LITHOSTRATIGRAPHY, HYDROTHERMAL ALTERATION, AND LITHOGEOCHEMISTRY OF NEOARCHEAN ROCKS IN THE LOWER AND SOUDAN MEMBER OF THE ELY GREENSTONE FORMATION, VERMILION DISTRICT, NORTHEASTERN MINNESOTA: IMPLICATIONS FOR VOLCANOGENIC MASSIVE SULFIDES

A THESIS
SUBMITTED TO THE FACULTY OF THE GRADUATE SCHOOL
OF THE UNIVERSITY OF MINNESOTA
BY

ADAM TIMOTHY HOFFMAN

IN PARTIAL FULFILLMENT OF THE REQUIRMENTS FOR THE DEGREE OF
MASTER OF SCIENCE

JANUARY, 2007

UNIVERSITY OF MINNESOTA

This is to certify that I have examined this copy of a master's thesis by

Adam Timothy Hoffman

and have found that it is complete and satisfactory in all respects,
and that any and all revisions required by the final
examining committee have been made.

Dean M. Peterson	George J. Hudak
Name of Faculty Adviser	Name of Faculty Co-Adviser
[redacted]	[redacted]
Signature of Faculty Adviser	Signature of Faculty Co-Adviser

12/26/2006 1/3/2007

Date

GRADUATE SCHOOL

Acknowledgements

First and foremost I would like to thank my advisors and mentors Dean Peterson, George Hudak and Richard Patelke for sharing with me their intimate knowledge of the geological sciences. I have benefited greatly from your support and friendship during the completion of this thesis. John Swenson and Joe Werne are thanked for serving on my committee. Luke Johnson and Ron Morton assisted with fieldwork. Karl Wirth and Jeff Thole are sincerely thanked for teaching me XRF techniques at Macalester College. Steve Hauck (NRRI), the Society of Economic Geologists' Newmont Student Research Grant, and the University of Minnesota Duluth Student Block Grant Program provided funding for this thesis. I would like to thank the faculty and staff in the Department of Geological Sciences at UMD; I have yet to find a friendlier group of professionals. Thank you to my good friend Paul Albers for encouraging me to finish this thesis. The staff at Newmont's Midas Operations provided a great amount of support and patience. I would like to thank my parents Miriam, Dan and Ann Hoffman for always encouraging me to make good life decisions, and for providing me the chance to receive a college education. Lastly I would like to thank my best friend and wife Jessica for the tremendous amount of love, encouragement and patience you have shown me in the last two years. This dissertation would never have materialized without you.

Dedication

This thesis is dedicated to

Miriam J. Hoffman

And

Brandon K. Mueller

Thank you both for teaching me the true meaning of courage. Don't ever give up.

Table of Contents

List of Figures, Tables, and Plates

LIST OF FIGURES

LIST OF TABLES

Chapter 1

INTRODUCTION

Introduction

The western Vermilion District of northeastern Minnesota contains a lithologically and structurally diverse geological setting located in the southern extension of the Wawa Subprovince of the Superior Province of the Canadian Shield (Card and Ciesielski, 1986) (Figure 1.01). The Wawa Subprovince is the host for a significant number of mineral deposits and showings, most notably lode gold and volcanogenic massive sulfides (VMS) (Fyon et al., 1992; Hudak et al., 2002b). In the Vermilion District, there has recently been a significant effort put forth to geologically and geochemically study areas that seem to represent environments favorable for hosting lode gold and VMS deposits (Peterson, 2001; Peterson and Jirsa, 1999a; Peterson and Jirsa, 1999b; Hudak et al., 2002b; Peterson et al., 2005; Hudak et al., 2004). Advocates of mineral exploration include the Natural Resources Research Institute of the University of Minnesota, the Minnesota Geologic Survey, the Minnesota Department of Natural Resources, and the Minerals Coordinating Committee that administers the mineral diversification plan of the Minnesota State Legislature. Since the early 1960's the state has supported mineral exploration through: 1) a large program of reconnaissance and detailed geologic mapping; 2) high-definition geophysical surveys including aeromagnetic, gravity, and EM Loop; 3) the construction of a centralized facility for housing drill cores and geologic data files; 4) the construction of a data storage and distribution system for archival and current exploration data; and 5) financial support for minerals-industry-related geological research (Southwick et al., 1998).

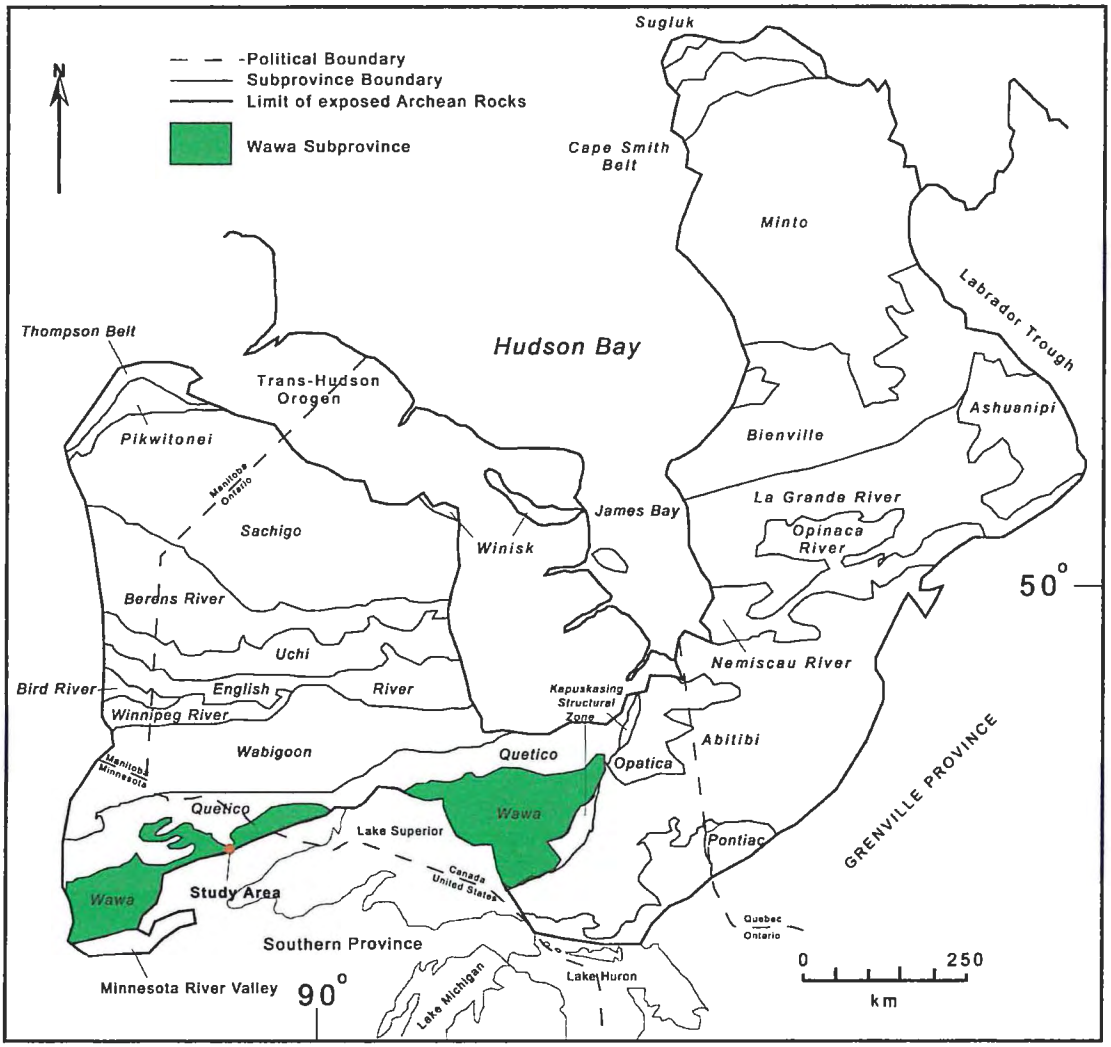

Figure 1.01. Location of the Wawa Subprovince of the Superior Province of the Canadian Shield (after Card and Ciesielski, 1986). Study area is shown in red.

During the summer of 2003, detailed geologic mapping (1:2000) was completed to assist the possible construction of a Deep Underground Science and Engineering Laboratory (DUSEL) adjacent to the Soudan Mine, formally proposed to the NSF as NUSEL (National Underground Science and Engineering Laboratory) (Peterson and Patelke, 2003). DUSEL planning and development required a better understanding of the regional and detailed geology, as well as the geological history of the area. Continued support from the NSF for DUSEL was awarded to the Homestake Mine (South Dakota) and the Henderson Mine (Colorado) during 2005.

Purpose of Study

This thesis project is part of a continuing research effort to understand the regional stratigraphy, volcanology, hydrothermal alteration, and possible base and precious metal mineralization, in the Lower and Soudan members of the Ely Greenstone Formation in the vicinity of the Soudan Mine. This work identifies the volcanic, hypabyssal, and sedimentary lithologies present near the Soudan Mine, reconstructs the geological processes and geological environments associated with their genesis, and discusses their syn- and post-volcanic hydrothermal alteration and structural modification. Glacial erosion has created numerous outcrop exposures in this area which provide an unparalleled opportunity to study a paleo seafloor geological system of Neoarchean age (Hudak pers. comm., 2005). Prospects including the Fivemile Lake, Purvis Lake, Eagles Nest, Skeleton Lake, and Needleboy Lake, all located within 5-15 km of Soudan, continue to challenge geologists studying northern Minnesota's base and precious metal mineral potential. These prospects are also contained within the Lower

member of the Ely Greenstone Formation and are interpreted to be geologically and stratigraphically linked to the Soudan Mine area (Hudak and Peterson, pers. comm. 2005). A detailed study of the stratigraphy, lithogeochemistry, and hydrothermal alteration has, to date, not been completed for the Soudan area. A detailed analysis of this area may indicate the occurrence of economic mineral deposits, and can further refine our understanding of the genesis of the Ely Greenstone Formation.

Objectives

The objectives of this study are: 1) to provide the state of Minnesota with a detailed geologic bedrock and hydrothermal alteration map, which will enable geologists to further understand the local stratigraphy, and encourage future geological studies in the area; 2) increase the understanding of the lithostratigraphy of the Soudan area, in particular, the eruption products and deposits, eruptive mechanisms, processes of emplacement and landforms produced; and 3) promote interest in the economic potential of the area by understanding the distribution, composition, paragenesis and processes associated with hydrothermally altered rock which will further enhance our understanding of the potential for discovering VMS deposits in this part of the Wawa Greenstone Belt.

Data obtained in this study will: 1) lead to a better understanding of the physical and chemical processes responsible for the genesis of the Lower and Soudan Members of the Ely Greenstone; 2) provide surficial geologic data which will contribute to a cross-sectional view of an Archean subaqueous hydrothermal seafloor system when combined with geological data to the east (Hudak and Morton, 1999; Peterson and Jirsa, 1999a;

Hovis, 2001; Peterson, 2001; Hudak et al., 2002a; Hudak et al., 2002b, and southeast (Hudak et al., 2002b; Giagrande, 1981).

Location, Access, and Terrain

The field area for this study is located in north-central St. Louis County in the Lower Member of the Ely Greenstone Formation. It comprises Sections 23, 24, 25 and 26 of Township 62 North, Range 15 West. The field site is approximately seventy miles (123 km) north of Duluth MN, 20 miles (35 km) southwest of Ely MN, and lies southeast of Vermilion Lake and northeast of the Soudan Iron Mine (1883-1962) and Soudan Mine State Park. The area may be accessed by traveling north from Duluth on U.S. Highway 53 to Virginia MN, and then north on Highway 169 to Soudan MN.

The western boundary of the field area lies within Soudan Mine State Park. The Oliver Mining Division of the United States Steel Corporation owns the remainder of the area. Terrain encompassing mostly shallow swampy wetlands contains mainly pine, birch, alder, and cedar trees (Figure 1.02). Outcrop access is tricky at times despite the fact that outcrops are well-dispersed throughout the field area. Exposed rock has a fine veneer of lichen and, in many cases, detailed mineralogical and texture analysis is difficult. Initially more than ninety percent of all outcrops mapped were covered with moss and small tree roots. Outcrops covered with vegetation were stripped by manually peeling moss layers, subsequently cleaning with a wisk broom, and then letting rain clean any additional debris off the exposed surfaces. Roots were cut with the butt end of a rock hammer. This made it easier to examine and interpret the physical characteristics of the outcrops, including color, texture, mineralogy, and structures.

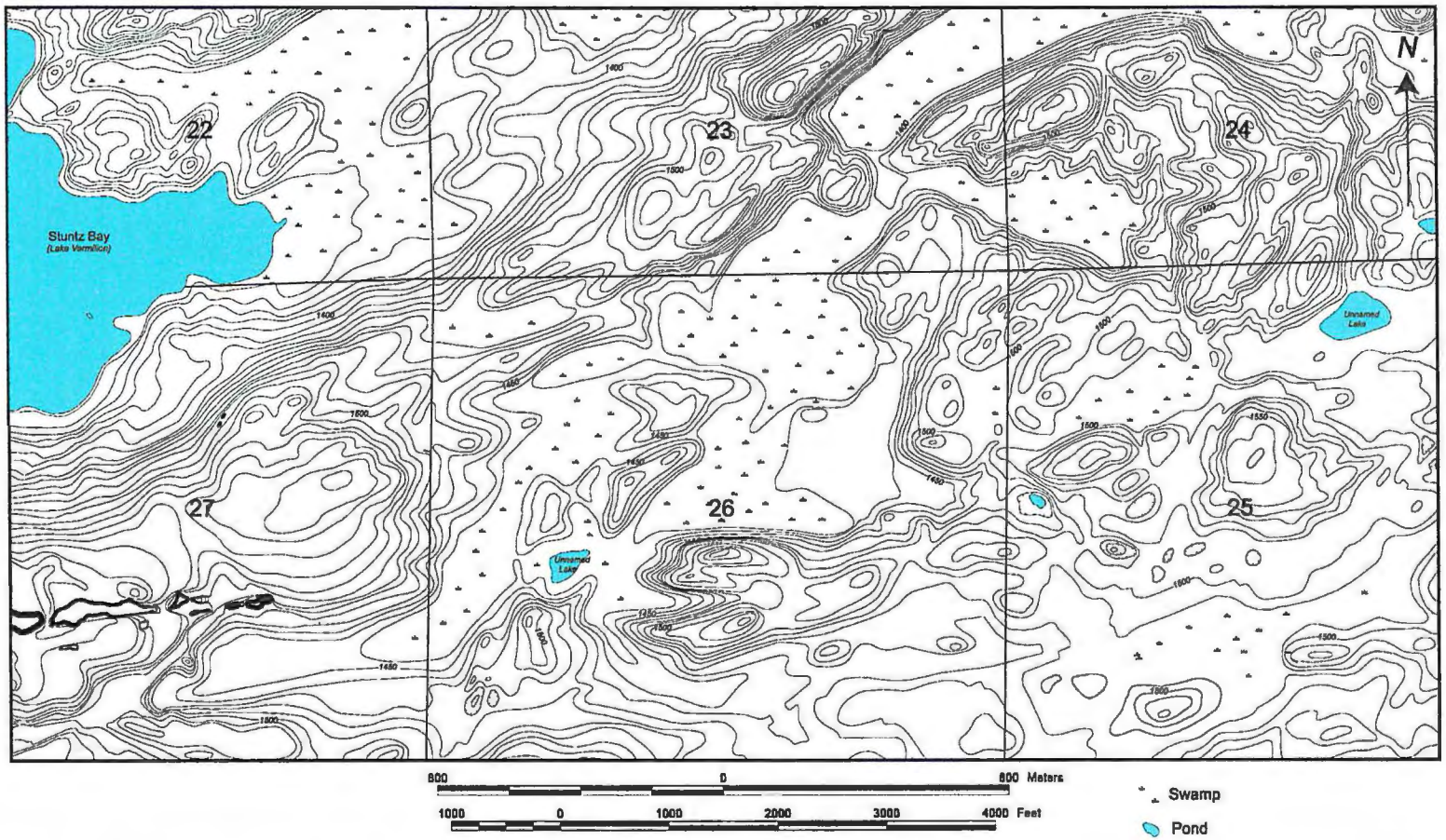

Figure 1.02. Topographic map of the Soudan Mine area. Low lying swamps are depicted by areas where contour lines are absent. Contour interval is 10 feet.

Methods

Bedrock geologic mapping was competed at a scale of 1:2000 on preprinted topographic map sheets designed by Peterson and Patelke (2003). Topography (10-foot contour interval) and a pre-printed (UTM) grid (100-m spaced) were included on the mapping sheets. Information recorded on the field sheets included traverse route, outcrop location, outcrop shape, sample locations, rock type, structural measurements, glacial features, pillow morphology, pillow selvege width, fault and lithological contact data, and other significant geologic information. Field data was entered into a continuously revised ArcView GIS database that was inherited from Peterson and Patelke (2003), for use in this study.

The field portion of this thesis was completed in two phases. *Phase 1* comprised a four-week period of bedrock mapping between May and June of 2003. This mapping served two purposes: 1) to create a geologic bedrock map of the Soudan Mine area for the possible construction of the DUSEL; and 2) to create a foundation for the Masters thesis study. *Phase 2* comprised a three week period and took place during June, 2004. Pre-selected field locations were further investigated based on information obtained via hand sample and petrographic analysis. Much of Phase 2 was spent examining and mapping (1:2000 scale) alteration mineral (Quartz + Epidote) assemblages suggestive of zones of intense ancient hydrothermal activity. The goal of Phase 2 was to further map volcanological facies and hydrothermal alteration patterns.

The author examined eighty-two standard thin sections in detail to identify rock type, mineralogy, volcanic fragments, volcanic textures, and mineral alteration assemblages (see Appendix: 2). Samples for petrographic analysis included each of the

various rock types in an attempt to accurately represent the study area. The author entered interpretations into custom petrography data sheets designed by Hudak et al. (2002b).

Nine days (September 7-14th, October 19th-20th) were spent at Macalester College in St. Paul Minnesota preparing thirty-seven rock samples for lithogeochemical analysis. X-ray fluorescence methods were used to generate whole rock and trace element data. The following analytical protocol was used to obtain the lithogeochemical data:

Selected rock samples were crushed in a Braun Chipmunk to approximately 1 centimeter by a half centimeter chips. Approximately 30 milliliters of sample was placed in a tungsten carbide bowl for whole rock analysis, and a cast iron bowl for trace element analysis. 27 milliliters of Vertrel® solution was added to the bowl. The bowls were sealed and each placed in a shatter box for four minutes. The powders were brushed out and collected in 60 milliliter Nalgene bottles. For each sample a pellet (trace elements) and a glass bead (major oxides) were made. Pellets were constructed by placing 10 grams of iron processed powder into a press at six tons of pressure for one minute. Pellets were dried in an oven at 70°C for one hour. Glass beads were made by melting a mixture of 1 gram tungsten carbide processed powder, five grams of flux, and 0.01 grams of ammonium nitrate. This mixture was melted in a platinum and gold alloy crucible at 1000-2100°C for approximately 13 minutes. Pellets and beads were then placed in an XRF for two weeks. Each sample was run six times, three times for the pellet, and three times for the bead. This method was used to average out element and compound concentrations to get a more accurate analysis.

Plate 1 shows the limits of recent mapping and the distribution of outcrops mapped in the field area with rock samples taken for lithogeochemical and petrographical analysis.

Terminology of Volcaniclastic and Volcanic Rocks

In previous years, the variability of volcanic terminology has been the subject of discussion (Fisher and Schmincke, 1984; Cas and Wright, 1987; Stix, 1991; McPhie et al., 1993; White, 1994; Orton, 1996; Gibson et al., 1999; Mueller and White, 2004). There are two dominant geologic facies in the Soudan Mine area: 1) coherent geologic facies that include felsic, mafic and intermediate lavas sequences and mafic and intermediate synvolcanic intrusions; and 2) volcaniclastic facies that include dominantly volcanic derived sediments formed from volcanic eruptions and volcanic weathering including tuff, lapillistone and breccia deposits. The nomenclature used in this thesis to describe these rock types is based on the criteria of Fisher (1961 and 1966) (Figure 1.03) and Mueller and White (2004).

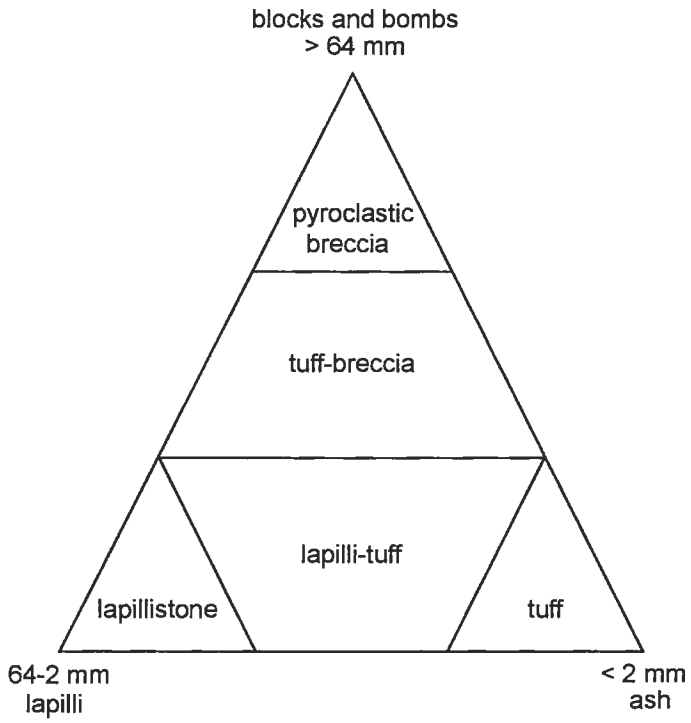

Figure 1.03. Grain size terms used for primary pyroclastic rocks (Fisher, 1966).

By definition, clastic rocks containing abundant volcanic material are referred to as volcaniclastic irrespective of the material origin or environment. The term volcaniclastic encompasses pyroclastic, autoclastic and epiclastic deposits and can be used for Precambrian rocks where particle origin remains enigmatic (Mueller and White, 2004). Table 1.01 introduces the volcaniclastic rock nomenclature used in this thesis.

Grain Size	Unconsolidated Deposit Name	Rock Name	Complete Rock Name
(< 0.0625 mm)	Mud-grade ash	Mud-grade tuff	Mudstone-grade tuff
(0.0625-0.125 mm)	Very fine ash	Very fine tuff	Very fine-grained tuff
(0.125-0.25 mm)	Fine ash	Fine tuff	Fine-grained tuff
(0.25-.5 mm)	Medium ash	Medium tuff	Medium-grained tuff
(0.5-1 mm)	Coarse ash	Coarse tuff	Coarse-grained tuff
(1-2 mm)	Very coarse ash	Very coarse tuff	Very coarse-grained tuff
(2-4 mm)	Fine lapilli	Fine lapillistone	Fine lapillistone
(4-16 mm)	Medium lapilli	Medium lapillistone	Medium lapillistone
(16-64 mm)	Coarse lapilli	Coarse lapillistone	Coarse lapillistone
(>64 mm)	Blocks/Bombs	Breccia	Breccia

Table 1.01. Expanded Wentworth-based, grain size scheme for volcaniclastic rocks (after Mueller and White, 2004) using the criteria of Fisher (1961, 1966).

Regional Geology

The study area is located in the western portion of the Neo-archean (2.5-2.8 Ga) Vermilion Greenstone Belt of the Vermilion District of northeastern Minnesota. The Vermilion District is situated in the southwestern part of the Wawa Subprovince of the Superior Province of the Canadian Shield (Card and Ciesielski, 1986). The Superior Province, part of the Laurentian Precambrian core of North America, is composed of rocks ranging in age from 3.1 Ga to 2.6 Ga, is exposed over an area of more than 2 million km^2, and is the world's largest relatively undisturbed Archean craton (Card and Ciesielski, 1986). The Vermilion Greenstone Belt is bounded to the north-northeast by

the Vermilion Granitic Complex of the Quetico Subprovince, on the east by the Saginaw Batholith, in the west is covered by thick glacial deposits, and to the southeast it is bounded by the Archean Giants Range Batholith (Sims, 1976; Shultz, 1980) (Figure 1.04). The Vermilion District is composed dominantly of well-defined areas of volcanic and volcanically-derived rock metamorphosed to greenschist and amphibolite facies. These rocks vary in composition from komatiite and basalt to dacite and rhyolite with defined assemblages of clastic and chemical sedimentary rocks that are separated by large pseudo-linear domains of plutonic rocks (Williams et al., 1991). Although pervasive greenschist or amphibolite facies alteration occurs throughout the Vermilion District, the prefix "meta" has been eliminated from all lithologic descriptions, for simplicity.

The Vermilion District contains lithological, structural, and stratigraphic architecture common to many other Archean greenstone belts (Southwick et al., 1998). It comprises a large folded (west-northwest plunging anticline) succession of moderately to steeply north-dipping supracrustal rocks, disrupted by an assortment of intrusive suites; all dissected by an array of syn- to post-depositional faults.

Five dominant formations or large lithologic domains make up the Vermilion District. These are, from oldest to youngest, the Ely Greenstone, the Gafvert Lake Volcanic Complex, the Lake Vermilion Formation, the Knife Lake Group, and the Bass Lake Sequence (Figure 1.04). Below is a general lithologic description of these rock domains.

The oldest rocks of the Vermilion District are the Ely Greenstone Formation. Subdivisions of the Ely Greenstone include the Lower, Soudan, and Upper members

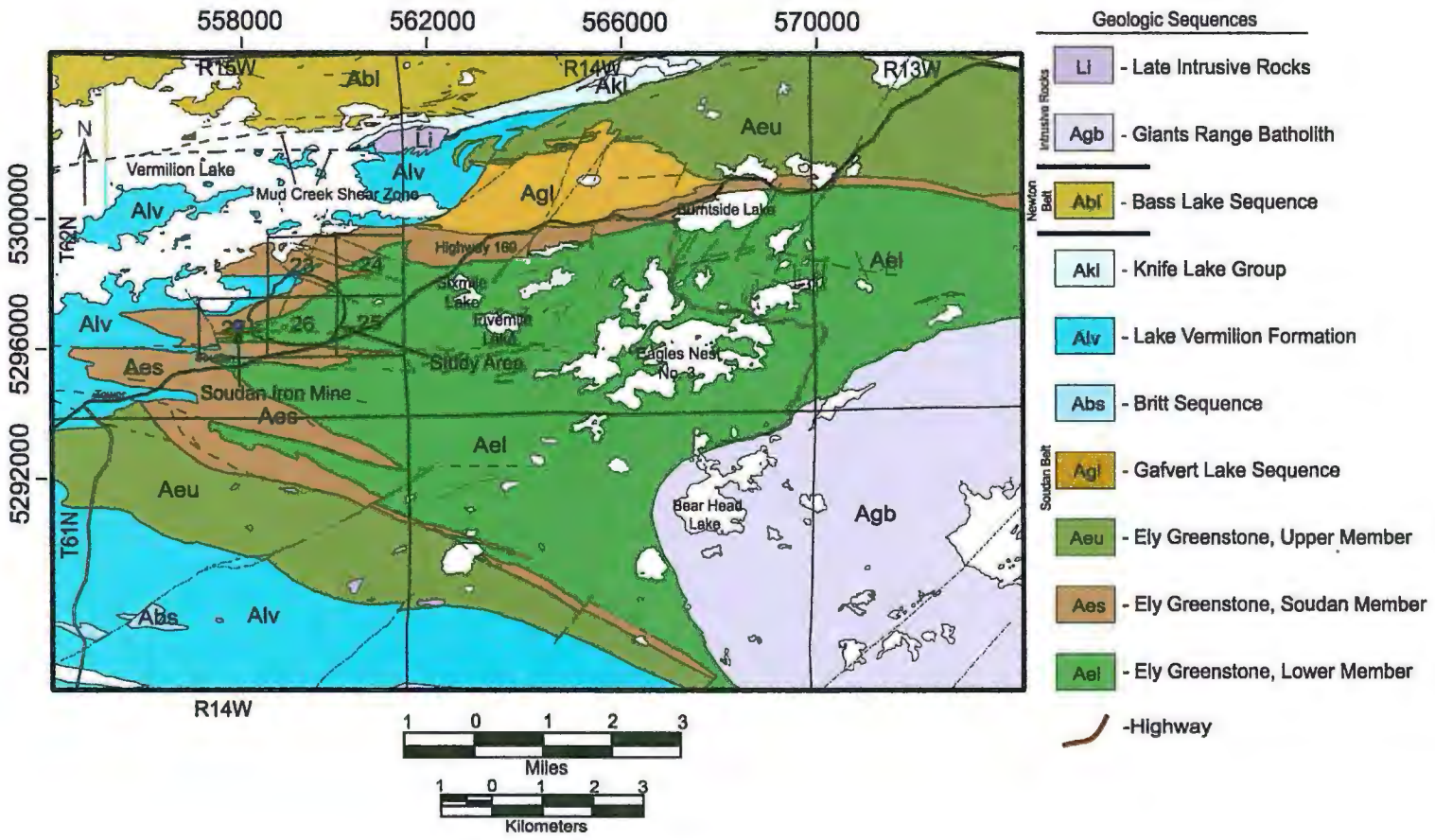

Figure 1.04. Simplified geologic stratigraphy of the western Vermilion District depicted with UTM NAD-83 coordinates (after Peterson and Patelke, 2003). The location of the study area is also indicated.

(Morey et al., 1970). Prior to 2003, the Lower Member of the Ely Greenstone was interpreted to be composed primarily of pillowed and massive calc-alkaline to tholeiitic basalt to andesite lavas with local felsic volcaniclastic rocks (Sims and Southwick, 1985). Recent detailed mapping by Peterson (2001), Hudak et al. (2002a), Hudak et al. (2002b), Peterson and Patelke (2003), and the author of this study, have revealed a wider variety of rock types than previously documented. Newly discovered lithologies consist of felsic and mafic intrusions, an abundant array of felsic, intermediate and mafic dikes, and felsic volcanic and volcaniclastic strata. Rocks in the Lower Member of the Ely Greenstone are believed to be correlative with rocks mapped by Hudak et al. (2002a) and Hudak et al. (2002b), in the Fivemile Lake, Needleboy Lake, and Sixmile Lake areas.

The Soudan Member of the Ely Greenstone is an Algoma-type oxide facies (Gross, 1965) iron formation varying from laminar to highly convoluted and is dominantly composed of interbedded jasper and hematite with smaller amounts of magnetite and chert (Peterson and Patelke, 2003).

The Upper Member of the Ely Greenstone contains mafic pillowed and massive calc-alkaline to tholeiitic basalt and andesite lavas and regional ultramafic komatiitic rocks with local horizons of felsic volcaniclastic rocks.

The Gafvert Lake Volcanic Complex has been interpreted to represent one or more Archean stratovolcanoes that were built upon the Lower and Soudan Members of the Ely Greenstone. Lava flows, tuffs, debris flows, peperites, and plutonic rocks of dacitic composition make up the complex (Peterson, 2001; Hudak et al., 2002b; Heiling, 2003).

The Lake Vermilion Formation and Knife Lake Group consist of graywackes, slates and conglomerates. The uppermost strata of the Vermilion District are mafic lavas, intrusions and clastic sedimentary rocks of the Newton Lake Formation.

Structural Geology

The Western Vermilion District is divided into two structural domains, the Soudan Belt (to the south) and the Newton Belt (to the north; Figure 1.04). The Soudan Belt is characterized by steeply plunging folds and a lithologically consistent, well-defined, east-west trending, 2-3 km thick stratigraphic section comprising calc-alkaline and tholeiitic rocks (Southwick, 1993; Hudak et al., 2002b; Peterson, 2001). The Newton Belt contains numerous homoclinal, north-dipping, east-west-trending, fault-bounded, poorly-correlated slabs of volcanic and sedimentary rocks (Southwick, 1993; Peterson, 2001). Both domains contain unconformable Timiskaming-type sequences composed of calc-alkalic volcanic rocks, conglomerates, and finer-grained sedimentary rocks. Volcanic rocks of the Newton Belt are compositionally distinct from those of the Soudan Belt because they contain komatiite flows and peridotite sills (Peterson and Patelke, 2003).

The boundary between the Soudan and Newton Belt can be traced geophysically across the width of Minnesota and is locally termed the Leech Lake disconformity (Jirsa et al., 1992). The Leech Lake disconformity is a curvilinear structure that locally trends northeast-southwest and coincides with such structures as the Mud Creek Shear Zone (Hudleston et al., 1988), the Bear River Fault (Jirsa et al., 1992), and the Wolf Lake Faults (Sims and Southwick, 1985). The relationship between stratigraphic units within

each Belt is correlated on a large scale, but faults truncate contacts locally (Figure 1.05) (Peterson and Patelke, 2003). Peterson et al. (2001) have correlated the Soudan Belt with the Saganagons Assemblage of Northwestern Ontario, and the Newton Belt with the Greenwater/Burchell Assemblage of Northwestern Ontario. These correlations are based on lithological, geochronological, and structural similarities (Figure 1.05).

Several studies (Jirsa et al., 1992; Boerboom and Zartman, 1993; Corfu and Stott, 1998; Peterson et al., 2001) have determined that the rocks in the western Vermilion District were subjected to at least three major structural deformation events. The earliest deformational event (D_1) produced broad, locally recumbent folds within the Soudan Belt. The effect of D_1 in the Newton Belt was predominately thrust imbrication of large crustal blocks resulting in north-dipping volcanic strata (Jirsa, 2000). D_1 was most likely the most dramatic deformational event, though it is difficult to find physical evidence in the field due to lack of cleavage. Field relationships indicate that uplift, faulting, and the deposition of Timiskaming-type clastic sequences in fault-bounded basins occurred late in D_1 (Figure 1.05) (Jirsa, 2000). The structural differences in the Newton and Soudan Belt are related primarily to D_1. These differences can be explained by Archean accretionary tectonics during the late stages of subduction where large topographic features on the subducting plate (near the trench) slowed subduction and caused initial thrust faulting (Newton Belt), and later broad recumbent folding (Soudan Belt) (Hoffman, 1990).

The best-defined large fold in the Soudan Belt related to D_1 deformation is the Tower-Soudan Anticline. The Tower-Soudan Anticline is a dominantly west-plunging structure near the Soudan Mine; however its orientation is highly variable further west,

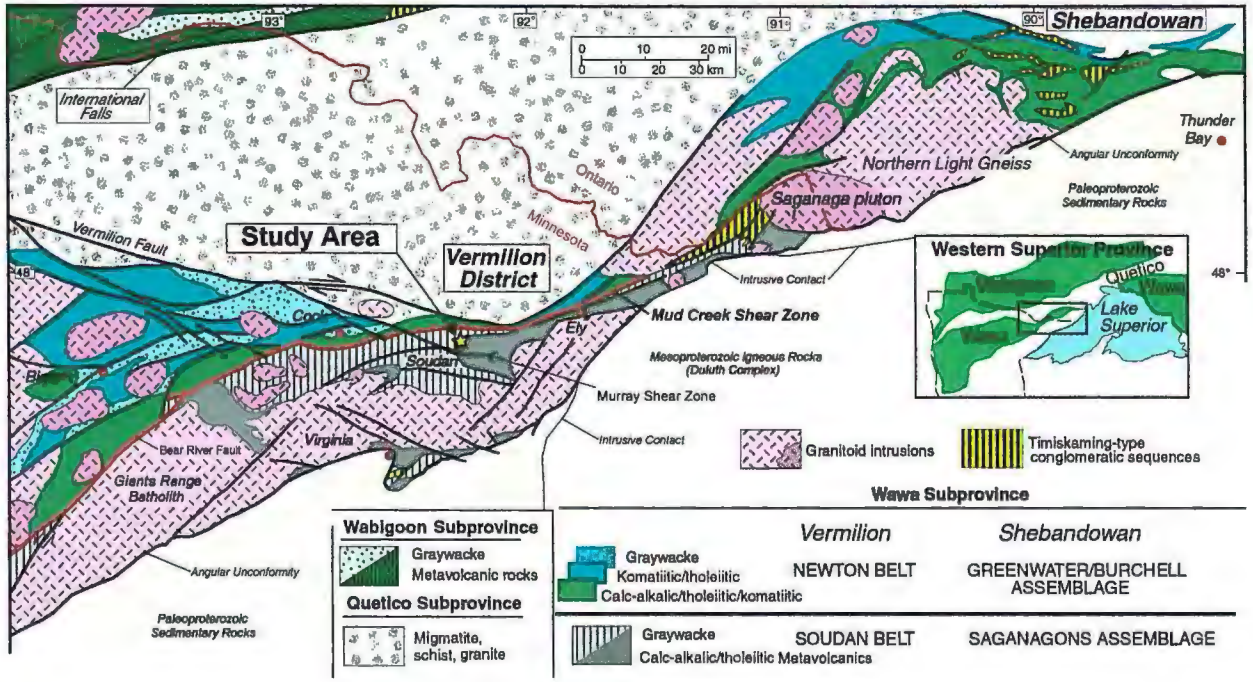

Figure 1.05. Regional geology, structure, and location of the western Vermilion district in northeastern Minnesota (after Peterson and Patelke, 2003).

ranging from nearly vertical in the Lower Member of the Ely Greenstone basalts, to shallowly northeasterly plunging in the western sedimentary rocks of the Lake Vermilion Formation (Bauer, 1985; Hooper and Ojakangas, 1971; Hudleston, 1976; and Jirsa et al., 1992).

The second deformation event (D_2) has been dated at 2674 to 2685 Ma (Boerboom and Zartman, 1993), and further refined to 2680 to 2685 Ma (Corfu and Stott, 1998). The D_2 event resulted in: 1) regional greenschist facies metamorphism; 2) the development of regional, generally east-west trending foliation, small folds, metamorphic fabric (well-developed cleavage), and lineations (Hovis, 2001); and 3) large deep crustal structures having mainly dextral asymmetry (Peterson and Patelke, 2003). Major D_2 structures located in the Vermilion District include the Murray Shear Zone, the Mine Trend Shear Zone (Peterson and Patelke, 2003), and the Mud Creek Shear Zone (Figure 1.06). These structures are interpreted to have resulted from compressional to transpressional tectonics associated within the late stages of D_2 (Peterson, D.M., personnel communication, 2003).

The third deformational event (D_3) is represented by northeast-and northwest-trending post-volcanic faults that dissect the stratigraphic assemblage (Peterson, 2001). D_3 related structures include the Waasa and Camp Rivard faults east of the Soudan Mine area, and the large, well-defined crustal scale Vermilion and related faults that form the Wawa-Quetico Subprovince boundary (Figure 1.05) (Peterson and Patelke, 2003).

Southwick et al. (1998) suggest that the lithological and structural history of the western Vermilion District area are generally analogous to those observed in Mesozoic to Holocene volcanic arcs of the western Pacific, and evolved in a similar tectonic setting.

Hudak et al. (2002b) have found that rocks in the Lower Member of the Ely Greenstone, near Fivemile Lake, have geochemical attributes that are consistent with volcanic rocks formed in an arc-setting.

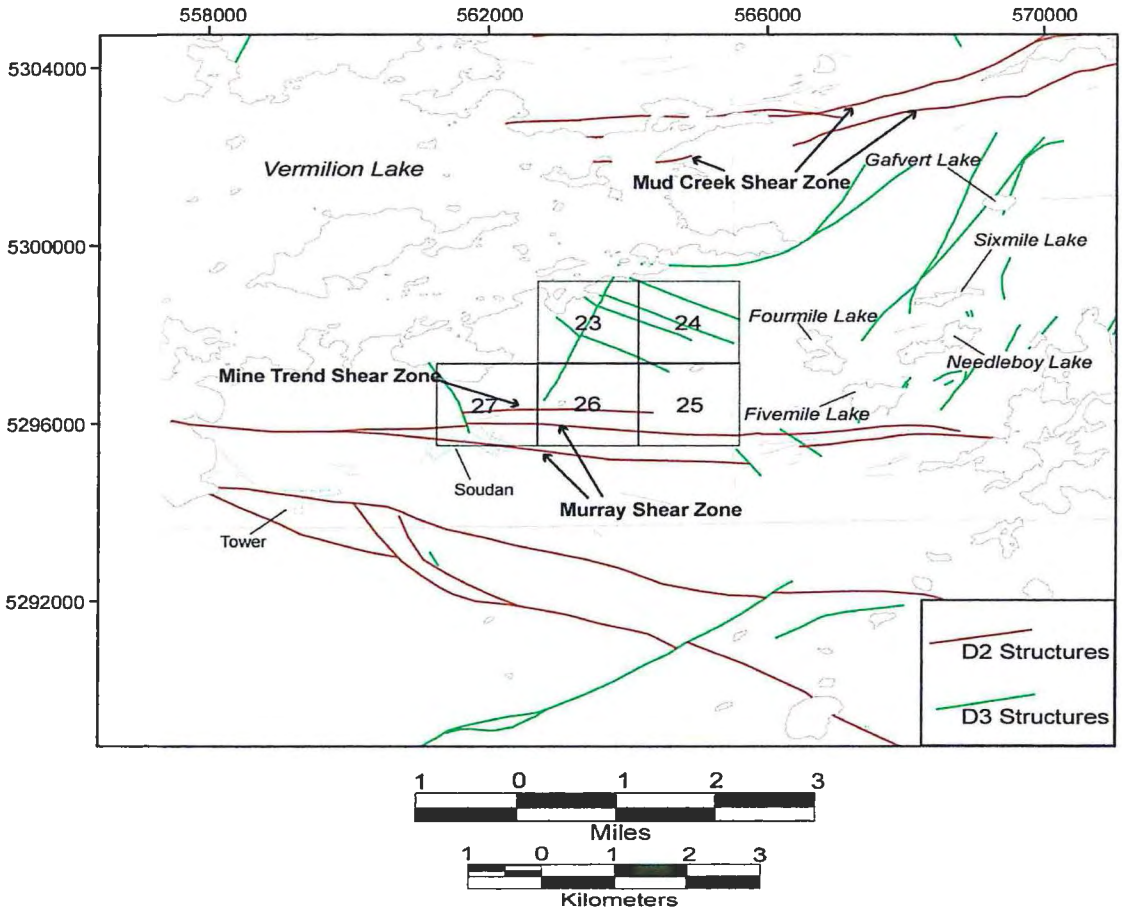

Figure 1.06. Location of major structural features in the western Vermilion District depicted by UTM NAD-83 coordinates.

Previous Work

The first major publication describing the geology of the Vermilion District, titled "The Vermilion Iron-Bearing District of Minnesota" was published by J. Morgan Clements in 1902. Since then, the western Vermilion District has been the focus of

mapping projects by the Minnesota Geological Survey (Southwick, 1993; Peterson and Jirsa, 1999b; Morey et al., 1970; Southwick et al., 1998; Jirsa et al., 2001), The United States Geological Survey (Sims and Southick 1980, 1985), academic theses (Giagrande, 1981; Hovis, 2001; Heiling in progress, 2003), the Natural Resources Research Institute (Hudak et al., 2002a, Hudak et al., 2002b; Hocker et al., 2003; Peterson and Patelke, 2003), the Minnesota Department of Natural Resources (Hudak and Morton, 1999), and numerous exploration and mining companies. Most recently, Carrie Heiling a graduate student at the University of Minnesota Duluth has completed fieldwork in the area. Her focus is characterizing peperites found in the Gafvert Lake Volcanic Complex (Heiling, 2003).

VMS Exploration and Prospects

The Lower Member of the Ely Greenstone hosts four volcanogenic massive sulfide (VMS) showings and two lode gold prospects. The VMS prospects include 1) the Skeleton Lake VMS Prospect (drilled by Exxon, 1972); 2) the Eagles Nest VMS Prospect (drilled by Newmont, 1988); 3) the Purvis Road Prospect (drilled by Rendrag, 1999); and 4) the Fivemile Lake Prospect (drilled by Teck, 1994) (Peterson, 2001; Hudak et al., 2002b, Peterson and Patelke, 2003).

The Skeleton Lake VMS Prospect

The Skeleton Lake VMS Prospect is located in central St. Louis County approximately five kilometers southeast of the Soudan Iron Mine. Exxon Corporation explored the Skeleton Lake area in the 1970s drilling three diamond drill holes, two of

which intersected a horizon of pyrite-pyrrhotite-chalcopyrite mineralization five to seven meters thick (Hudak et al. 2002a). Exxon dropped the property and the Minnesota DNR conducted its own geophysical survey in 1975 and 1976. In the early 1980s, Lehmann Exploration drilled six drill holes as part of their Polaris joint venture (Hudak et al. 2002b). The Skeleton Lake area was also the subject of two research studies (Giagrande, 1981; Hudak et al., 2002b). Investigation by Hudak et al. (2002b) suggests that mineralization at the Skeleton Lake VMS Prospect is similar to mineralization that occurs in Noranda-type VMS deposits. Conclusions were reached by the presence of semi-conformable epidote + chlorite + actinolite alteration that is consistent with alteration associated with Noranda-type deposits (Morton and Franklin, 1987; Santaguida et al., 1999). Work by Hudak et al. (2002b) suggests that the Skeleton Lake VMS Prospect has similar attributes to rocks mapped in the Five Mile Lake area (Hudak et al. 2002b) and the Eagles Nest (Hovis, 2001).

The Eagles Nest Prospect

The Eagles Nest VMS Prospect is located within the Lower Member of the Ely Greenstone approximately nine kilometers east of the Soudan Mine. It is composed dominantly of pillowed and massive mafic lavas with local felsic volcaniclastic deposits and small plutons (Hovis, 2001). The entire sequence is metamorphosed to greenschist grade (Peterson, 2001). In the summer of 1999, Steve Hovis (University of Minnesota Duluth) inspected a 2.5 square mile area to interpret the physical volcanology and hydrothermal alteration of footwall rocks in the Eagles Nest area (Hovis, 2001). Hovis (2001) determined that the Eagles Nest Prospect is situated in a sequence of subaqueous calc-alkaline andesite lava flows formed during island arc-type volcanism in the late

Archean. Hovis (2001) indicated that alteration mineral assemblages at this prospect formed from mostly low temperature hydrothermal systems. The low solubility of Cu and Zn under these conditions suggested that Cu and Zn were not apparently leached from the lavas, and therefore no significant massive sulfide mineralization occurred in the area (Hovis, 2001).

The Purvis Road Prospect

The Purvis Road Copper-Zinc Prospect is located approximately 10 miles north of Babbitt MN and lies within the Lower Member of the Ely Greenstone Formation. The area is located in the northeast part of the Eagles Nest. The Minnesota Geological Survey and United States Geological Survey conducted reconnaissance mapping to the south of Purvis Lake. This mapping was completed around 1970 and was published in 1985 (Sims and Southwick, 1985). Geologic mapping by Peterson (1998) along with the Purvis Forest Management led to the discovery of a large tonalitic pluton. The field relationships of the pluton with the surrounding volcanic rocks indicated that its timing was synvolcanic. Copper-rich mineralization within the pluton and surrounding volcanic rocks, along with extensive alteration (quartz-epidote, chlorite, porphyry-style veining), the occurrence of massive sulfide boulders in basal till, and the presence of a geophysical anomaly indicated the area highly favorable for hosting VMS.

The Fivemile Lake Prospect and the Needleboy Lake/Six-Mile Lake Areas

The Fivemile Lake Prospect is located approximately 2-3 kilometers east of the Soudan Mine area. Since the summer of 2000, detailed field mapping (1:100-1:5000

scale), petrographic studies, and lithogeochemical evaluations of the volcanic, intrusive, and sedimentary strata at the Fivemile Lake Prospect were conducted by Dr. George Hudak, Mr. Trent Newkirk, Mr. Jason Odette, Ms. Stephanie Hocker (UW-Oshkosh), Mr. John Heine, and Mr. Steven Hauck (NRRI) (Hudak, et al., 2002b).

Hudak et al. (2002b), Newkirk et al. (2001), Odette et al. (2001), and Hocker et al. (2003) found that the Fivemile Lake area is composed dominantly of mafic to intermediate lavas and volcaniclastic rocks, with subordinate felsic lavas and volcaniclastic rocks, as well as mafic to intermediate synvolcanic intrusions.

Hudak et al. (2002b) and Odette et al. (2001) defined a large semi-conformable alteration zone dominated by quartz + epidote-bearing mineral assemblages that exhibit mineralogical and geochemical characteristics of metal-depleted rocks found within the deep parts of subaqueous convective hydrothermal cells. Hocker et al. (2003) identified two distinct types of alteration zones within volcanic and volcaniclastic rocks associated with VMS mineralization in the Fivemile Lake area. These included regional semi-conformable alteration zones of various proportions of quartz + epidote ± amphibole ± chlorite ± plagioclase feldspar that are locally crosscut by several relatively narrow, northeast trending disconformable zones of fine-grained chlorite and/or sericite that are closely associated with synvolcanic fault zones. Microprobe analysis determined that the alteration mineral chemistry (epidote, chlorite, sericite) at the Fivemile Lake Prospect is remarkably similar to that from the Noranda VMS mining camp of Canada as well as other significant Archean VMS ore bodies.

Ultimately, Hudak et al. (2002b) concluded that: 1) large amounts of pillow-dominated sections suggest rapid deposition of mafic lavas on the seafloor, therefore not

providing ample time to develop a significant economic VMS alteration system and only small VMS deposits may have been formed in the relatively short-lived hiatuses between pillow lava flows; 2) a one-to two kilometer thick stratigraphic section of the Lower Ely Greenstone north of the Five Mile Lake area has excellent potential to host VMS mineralization (Hudak et al., 2002b); 3) strata up-section from the Fivemile Lake Prospect needs to be further evaluated for volcanogenic massive sulfides; and 4) geophysical conductors that were found during their investigation should be further evaluated for syn- and/or post-magmatic mineralization (Hudak et al., 2002b).

In August of 2001 and 2002 Dr. George Hudak, John Heine, Stephanie Hocker, and Steven Hauck investigated Needleboy Lake and the Six Mile Lake area for VMS mineral potential. Field mapping within the Needleboy Lake area investigated all outcrops within a 100-200m perimeter of the lake. Mapping of Six Mile Lake included three detailed north-south traverses (Hudak et al., 2002a). This work involved evaluating the stratigraphic succession, hydrothermal alteration, and the syn- and post-volcanic structures in an effort to understand the VMS potential in the Lower Ely Greenstone region (Hudak et al., 2002a).

Gold Exploration and Prospects

Exploration programs for gold in the Ely Greenstone Formation occurred from the mid 1980's to the early 1990's. These programs included mineral exploration in the Murray and Eagles Nest Prospects and the Mud Creek Shear Zone. Other gold exploration projects occurred both east and west of Lake Vermilion from the 1980's to

the early 1990's, by companies including Cyprus, Freeport, Noranda, Normin, Kerr-McGee, BHP, American Shield, Lehmann, and Mapco.

Murray Shear Zone

Newmont Exploration Limited completed lode gold mineral exploration in the Lower Member of the Ely Greenstone in the mid- to late- 1980s, and discovered gold mineralization at the Murray Prospect (Hovis, 2001). Newmont discovered gold mineralization along the northern edge of the Murray shear zone during reconnaissance mapping and sampling of rocks, soil, and stream sediments in the area (Peterson, 2001). Encouraging results led to an extensive exploration program across the Lower Member of the Ely Greenstone.

Eagles Nest Prospect

Newmont Exploration Limited also conducted a gold exploration program over the Eagles Nest Prospect from 1986-1988 (Peterson, 2001). Newmont performed magnetic and EM loop geophysical surveys, geochemical sampling, and diamond drilling at the site (Hovis, 2001). The project was discontinued after Newmont considered the drilling results unfavorable for gold mineralization. However, these drilling results indicate the presence of up to four meters of VMS mineralization (Hudak and Morton, 1999).

Mud Creek Shear Zone

Dr. Dean Peterson and Richard Patelke of the Natural Resources Research Institute are currently investigating the eastern Mud Creek Shear Zone for lode gold mineralization. This project aims to complete geologic bedrock maps of numerous gold prospects located north of the Mud Creek Shear Zone in the Archean Bass Lake Sequence. The goal is to increase economic interest in the area by incorporating previous and contemporaneous geologic data into a GIS database to better characterize the potential for mesothermal lode gold (Peterson et al., 2005).

Iron Exploration

The United States Steel Corporation (U.S. Steel) has done exploration in the area since the early 1900s and found localized iron formation and massive pyrite horizons, as well as local anomalous gold mineralization (Peterson, 2001). The Soudan Mine area is recognized for its massive hematite ores (>60%) that were mined from 1883 to 1962 (Peterson and Patelke, 2003). Ore was extracted with dynamite and carried by man, mule, or rail. Railroad grades, mine dumps, open pits and shafts are still recognized in the Soudan Mine area. Mining usually started in open pits and progressed underground into steep walled shafts that became increasingly dangerous. Ore bodies located in the mine area were irregular in shape and derived from lower grade iron-formation by uncertain processes. Peterson and Patelke (2003) describe the "most likely" formation of ore by "the contemporaneous leaching of silica and precipitation of hematite by hydrothermal solutions active during the D_2 shear-dominated deformation."

In the late 1900s, the Oliver Mining Company, a division of U.S. Steel, conducted test pit programs and dip-needle surveys. This work suggests that other near surface massive hematite bodies are absent in the immediate area (Peterson and Patelke, 2003). The Minnesota Injector Neutrino Oscillation Search (MINOS) lab is currently operating in the Soudan Mine.

Chapter 2

LITHOLOGY, STRATIGRAPHY, STRUCTURE AND PETROCHEMISTRY

Introduction

Volcanic and volcaniclastic strata were characterized in the Soudan Mine area based on field mapping, petrographic analysis, and lithogeochemical data. More specific criteria include the detailed analysis of volcanic textures, rock color, lava morphology, crystal size and morphology, rock distribution, rock composition, sedimentary features and contact relationships. Together these data have played a major role in defining the stratigraphy and constraining lithology boundaries, and have provided useful information that have aided in determining the potential for base metal sulfide mineralization in the field area.

Definition of Lithologic Terms

The Natural Resources Research Institute submitted a report (Peterson and Patelke, 2003) to the state of Minnesota titled "National Underground Science and Engineering Laboratory: Geological Site Investigation for the Soudan Mine". This report describes the geologic setting near the Soudan Mine, and was submitted in order to determine if the bedrock in the Soudan Mine area was a practical location to host the proposed Deep Underground Science and Engineering Laboratory (DUSEL). For the sake of convention throughout the Vermilion District, the rock classification format used in this thesis is similar to the classification used by Peterson and Patelke (2003) and others that have conducted studies in the Vermilion District (Peterson, 2001; Peterson

and Jirsa, 1999a; Hudak et al., 2002a; Hudak et al., 2002b) (Table 2.01). This classification system utilizes descriptive field based observations, by naming rock types solely on physical characteristics and omitting nomenclature that is influenced by genetic processes. Genetic rock classification will be discussed further in the interpretation section for each rock sequence. The nomenclature used in this thesis is consistent with that of Fisher (1961 and 1966), Mueller and White (2004).

Peterson and Patelke (2003) divided the Lower and Soudan members into five distinct supracrustal sequences based on textural and compositional differences. These are listed from oldest to youngest and include: 1) the Fivemile Lake Sequence (FMxx), composed dominantly of, but not limited to, mafic and intermediate pillowed and massive lava flows; 2) the Central Basalt Sequence (CBxx), composed dominantly of, but not limited to, mafic and intermediate pillowed and massive lava flows; 3) the Upper Sequence (USxx), consisting dominantly of chemical and volcaniclastic sediments; 4) the Gafvert Lake Sequence (GLxx), consisting dominantly of volcaniclastic sediments; 5) Intrusive Rocks (Xy, XXXX) of mafic to intermediate composition; and 6) Sheared Rocks (5xxx), or schists with varying mineral assemblages (Figure 2.01).

Peterson and Patelke (2003) grouped the following rock types into the Upper Sequence: 1) felsic volcaniclastic rocks at the base of the Soudan Iron Formation; 2) chemical sediments that comprise the Soudan Iron Formation; and 3) volcaniclastic rocks that comprise the base of the Gafvert Lake Sequence. This study differentiates volcaniclastic rocks of the Gafvert Lake Sequence and does not include them as part of the Upper Sequence. The segregation of the Upper Sequence for this thesis is based on data gathered during field work (Phase 2), which better defines the physical and spatial

relationship between the Soudan Iron Formation and the Gafvert Lake Sequence. Therefore, rock sequences for this study are described below from oldest to youngest and are listed for reference in Table 2.01.

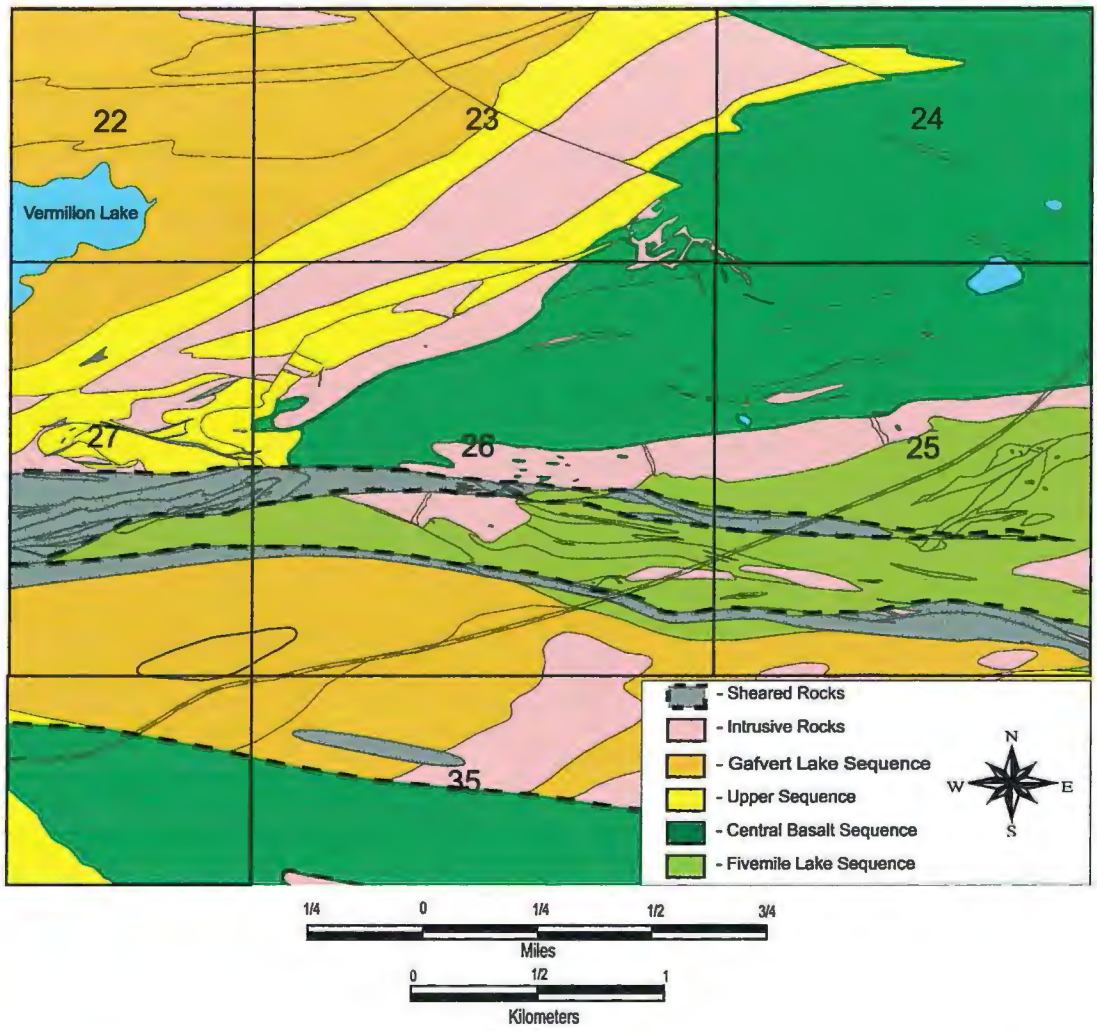

Figure 2.01. Location of major geologic sequences in the Soudan Mine area.

SUPRACRUSTAL SEQUENCES

FMxx – Fivemile Lake Sequence Rocks

CBxx – Central Basalt Sequence Rocks

USxx – Upper Sequence Rocks

GLxx – Gafvert Lake Sequence Rocks

Xy or XXXX – Intrusive Rocks

5x – Sheared Rocks

1 – MAFIC VOLCANIC ROCKS (Basalt and Andesite)

1a – Massive Lava Flows

1b – Pillowed Lava Flows

1c – In-situ and Resedimented Hyaloclastite

1e – Mafic Tuff Deposits

1h – Lapillistone Deposits

1i – Foliated Lava Flows

2 – FELSIC VOLCANIC ROCKS (Rhyolite and Rhyodacite-Dacite)

2a – Massive Lava Flows

2b – Lapillistone and Breccia Deposits

2c – Lapilli-Bearing Tuff Deposits

3 – CLASTIC SEDIMENTARY ROCKS

3a – Volcaniclastic Greywacke and Argillites

4 – CHEMICAL SEDIMENTARY ROCKS

4a – Oxide Facies Banded Iron Formation

5 – SHEARED ROCKS (Mineralogical Codes Below)

b – Sericite Schist

c – Ankerite Schist

e – Chlorite Schist

p – Pyrite Schist

INTRUSIVE ROCKS

Gb – Gabbro

Db – Diabase

QFSD – Quartz Feldspar Syeno-diorite

FPDD – Feldspar Porphyry Diorite

D – Diorite Porphyry

Table 2.01. Rock unit codes used in the Soudan Mine area (revised from Peterson and Patelke, 2003).

Fivemile Lake Sequence (FM)

The oldest volcanic strata in the Soudan Mine study area comprise the Fivemile Lake Sequence (Plate 1). The Fivemile Lake Sequence is a north-facing, steeply-dipping (75°-85°) bimodal succession (Barrie and Hannington, 1999) of subaqueous mafic to intermediate, pillowed to massive, calc-alkaline to tholeiitic rocks and felsic volcanic and volcaniclastic rocks. The type locality of this sequence is the thoroughly studied Fivemile Lake area (*see* Peterson and Jirsa 1999a; Hudak and Morton, 1999; Peterson, 2001; Hudak et al., 2002a; Hudak et al., 2002b). Due to the occurrence of highly vesiculated pillow basalts and andesites, multiple pillow rinds, and stringer epithermal-like zinc mineralization, Hudak et al. (2002b), Hudak et al. (2004) and Peterson (2001) have interpreted this volcanic succession to have erupted in a relatively shallow subaqueous environment. Rock types in the Fivemile Lake Sequence near Soudan, include mafic to intermediate pillowed and massive lavas, mafic tuff and lapillistone deposits, felsic lava flows and lapillistone and breccia deposits. Geographic Information Systems (GIS) analysis performed on the study area map indicates that Fivemile Lake Sequence volcanic and volcaniclastic rocks make up approximately 13% (by area) of volcanic strata in the Soudan Mine study area.

Mafic to Intermediate Volcanic Rocks in the Fivemile Lake Sequence

Four samples (LE-289, LE-295, LE-1507, LE-1512) in the Fivemile Lake Sequence were geochemically analyzed. The cores of pillowed and foliated lavas, and the matrix + lapilli fragments (unbiased sample) of lapillistone deposits were selected for analysis. Compositional classification using the relatively immobile trace elements Zr,

Nb and Y and the relatively immobile oxides P_2O_5 and TiO_2 (Winchester and Floyd, 1976; Winchester and Floyd, 1977; Barrett and Mclean, 1999), indicate that mafic to intermediate volcanic and volcaniclastic rocks in the Fivemile Lake Sequence vary from basalt to andesite in composition and have a calc-alkaline to tholeiitic affinity (Figures 2.02-2.05).

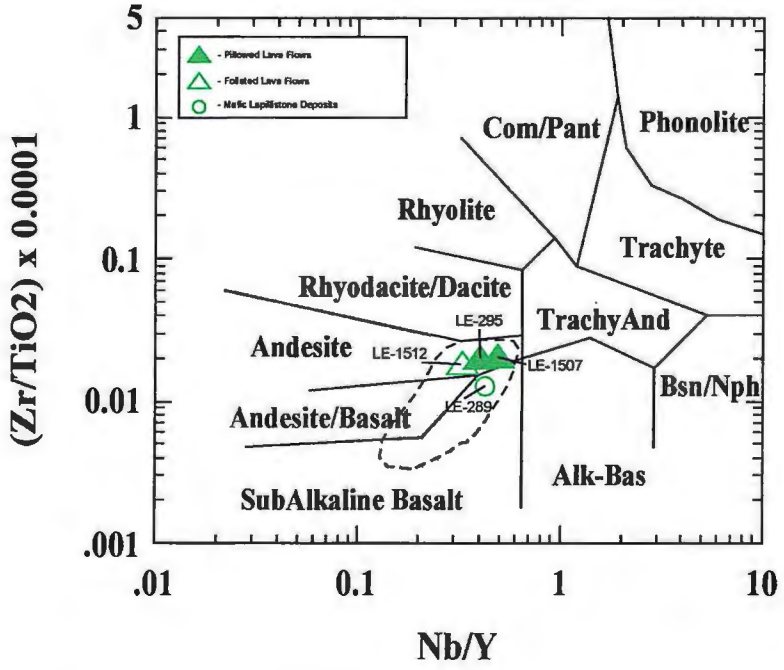

Figure 2.02. Immobile element classifications of mafic to intermediate volcanic rocks in the Fivemile Lake sequence by means of Zr, TiO_2, Nb, and Y concentrations (after Winchester and Floyd, 1977). Dashed line indicates the approximate field of compositions at Fivemile Lake (after Hudak et al., 2002b).

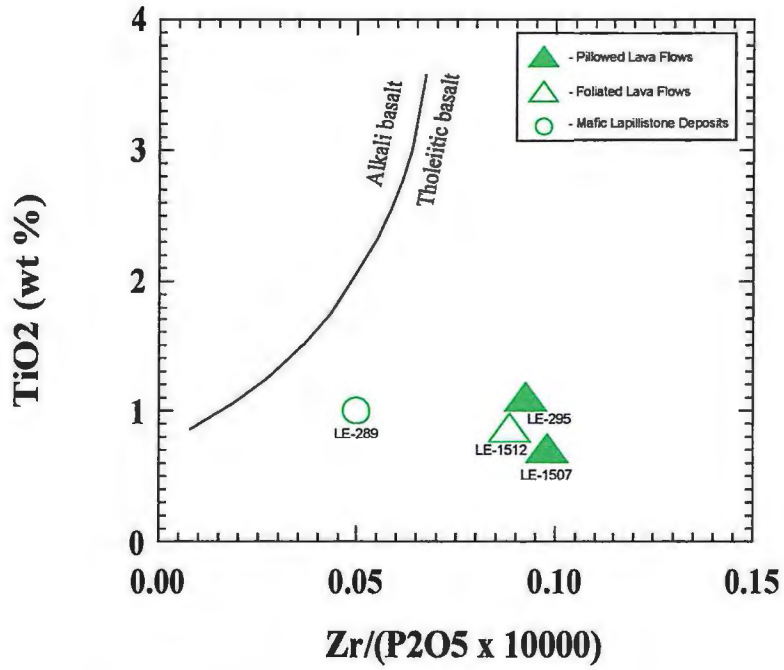

Figure 2.03. The TiO_2-Zr/(P_2O_5x10^4) diagram (after Winchester and Floyd 1976). Fivemile Lake mafic and intermediate volcanic and volcaniclastic rocks plot as tholeiitic basalts. Zr concentration in parts per million.

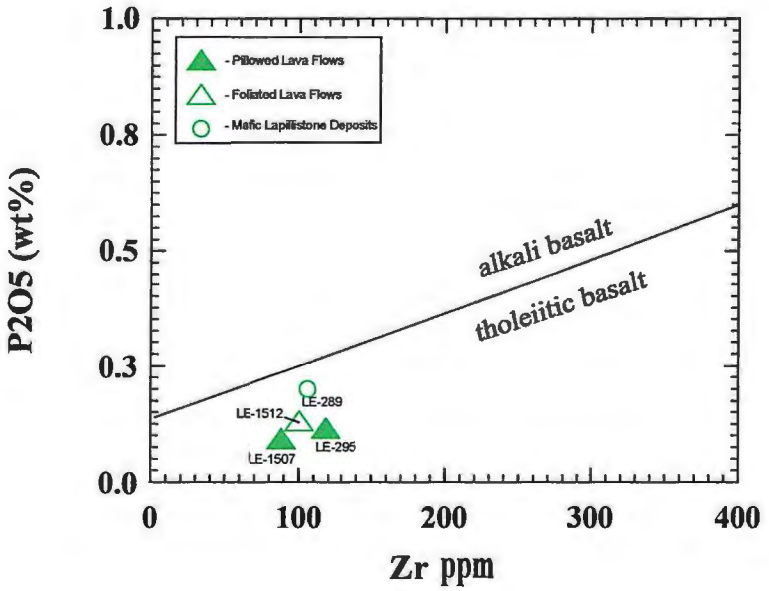

Figure 2.04. The P_2O_5-Zr discrimination diagram for Fivemile Lake Sequence mafic to intermediate volcanic and volcaniclastic rocks in the vicinity of the Soudan Mine (after Winchester and Floyd, 1976). Fivemile Lake lavas plot as tholeiitic basalts. Concentrations in parts per million.

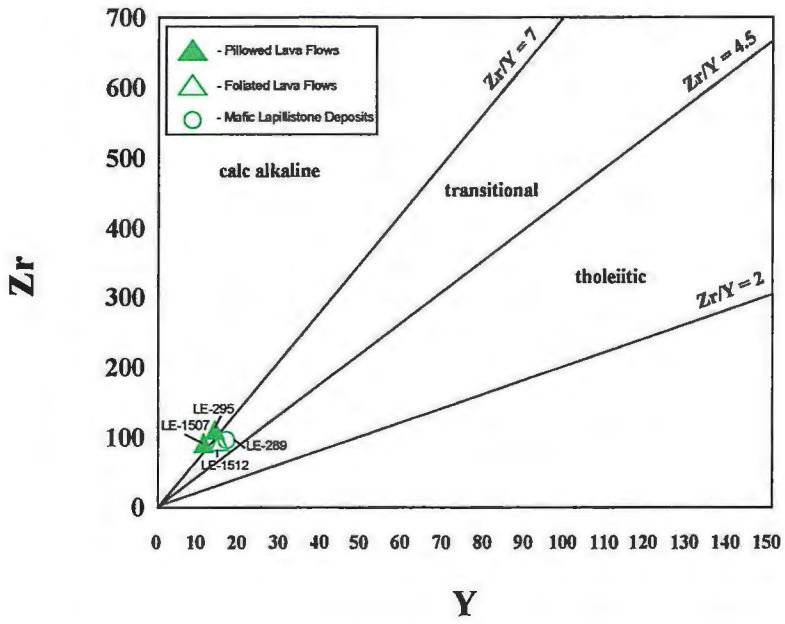

Figure 2.05. Immobile trace element plot of Zr vs. Y for Fivemile Lake Sequence mafic and intermediate rocks near the Soudan Mine (after Barrett and Mclean, 1999). Mafic and intermediate rocks plot as calc-alkaline to transitional basalts. Concentrations in parts per million.

The relative enrichment of light rare earth elements (LREE) is depicted on chondrite normalized and primitive mantle normalized rare earth element spider diagrams (Figures 2.06 and 2.07). LREE enrichment suggests that the rocks have a highly fractionated calc-alkaline trend and have geochemical signatures that are consistent with rocks that formed in an arc setting (e.g. negative Nb anomaly).

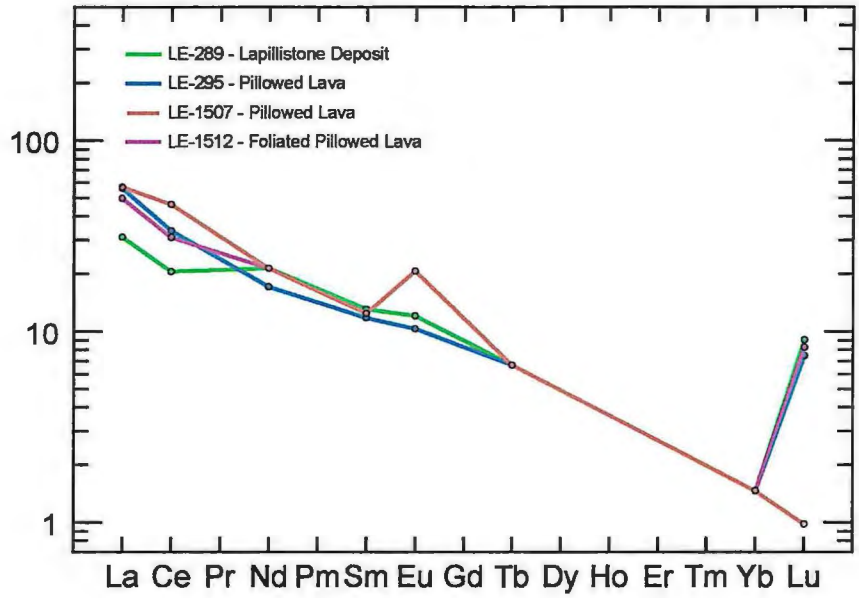

Figure 2.06. Chondrite normalized rare earth element spider diagram (after Sun and McDonough, 1989) for mafic volcanic and volcaniclastic rocks in the Fivemile Lake Sequence. Notice the enrichment of the LREE.

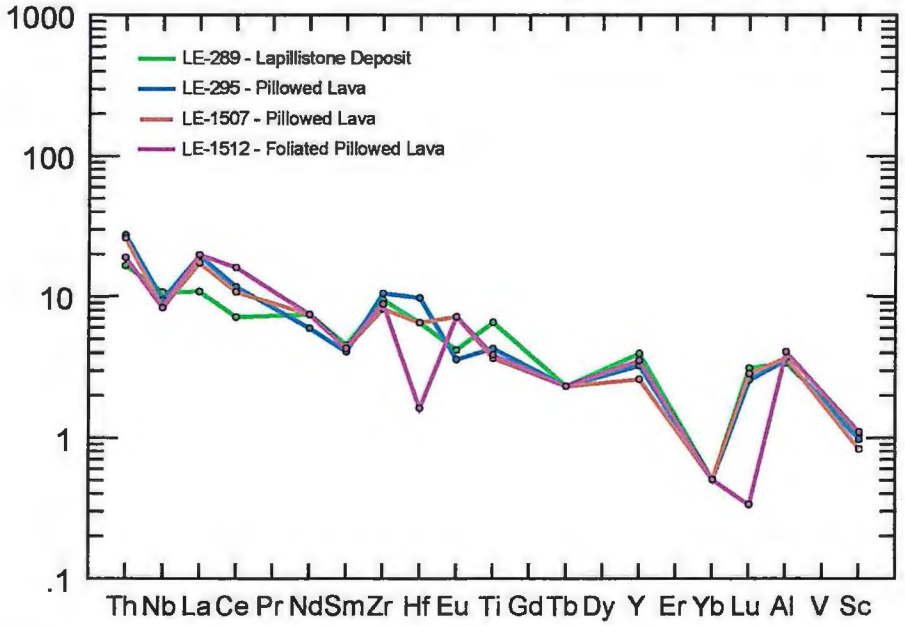

Figure 2.07. Primitive mantle normalized rare earth element spider diagram (after Sun and McDonough, 1989) for mafic volcanic and volcaniclastic rocks in the Fivemile Lake Sequence. Notice the enrichment of LREE and the negative Nb anomaly characteristic of a volcanic-arc environment.

Tectonic diagrams (Winchester and Floyd, 1976; Pearce and Gale, 1977) suggest that the rocks are similar in affinity to plate-margin, island-arc basalts (Figures 2.08-2.09). Plots using relatively immobile trace elements (Figures 2.10) developed by Pearce and Cann (1973), indicate that these volcanic rocks have a calc-alkaline volcanic-arc affinity.

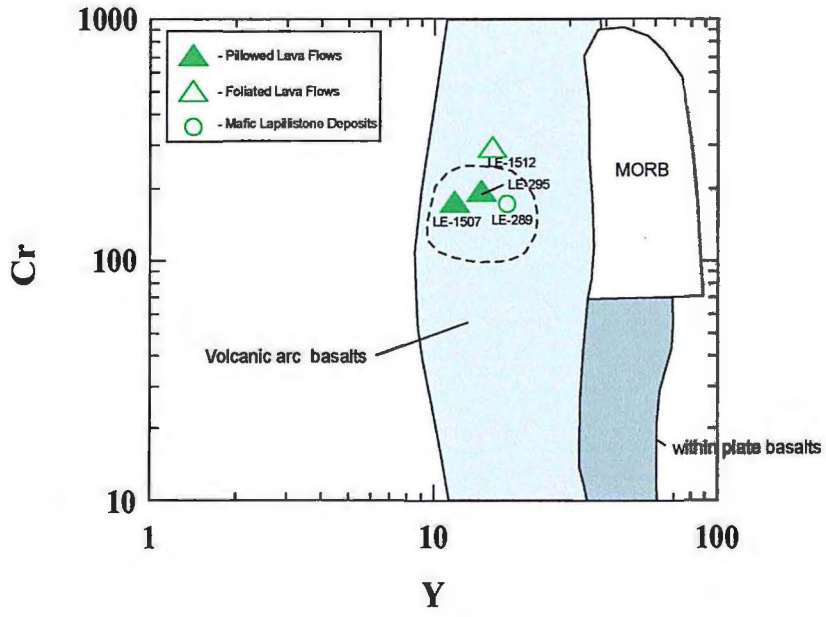

Figure 2.08. The Cr-Y discrimination diagram for Fivemile Lake Sequence mafic to intermediate lavas near the Soudan Mine (after Winchester and Floyd, 1976). Fivemile Lake mafic and intermediate lavas fall into the volcanic-arc field for basalts. Dashed line shows the approximate field for mafic and intermediate lavas at Fivemile Lake (after Hudak et al., 2002b). Concentrations in parts per million.

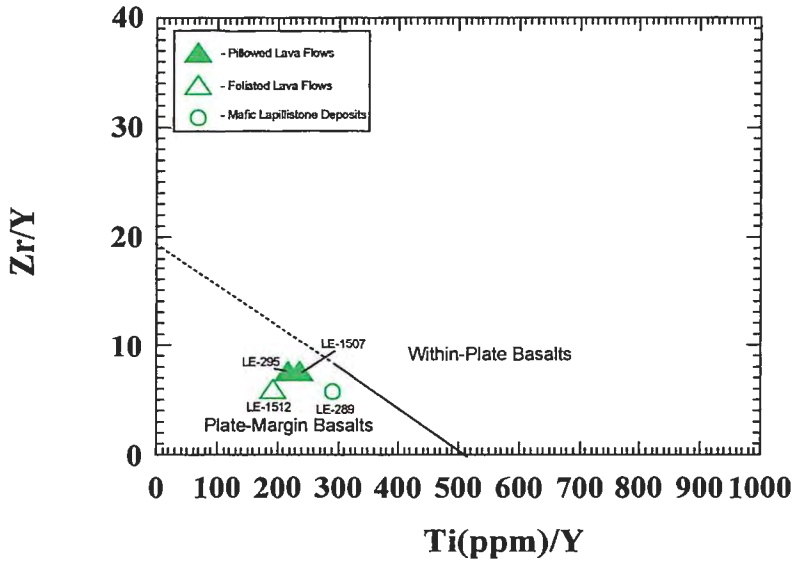

Figure 2.09. The Zr/Y vs. Ti (ppm)/Y plot (after Pearce and Gale, 1977) for Fivemile Lake Sequence mafic to intermediate lavas near the Soudan Mine. Fivemile Lake mafic to intermediate rocks consistently plot as plate-margin basalts.

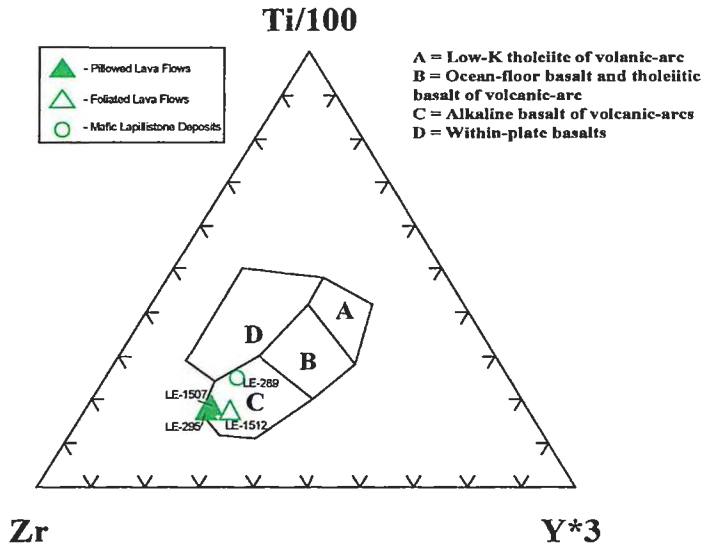

Figure 2.10. The Ti-Zr-Y discrimination diagram for Fivemile Lake Sequence mafic to intermediate lavas near the Soudan Mine. Fivemile Lake mafic to intermediate rocks classify as alkaline volcanic-arc basalts (after Pearce and Cann, 1973). Concentrations in parts per million.

Lithogeochemical data from the Soudan Mine area are relatively consistent with those from the Fivemile Lake area located 5 km to the east (Figure 2.02). These lithogeochemical similarities, as well as various physical similarities, suggest that volcanic rocks at Soudan are correlative with those near Fivemile Lake.

Massive Andesite (*unit FM1a*)

Near Soudan, massive andesite lavas in the Fivemile Lake Sequence occur in the southwest quarter of Section 25 (Plate 1). The upper contact between massive lava flows and pillowed lava flows was not observed in outcrop (OC-586); therefore the thickness of the massive lava flow unit was approximated and is estimated to be 8-10m thick. Massive lava flows display a sharp basal contact with a 0.1 m thick tuff unit (FM1e) (Figure 2.11). Approximate contacts with other adjacent units (e.g. FM1b, FM1h) were laterally approximated due to a lack of outcrop (Plate 1). Outcrops generally are rounded to elongated and form relatively flat to gentle topography.

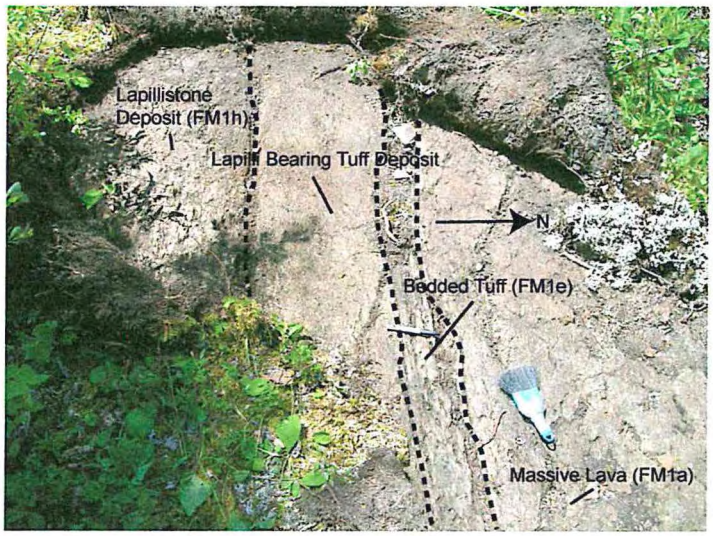

Figure 2.11. Contact relationship between massive lava (FM1a) and tuff deposit (FM1e). Upper contact of massive lava flows were not present in the field, therefore the thickness of this unit was approximated. Brush is 12 cm for scale. Outcrop 586.

In outcrop, massive lava flows appear green to green-gray in color and have an orange tint. Massive lava flows are fine-grained, aphyric to plagioclase-phyric and have a felty texture (Figure 2.11). Plagioclase is finely disseminated and appears to make up approximately 40-50 % of the rock. The groundmass is massive and mineral percentages were not estimated due to their fine-grained nature.

One sample was analyzed via petrographic analysis (LE-371). This sample is located to the east, and is out of the current study area for this thesis, but was included in the area mapped by Peterson and Patelke (2003). Petrographic analysis indicates that massive andesite lava flows in the Fivemile Lake Sequence contain approximately 90% groundmass and 10% phenocrysts. Groundmass consists of: 54% albite plagioclase microlites that are <<1mm, anhedral to subhedral, and appear to be recrystallized; 16% Mg-chlorite, that occurs as 1-1.5mm anhedral pod-like aggregates; 8% epidote that is <<1mm in diameter and occurs as well-dispersed anhedral aggregates; 8% quartz that occurs as <1mm anhedral groundmass; 3% sericite that occurs as <<1mm anhedral crystals, and also occurs in groundmass and commonly pseudomorphs plagioclase; and <1% actinolite that occurs as 1-1.5mm anhedral crystal aggregates which are rounded to curvilinear. Albite plagioclase phenocrysts (10%) occur as 1-2mm euhedral crystals. In thin section the rock has a felty texture.

The scarcity of massive andesite lavas in the Fivemile Lake Sequence may be due to an abundance of pillow-dominated volcanism on the seafloor. The transition from pillowed to massive flows, within a single flow or between flows, could reflect an increase in discharge rate or a rapid change in viscosity (Cas and Wright, 1987). These rocks are interpreted by the author to represent massive subaqueous sheet flows. Due to

lack of outcrop control, some massive lava may be interpreted as hypabyssal diabase sills or the basal portions of large pillowed flow units.

Pillowed Andesite (*unit FM1b*)

Pillowed lava flows in the Fivemile Lake Sequence occur in the southeast quarter-section of Section 26, and comprise the dominant lithology in the lower half of Section 25 (Plate 1). Near Soudan, the unit is 50-1000 meters thick and can be mapped along strike (80-110°) for approximately 2.2 kilometers, east to the project boundary (eastern edge of Section 25, Plate 1, limits of thesis mapping). Pillowed lava flows are in contact with intrusive rocks along the northern edge of the field area and are fault bounded by sheared rocks along the southern edge of the field area. Internally the pillowed lava flows are locally interlayered with thin units comprising felsic volcanic and volcaniclastic rocks, mafic volcaniclastic rocks, sheared rocks, foliated pillowed lavas, and dike- and stock-like intrusions of mafic and intermediate composition (Plate 1). All contacts between pillowed lava flows and adjacent units are sharp. All other contact relationships that are not reflected in outcrop (Plate 1) were not observed and are therefore approximated. Outcrops are generally flat, vary in size and shape, and form relatively shallow slopes and mounds throughout the sequence.

In outcrop, pillows in the Fivemile Lake Sequence are mainly amoeboid- or mattress-shaped, but oval- or lens-shaped pillows are common (Figure 2.12). Pillow size ranges from 50-150 cm along strike (horizontal) and are approximately 30-75 cm thick (vertical). Least altered pillowed lavas are light blue to green and are aphyric to plagioclase-phyric. In general, pillowed basalt and andesite comprises 30% 1-2 mm

subhedral to euhedral randomly oriented albite plagioclase microlites, and 70% < 1 mm aphyric groundmass. Plagioclase microlites give the rock a felty texture. Due to the fine-grained nature of the groundmass, modal percentages were difficult to estimate in the field. In general, individual pillows are surrounded by 2-25 cm zones of interpillow hyaloclastite (Figure 2.12). Interpillow hyaloclastite contains approximately 30-50% 1-10 mm light gray to blue-gray, matrix-supported, angular to subangular revitrified glass shards composed of chlorite, epidote, and actinolite and up to 50% <1 mm matrix, consisting of variable amounts of epidote, chlorite, actinolite, sericite, and carbonate. Locally 1-2% <1-1mm euhedral-subhedral finely disseminated pyrite is present.

Figure 2.12. Typical appearance of pillowed lavas in the Fivemile Lake Sequence. Notice dark zones of interpillow hyaloclastite and weathered amygdules. Hammer is 30 cm for scale. Outcrop 037.

The matrix within the interpillow hyaloclastite is typically dark blue-gray and aphyric so accurate modal percentages for individual minerals were difficult to estimate. Pillow cores contain 20-40% 1-6 mm well-rounded, well-dispersed weathered quartz amygdules. Pillow margins contain 5-35% 1-15 mm well-rounded weathered quartz amygdules.

Flow direction in pillowed sequences can be approximated by evaluating budding directions (Hargraves and Ayers, 1979; Gibson, 1989; Gibson et al., 1999). At Soudan, a lack of observed pillow buds precludes accurate determination of flow direction. In contrast, pillows at Fivemile Lake have a consistent budding direction that indicates flow propagation from west to east (Hudak et al., 2002b). Lavas at Soudan may be either derived from a different vent source than the lavas at Fivemile Lake, or flow propagation is more or less parallel to the dip direction.

Petrographic analysis on six samples (LE-188, LE-295, LE-297, LE-299, LE-371, LE-1004) indicates that pillowed lavas in the Fivemile Lake Sequence contain 0-60% phenocrysts, 40-100% groundmass and 0-15% amygdules. Phenocrysts comprise 1-25% 1-2 mm anhedral-euhedral well-dispersed albite plagioclase crystals, 0-5% 1-2 mm well-dispersed anhedral to subhedral orthoclase crystals, and 0-1% 1-2mm well-dispersed anhedral to subhedral Fe-carbonate crystals. Primary groundmass includes up to 50% <1-1mm well-dispersed anhedral to subhedral felty albite microlites (Figure 2.13). Secondary groundmass includes 15-40% <1mm epidote which occurs both as euhedral crystals and well-dispersed semi-opaque spherical aggregates; 1-20% <<1mm anhedral to subhedral well-dispersed actinolite lathes; 10-16% <1mm well-dispersed anhedral to subhedral Mg-chlorite aggregates; 8-50% <1mm anhedral finely disseminated recrystallized quartz crystals; 8% <1mm anhedral Fe-chlorite, which occurs as platy

aggregates and as interstitial groundmass; 3-10% <1mm anhedral to subhedral sericite, that commonly pseudomorphs plagioclase; 2% <1-1mm subhedral disseminated opaque minerals; <1% <<1mm anhedral localized limonite; and <1% <1 mm anhedral localized stilpnomelane. 1-8 mm spherical to semi-deformed well-dispersed amygdules (15%) typically have a zoned texture. The amygdule center comprises subhedral epidote and the amygdule rim comprises fine-grained recrystallized quartz. The location and distribution of secondary minerals is highly variable and will be discussed further in Chapter 3.

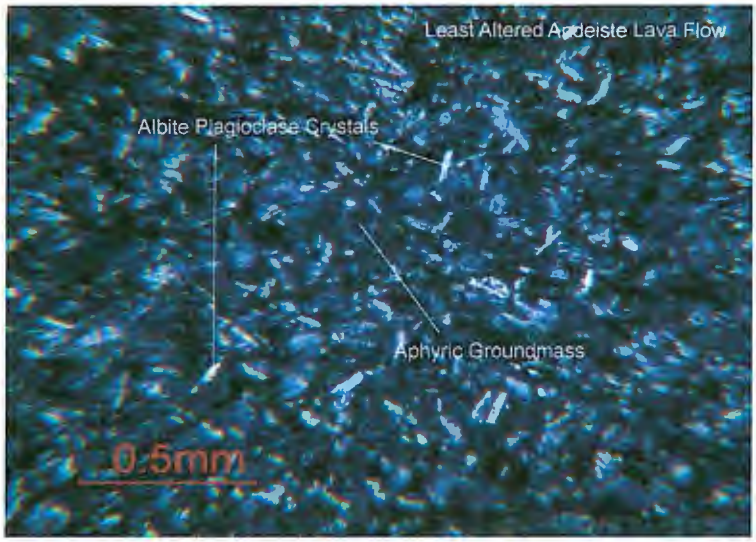

Figure 2.13. Photomicrograph of pillowed andesite lava from the Fivemile Lake Sequence. This sample has approximately 56% subhedral albite plagioclase crystals and 44% fine-grained groundmass composed of 16% Mg-chlorite, 8% epidote, 8% quartz, 3% sericite and <1% actinolite. Field of view 2.5 mm. Cross-polarized light. LE-371.

Foliated Andesite (*unit FM1i*)

Foliated andesite lavas are located mainly in the southeast and southwest quarter-sections of Section 25, southeast and southwest quarter-sections of Section 26, and the southeast quarter-section of Section 27. Well-foliated units are located adjacent to the

Murray and Mine Trend shear zones (Plate 1). Foliated lavas range in thickness from 8-190 m. Sharp contacts between non-foliated pillow lavas and foliated lavas were observed in the field. Along these contacts, pillow features (pillow selveges, pillow cores and interpillow hyaloclastite) are highly attenuated. Contacts between foliated lavas and all other adjacent units (Plate 1) were not observed, and are therefore approximated. Outcrop appearance is similar to non-foliated pillowed lavas and form shallow sloping mounds.

In outcrop, foliated andesite lavas are transitional between pillow andesite lavas (unit FM1b) and chlorite schist (unit 5e). Due to a lack of complete shear deformation, foliated lavas are classified as a separate map unit. Foliated lavas are green to green-blue and dominantly aphyric, so modal percentages are difficult to estimate. Foliation within pillows and along pillow margins consistently trends at 80-110° and is defined by parallel alignment of fine-grained (<1 mm) chlorite that forms 1-4 mm well-dispersed sub-rounded crystal aggregates. Weathered amygdules (15-35%, 1-6 mm) are flattened and elongated parallel to the regional foliation. Pillow selvages and interpillow hyaloclastite do not retain their primary textures and appear to be altered to a light blue to purple, very fine-grained recrystallized chlorite + quartz (Figure 2.14).

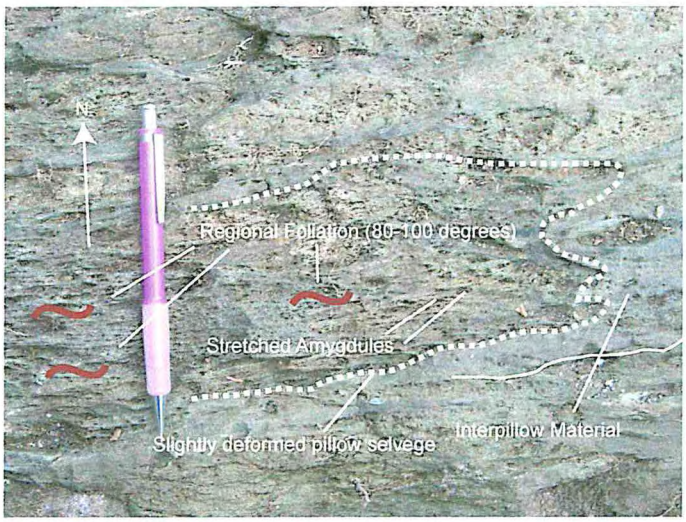

Figure 2.14. Regional D_2 foliation (80-100°) overprinting primary pillow textures in foliated Fivemile Lake Sequence pillowed lava flow. Pencil is 11 cm for scale. Outcrop 544.

Petrographic analysis on two samples (LE-212, LE-1500) indicates that foliated lavas are aphyric, and contain approximately 30% deformed amygdules. All minerals present within this unit appear to be secondary. Groundmass consists of 40% <<1 mm anhedral well-dispersed fine-grained recrystallized quartz, 25% <<1 mm anhedral imbricated platy Fe-chlorite crystals, 20% <<1-1 mm well-dispersed subhedral-euhedral albite plagioclase microlites, 5-18% <<1-1.5 mm subhedral Fe-carbonate blebs, which also occurs in 4-5 mm veinlets, 12% <1 mm anhedral imbricated platy sericite crystals, 10% <1-1.5 mm subhedral disseminated sub-cubic opaque minerals, 2% <1 mm, well-dispersed anhedral platy biotite crystals, 2% <<1 mm subhedral zoisite crystals, 1% <1 mm anhedral semi-opaque spherical aggregates, and 20-30% 1-1.5 mm diameter deformed quartz + carbonate amygdules. The rock has a foliated and felty texture and comprises a mineral assemblage dominantly composed of quartz + chlorite.

Foliated lava flows in the Fivemile Lake Sequence near the Soudan Mine are strongly foliated (80-110°) and altered to a variable quartz + chlorite mineral assemblage. The more or less east-west trending foliation that is present is consistent with their genesis during the regional D_2 deformation event.

Andesite Tuff (*unit FM1e*)

One occurrence of andesite tuff is located in the southwest quarter of Section 25 (Plate 1, Figure 2.11). The true thickness of this unit is approximately 0.1m. Andesite tuff is bounded up-section by massive andesite lava flows and shows a gradational contact with lapilli-bearing tuff into lapillistone (FM1h) down-section (Figure 2.11). The contacts between the two adjacent units are sharp and strike at approximately 270° and dip 82° north. The lateral continuity of this deposit is restricted to outcrop exposure, therefore the contact relationships between adjacent units beyond the extents of exposure (OC-586) are approximated.

In outcrop, andesite tuff is dark green-black with an orange hue, and comprises well-sorted mud sized (<0.0625 mm) recrystallized grains that are laminated to very thinly bedded and have no visible grading. Andesite tuff is comprised of approximately 85% mud sized grains and 10-15% 1-2 mm subhedral well disseminated pyrite. Due to the fine-grain size, modal percentages were difficult to estimate without petrographic analysis, which was not conducted for this unit. Lithogeochemical analysis was not conducted for this unit.

The deposit is interpreted to be the metamorphosed equivalent of reworked very fine-grained hyaloclastite or mud-grade tuff. The contact relationships between the adjacent units suggest that the mafic tuff deposit formed conformably.

Basaltic Lapillistone Deposits (*unit FM1h*)

Two distinct locations of basaltic lapillistone occur in the Fivemile Lake Sequence. They are dominantly located in the central portion of Section 25 and form a thin 8 m thick deposit in the southwest quarter-section of Section 25 (Plate 1). More prolific mafic lapillistone deposits are 50-130 m thick and can be mapped along strike for 180-350 meters. Adjacent units include pillowed lava flows (FM1b), felsic lava flows (FM2a), andesite tuff (FM1e), felsic lapilli-bearing tuff (FM2c), and cross-cutting dikes of intermediate composition (FPDD). The contacts between adjacent units are sharp and strike at approximately 75-90° and dip at 85° to the north. In general, contacts cannot be mapped continuously along strike so unit thickness was approximated. Outcrops are rounded to slightly elongated and form either relatively flat or gently sloping terrain.

In outcrop, basaltic lapillistone deposits are dark blue-green in color; dominantly matrix supported and locally clast supported. Basaltic lapillistone deposits are thickly to very thickly bedded (30->100 cm), poorly sorted and poorly graded (Figure 2.15).

Figure 2.15. Thickly to very thickly bedded lapillistone deposits in the Fivemile Lake Sequence. Notice weathered scoria lapilli. Hammer head is 15 cm wide for scale. OC-501.

Basaltic lapillistone deposits have approximately 65% scoria lapilli to block-sized fragments that are set in a recrystallized fine-medium ash (35%). Individual lapilli and block fragments are aphyric so modal percentages were difficult to estimate in the field. Fine- to medium-recrystallized ash is dark blue-green and shows no grading or bedding. Commonly, lapilli- and block-sized fragments appear to be strongly weathered and show negative relief. Scoria clast size is highly variable and generally comprises 50% fine-medium, rounded to subrounded lapilli, 45% coarse, rounded to subrounded lapilli and 5% rounded to subangular block-sized fragments that are locally up to 155 mm. In general, lapilli- and block-sized fragments contain approximately 15-40% quartz + chlorite filled amygdules which are locally weathered out. Outcrops commonly exhibit a strong regional east-west trending D_2 foliation.

Petrographic analysis on one sample (LE-496) indicates that mafic lapillistone deposits are highly altered. They are comprised of approximately 40% <1mm well-dispersed anhedral sericite, 35% <1mm anhedral well-dispersed quartz, 15% <1mm anhedral crystal spherical aggregates of epidote, 6% 1mm anhedral limonite that locally occur in 1-2 mm curvilinear foliation planes, 2% <1 mm anhedral well-dispersed Fe-carbonate, 2% <1 mm well-dispersed subhedral play chlorite crystals and 15% 1-3mm zoned quartz + chlorite filled amygdules. The amygdules are zoned in such a way that quartz lines the exterior and chlorite fills the center of the amygdules.

Lapillistone deposits in the Fivemile Lake Sequence near Soudan are laterally restricted. They comprise matrix- to clast-supported rounded to subrounded fine-lapilli to block-sized clasts that are thickly- to very thickly bedded, poorly sorted, ungraded, and have 15-40 % weathered quartz + chlorite amygdules. It is difficult to determine the origin of these deposits. Modern and ancient scoria cones are laterally restricted, have steep angles of repose (33°), are reversely graded and commonly contain cow dung and spindle bombs (Cas and Wright, 1987). Alternatively, scoria flow deposits are compositionally homogeneous, internally massive and may contain accretionary lapilli (Cas and Wright, 1987). It is evident that lapillistone deposits in the Fivemile Lake sequence do not directly fit the criteria of scoria cones and/or scoria flow deposits. However, according to Cas and Wright (1987) scoria cones and scoria flow deposits are highly susceptible to weathering and erosion, which may alter their morphology and inhibit the ability for proper identification. Therefore, it is reasonable to assume that mafic lapillistone deposits in the Fivemile Lake Sequence may be the weathered or resedimented equivalent of scoria derived from a scoria cone or scoria flow deposit.

Felsic Volcanic and Volcaniclastic Rocks in the Fivemile Lake Sequence

Felsic volcanic and volcaniclastic rocks occur in the southeastern portion of the field area in the central portion of Section 25 (Plate 1). Three distinct lithologies occur: 1) rhyodacite-dacite lava flows (*unit FM2a*); 2) coarse lapillistone and breccia deposits (*unit FM2b*), and; 3) lapilli-bearing tuff deposits (*unit FM2c*).

Two samples (LE-288, LE-500) from the massive facies of unit FM2a were lithogeochemically analyzed (Plate 1). Compositional classification for felsic rocks was determined using relatively immobile trace element and oxide ratios (Zr, TiO_2, Nb, Y, Rb) (Winchester and Floyd, 1977), and indicates that felsic lava flows in the Fivemile Lake Sequence are rhyodacite-dacite in composition (Figure 2.16).

Pearce et al.'s (1984) method for classifying granites is used for felsic volcanic rocks. Granitic rocks represent intrusive equivalents of felsic volcanic rocks; therefore this classification scheme should reasonably assess the tectonic environment in which the felsic extrusive rocks were formed. Felsic volcanic rocks in the Soudan area have lithogeochemical characteristics of granites that formed in a syn-collisonal volcanic-arc setting (Figures 2.17 and 2.18).

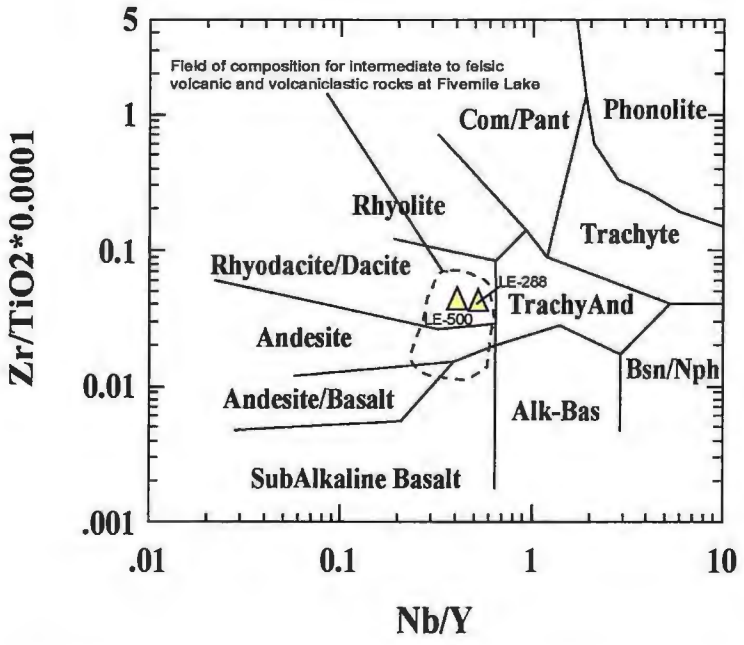

Figure 2.16. Immobile element classification for felsic volcanic rocks in the Fivemile Lake Sequence near the Soudan Mine (after Winchester and Floyd, 1977).

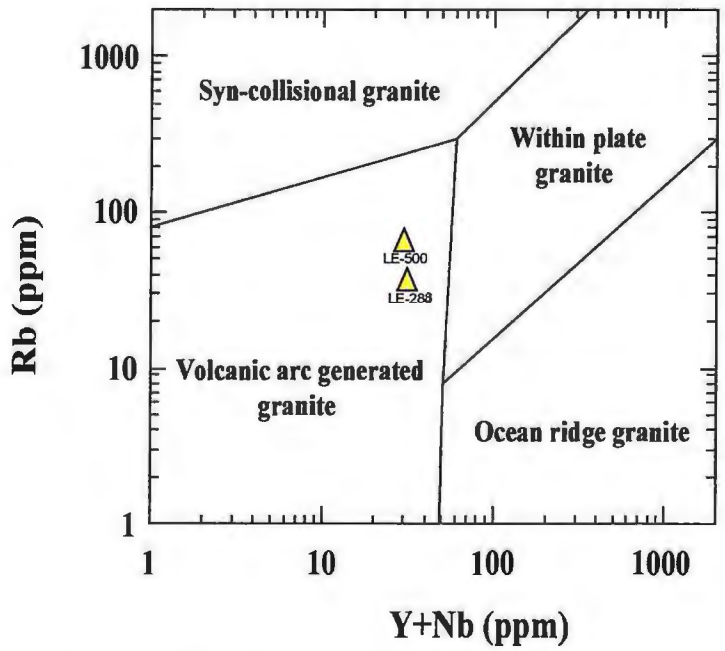

Figure 2.17. The Rb- (Y + Nb) discrimination diagram for granites (after Pearce et al., 1984). Fivemile Lake Sequence felsic volcanic rocks near the Soudan Mine plot as volcanic-arc generated granites.

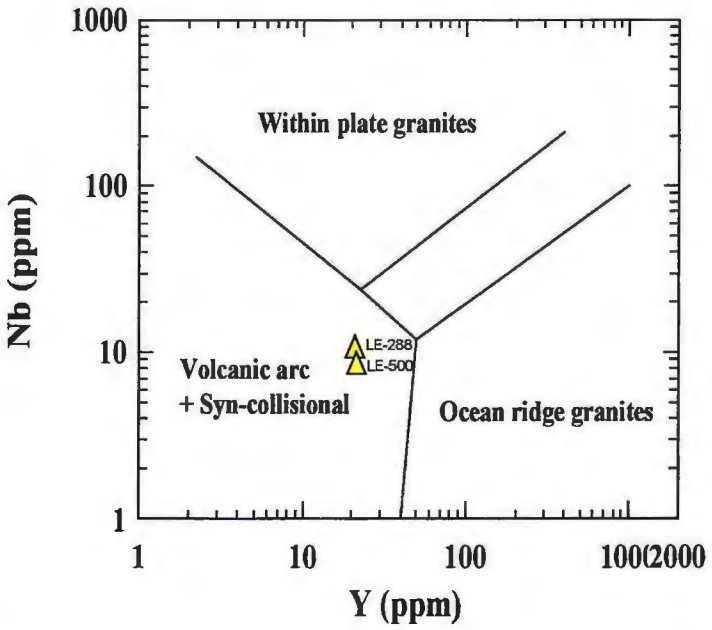

Figure 2.18. The Nb-Y discrimination diagram for granites (after Pearce et al., 1984). Fivemile Lake Sequence felsic volcanic rocks near the Soudan Mine plot as volcanic-arc/syn-collisional granites.

The relative enrichment of light rare earth elements (LREE) in unit FM2a is depicted by chondrite normalized and primitive mantle normalized rare earth element spider diagrams (Figures 2.19 and 2.20). LREE enrichment suggests that rhyodacite-dacite lava flows have a highly fractionated calc-alkaline trend and have geochemical signatures that are consistent with rocks that formed in an arc setting (e.g. negative Nb anomaly, La_n/Lu_n = 9.8-14.5). Notice that the LREE's (which are more incompatible) are enriched relative to LREE's in andesite from the Fivemile Lake Sequence (Figure 2.06 and 2.07). According to Rollinson (1993), LREE enrichment is typically more abundant in felsic rocks when compared to mafic rocks, because felsic melts typically undergo more fractionation or enrichment in incompatible (LREE) elements during their genesis.

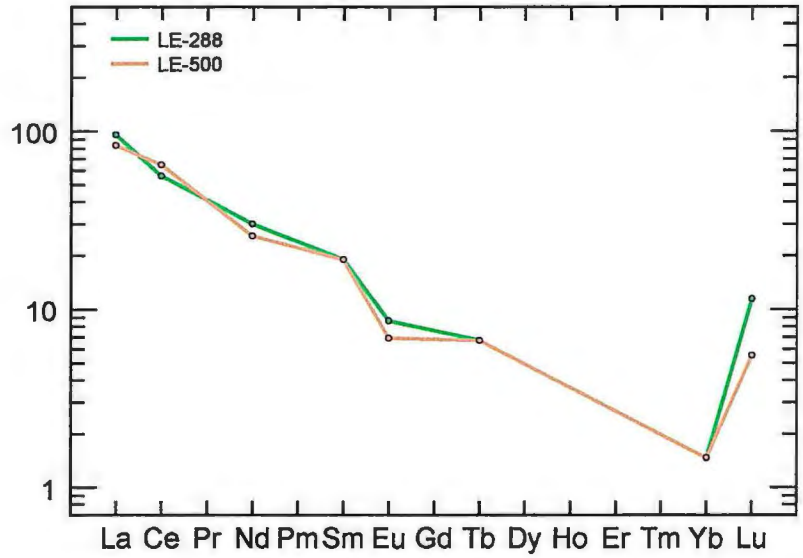

Figure 2.19. Rock vs. chondrite rare earth element spider diagram (after Sun and McDonough, 1989) for rhyodacite-dacite lava flows in the Fivemile Lake Sequence. Notice the enrichment of the LREE.

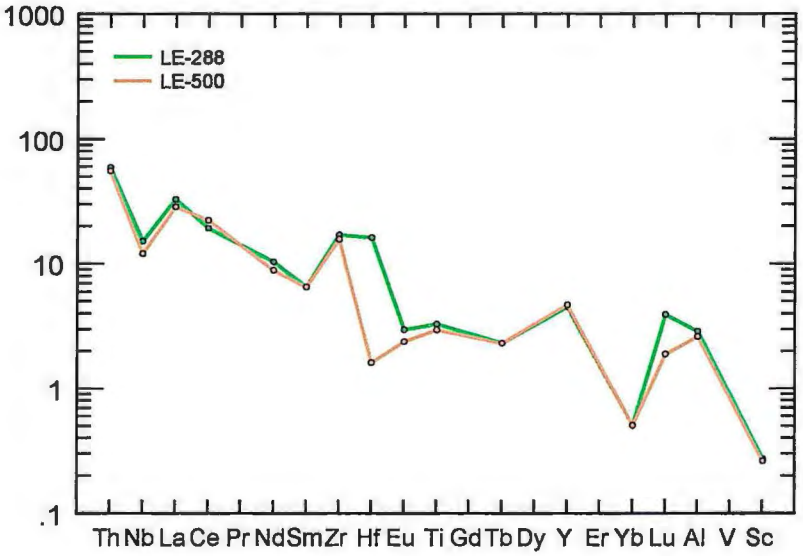

Figure 2.20. Rock vs. primitive mantle rare earth element spider diagram (after Sun and McDonough, 1989) for rhyodacite-dacite lava flows in the Fivemile Lake Sequence. Notice the enrichment of LREE and the negative Nb anomaly typically associated with a volcanic-arc related environment.

High field strength elements (HFSE) and rare earth elements (REE) have been used by numerous geoscientists (Lesher et al., 1986; Barrie et al., 1993; Barrie and Hannington, 1997; Lentz,1998; Hart et al., 2004) in order to evaluate the prospectivity of various felsic volcanic rocks for hosting VMS deposits (Hudak et al., 2004b). Lesher et al. (1986) distinguished four types of felsic volcanic groups based on rock type, the normalized ratio of La/Yb (La/Yb_n), Eu anomalies, the ratio of Zr/Y, the abundance of high field strength elements and the Sr contents of the rocks (Table 2.02). Lesher et al. (1986) found that Archean VMS deposits are typically associated with tholeiitic felsic rocks containing intermediate to high contents of HFSE and REE, low La/Yb_n, and low Zr/Y ratios. These felsic rocks are known as FIIIa- and FIIIb-type volcanic rocks. Hart et al. (2004) suggests that the geochemical attributes that define FI-, FII- and FIII-type volcanic rocks are dependant on the depth of formation, degrees of partial melting of mafic sources, composition of the source region, pressure and temperature of melting, and to a lesser extent, fractionation processes.

	FI	FII	FIIIa	FIIIb
Lithology	Dacite-rhyolite	Dacite-rhyolite	Rhyodacite-high silica rhyolite	Rhyodacite-high silica rhyolite
La/Yb_n	5.8-34	1.7-8.8	1.5-3.5	1.1-4.9
Eu/Eu*	0.87-1.5	0.35-0.91	0.37-0.94	0.2-0.6
Zr/Y	8.8-31	3.2-12.12	3.9-7.7	1.7-6.2
HFSE	Low	Medium	Medium	High
Sr	High	Medium	Medium	Low
Sc	-	-	High	Low
Ore Potential	Barren	VMS Occasionally	High	High
VMS Deposit Example	None	Sturgeon Lake/Kuroko	Noranda	Crandon
Eu° calculated by linear interpolation between chondrite-normalized Sm and Tb				

Table 2.02. Lithogeochemical classification scheme for felsic volcanic rocks and their susceptibility for hosting massive sulfide deposits (after Lesher et al., 1986; Hart et al., 2004).

Analysis of felsic volcanic rocks in the Fivemile Lake area indicates that these rocks are FII-type (Figure 2.21). Felsic volcanic rocks with FII affinities (e.g. Sturgeon Lake Caldera Complex VMS) may occasionally host massive sulfide deposits (Lesher et al., 1986). The geochemical methodology of Lesher et al. (1986) and Hart et al. (2004) should be used as an exploration tool, and not as a single means to define the potential for VMS deposits. Therefore, the classification of F-II type granites in the Fivemile Lake Sequence does not suggest that this volcanic terrain unequivocally hosts VMS.

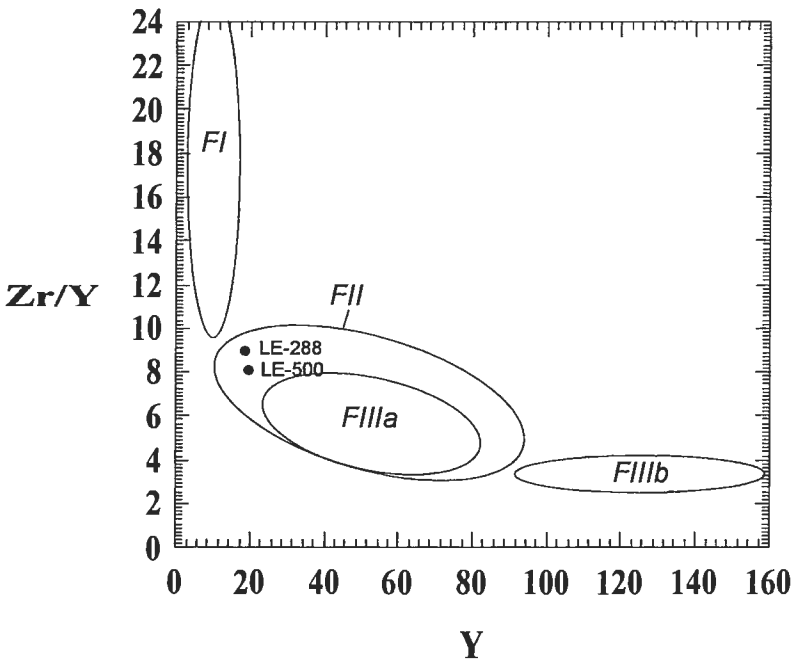

Figure 2.21. Zr/Y vs. Y diagram for Fivemile Lake rhyodacite-dacite lava flows near the Soudan Mine (after Piercey et al., 2001). Felsic rocks plot as FII-type rhyolites (Lesher et al., 1986; Hart et al., 2004). Concentrations in parts per million.

Rhyodacite-Dacite (*unit FM2a*)

Rhyodacite-dacite lava flows occur in the southeast quarter-section of Section 25. Two semi-parallel lava flows are each approximately 10-50 meters thick. Rhyodacite-

dacite lava flows can be mapped along strike (255°) for approximately 400-550 meters. Adjacent units include pillowed andesite (FM1b), basaltic lapillistone deposits (FM1h), and lapillistone and breccia deposits (FM2b), and foliated basalt and andesite (FM1i) by means of faulting. Contacts between adjacent units were not mapped in the field and are therefore approximated. Outcrops are generally sub-rounded to elongated and form relatively flat terrain. According to Peterson et al. (2001), quartz-phyric lavas near Fivemile Lake have a $^{207}Pb/^{206}Pb$ age of approximately 2722.6 ± 0.9 Ma.

In outcrop, rhyodacite-dacite lava flows are massive, green-gray-tan in color and are aphyric to quartz-plagioclase phyric. Groundmass comprises 90-95% of the rock and phenocrysts comprise 5-10%. Due to the fine-grained nature of the groundmass it is difficult to estimate modal percentages in outcrop; however secondary minerals form 1-200 mm blue-gray patchy aggregates of chlorite and sericite that is easily distinguishable from the more ubiquitous groundmass. Phenocrysts comprise 1-3 mm subhedral well-dispersed plagioclase crystals. A distinct fabric is present in outcrop that trends at 265° and is defined by the parallel alignment of chlorite that forms 1-3 mm rounded crystal aggregates. Easily distinguishable curvilinear cooling cracks and a high concentration of cross-stratal 1-3 mm quartz veinlets are also common and give the rocks a fragmental appearance (Figure 2.22). Brittle deformation along with cooling cracks and subtle flow-banding suggests that these lavas were once highly viscous (Figure 2.23).

Rhyodacite-dacite lava flows locally contain <10% medium lapilli- to block-sized (6-70 mm) angular to sub-rounded felsic accessory fragments. Felsic accessory

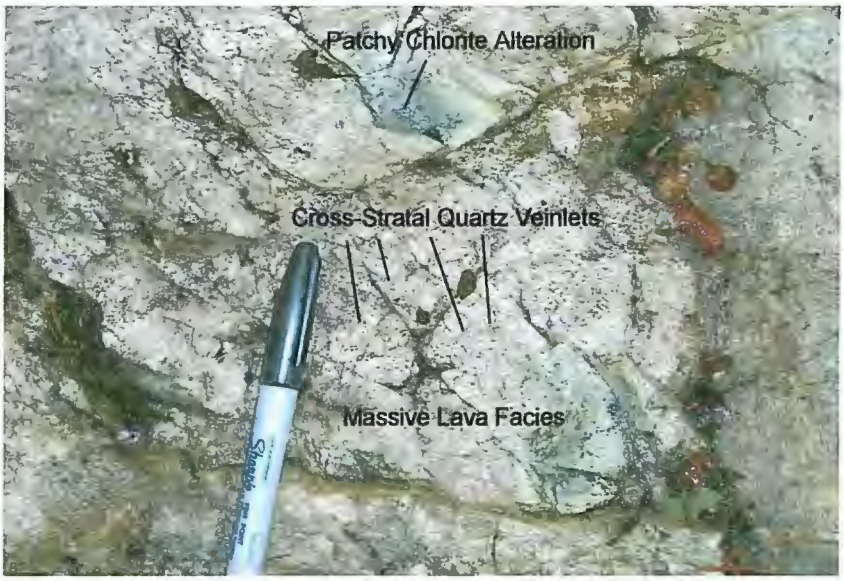

Figure 2.22. Fivemile Lake Sequence massive green-gray to light tan rhyodacite-dacite lava facies in the Soudan Mine area (unit FM2a). Notice the high concentration of cross-stratal quartz veinlets that gives rock a fragmental appearance. Blue to green patchy chlorite alteration is also common. Pen is 14 cm for scale. Outcrop 273.

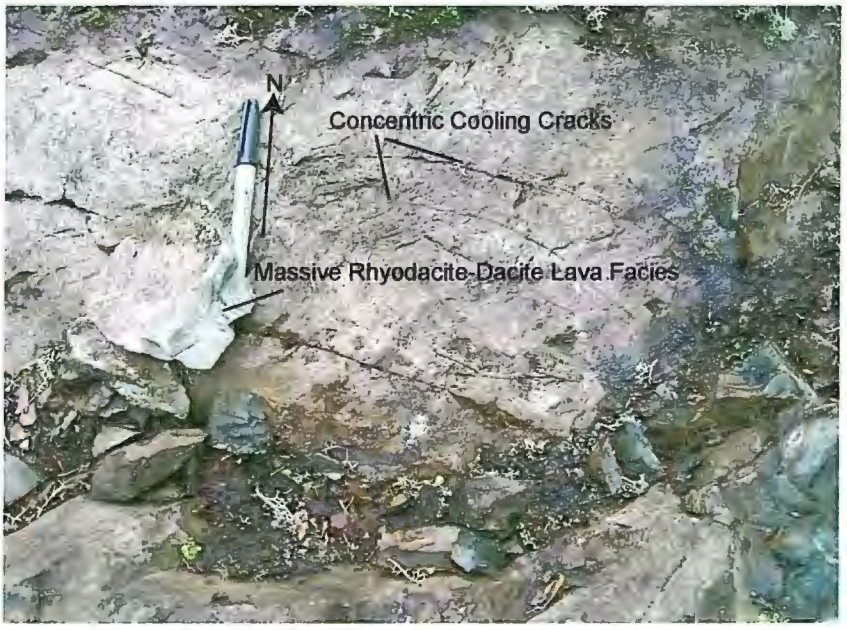

Figure 2.23. Fivemile Lake Sequence massive green-gray to light tan rhyodacite-dacite lava facies in the Soudan Mine area (unit FM2a). Notice concentric cooling cracks. Pen is 14 cm for scale. Outcrop 276.

fragments occur as three distinct lithologies: 1) 6% 5-25 mm diameter subangular to slightly elongated lava which is similar in appearance to the massive lava facies; 2) 2% 5-70 mm subrounded aphyric pumice that contains 20-30% 1-3 mm quartz and carbonate amygdules; and 3) 2% 5-25 mm diameter subangular to elongate chert fragments. Larger block sized accessory fragments appear to be contained with subtle anastomozing flow-banding.

Petrographic analysis on two samples (LE-288, LE-362) indicates that rhyodacite-dacite lava flows are comprised of 92% aphyric groundmass and 8% phenocrysts (Figure 2.24). Primary groundmass includes 20-75% <1-1mm anhedral quartz that occurs interstitially and 5% <1 mm subhedral-euhedral well-dispersed orthoclase crystals. Secondary groundmass consists of 20% < 1mm subhedral well-dispersed tabular Mg-chlorite, 5-12% < 1mm anhedral cross-cutting sericite stringers, 5-10% <<1mm anhedral to subhedral epidote that occurs as well-dispersed spherical aggregates, <1-3% <<1mm anhedral to subhedral Fe-carbonate that occurs as well-dispersed elongated crystal masses, 2% <1mm disseminated sub-cubic pyrite crystals, <1% <1mm anhedral well-dispersed biotite crystals, 5% slightly deformed 1-3 mm subhedral chlorite amygdules and 1% 1-3mm subhedral Fe-carbonate amygdules. Rhyodacite-dacite lava flows have a silicified and felty texture.

Rhyodacite-dacite lava flows in the Fivemile Lake Sequence are generally massive lavas with local occurrences of medium lapilli- to block-sized accessory fragments. Curvilinear cooling cracks and a high concentration of cross-stratal 1-3 mm quartz veinlets are also common and give the rocks a fragmental appearance. Slight deformation of amygdules along with cooling cracks and subtle anastomozing flow-

banding around accessory fragments suggests that these rocks resulted from highly viscous flows.

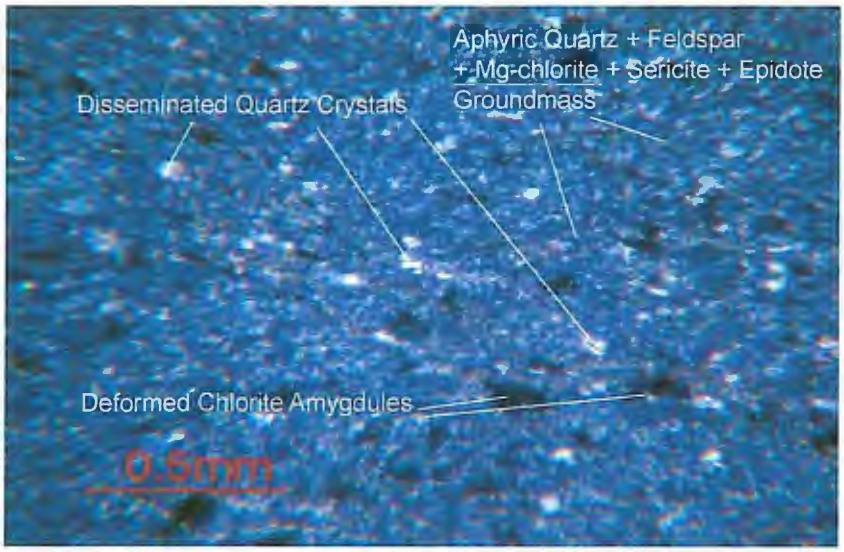

Figure 2.24. Photomicrograph of Fivemile Lake Sequence rhyodacite-dacite lava flow near the Soudan Mine. Notice light quartz crystals and dark deformed chlorite amygdules set in a fine-grained quartz + feldspar + chlorite + sericite + epidote groundmass. Field of view 2.5 mm. Cross-polarized light. LE-288.

Felsic Lapillistone and Breccia Deposits (*unit FM2b*)

Coarse felsic lapillistone and breccia deposits are located in the southeast quarter-section of Section 25 along the eastern field area boundary. These lapillistone and breccia deposits are approximately 65-85 meters thick and can be mapped approximately 200 meters along strike to the eastern project boundary (Plate 1). Adjacent rock units include pillowed andesite (FM1b) and rhyodacite-dacite lava flows (FM2a). Unit contacts with adjacent rocks where not observed and are therefore approximated. Outcrops generally occur in small clusters, are rounded to elongated in shape and form gentle topography.

Lapillistone and breccia deposits are tan-brown-light green in color, poorly-bedded, poorly sorted and locally clast supported. Lapillistone and breccia deposits comprise 50-70% tan, rounded-subangular, silicified, aphyric vesicular (20-40%) fine-lapilli- to block-sized pumice, and angular fine- to medium-lapilli-sized rhyodacite lava fragments that are well-dispersed and set in 30-50% brown-tan quartz phyric recrystallized coarse ash (0.5-1 mm) matrix (Figure 2.25). Block and lapilli fragments differentially weather in positive relief, approximately 5 mm above the matrix. Due to their aphyric nature, modal mineral percentages were difficult to estimate in the field in block and lapilli fragments.

Figure 2.25. Pumice blocks and fine- to medium- pumice lapilli fragments set in a recrystallized coarse-ash matrix. Long axis of paper is 7 cm for scale. Outcrop 351.

Recrystallized coarse-ash comprises 5-10% 1-3 mm anhedral, rounded, well-dispersed quartz amygdules, approximately 8-10% 1-3 mm rounded well-dispersed chlorite + quartz amygdules and 80% well-dispersed recrystallized coarse-ash sized fragments.

Modal mineral percentages were therefore difficult to estimate in the matrix. The regional D_2 fabric is present in breccias and lapillistone deposits, and is depicted by light blue to yellow schistose chlorite-sericite-carbonate alteration forming anastomozing bands which generally trend northeast-southwest around block and coarse-lapilli clasts. Anastomozing bands may also have formed from slight remobilization of ash after deposition. Petrographic data is not available for this unit.

Lapillistone and breccia deposits in the Fivemile Lake Sequence near Soudan are laterally restricted deposits. They comprise recrystallized coarse-ash supported rounded-subangular fine-lapilli to block-sized clasts that are poorly bedded, poorly sorted, non-graded and have 5-10 % anhedral well-rounded, well-dispersed quartz and chlorite amygdules. Non-welded ignimbrite deposits are compositionally homogenous internally massive, up to tens of meters thick and may contain gas segregation features (vesicles). Co-ignimbrite deposits (previously known as "lag-fall" deposits) are defined as coarse, lithic-rich deposits that consist mainly as pyroclasts that are too large and heavy for the eruption column to support (Cas and Wright, 1987). The absence of fine grained fall units (<2 mm) and the lack of discrete bedding was thought to be evidence for rapid accumulation from a continuous, vigorous eruption column with only minor variations in eruption intensity (Cas and Wright, 1987). Based on the physical features and textures present in the lapillistone and breccia deposits in the Fivemile Lake Sequence near Soudan, I interpret these deposits to be the products of non-welded or co-ignimbrite eruptions.

Lapilli-Bearing Tuff Deposits (*unit FM2c*)

Felsic lapilli-bearing tuff deposits occur in the southeast quarter-section of Section 26, and the southeast quarter-section of Section 25. Near Soudan, lapilli-bearing tuff deposits are found up-section from felsic lava flows in the southeast quarter-section of Section 26. In the eastern part of Section 25, these deposits are adjacent to basaltic scoriaceous deposits (Plate 1). Lapillistone and breccia deposits are approximately 2.5-4 meters thick. Contacts between all adjacent units strike at approximately 80-95° and dip at 80-85° to the north. The contacts between all adjacent units were mapped in the field and are sharp. Outcrops are generally flat, elongated in shape and form gentle topography.

In outcrop, felsic lapilli-bearing tuff deposits are laterally discontinuous, tan-brown, laminated to very thinly bedded (1-3 cm), non-graded and are quartz-phyric. They have sharp lamination and bedding contacts that are slightly curvilinear in nature. Lapilli-bearing tuff deposits comprise approximately 60-70% massive, aphyric recrystallized fine-ash matrix; 15-30% well-dispersed, matrix-supported, aphyric, medium-lapilli sized, sub-rounded to elongated vesicular (<10 %) flattened pumice fragments; 4 cm diameter, well-dispersed, angular to sub-rounded fine- felsic lava lapilli; and 10-15% 1-2 mm subhedral well-dispersed quartz crystals (Figure 2.26). Lapilli are chlorite altered. Gifkins and Allen (2001) suggest that pumice may differentially weather to phyllosilicates during seafloor alteration, and subsequent deformation may result due to lithostatic overburden. Lithogeochemical and petrographic data is not available for this unit.

Felsic lapilli-bearing tuff deposits are laterally discontinuous, laminated (<1cm) to very thinly bedded, non-graded, and quartz-phyric. Lapilli-bearing tuff deposits comprise approximately 60-70% massive recrystallized fine-ash matrix, 15-30% well-dispersed medium-lapilli sized flattened pumice fragments, angular to sub-rounded felsic lava lapilli and 10-15% well-dispersed quartz crystals. Lapilli-bearing tuff deposits are bound both up-section and down-section by pillowed lava flows; therefore, these deposits may represent either primary or secondary accumulations of pyroclastic debris resulting from explosive volcanism.

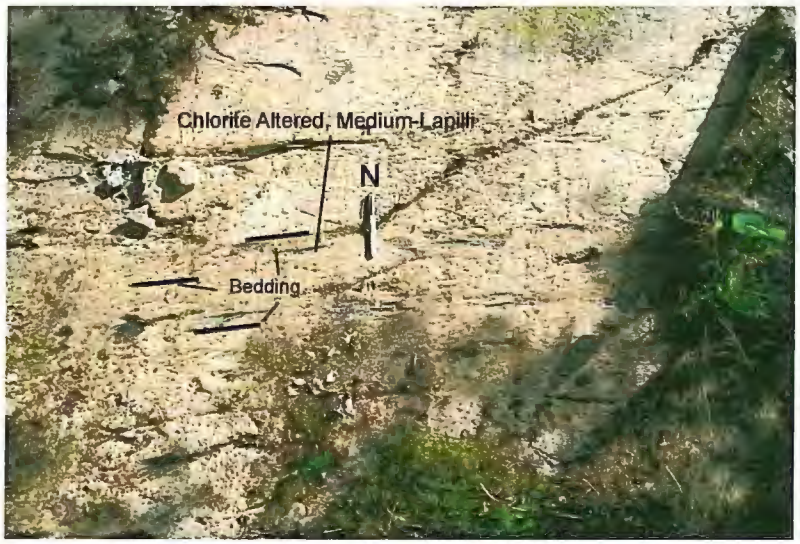

Figure 2.26. Laminated to very thinly bedded lapilli-bearing tuff deposit. Bedding trace depicted by black lines. Notice the differential alteration of pumice to chlorite and subsequent deformation by lithostatic overburden. Pen is 14 cm for scale. Outcrop 560.

Chemical Sedimentary Rocks in the Fivemile Lake Sequence

Banded Iron Formation *(unit FM4a)*

A single occurrence of oxide facies banded iron formation (BIF) (Gross, 1965) occurs in the southeastern portion of Section 25. Banded iron formation is bounded by

andesite pillowed lavas. Contacts were not observed in the field and are therefore inferred. The unit thickness is approximated to be <3 m. BIF can be mapped along strike for approximately 10 meters (Plate 1).

In outcrop, the unit is characterized by alternating white chert and black magnetite laminae that is highly convoluted. Bedding thickness ranges from laminated (<1 cm) to very thinly bedded (1-3 cm). Structural analysis on bedding convolution was not studied in detail for this thesis; however, Lundy (1985) has indicated that much of the folding is these strata resulted from soft sediment deformation. Lithogeochemical and petrographic data are not available for this rock unit.

Interpretation of the Fivemile Lake Sequence

Field geology, petrography, and lithogeochemical analysis of rocks in the Fivemile Lake Sequence suggest that lithologies formed in relatively shallow water, in a syn-collisonal volcanic-arc setting. These rocks were subject to syn-volcanic, seawater-dominated hydrothermal alteration immediately, or soon after deposition. Subsequent structural deformation during the regional D_2 deformation event locally resulted in well developed east-west trending rock foliation.

The Fivemile Lake sequence appears to make up part of a large mafic bimodal shield complex that formed on the Archean seafloor. The Fivemile Lake Sequence comprises pillowed and massive lava flows that are locally interbedded with banded iron formation. There are several transitions from pillowed to massive flows. The transition from pillowed to massive flows, within a single flow or between flows, could reflect an increase in discharge rate, a rapid change in viscosity (Cas and Wright, 1987), or a lateral

facies change (Dimroth et al., 1978). The presence of thin BIF and felsic units suggests that there were local hiatuses in mafic dominated volcanism in which hydrothermal activity prevailed.

Based on geologic criteria from Cas and Wright (1987), felsic volcanic and volcaniclastic rocks resemble what appears to be non-welded or co-ignimbrite deposits that were preceded by rhyodacite-dacite lava flows and possibly resedimented lapilli-bearing subaqueous tuff deposits. The presence of these rocks suggests that a break in andesite volcanism occurred and felsic volcanism was periodically dominant.

The lithogeochemical data for intermediate and felsic volcanic and volcaniclastic rocks near Soudan are consistent with lithogeochemical data for mafic and felsic volcanic and volcaniclastic rocks near Fivemile Lake (see discrimination diagrams). Hudak et al. (2002b) used similar immobile element discrimination diagrams (Winchester and Floyd, 1977; Pearce et al., 1984; Gordan and Schandl, 2000; Harris et al., 1986) to determine that rocks near Fivemile Lake are also basalt to andesite and rhyodacite-dacite in composition, and have chemical affinities (calc-alkaline to tholeiitic) similar to basalt-andesite and granitic rocks found in a syn-collisional volcanic-arc setting. These two locations clearly belong to the same Archean volcanic package and underwent similar post depositional physical and chemical changes during their genesis.

Central Basalt Sequence (CB)

The Central Basalt Sequence is a north-facing, steeply dipping (75°-85°), mafic to intermediate-dominated, bimodal succession of subaqueous volcanic, volcaniclastic, intrusive, and chemical sedimentary rocks that are locally deformed, texturally well-

preserved, and moderately to extensively hydrothermally altered. Rock types in the Central Basalt Sequence include mafic to intermediate pillowed and massive lavas, mafic volcaniclastic deposits, felsic volcanic and volcaniclastic deposits, and chemical sedimentary rocks. The volcanic sequence is intruded by syn- and post-volcanic sill-like intrusions and structurally controlled porphyry dikes. By percentage (>50% mafic rocks and >3% felsic rocks), the Central Basalt Sequence can be classified as a mafic bimodal sequence (Barrie and Hannington, 1999). Geographic information systems (GIS) analysis performed on the study area map indicate that the Central Basalt Sequence volcanic and volcaniclastic rocks make up approximately 29% (by area) of volcanic strata in the Soudan Mine study area. The Central Basalt Sequence is located within the Lower Member of the Ely Greenstone Formation, and sits stratigraphically above the Fivemile Lake Sequence and stratigraphically below the Upper Sequence (Plate 1).

Mafic to Intermediate Volcanic Rocks in the Central Basalt Sequence

Eleven samples (LE-055, LE-222, LE-225, LE-227, LE-337, LE-402, LE-413, LE-420, LE-425, LE-437 and LE-451) in the Central Basalt Sequence were geochemically analyzed. The cores of pillows, the massive facies of massive lava flows (LE-225), and interpillow hyaloclastite (LE-420, LE-437) were analyzed. Compositional classification was determined using relatively immobile trace elements Zr, Nb, Y and the relatively immobile oxides P_2O_5 and TiO_2 (Winchester and Floyd, 1976; Winchester and Floyd, 1977, Barrett and Mclean, 1999). Lithogeochemical analysis indicates that lavas in the Central Basalt Sequence vary from basalt to andesite in composition and have a transitional to tholeiitic affinity (Figure 2.27-2.30).

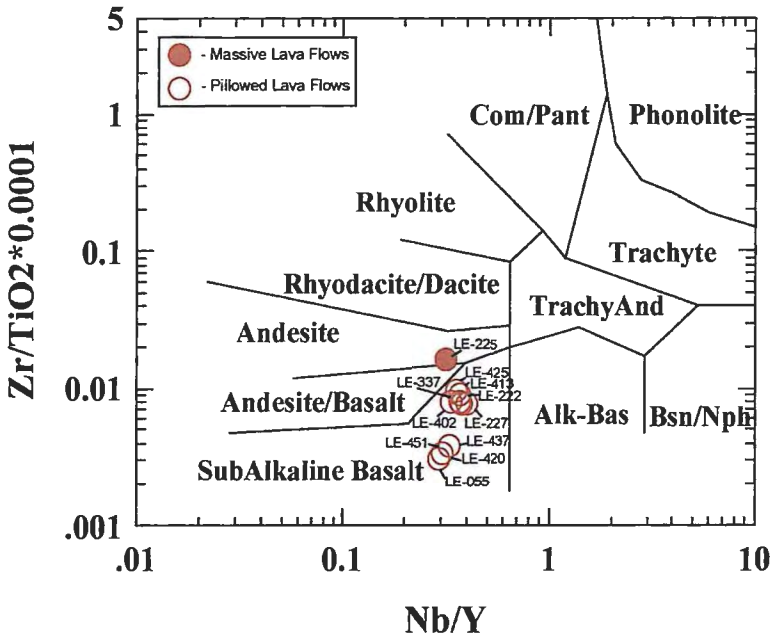

Figure 2.27. Immobile element classifications of mafic to intermediate volcanic rocks in the Central Basalt Sequence by means of Zr, TiO_2, Nb, and Y concentrations (after Winchester and Floyd, 1977).

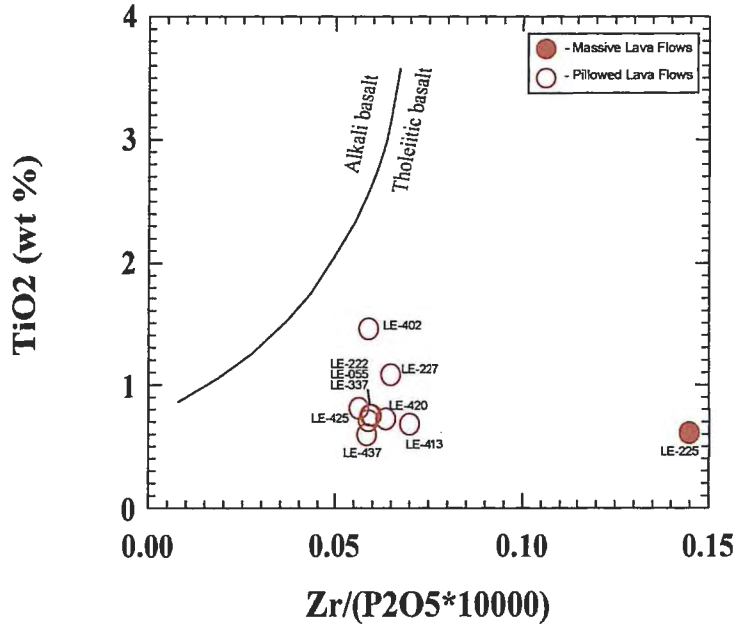

Figure 2.28. The TiO_2-Zr/(P_2O_5x10^4) diagram (after Winchester and Floyd 1976). Central Basalt Sequence mafic and intermediate lavas plot as tholeiitic basalts. Concentration in parts per million.

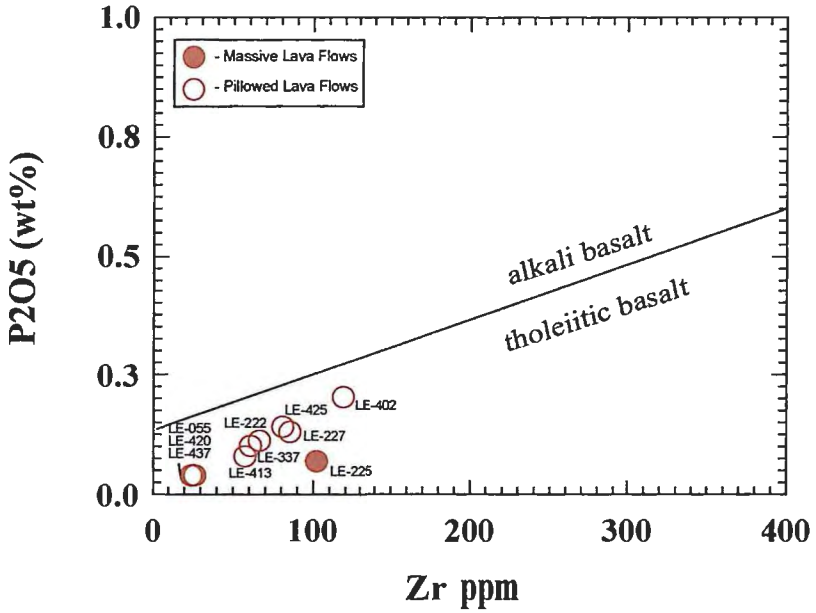

Figure 2.29. The P_2O_5-Zr discrimination diagram for Central Basalt Sequence mafic and intermediate rocks in the vicinity of the Soudan Mine (after Winchester and Floyd, 1976). Central Basalt Sequence lavas plot as tholeiitic basalts. Concentrations in parts per million.

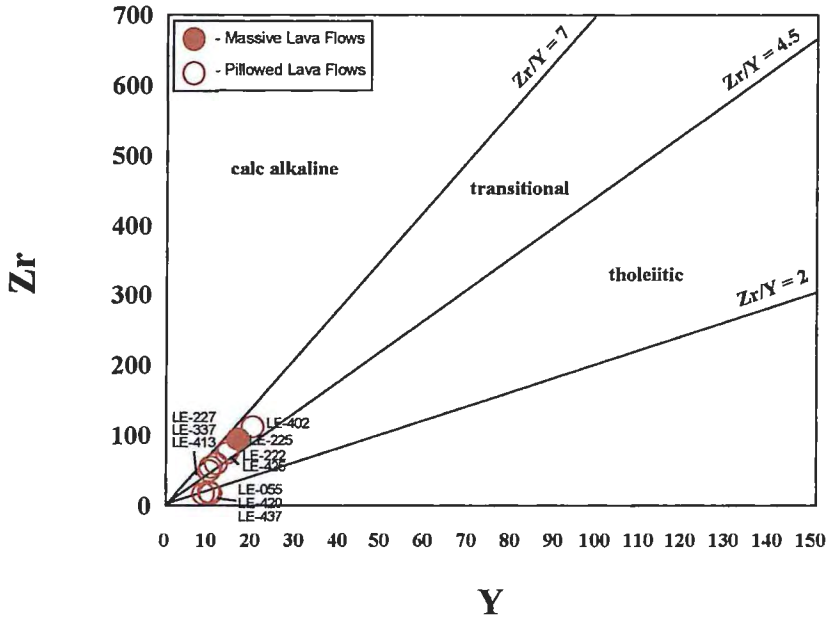

Figure 2.30. Immobile trace element plot of Zr vs. Y after Barrett and Mclean (1999). Mafic and intermediate rocks in the Central Basalt Sequence plot in the transitional to tholeiitic fields for basalts. Trace element concentrations in parts per million.

The relative enrichment of light rare earth elements (LREE) is depicted on chondrite normalized and primitive mantle normalized rare earth element spider diagrams (Figures 2.31 and 2.32). LREE enrichment in samples LE-222, LE-225, LE-227, LE-402 and LE-425 suggests a highly fractionated calc-alkaline trend that is consistent with rocks that formed in an arc-setting (e.g. negative Nb anomaly). The relatively flat pattern of the light rare earth elements (LREE) and middle rare earth elements (MREE, Sm-Ho) in samples LE-055, LE-337, LE-413, LE-420, LE-437 and LE-451 is more suggestive of magma generation from an upper mantle REE and MREE depleted source.

Tectonic diagrams (Winchester and Floyd, 1976; Pearce and Gale, 1977) suggest that the rocks are similar in affinity to plate-margin to within-plate, island-arc basalts (Figures 2.33-2.35). Conversely, the tectonic diagram after Pearce and Cann (1973) suggests that pillowed lavas plot as island-arc tholeiites and within-plate basalts, and massive lavas plot as calc-alkaline basalts (Figure 2.35).

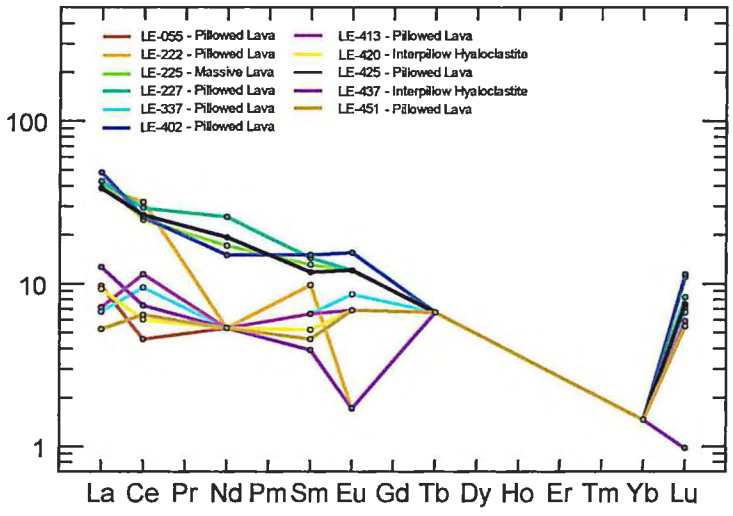

Figure 2.31. Rock vs. chondrite rare earth element spider diagram (after Sun and McDonough, 1989) for mafic and intermediate volcanic rocks in the Central Basalt Sequence.

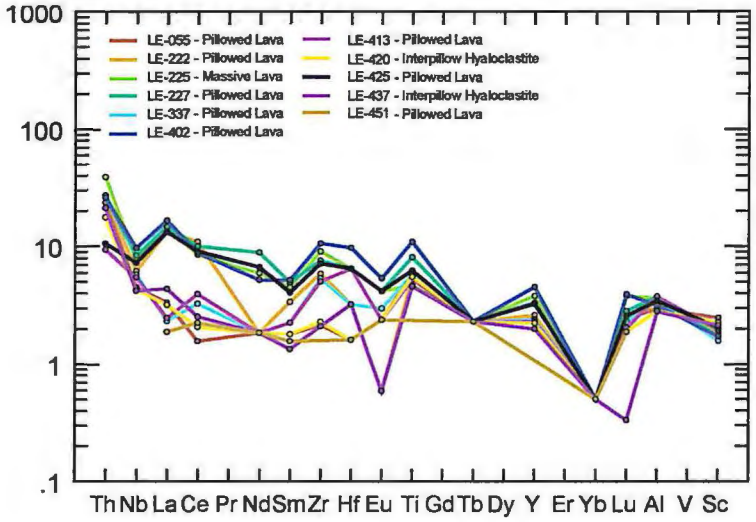

Figure 2.32. Rock vs. primitive mantle rare earth element spider diagram (after Sun and McDonough, 1989) for mafic and intermediate volcanic rocks in the Central Basalt Sequence. Notice the relative depletion of LREE and MREE (LE-055, LE-337, LE-413, LE-420, LE-437, LE-451) when compared to the REE concentration of the Fivemile Lake Sequence mafic to intermediate volcanic and volcaniclastic rocks.

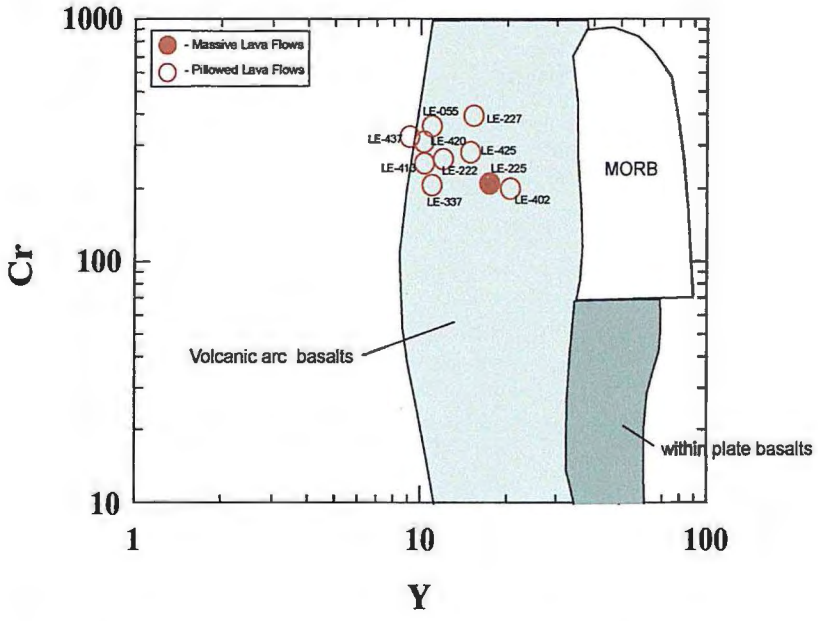

Figure 2.33. The Cr-Y discrimination diagram (after Winchester and Floyd, 1976). Central Basalt Sequence mafic to intermediate lavas fall in the volcanic-arc field. Concentrations in parts per million.

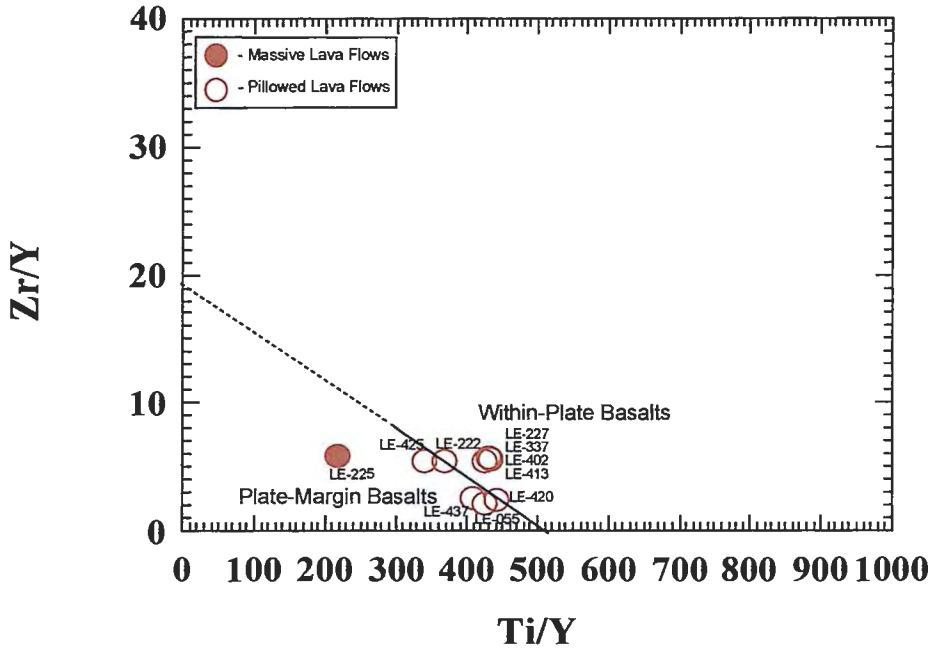

Figure 2.34. The Zr/Y vs. Ti/Y plot (after Pearce and Gale, 1977) for mafic and intermediate lavas in the Central Basalt Sequence.

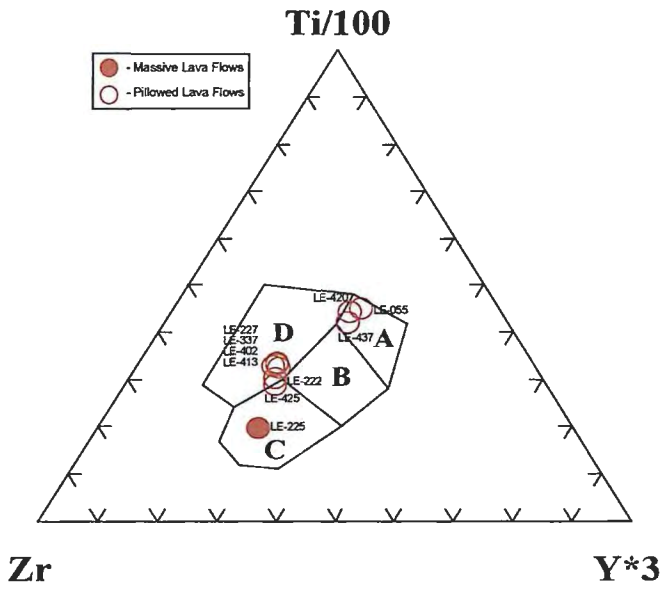

Figure 2.35. The Ti-Zr-Y discrimination diagram for basalts (after Pearce and Cann, 1973). A is the field of island-arc tholeiites, B is the field of MORB, C the field of calc-alkali basalts and D is the field of within-plate basalts (Rollinson, 1993). Central Basalt Sequence lavas plot mostly in the island-arc tholeiites and within-plate basalt fields. Concentrations in parts per million.

Massive Andesite (*unit CB1a*)

Massive andesite lavas in the Soudan Mine area occur in the southeast quarter-section of Section 23, northeast quarter-section of Section 26, and northwest quarter-section of Section 25. Massive lavas are approximately 12-250 m thick with individual flow units ranging from 1-10 meters thick. They can be mapped along strike (~75-85°) for approximately 370-700 m. Sharp contacts with adjacent units (CB1b, CB1i, US4a, QFSD, FPDD) were observed in the field, and contacts with other units (CB2b, US2b, DbU, Gb) were not observed and are therefore inferred (Plate 1). Outcrops vary considerably in size and shape and generally form large areas of relatively steep hilly terrain (Plate 1).

In outcrop, massive lava flows appear green-gray-blue in color, and are fine-grained (Figure 2.36). Locally, massive lava flows are interbedded with thin 1-2 m pillowed flow units. Massive lavas are dominantly aphyric. Primary groundmass is massive and mineral percentages were not estimated due to the rocks' fine-grained nature. Secondary minerals include <5% to locally 15% well-disseminated pyrite with local occurrences (<5%) of chalcopyrite. A general pervasive alteration comprising <1-2 mm epidote (20-35%) appears to give the rock its blue-gray appearance. Local concentrations of patchy Fe-oxide, Fe-chlorite, sericite, epidote + quartz, garnet, magnetite, and cross-stratal 1-4 cm quartz + epidote veins are highly variable in both distribution and concentration and will be discussed more thoroughly in Chapter 3. Well rounded, well-dispersed epidote + quartz + chlorite filled amygdules (5-10%, 1-5mm), and 1-6 cm cross-stratal garnet filled pipe vesicles (<1%, 1-8 mm long) are common locally.

Five samples were analyzed via petrographic analysis (LE-002, LE-003, LE-154, LE-225, and LE-333). Petrographic analysis indicates that massive lava flows in the Central Basalt Sequence are dominantly aphyric. 35% primary, well-dispersed subhedral plagioclase (albite) is present. Secondary minerals include: 5-60% epidote that occurs as <1-1mm anhedral well-dispersed semi-opaque spherical aggregates, and as <1 mm anhedral crystals, with local occurrences of up to 5mm well-dispersed subhedral crystals; 2-55% <1mm anhedral to subhedral well-dispersed platy sericite, which also occurs as 1-2mm wide and 1-4 mm long cross-cutting stringers; 20-40% <1-1.5mm

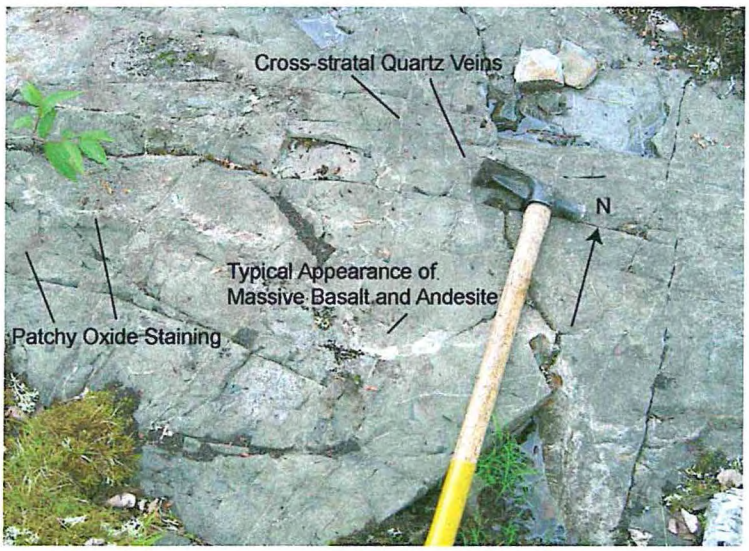

Figure 2.36. Common field appearance of massive basalt and andesite in the Central Basalt Sequence. Notice cross-stratal quartz veins and patchy oxide staining. Hammer is 68 cm long for scale. Outcrop 001.

anhedral to subhedral well-dispersed Mg-chlorite, which also occurs as cross-cutting stringers; 5-35% <1mm anhedral recrystallized quartz, which commonly occurs as well-dispersed groundmass; up to 25% <1mm well-dispersed but locally concentrated Fe-chlorite crystals; 2-25% <1-2mm anhedral to subhedral well-dispersed and locally concentrated Fe-carbonate crystals and crystal aggregates; 5-12% <1-2mm anhedral to

subhedral well-dispersed actinolite lathes; up to 5% <1mm subhedral to euhedral well-dispersed zoisite crystals; <1-5% well-dispersed <1-2mm subhedral-euhedral sub-cubic opaque minerals, probably pyrite; and 3% <1mm anhedral stilpnomelane which locally occurs in small veins and fractures. Well rounded quartz + chlorite amygdules (2-5%, 4-5mm) and 1-4 mm oxide and sulfide concentrations (<5%) were also observed in thin section. In general, massive lava flows have a massive felty texture.

Ballard et al. (1979) suggests that sheet flows are analogous to modern subaerial unchannelled pahoehoe flows that erupted at high discharge rates. Therefore, extensive changes in the discharge rates of lava during the eruptions of the Central Basalt Sequence, may account for the alternating massive to pillowed lava flows.

Pillowed Basalt (*unit CB1b)*

Pillowed lava flows in the Central Basalt Sequence occur in the southeast quarter-section of Section 23, southern half of Section 24, northern half of Section 25 and northern half of Section 26. The unit ranges in thickness from approximately 250 m on the western contact (Section 26/27 boundary, where it is deformed by the Soudan anticline), to 1700 m near the eastern mapping limit (see thesis limits of mapping, Plate 1). It can be mapped to the east, along strike (~75°-85°) for approximately 2.1 km. East of the project boundary, the sequence continues to thicken before it is truncated by the Giants Range Batholith (see Sims and Southwick, 1985). Adjacent units at the base of pillowed flows include sharp contacts with a diabase sill (DbSM) and fault bounded contacts with chlorite dominant schist (5e) that were not observed in the field and are therefore approximated. Within the Central Basalt Sequence, pillowed lavas form sharp

contacts with massive lava flows (CB1a), foliated lava flows (CB1i), intermediate dike rocks (QFSD), and have inferred contacts with stock-like diorite (D) and sill-like diabase (DbU) intrusions. At the top of the Central Basalt Sequence, pillowed lava flows are in sharp contact with oxide facies banded iron formation (US4a) and have inferred contact relationships with felsic breccia and lapillistone deposits (US2b) and a gabbro sill-like intrusion (Gb). Pillowed outcrops are highly variable in size and shape and form a variety of landscapes throughout the field area.

In outcrop, pillows in the Central Basalt Sequence consistently strike 80°-100°. They are mainly ovoid in shape with some amoeboid shaped pillows occurring locally. Pillows generally range in size from approximately 8-75 centimeters along strike (horizontal), approximately 7-40 centimeters thick (vertical), and are relatively small when compared to pillows of the Fivemile Lake Sequence. Least altered pillowed lavas are variable greens to gray-black in color, are aphyric to plagioclase-phyric and have 1-2 cm orange-brown pillow selvages (Figure 2.37).

In general, pillowed basalt and andesite comprises 15-20% primary 1-2 mm subhedral to euhedral randomly oriented plagioclase microlites, and 80-85% groundmass. Plagioclase microlites give the rock a felty texture. Due to the fine-grained nature of the groundmass, modal percentages were not estimated in the field. In general, individual pillows are contained within 1-10 cm thick, iron stained zones of well-preserved interpillow hyaloclastite (Figure 2.37). Interpillow hyaloclastite contains approximately 10-20% <1-4mm light gray to black, matrix-supported, angular to subangular recrystallized glass shards with up to 80% <1 mm matrix, consisting of variable amount of epidote, Fe-oxide, chlorite, actinolite, sericite, and carbonate and locally 1-5% <1-2

mm subhedral-euhedral finely disseminated pyrite. The matrix within the interpillow hyaloclastite is typically dark blue to orange and aphyric so accurate modal percentages for individual minerals are difficult to estimate. In the field, pillow cores contain approximately 2-3% 1-2 mm well-rounded to oval and lens-shaped, well-dispersed epidote + quartz + chlorite amygdules. Pillow margins contain 4-7% 1-5 mm well-rounded to deformed epidote + quartz + chlorite amygdules.

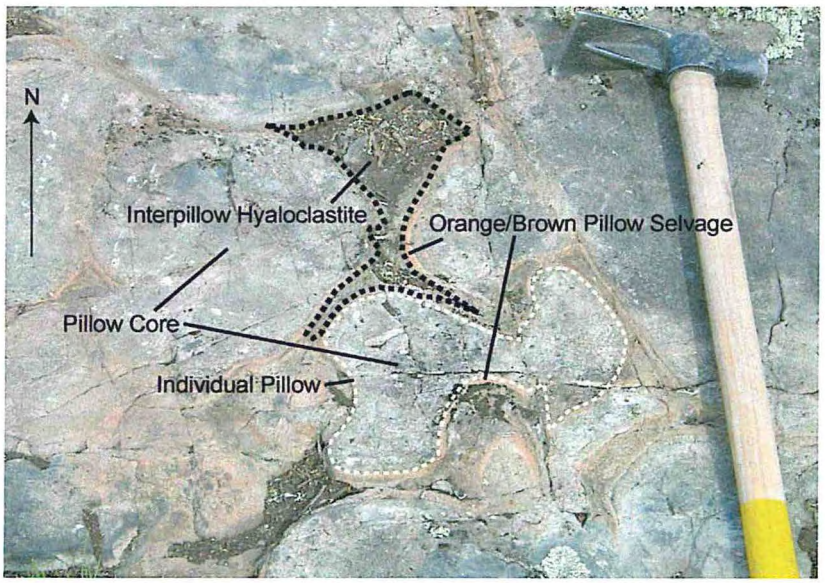

Figure 2.37. Typical field appearance of pillowed lavas in the Central Basalt Sequence. Notice the lack of vesicles and brown/orange rusty selvages characteristic of this sequence. Hammer is 68 cm long for scale (after Peterson and Patelke, 2003).

Evidence for flow direction by analysis of reentrant selvage orientation or pillow budding direction was not possible due an absence of these features. Like the Fivemile Lake Sequence lavas, Central Basalt Sequence basalts appear to have a flow propagation that is more or less parallel to the dip direction.

Petrographic analysis on fifteen samples (LE-007, LE-008, LE-126, LE-217, LE-218, LE-222, LE-226, LE-227, LE-312, LE-337, LE-401, LE-402, LE-413, LE-419 and LE-469) indicates that pillowed lavas in the Central Basalt Sequence contain 45-100% groundmass and locally 25-55% porphyroblasts. Primary mineralogy consists of: ~1-35% <1mm subhedral to euhedral albite plagioclase crystal aggregates and 8% <<1-1mm anhedral to subhedral hornblende. Secondary groundmass consists of: 5-70% epidote, which occurs as <1-1mm well-dispersed semi-opaque spherical aggregates, <1-2 mm well distributed patchy crystal aggregates, and 1-2 mm anhedral well-dispersed crystals. Epidote also occurs in 1-4 mm sigmoidal quartz veins as 1-3 mm euhedral crystals. Actinolite (6-40%) occurs as <1-1mm subhedral to euhedral well-dispersed lathes, <1 mm subhedral tabular crystals, <1 mm subhedral needle-like lathes and occurs in veins as <1-1mm felty lathes. Sericite (2-55%) occurs as <1 mm anhedral to subhedral well-dispersed platy crystals, and as <1 mm anhedral to subhedral platy crystal aggregates that commonly pseudomorph plagioclase. Anhedral to euhedral garnet (18-55%, 1-6mm) commonly occurs in 1-4 mm veinlets, 1-3 mm amygdules, and 1-6 cm long pipe amygdules. Quartz (2-35%) dominantly occurs as <<1 mm anhedral, well-dispersed recrystallized groundmass, and locally occurs as 1-2 mm anhedral crystals, and occurs along the rims of amygdules. Mg-chlorite (5-20%) occurs as <1-1mm anhedral crystal aggregates and 1-1.5 mm wide cross-cutting stringers. Fe-chlorite (~1-20%) occurs as <1-1mm subhedral tabular crystals, <<1mm anhedral well-dispersed groundmass and <1 mm anhedral to subhedral crystal aggregates. Other minerals include 15% <1-1mm subhedral to euhedral cubic pyrite; 15% 2-15mm irregular accumulations of 1-2 mm anhedral magnetite crystals; 1-15% Fe-carbonate, which occurs as <1-1 mm anhedral

blebs, 1-2mm subhedral to anhedral well-dispersed crystals, and 1-4 mm subhedral to anhedral crystals which are commonly associated with garnet porphyroblasts; 1-5% <1-1mm anhedral to subhedral local clinozoisite; 1-5% <1-1mm anhedral well-dispersed opaque minerals; 3% 1-3 mm euhedral crystal masses of zoisite also occur. Approximately 15% 1-2 mm well rounded variolites are common along the rims of pillows or within interpillow hyaloclastite. 5% 1-3 mm well-rounded and locally deformed, well-dispersed quartz + chlorite filled amygdules are also common in pillowed lavas. Locally, rocks may contain up to 15% 1-2 mm quartz + epidote + actinolite veinlets. In general, pillowed basalts have a felty and locally porphyritic texture. The distribution and concentration of secondary minerals will be more thoroughly discussed in Chapter 3.

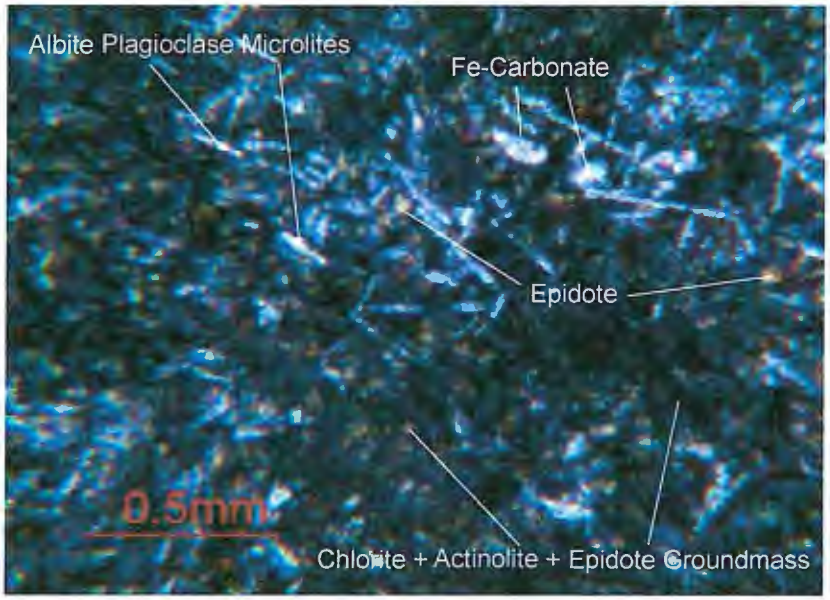

Figure 2.38. Photomicrograph of typical felty mafic lava from the Central Basalt Sequence. Notice white feldspar microlites, yellow-magenta epidote crystals, pastel color Fe-carbonate and dark chlorite/actinolite rich matrix. Field of view 2.5 mm. LE-419.

Two samples (LE-420, LE-437) of interpillow hyaloclastite were analyzed via petrographic analysis. These data suggests that interpillow material is composed of up to 20% devitrified glass shards and 80% groundmass. Glass shards are altered to: 60% <1mm-1mm anhedral to subhedral crystal aggregates of sericite, 1-30% <<1mm anhedral to euhedral 1-2 mm crystal aggregates of epidote that commonly alter the rims of glass shards, 12-30% <<1-<1mm anhedral to euhedral actinolite laths that commonly reside in the interiors of glass shards, 8-20% <1-3mm subhedral to euhedral Fe-carbonate crystals that commonly alter glass and reside in between glass shards, 2-5% <1mm anhedral to subhedral Fe-chlorite crystals that commonly reside in the centers of glass shards and appear to be intimately associated with actinolite lathes, 5% <1mm anhedral recrystallized quartz, 2% <1mm subhedral local clinozoisite crystals, and 1% ~1-1.5 mm subhedral sub-cubic pyrite crystals. 1-3 mm sigmoidal carbonate + actinolite + sericite veins are common locally.

Mafic Tuff Deposit (*unit CB1e*)

One occurrence of mafic tuff exists in the northwest quarter-section of Section 25. The true thickness is approximately 3 m. The unit can be mapped along strike for 40 meters before pinching out laterally. Mafic tuff is bounded up-section by massive lava flows (CB1a) at the top and by pillowed lava flows down-section (CB1b). The contacts between the two adjacent units are sharp and strike at approximately 65°.

In outcrop, mafic tuff is deep green to blue and comprises well-sorted recrystallized ash that is non-bedded, has no visible grading, and appears to be relatively

massive. Due to the fine nature of the grain size, modal percentages were difficult to estimate without petrographic analysis, which was not conducted for this unit.

The deposit is interpreted to be the reworked equivalent of very fine-grained hyaloclastite or tuff. The contact relationship between the adjacent units suggests that the mafic tuff deposit formed conformably. Lithogeochemical analysis was not conducted for this unit.

Foliated Basalt (*unit CB1i*)

Foliated basalt lavas are located in the northeast quarter-section of Section 26 (Plate 1). The unit is approximately 11 m thick. The deposit has a sharp up-section contact with mafic pillowed lavas. At the stratigraphic base, the contact was not observed so the unit thickness is approximated. The strike length of the deposit is limited to outcrop exposure; therefore, the strike length of this deposit was approximated beyond exposure.

In outcrop, foliated mafic and intermediate lavas are transitional between pillowed basalt and andesite lavas (unit CB1b) and chlorite schist (unit 5e). Due to their moderate shear deformation, foliated lavas are classified as a separate map unit. Foliated lavas are dark green-black, fine-grained and aphyric so exact modal percentages are difficult to estimate in the field. Metamorphic foliation within pillows and along pillow margins consistently trend between 102-108°, and is defined by the parallel alignment of fine-grained (<1 mm) chlorite that forms 1-6 mm well-dispersed sub-rounded crystal aggregates. Approximately 10% 1-3 mm flattened chlorite + quartz amygdules are common and are elongated sub-parallel to the regional foliation. Pillow selvages and

interpillow hyaloclastite do not retain their primary textures. They appear to be moderately attenuated along foliation and are altered to a light blue, very fine-grained chlorite + quartz assemblage. Well-foliated lavas in the Fivemile Lake Sequence are most commonly found either proximal to or bounded by, the two major east-west trending shear zones (Plate 1). However, foliated lavas in the Central Basalt Sequence appear to be isolated in nature. Lithogeochemical and petrographic analysis was not completed for this rock unit.

Foliated lava flows in the Central Basalt Sequence near the Soudan Mine are strongly foliated (102-108°) and altered to a variable chlorite + quartz mineral assemblage. The more or less east-west-trending foliation contained in the foliated lavas is consistent with their genesis during the regional D_2 deformation event.

Felsic Volcanic and Volcaniclastic Rocks in the Central Basalt Sequence

In the Central Basalt Sequence, felsic rocks are located in the southeastern corner of Section 23 and are found in only three small outcrops (Plate 1). Two distinct lithologies occur: 1) rhyolite lava flows (*unit CB2a*); and 2) felsic lapillistone deposits (*unit CB2b*).

Two samples (CBD2, CBD3) from the massive and spherulitic facies of unit CB2a were collected and lithogeochemically analyzed. Compositional classification of the felsic rocks in the Central Basalt Sequence was determined using relatively immobile trace element and oxide ratios (Zr, TiO_2, Nb, Y, Rb) (Winchester and Floyd, 1977; Pearce et al., 1984). Felsic rock units in the Central Basalt Sequence are rhyolite in

composition and have chemical affinities consistent with volcanic-arc and within-plate generated granites (Figures 2.39 and 2.40).

A relative enrichment of light rare earth elements (LREE), middle rare earth elements (MREE) and heavy rare earth elements (HREE) is depicted by chondrite normalized and primitive mantle normalized rare earth element spider diagrams (Figure 2.41 and 2.42). These data suggest that rhyolite lava flows have been enriched in REE element concentrations when compared to mafic and intermediate volcanic rocks in the Central Basalt Sequence. Crystal fractionation in magma chambers, which enriches the existing liquid phases in the more incompatible elements (LREE), is consistent with genesis of rhyolite magmas (Winter, 2001).

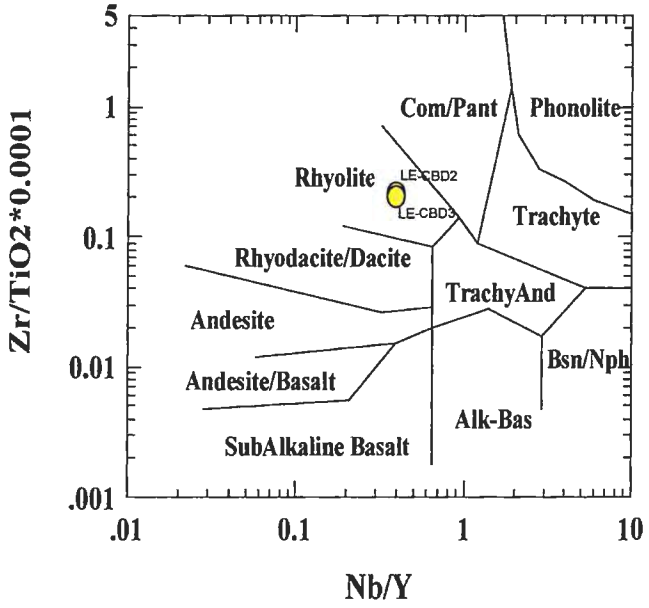

Figure 2.39. Immobile element classification of felsic volcanic rocks in the Central Basalt Sequence near the Soudan Mine (after Winchester and Floyd, 1977).

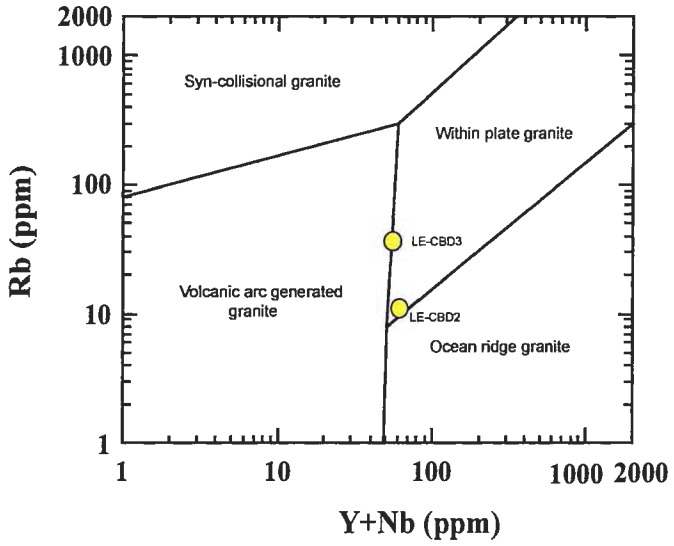

Figure 2.40. The Rb-(Y + Nb) discrimination diagram for granites (after Pearce et al., 1984). Central Basalt Sequence felsic rocks plot as within-plate granites. Concentrations in parts per million.

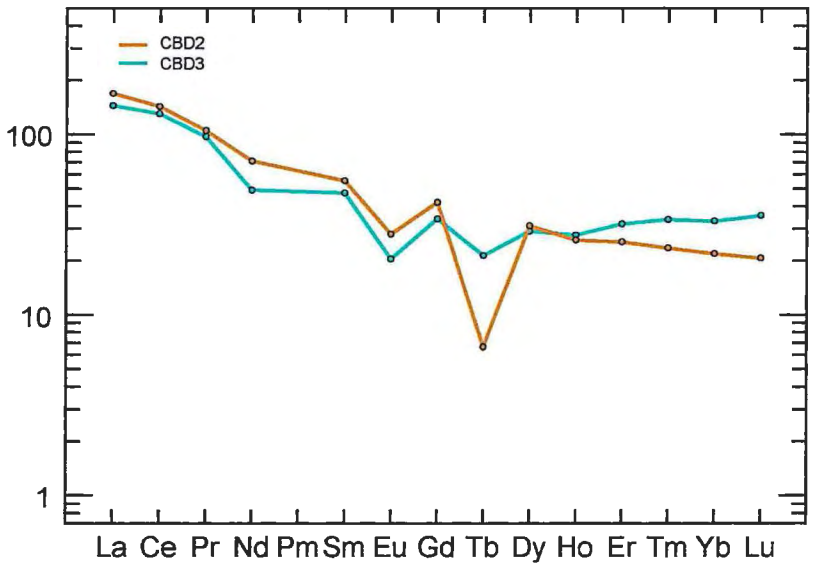

Figure 2.41. Rock vs. chondrite rare earth element spider diagram (after Sun and McDonough, 1989) for rhyolite lava flows in the Central Basalt Sequence. Notice the enrichment of the LREE, MREE and HREE.

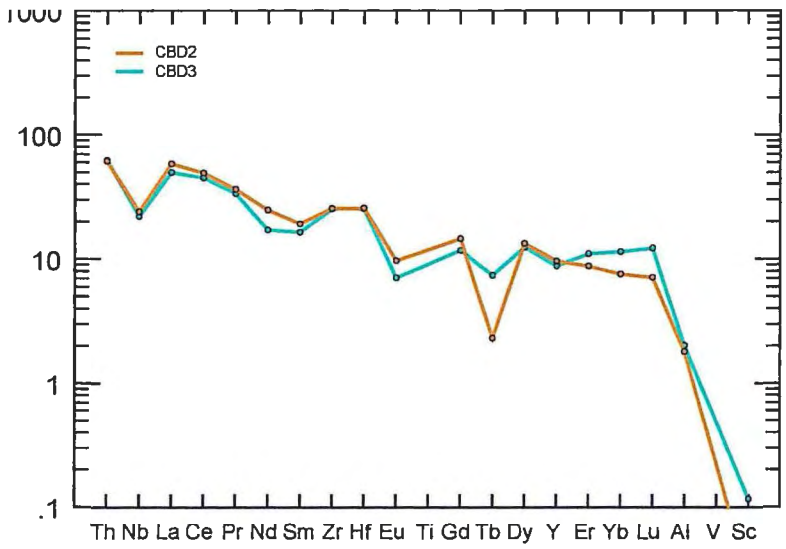

Figure 2.42. Rock vs. primitive mantle rare earth element spider diagram (after Sun and McDonough, 1989) for rhyolite lava flows in the Central Basalt Sequence. Notice the enrichment of the LREE, MREE and HREE when compared to mafic volcanic rocks in the Central Basalt Sequence.

Lithogeochemical analysis of felsic volcanic rocks in the Central Basalt Sequence indicates that these rocks are most similar to FIIIa-type rhyolites (Figure 2.38). However, La/Yb_n values for CBD2 (La/Yb_n = 1.82) and CBD3 (La/Yb_n = 1.1) suggests that the lavas are FIIIa- and FIIIb-type rhyolites respectively. In either case, rhyolites of this composition have been shown to have good prospectivity for hosting VMS deposits (Lesher et al., 1986; Hart et al., 2004). This method used alone, however, is not a definitive method to classify whether or not VMS deposits exist in the Central Basalt Sequence.

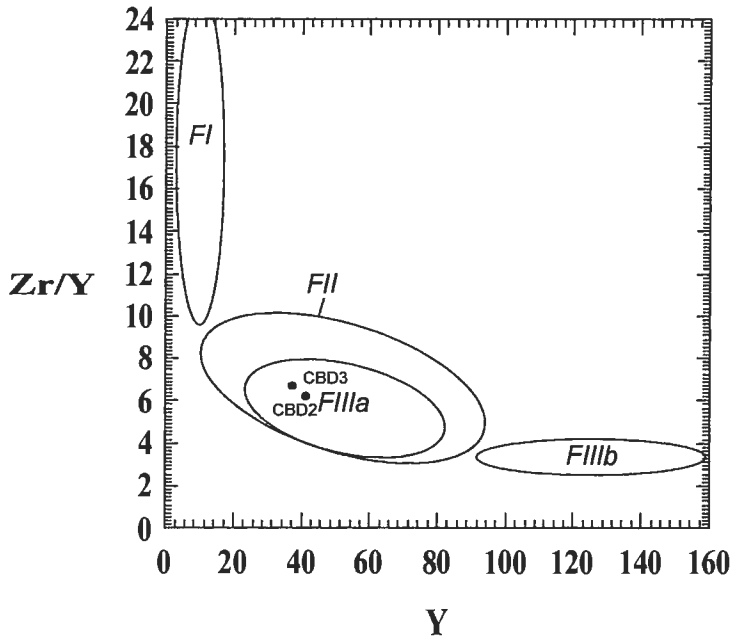

Figure 2.43. Zr/Y vs. Y diagram for Central Basalt Sequence felsic volcanic rocks near the Soudan Mine (after Piercey et al., 2001). Felsic rocks plot as FIIIa-type rhyolites. Concentrations in parts per million.

Rhyolite (*unit CB2a*)

Rhyolite lavas occur in the southeastern corner of Section 23. They can be mapped along strike for approximately 72 m. Basal contacts were mapped in the field; however overlying contacts were not observed. The unit thickness has been approximated to be 35 m thick. Rhyolite lavas are in contact with felsic lapillistone deposits (CB2b) in outcrop. Other adjacent units include massive and pillowed basalt flows (CB1a, CB1b) and compositionally intermediate cross-stratal dikes (QFSD). Contact relationships with these units were not observed in the field, and therefore contacts have been approximated. Outcrops are small, subrounded and form flat to moderately sloping topography.

In outcrop, rhyolites are yellow-tan-green in color, aphyric to plagioclase-phyric, and locally spherulitic. Groundmass comprises 98% of the rock and phenocrysts comprise 2%. Due to the fine-grained nature of the groundmass, it is difficult to estimate modal percentages in outcrop. However, locally dark yellow mottled 1- 3 cm wide subrounded patchy alteration zones are rich in quartz and sericite. Plagioclase phenocrysts are <1-1 mm, subhedral to euhedral, and well-dispersed. Locally, <1-2 mm spherulites are present and comprise 25-50% of the rock. Where spherulites are present, alteration intensity differs from massive lava flows. Spherulitic rhyolites have 1-5 cm subrounded zones of patchy chlorite + Fe-oxide (hematite). 1-2 mm subrounded quartz + chlorite amygdules (1-3%) are present locally. Near the base and within the central part of rhyolite lava flows, they locally contain < 1% 1-15 cm, subangular, spherical to elongated, medium- to coarse-lapilli to block sized massive rhyolite lava accessory fragments (Figure 2.44). Accessory fragments occur in both the massive and spherulitic facies.

Petrographic analysis on three samples (CBD2, CBD3, CBD3-2) indicates that rhyolite lavas are composed of 1% primary phenocrysts, 10% primary groundmass and 89% secondary groundmass (Figure 2.45). Primary phenocrysts comprise 1% <1-1mm subhedral to euhedral well-dispersed plagioclase crystals. Primary groundmass comprises 10% < 1-1mm anhedral well-dispersed orthoclase crystals. Secondary groundmass includes 20-60% anhedral to subhedral sericite that occurs as <1mm well-dispersed crystals and 1-3mm long and < 1mm wide stringers; 15-60% <1-1mm well-dispersed anhedral quartz crystals; locally 30% <1-1mm anhedral hematite, that locally occurs as patchy 1-3 mm zones and pervasively and partially alters spherulites; 8-15%

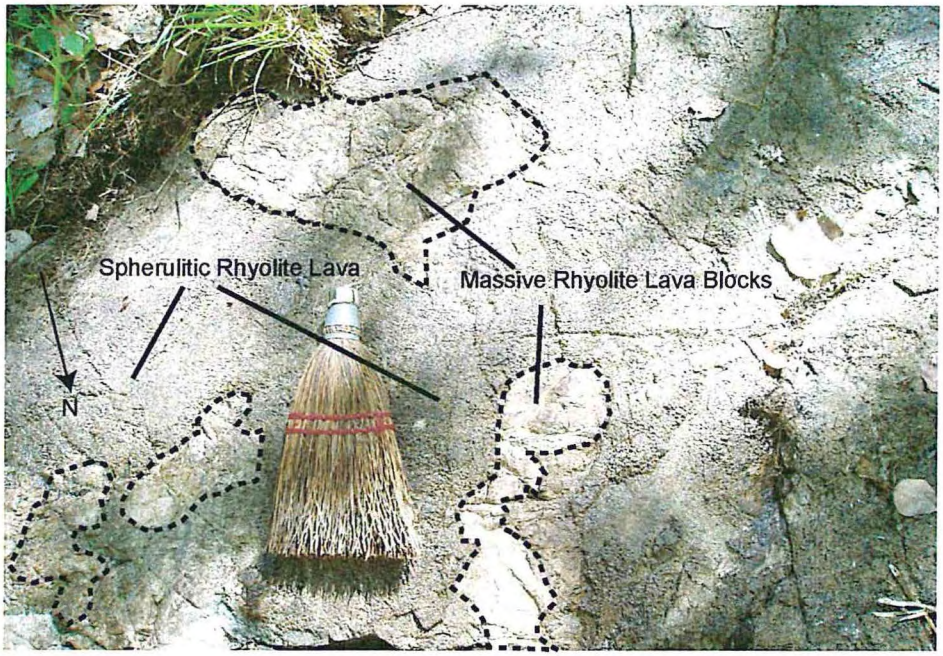

Figure 2.44. Spherulitic rhyolite lava flow with block sized massive rhyolite lava accessory fragments. Brush is approximately 15 cm for scale. Outcrop 227.

<1-1mm anhedral to subhedral cross-cutting Fe-chlorite stringers; 5% subhedral finely disseminated pyrite; and <1-5% < 1mm anhedral well-dispersed Fe-carbonate blebs. Local 1-3 mm subrounded chlorite + quartz rich amygdules are present. Radiating quartz + orthoclase spherulites (20%) are present and are locally pervasively to partially altered to hematite. Partially altered spherulites have hematite altered rims and quartz + orthoclase rich centers.

Rhyolite lava flows in the Central Basalt Sequence are generally massive to locally spherulitic. Local occurrences of medium- to coarse-lapilli to block sized accessory fragments are present. Local variations in alteration intensity will be discussed more thoroughly in Chapter 3. According to McPhie et al.(1993), spherulites in rhyolites are the product of the devitrification of glass by the nucleation and growth of crystals in

glass at subsolidus temperatures. Based on the bounding pillowed lava facies, the rhyolite lava flows were deposited in a subaqueous environment.

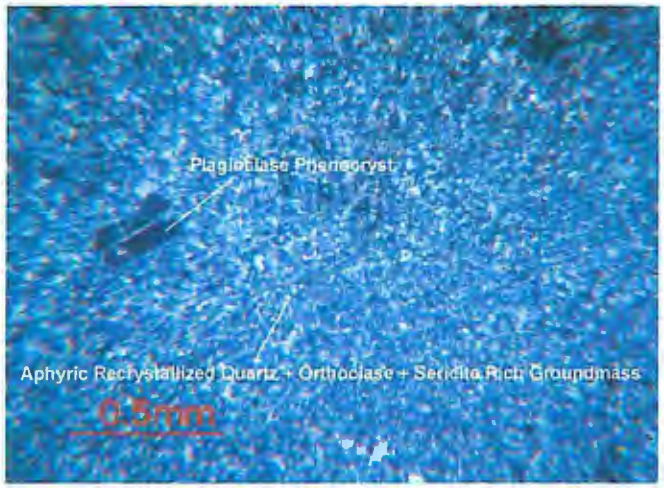

Figure 2.45. Photomicrograph of plagioclase-phyric massive rhyolite lava. Matrix is composed of very fine-grained recrystallized quartz + sericite + orthoclase. Cross Polarized light. Field of view is 2.5 mm. CBD2.

Felsic Lapillistone Deposits (*unit CB2b*)

A single outcrop of felsic lapillistone occurs in the southeast quarter-section of Section 23. Lapillistone deposits are 5-9 meters thick in outcrop and are estimated to be 20-25 meters thick beyond outcrop extents. Adjacent rock units include massive andesite (CB1a), massive and spherulitic rhyolite (CB2a) and cross-stratal dikes (QFSD). The contacts between cross-stratal dikes and felsic lapillistone are sharp. All other contacts between adjacent units were not observed and are approximated.

In outcrop, felsic lapillistone deposits are gray to light tan, non-bedded, non-sorted and dominantly matrix-supported. Felsic lapillistone comprises 40% <1-3 cm angular to subrounded lapilli clasts set in a <1-1 mm recrystallized fine- to coarse-ash

matrix (60%). Clasts are composed of 25% <1-4 cm angular well-dispersed rhyolite lava lapilli, 10% <1-3 cm angular to sub-rounded dark grey chert lapilli (Figure 2.46) and 5% 2-4 cm subrounded well-dispersed silicified pumice. Aphyric pumice contains 30-40% <1-1 mm quartz amygdules. The matrix consists of 40% recrystallized fine-ash, 18% <1-1mm angular recrystallized coarse-lithic-ash fragments, and 2% <1-1mm subhedral well-dispersed plagioclase grains.

Figure 2.46. Field appearance of felsic lapillistone deposits in the Central Basalt Sequence. Notice cherty accessory fragments set in recrystallized quartz rich matrix. Outcrop 228.

Petrographic analysis was conducted on the matrix of felsic lapillistone (CBD1). The analysis indicates that the matrix is composed of 50% < 1mm anhedral well-dispersed recrystallized interstitial quartz, which also occurs as 1- 2 mm angular crystal grains; 20% < 1mm anhedral to subhedral well-dispersed play interstitial sericite, which also commonly pseudomorphs plagioclase; 15% <1m-1mm angular well-dispersed orthoclase grains; 10% <1-1 mm well-dispersed subhedral plagioclase crystals, that also

occurs as <1-2 mm well-dispersed angular grains; 5% <1mm well-disseminated platy Fe-chlorite crystals; and <1% <1mm well-dispersed anhedral Fe-carbonate blebs.

Felsic lapillistone deposits in the Central Basalt Sequence are dominantly matrix-supported fine- to coarse-lapilli deposits that are spatially closely associated with rhyolite lava flows. Due to the intense recrystallization of the matrix, it is difficult to tell how the matrix is genetically related to the lapilli fragments. Cas and Wright (1987) have described some silicic hyaloclastite as unstratified, loose glassy sand-sized fragments containing angular lava lapilli and block fragments, of which some fragments are vesicular. These fragments may be associated with autobrecciation of the quenched surface of lava flows. Due to the close proximity of rhyolite lavas, and the physical similarities of felsic hyaloclastite described by Cas and Wright (1987), I interpret the felsic lapillistone deposits in the Central Basalt Sequence as the lateral brecciated facies of rhyolite lava flows (CB2a).

Chemical Sedimentary Rocks in the Central Basalt Sequence

Banded Iron Formation (*unit CB4a*)

Banded iron formation (BIF) in the Central Basalt Sequence occurs in the southeast corner of Section 23, the northeast corner of Section 26 and the northwest quarter-section of Section 25 (Plate 1). BIF is < 3 m to 40 meters thick, the strike length of these deposits ranges from 40-320m. BIF is bounded by massive andesite and pillowed basalt lava flows (CB1a, CB1b) and locally forms a sharp contact with intermediate intrusive rocks (QFSD) in the southeast corner of Section 23. Unit contacts between the bounding lava flows were not observed in the field, and therefore unit

thicknesses were approximated. Outcrops are rounded and typically correlate with areas defined by greater topography.

In outcrop, banded iron formation is composed of alternated gray magnetite and red jasper chert laminae. Bedding is highly convoluted and ranges from very thinly bedded to thinly bedded. Bedding convolution is interpreted to be the result of soft sediment deformation (Lundy, 1985). Lithogeochemical and petrographic data are not available for this rock unit.

Interpretation of the Central Basalt Sequence

Based on field mapping, petrographic analysis, and lithogeochemical data, the Central Basalt Sequence is interpreted to represent a suite of mafic to intermediate lava flows that formed in a volcanic-arc to within-plate setting. These rocks were subject to synvolcanic, seawater dominated hydrothermal alteration soon or immediately after deposition. Subsequent structural deformation during the regional D_2 deformation event locally resulted in well developed east-west trending rock foliation. With differences in chemical affinity, and the presence of major shear zones and intrusive rocks over unit contacts, it is difficult to determine whether or not the Central Basalt Sequence is conformable with the Fivemile Lake Sequence.

The Central Basalt Sequence appears to represent the upper stratigraphy of a large mafic dominated shield volcano complex that formed in a syn-collisional volcanic-arc to within-plate setting. The Central Basalt Sequence comprises massive and pillowed basalt and andesite flows that are locally interbedded with banded iron formation. There are four transitions from pillowed to massive flows. Massive lava flows in the Central Basalt

Sequence are much more substantial than massive lava flows in the Fivemile Lake Sequence. This might suggest long lived volcanism with increased discharge rates (Cas and Wright, 1987).

Massive and locally spherulitic rhyolite lava flows are flanked by felsic lapillistone deposits. The physical characteristics of felsic lapillistone deposits correlate well with Cas and Wrights (1987) description of autobreccia associated hyaloclastite. Therefore, these deposits are believed to form the lateral breccia facies of rhyolite flows. The presence of felsic lavas, suggests there was a break in mafic volcanism, and that felsic volcanism was periodically dominant.

The lithogeochemical data for mafic and felsic volcanic rocks in the Central Basalt Sequence suggests that these rocks are more variable chemically and more transitional in nature than the dominantly calc-alkaline Fivemile Lake Sequence. Therefore, it appears that the Central Basalt Sequence was formed during a different stage of arc-volcanism. Spider diagrams and REE discrimination diagrams show a wide distribution that includes island-arc tholeiites, within-plate basalts, and calc-alkaline basalts. This distribution may suggest that the Central Basalt Sequence began forming in an island-arc environment and then progressed into a post-collisonal within-plate environment. The advent of within-plate (ocean island) volcanism coeval with volcanic-arc volcanism is unclear but may represent the onset of volcanism in an extensional regime within the volcanic arc. The relationships between these environments, their geochemical attributes and their volcanological significance will be discussed more thoroughly in Chapter 5.

Upper Sequence (US)

The Upper Sequence is a north-northwest facing and steeply dipping (75°-85°), well preserved but locally deformed, suite of felsic and chemical sedimentary rocks that are well exposed throughout the field area. This sequence forms the transition between the Lower Ely Greenstone and the Gafvert Lake Sequence (Plate 1). Rock types in the Upper Sequence include felsic lapillistone and breccia deposits, felsic tuff deposits, and chemical sediments (banded iron formation) formally known as the Soudan Member of the Ely Greenstone (Plate 1). In the field, a gradational contact over several tens to hundreds of meters occurs between the underlying Lower Member and the overlying Soudan Member. Hudak (pers comm., 2006) has also observed a gradational contact between these two units in the vicinity of Sixmile Lake, ~5 km to the east of the study area. Throughout the Vermilion District the contact between the Lower and Soudan Member can be geophysically traced to the east until it is truncated by the Giants Range Batholith (Sims and Southwick, 1985; Peterson and Patelke, 2003). GIS analysis performed on the study area map indicates that Upper Sequence rocks make up approximately 30% (by area) of volcanic strata in the Soudan Mine study area.

Felsic Volcaniclastic Rocks in the Upper Sequence

Felsic volcaniclastic rocks occur in the northwest quarter-section of Section 26 and east-central portion of Section 27 (Plate 1). Two distinct lithologies occur 1) felsic lapillistone and breccia deposits (*unit US2b*); and 2) felsic tuff deposits (*unit US2c*).

Felsic Lapillistone and Breccia Deposits (unit US2b)

Felsic lapillistone and breccia deposits occur in the northwest quarter-section of Section 26 and east-central portion of Section 27. They can be mapped along strike (~260°) for approximately 1500 m. Felsic lapillistone and breccia deposits are approximately 90-125 m thick. In the east-central portion of Section 27, they are deformed so true thickness is difficult to estimate. Felsic lapillistone and breccia deposits display a sharp contact between chlorite schist (5e) and intrusive diabase (DbSS). Contacts between other adjacent units (CB1a, CB1b, US2c, US4a, 5,4, Gb) where not observed in outcrop and are therefore approximated. Outcrops are generally rounded to elongate and form gentle to steep terrain. Lithogeochemical analysis was not conducted for this unit.

In outcrop, felsic lapillistone and breccia deposits are monolithic, tan-white-gray in color, thinly to medium bedded or locally massive, poorly sorted and dominantly clast supported (Figure 2.47). Lapillistone and breccia deposits comprise approximately 66% white-tan subrounded to subangular fine- to block sized rhyolite lava fragments set in 34% tan to gray recrystallized medium- to very coarse-ash matrix. Fragments comprise 60% 2-4 mm subrounded to subangular well-dispersed fine- rhyolite lava lapilli, 5% 10-40 mm subrounded to subangular well-dispersed medium- to coarse- rhyolite lava lapilli and 1% 7-8 cm subangular well-dispersed rhyolite lava blocks. Due to the aphyric nature of the rhyolite lava lapilli, modal percentages were difficult to estimate. The matrix comprises: 25% < 1mm recrystallized fine-ash (of which modal mineral percentages were not estimated), 5% 0.5-1mm well-dispersed angular recrystallized rhyolite lava fragments, 2% 0.5-1mm well-dispersed angular plagioclase grains and 2% 0.5-1mm well-

dispersed angular quartz grains. Rhyolite lava lapilli comprise 80% fine-grained matrix, 10% 1-3 mm subrounded well-dispersed quartz amygdules and 10% <1-1mm subhedral to euhedral well-dispersed plagioclase phenocrysts.

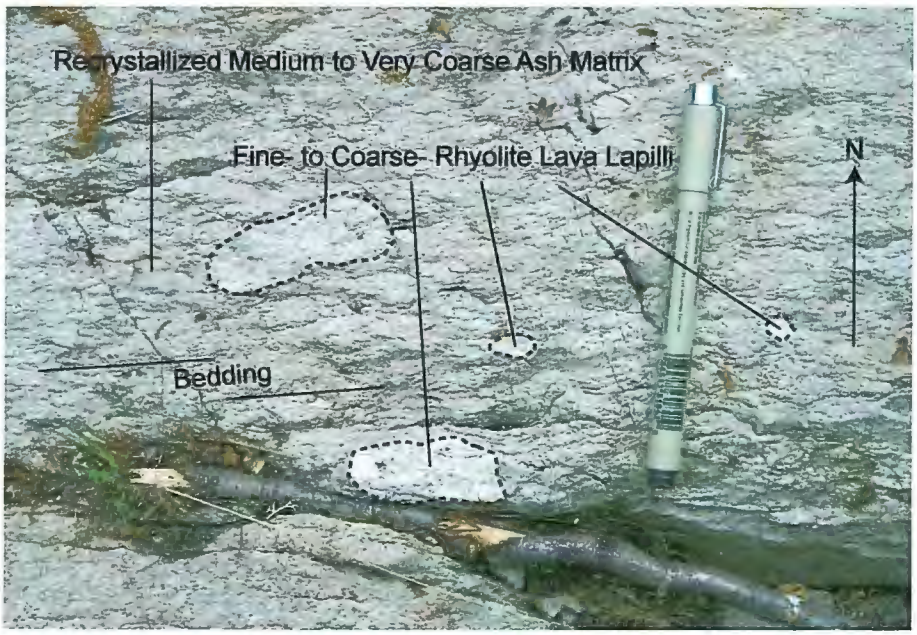

Figure 2.47. Typical field appearance of felsic lapillistone and breccia deposits. Notice the white to tan fine- to coarse- rhyolite lava lapilli set in a recrystallized medium to very coarse ash matrix. Pen is 9 cm for scale. Outcrop 008.

Petrographic analysis was completed on three samples (LE-135, LE-325, LE-356). The matrix (LE-135) and rhyolite lapilli (LE-325, LE-356) were analyzed. Petrographic analysis of LE-135 indicates that the matrix is composed of 85% groundmass and 15% angular crystal grains (Figure 2.48). The groundmass comprises 65% <<1 mm anhedral recrystallized quartz, which also exists as <<1-1mm subangular quartz grains, 15% < 1mm anhedral platy sericite crystals, 2% < 1mm anhedral spherical epidote aggregates, 2% <1-1mm sub-cubic disseminated pyrite crystals, 1% < 1mm,

anhedral Mg-chlorite crystals. Angular grains (15%), comprise 10% <1-1 mm subhedral angular plagioclase grains, 4% 1 mm anhedral angular quartz grains, and 1% < 1mm anhedral angular orthoclase grains. Petrographic analysis on LE-325 and LE-356 indicates that rhyolite lapilli are composed of 15-60% <1 mm well-dispersed anhedral recrystallized quartz groundmass, 10-40% <1 mm anhedral platy sericite crystals (that occur as 1-2 mm crystal aggregates that pseudomorph plagioclase), 5-15% 1-4 mm subhedral to euhedral patchy epidote crystals (which also occurs as < 1mm semi-opaque spherical crystal aggregates), 8% < 1mm subhedral to euhedral well-dispersed actinolite lathes (that locally form < 1-1mm crystal lathe aggregates), 8% 1-2 mm anhedral to subhedral Fe-carbonate crystals, 5% < 1mm anhedral to subhedral well-dispersed orthoclase crystals, and <1-2% < 1mm anhedral well-dispersed Fe-chlorite crystals. Rhyolite lava lapilli contain approximately 15% 1- 3 mm subrounded well-dispersed quartz + chlorite + carbonate amygdules.

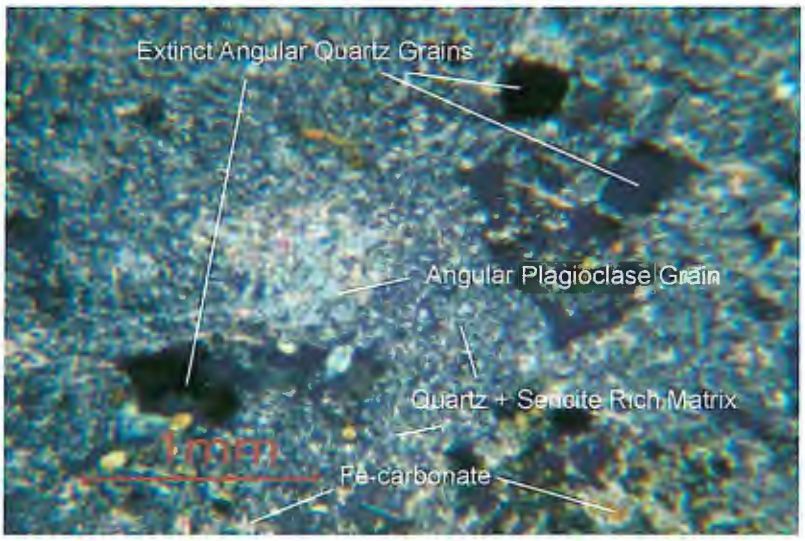

Figure 2.48. Photomicrograph of the matrix of felsic lapillistone and breccia deposits. Notice the extinct angular quartz grains and angular plagioclase grain set in a quartz + sericite rich matrix. Field of view is approximately 3 mm. Cross-polarized light. LE-315.

Felsic lapillistone and breccia deposits are monolithic, medium bedded but locally massive, poorly sorted and dominantly clast supported. Cas and Wright (1987) describe epiclastic redeposition deposits as compositionally homogenous to heterogeneous; disorganized to graded units with thicknesses up to hundreds of meters. Based on these criteria, the lapillistone and breccia deposits in the Upper Sequence may represent epiclastic deposits.

Felsic Tuff Deposits (*unit US2c*)

Felsic tuff deposits are located in the east-central portion of Section 27. The unit ranges in thickness from 35 to 100m; however, these thicknesses do not represent the true unit thickness because of post-depositional deformation (Plate 1). Contacts between adjacent units (DbSS, US2b, US4a, 5,4, 5e) were not observed in the field and are therefore inferred. Outcrops are generally rounded and are located in relatively moderate to flat terrain.

In outcrop, felsic tuff is light tan-orange, laminated to very thinly bedded, non-graded and quartz- and plagioclase-phyric. Bedding is well defined and bedding contacts are slightly curvilinear (Figure 2.49). Felsic tuff deposits comprise approximately 98% matrix and 2% phenocrysts. Matrix is composed of 98% recrystallized fine- to medium-ash. Modal percentages were not estimated in the field due to the fine-grained nature of the matrix. Phenocrysts comprise 1% 1-2 mm angular to subrounded well-dispersed quartz grains and 1% 1-2mm angular to subrounded well-dispersed plagioclase grains. Locally, < 1% 1- 4 mm subrounded to subangular matrix supported aphyric fine- rhyolite lava lapilli are present. Yellow to tan patchy sericite alteration (1-4 cm in diameter) is

common. 1 - 3 cm domains of recrystallized fine-grained tuff with lapilli sized fragments are separated by a sericite-chlorite foliation, which in this location is sub-parallel to bedding.

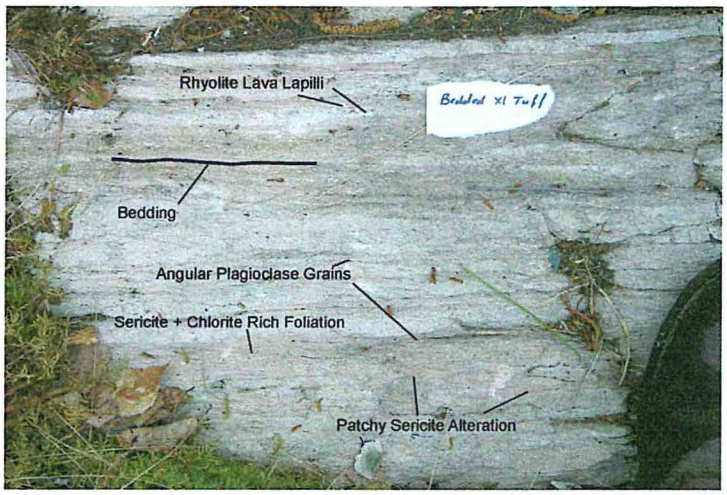

Figure 2.49. Typical outcrop appearance of felsic tuff deposits. Notice the rhyolite lava lapilli and angular plagioclase grains. Patchy sericite alteration and sericite + chlorite rich foliation is common. Paper is 5 cm wide for scale. Outcrop 009.

Petrographic analysis on three samples (LE-245, LE-246, LE-409) indicates that felsic tuff deposits are comprised of 98% matrix and 2% phenocrysts (Figure 2.50). The entire matrix is interpreted to be comprised of secondary minerals including 15-75% < 1mm anhedral platy sericite crystals (which also occurs in < 1-3 mm curvilinear foliation planes), 25-70% < 1-1mm anhedral recrystallized quartz, 10% < 1mm anhedral Fe-chlorite aggregates (which also occurs in 1-2 mm foliation planes), 2% 1mm anhedral well disseminated epidote that occurs as crystal aggregates, <1% < 1mm anhedral stilpnomelane crystals (which occurs mostly as staining in foliation planes), < 1% < 1mm interstitial Mg-chlorite (which also lines the rims of amygdules and <1% < 1mm anhedral to subhedral well-dispersed crystals). Phenocrysts are composed of 2% 1- 2mm angular

to subrounded well-dispersed quartz grains. Locally, < 1% 1- 2mm rounded chlorite + quartz amygdules are present. Chlorite typically fills the center and quartz lines the rims of the amygdules.

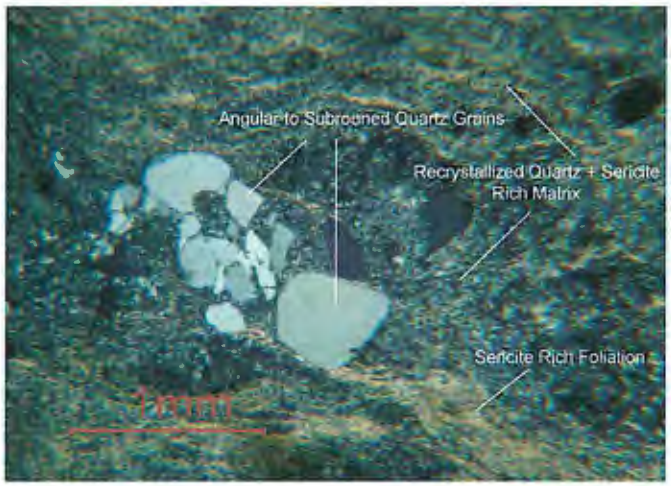

Figure 2.50. Photomicrograph of Upper Sequence felsic tuff deposit. Notice the angular to subrounded quartz grains set in a recrystallized quartz + sericite rich matrix. Foliation planes parallel bedding and are rich in sericite. Field of view 3 mm. Cross-polarized light. LE-409.

Felsic tuff deposits in the Upper Sequence are laminated to very thinly bedded, non-graded and quartz- and plagioclase-phyric. Bedding is well-defined and bedding contacts are slightly curvilinear. Peterson and Patelke (2003) have observed outcrops that contain crystal lithic tuffs interbedded with lapillistone deposits. Based on the presence of underlying pillowed and massive lavas and overlying banded iron formation, the felsic tuff deposits in the Upper Sequence are interpreted to represent primary or resedimented subaqueous tuffs that were formed from explosive volcanism.

Chemical Sedimentary Rocks in the Upper Sequence

Banded Iron Formation (*unit US4a*)

The formally named Soudan Member of the Ely Greenstone crops out in the central portion of Section 27 and can be mapped east-northeast along strike for approximately 2,300 meters through the northwest quarter-section of Section 26 and into the east-central portion of Section 23 (Plate 1). Near Soudan this unit is approximately 500-600 meters thick and can be geophysically traced throughout the Vermilion District as a marker bed that defines the Tower-Soudan anticline. Sharp contacts between adjacent units (CB1a, DbSS) were mapped in the field. Contacts with all other units (US2b, US2c, 5,4, GL2b and QFSD) were not observed in the field and were therefore inferred. The Soudan Iron Formation has the largest and most prolific outcrops mapped in the field area. Outcrops typically are large, and have steep margins up to 3-10m in height. Glacial erratics are common, and glacial striations can be found on almost every smoothly polished outcrop surface.

In outcrop, the Soudan Iron Formation is a grey-red-black-white, laminated to thinly bedded oxide facies BIF composed dominantly of interbedded jasper and hematite (Figure 2.51) with lesser amounts of magnetite and chert. Bedding is commonly highly convoluted and may locally be disrupted by meter scale breccia zones that are healed by 1-3 mm wide cross-stratal quartz and carbonate veins. In the lowermost half of the Soudan BIF, individual laminations and beds vary in thickness from <1-2 cm. Laminations and beds are more commonly composed of alternating red jasper and steel-gray hematite with lesser amounts of magnetite. In the upper half of the Soudan BIF, laminations are absent and individual beds range from 1-4 cm thick. Beds are more commonly composed of interbedded red jasper and hematite with local occurrences of alternating white and black chert interbedded with black magnetite.

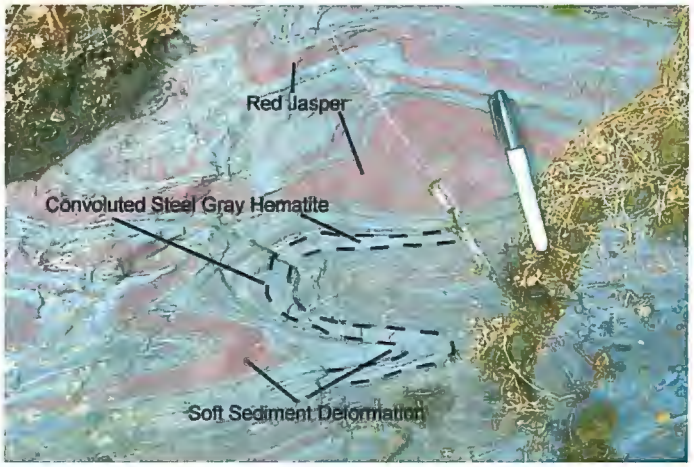

Figure 2.51. Common appearance of red and steel gray laminated jasper and hematite in Banded Iron Formation. Convolution has been interpreted to be generated from soft sediment deformation. Pen is 9 cm for scale. Outcrop 532.

One sample was analyzed petrographically (LE-253), and indicates that banded iron formation is comprised of alternating bands of 25% <<1 mm anhedral spherical quartz aggregates, 25% <<1mm red spherical jasper aggregates, 25% <<1mm anhedral opaque spherical hematite aggregates and 25% <<1mm spherical gray chert aggregates.

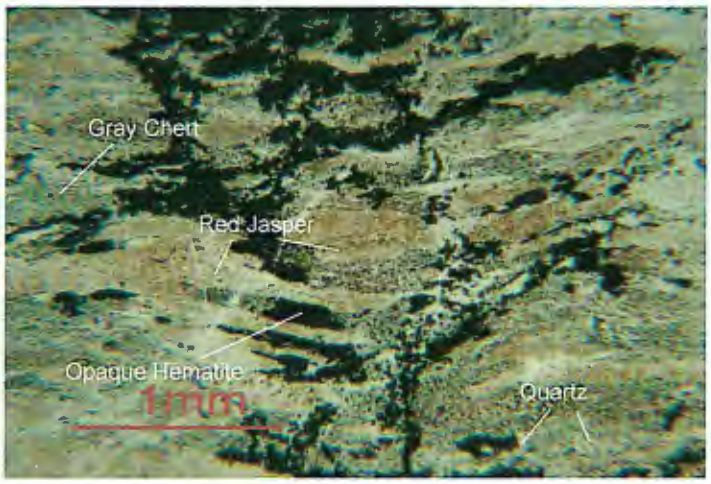

Figure 2.52. Photomicrograph of Soudan Member Banded Iron Formation. Notice alternating band of gray chert, red jasper, quartz and hematite. Mineral accumulations are comprised of <<1 mm spheroids. Field of view is 3 mm. Plane-polarized light. LE-253.

Alternating bands are 0.2-0.9 mm thick and are generally not continuous along bedding (Figure 2.52).

Interpretation of the Upper Sequence

Field geology and petrology of rocks in the Upper Sequence suggest that these rocks represent a relative decrease in mafic to intermediate volcanism, and an increase in both clastic and chemical sedimentation. During this time, a laterally extensive, relatively low temperature hydrothermal system chemically precipitated the Soudan BIF on the underlying Fivemile Lake Sequence, Central Basalt Sequence and volcaniclastic rocks of the Upper Sequence. The contact relationship between the Soudan Member and the Lower Member of the Ely Greenstone appears to be conformable.

Felsic volcaniclastic rocks in the Upper Sequence appear to make up a series of epiclastic deposits that were overlain by primary or resedimented subaqueous tuffs. These interpretations are based on the criteria of Cas and Wright (1987). Bedding convolution in the Soudan Iron Formation may be related to a soft-sediment deformation phenomenon that predates lithification (Lundy, 1985; Peterson and Patelke, 2003). Convolution may result from post-deposition deformation of the seafloor. Post-deposition deformation may have caused gravitational instability, resulting in slumping and the redeposition of lithified chemical sediments.

Gafvert Lake Sequence (GL)

The youngest volcanic strata in the Soudan Mine study area comprise the base of the Gafvert Lake Sequence (Plate 1). The base of Gafvert Lake Sequence is a north-

northwest facing steeply-dipping (75-85°) felsic volcaniclastic dominated succession. The base of the Gafvert Lake Sequence is comprised of felsic lapillistone and breccia deposits. The Gafvert Lake Sequence is regionally overlain by a thick sequence of residemented very-fine to fine-tuff, previously termed volcanogenic greywacke (Sims and Southwick 1980; Sims and Southwick, 1985; Peterson, 2001; Peterson and Patelke, 2003). Geographic Information Systems (GIS) analysis performed on the study area map indicates that Gafvert Lake Sequence rocks make up approximately 7% (by area) of volcanic strata in the Soudan Mine study area.

Felsic Volcaniclastic Rocks in the Gafvert Lake Sequence

Two samples (LE-1014, LE-1018) were collected and lithogeochemically analyzed. These samples comprise both the clasts and matrix. Compositional classification for felsic volcaniclastic rocks in the Gafvert Lake Sequence was determined using relatively immobile trace element and oxide ratios (Zr, TiO_2, Nb, Y, Rb) (Winchester and Floyd, 1977 and Pearce et al., 1984). Lithogeochemical analysis indicates that felsic volcaniclastic rocks in the Gafvert Lake Sequence are rhyodacite/dacite to trachyandesite in composition and have chemical affinities consistent with volcanic-arc, syn-collisional generated granites (Figures 2.53 and 2.54).

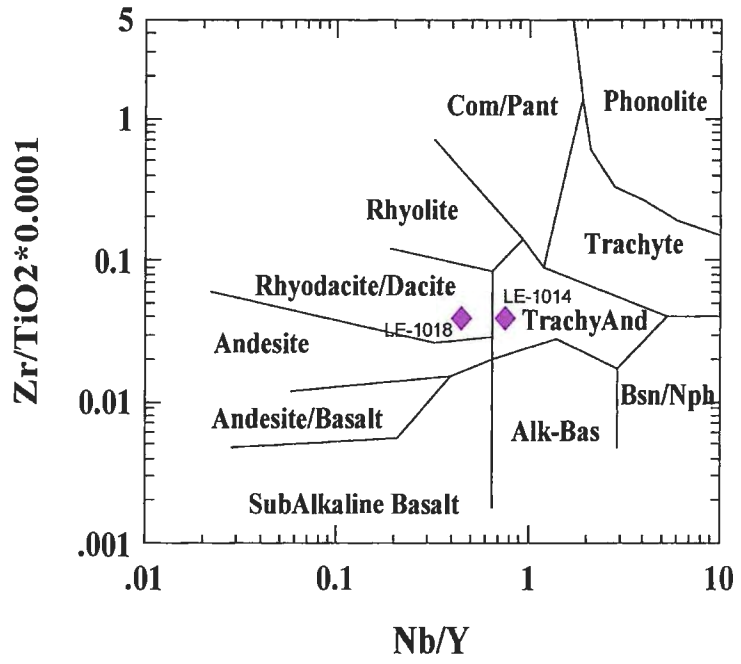

Figure 2.53. Immobile element classification of felsic volcanic lapillistone and breccia deposits in the Gafvert Lake Sequence (after Winchester and Floyd, 1977). Matrix + breccia material plots as rhyodacite/dacite to trachyandesite in composition.

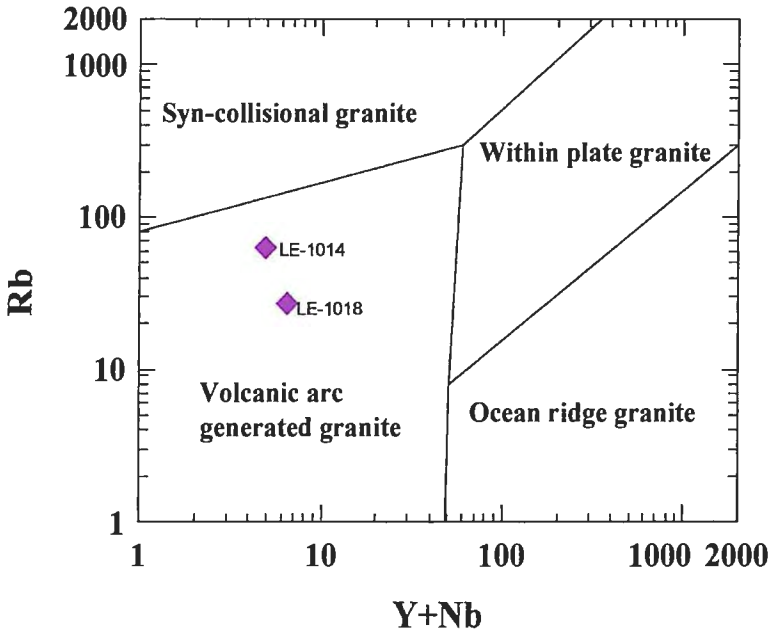

Figure 2.54. The Rb-(Y + Nb) discrimination diagram for granites (after Pearce et al., 1984). Gafvert Lake lapillistone and breccia deposits plot as volcanic-arc generated granites. Concentrations in parts per million.

A relative enrichment of light rare earth elements (LREE) and the depletion of heavy rare earths (HREE) is depicted by chondrite normalized and primitive mantle normalized rare earth element spider diagrams (Figures 2.55 and 2.56) These data suggest that rhyodacite/dacite to trachyandesite volcaniclastic rocks in the Gafvert Lake Sequence have a protolith that has a fractionated calc-alkaline affinity and is consistent with rocks that formed in a volcanic-arc setting (e.g. negative Nb anomaly).

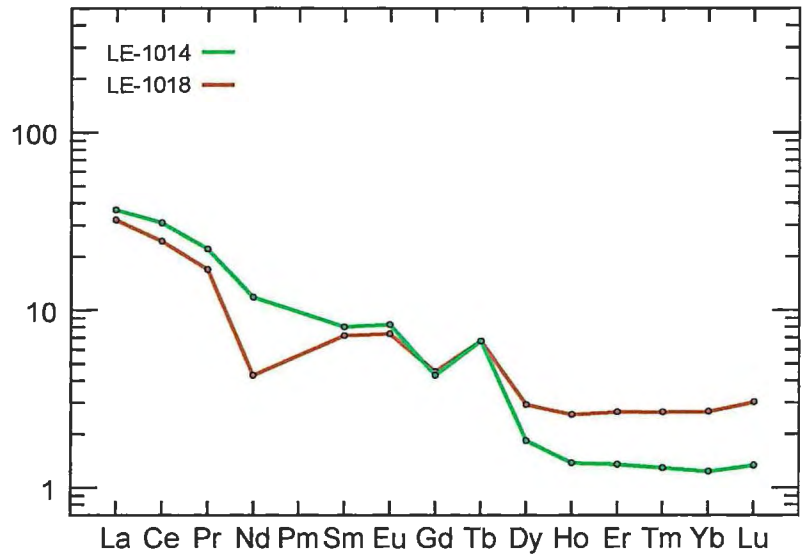

Figure 2.55. Rock vs. chondrite rare earth element spider diagram (after Sun and McDonough, 1989) for rhyodacite/dacite and trachyandesite volcaniclastic rocks in the Gafvert Lake Sequence. Notice the enrichment of the LREE versus relative depletion of the heavy rare earth (HREE) which is indicative of a highly fractionated calc-alkaline affinity.

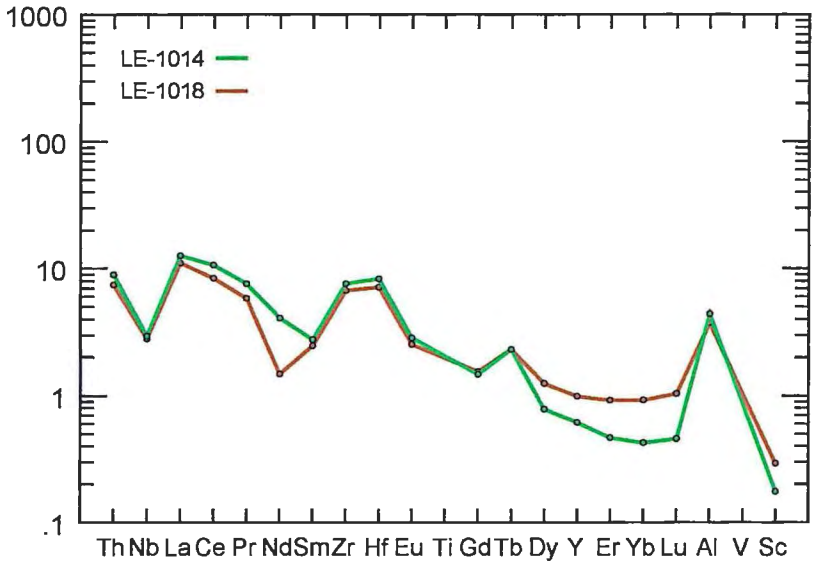

Figure 2.56. Rock vs. primitive mantle normalized rare earth element spider diagram (after Sun and McDonough, 1989) for rhyodacite/dacite and trachyandesite volcaniclastic rocks in the Gafvert Lake Sequence. Notice the negative Nb anomaly that is typically associated with rocks that form in a volcanic-arc setting.

Lithogeochemical analysis indicates that felsic volcaniclastic protoliths in the Gafvert Lake Sequence near the Soudan Mine classify as FI-type rhyolites (Figure 2.57). Geochemical data from Heiling (2003) indicates that volcanic and volcaniclastic protoliths in the Gafvert Lake Sequence are FI- and FII-type rhyolites. Both Lesher et al. (1986) and Hart et al. (2004) suggest that rhyolites of these compositions generally have low prospectivity for hosting VMS deposits.

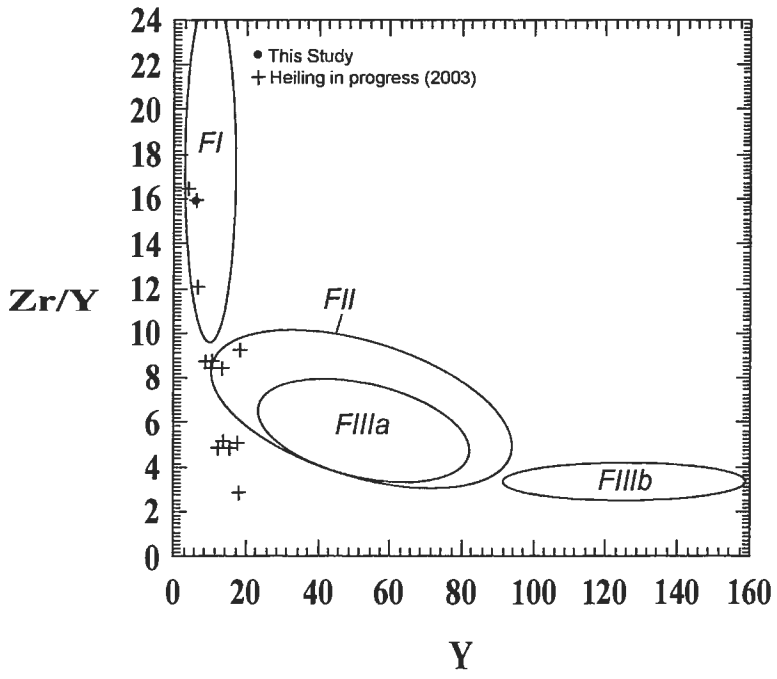

Figure 2.57. Zr/Y vs. Y diagram for felsic volcanic and volcaniclastic rocks in the Gafvert Lake Sequence (after Piercey et al., 2001). Felsic rocks plot as FI- and FII-type rhyolites. Concentrations in parts per million.

Rhyodacite/Dacite to Trachyandesite Lapillistone and Breccia Deposits (*unit GL2b*)

Felsic lapillistone and breccia deposits occur in the lower half of Section 23. These deposits can be mapped along strike for approximately 450 m. Unit thickness has been approximated to be 150-360 m; however, unit thickness was difficult to estimate because of a lack of outcrop exposure, and because the upper contact was beyond the mapping limits for this thesis (Plate 1). The overlying adjacent unit is US2e (Felsic Tuff; Peterson and Patelke, 2003), which was not mapped in the field for this thesis. Therefore, the upper contact between felsic lapillistone and breccia deposits and felsic tuff deposits was inferred. At the base, unit GL2b is in contact with the Soudan Member of the Ely Greenstone; this contact was not observed in the field, but was inferred within

1-2 m of the Soudan Member based on outcrop exposure of the two units. Outcrops are generally subrounded to elongated and form steep hilly terrain.

In outcrop, felsic lapillistone and breccia deposits are tan-white, poorly sorted, dominantly clast supported but locally matrix supported, non-graded, massive deposits. Felsic lapillistone and breccia deposits comprise approximately 55% angular to subrounded medium-lapilli- to block-sized fragments set in dominantly angular recrystallized fine- to coarse- ash to fine-lapilli matrix (45%). Clasts are composed of 30% angular to rounded, well-dispersed 4 -75mm diameter quartz and plagioclase phyric lava fragments, 5-10% well-dispersed, rounded to subrounded, 5-6 mm aphyric pumice fragments that contain 20% 1-2 mm subrounded well-dispersed quartz amygdules, 5-10% 4-6 mm well-dispersed angular white-gray chert fragments, and 2-3% 4-5 mm well-dispersed angular black chert fragments (Figure 2.58).

Figure 2.58. Felsic lapillistone and breccia deposit in the Gafvert Lake Sequence. Notice plagioclase and quartz phyric rhyolite lava lapilli and lava blocks, and angular black chert lapilli fragments set in coarse-ash to fine-lapilli matrix. Finger is approximately 1 cm wide for scale. Outcrop 713.

Figure 2.59. Angular to subangular block sized BIF rip-up clasts within 1-2 meters of the Soudan BIF-Gafvert Lake Sequence contact. Scale bar 15 cm for scale. Outcrop 712.

Locally, within 1-2 m of the basal contact of the Gafvert Lake Sequence and the Soudan Iron Formation, 10-40 cm block sized angular to subrounded BIF rip-up clasts are present (Figure 2.59). The matrix (25-35%) is aphyric. 10% <1-3 mm angular to subrounded well-dispersed aphyric fine- lava lapilli, 5% <1-2 mm angular to subrounded well-dispersed quartz grains and 1-2% subhedral angular to subrounded plagioclase grains are present.

Petrographic analysis (LE-1018) indicates that lapillistone and breccia matrix is composed of 40% <1mm angular to subrounded anhedral recrystallized quartz, 30% <1-2 mm angular to subrounded well-dispersed quartz grains, 10% <1-1mm subhedral well-dispersed plagioclase grains, 10% < 1mm anhedral well-dispersed sericite crystals, 8% 1-2 mm angular to subrounded aphyric lava clasts (which comprise 70% <1mm anhedral

recrystallized quartz, 20% <<1mm anhedral local sericite, 5% <1mm well-dispersed anhedral quartz phenocrysts and 5% < 1mm anhedral to

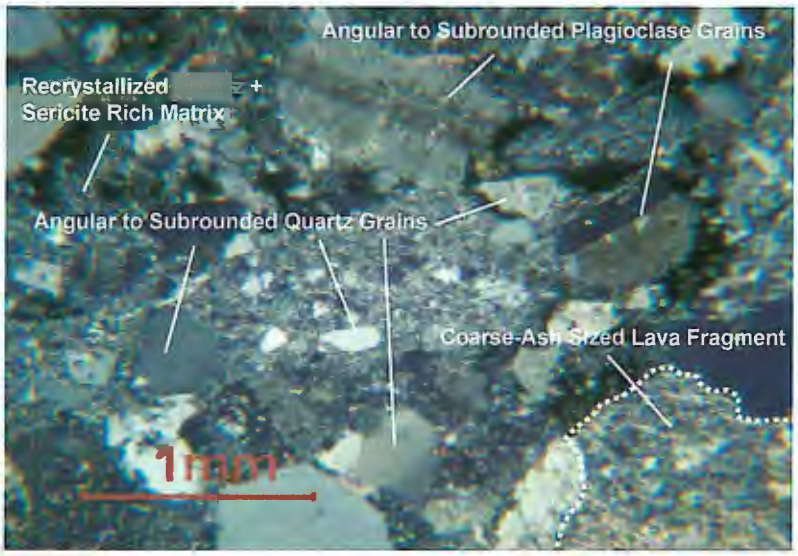

Figure 2.60. Photomicrograph of felsic lapillistone and breccia deposit in the Gafvert Lake Sequence. Notice angular quartz and feldspar grains and coarse-ash sized aphyric lava fragment set in a recrystallized quartz and sericite rich matrix. Field of view 3 mm. LE-1018.

subhedral well-dispersed plagioclase phenocrysts), <1% anhedral Fe-carbonate blebs, <1% <1mm anhedral to subhedral epidote crystals and <1% <1mm anhedral well-dispersed Fe-chlorite (Figure 2.60).

Interpretation of the Gafvert Lake Sequence

Field geology, petrographic analysis and lithogeochemistry indicate that rhyodacite/dacite to trachyandesite lapillistone and breccia deposits in the Gafvert Lake Sequence are dominantly heterolithic, clast supported but locally matrix supported, poorly sorted, non-graded, massive deposits. Cas and Wright (1987) suggest that mass

flow redeposition deposits typically have compositionally heterogeneous angular to subrounded clasts which may be disorganized and may contain tractional structures at their base. The occurrence of 4 mm - 4 cm grey-black angular chert fragments and 10-40 cm block sized angular to subrounded BIF rip-up clasts may have resulted from scouring of the lithified Soudan Member by the deposition of the Gafvert Lake Sequence. Therefore, the rocks in the Gafvert Lake Sequence are interpreted to be associated with a mass flow redepositional event that occurred after lithification of the Soudan Member of the Ely Greenstone. This may have occurred a significant period of time after the Soudan BIF was deposited; therefore, it is unclear if the contact between the Soudan BIF and the overlying Gafvert Lake Sequence is a disconformity.

Intrusive Rocks (Xy or XXXX)

Intrusive rocks in the Soudan Mine area are interpreted to be syn-volcanic with respect to the Ely Greenstone Formation based on the following criteria: 1) the occurrence of structural fabric, which would imply pre-D_2 emplacement; 2) the occurrence of hydrothermal alteration associated with syn-volcanic seafloor metamorphism; 3) cross-stratal relationships; and 4) lithogeochemical comparisons to volcanic rocks. These criteria were evaluated in the field and by subsequent petrographic and lithogeochemical analysis.

Intrusive rocks occur along major sequence contacts, within sequences, or as 1-4 m wide east-west-trending sills and northwest-northeast-trending dikes. Intrusive rocks in the field area include: 1) compositionally mafic to intermediate dikes (units FPDD, DbU) located in the Fivemile Lake Sequence; 2) intermediate dikes (FPDD, QFSD) in

the Central Basalt Sequence; 3) small sills (units DbU, Gb, D) in both the Central Basalt Sequence and Fivemile Lake Sequence; 4) a large massive sill that intrudes the Fivemile Lake and Central Basalt Sequence contact (unit DbSM), informally named the Sugar Mt. Sill; and 5) a large sill that intrudes the Soudan Member and is laterally extensive throughout the western Vermilion District (unit DbSS), informally named the Soudan Sill. Geographic Information Systems (GIS) analysis indicates that intrusive rocks make up approximately 14% of the field area.

Mafic Intrusive Rocks

Nine samples of mafic intrusive diabase were analyzed in the field area. Four samples were analyzed from the informally named Sugar Mountain Sill (LE-050, LE-086, LE-141, LE-360), three samples were analyzed from the informally named Soudan Sill (LE-180, LE-254, LE-431) and two samples of undifferentiated diabase (LE-063, LE-259) were analyzed. Generally, classification of intrusive rocks can be done based on primary mineralogy (Streckenstein, 1976) or primary chemistry (Cox et al., 1979; LeMaitre, 1984). However, due to alteration and metamorphism, classification for intrusive rocks is based on immobile trace elements. Compositional classifications for mafic intrusive rocks in the Soudan area were determined using relatively immobile trace elements Zr, Nb and Y and relatively immobile oxides P_2O_5 and TiO_2 (Winchester and Floyd, 1977; Barrett and Mclean, 1999) and indicate that mafic intrusive rocks plot as gabbros that have a dominantly tholeiitic affinity (Figures 2.61- 2.64).

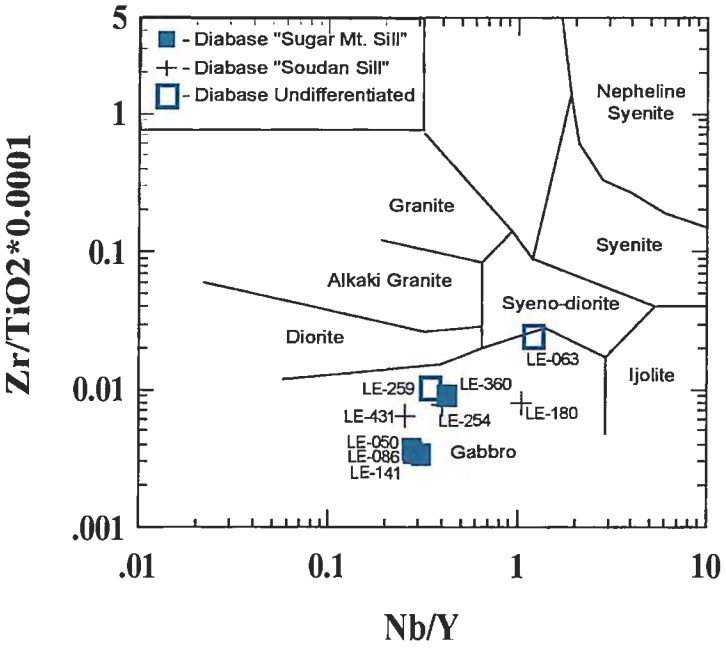

Figure 2.61. Immobile element classification of mafic intrusive rocks in the old Soudan Mine area by means of Zr, TiO_2, Nb, and Y concentrations (after Winchester and Floyd, 1977). Mafic intrusive rocks in the Soudan Mine plot as gabbros.

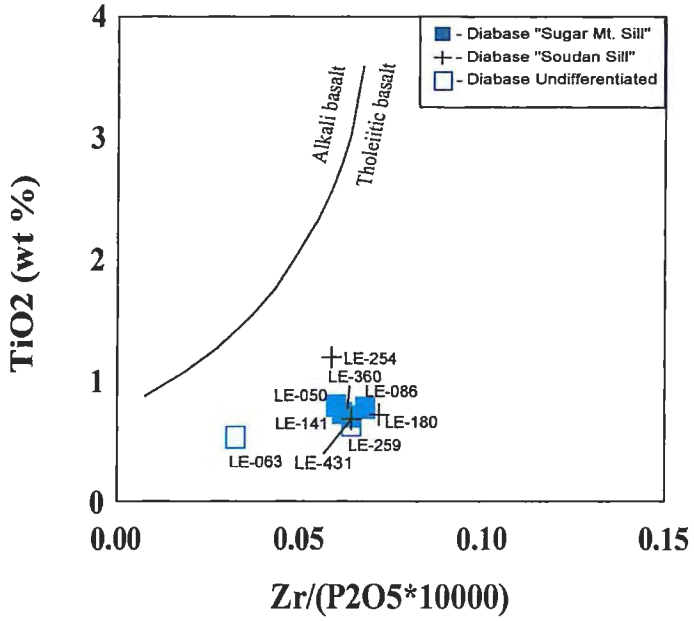

Figure 2.62. The TiO_2-$Zr/(P_2O_5x10^4)$ diagram (after Winchester and Floyd 1976). Mafic intrusive rocks in the Soudan mine area plot as tholeiitic basalts.

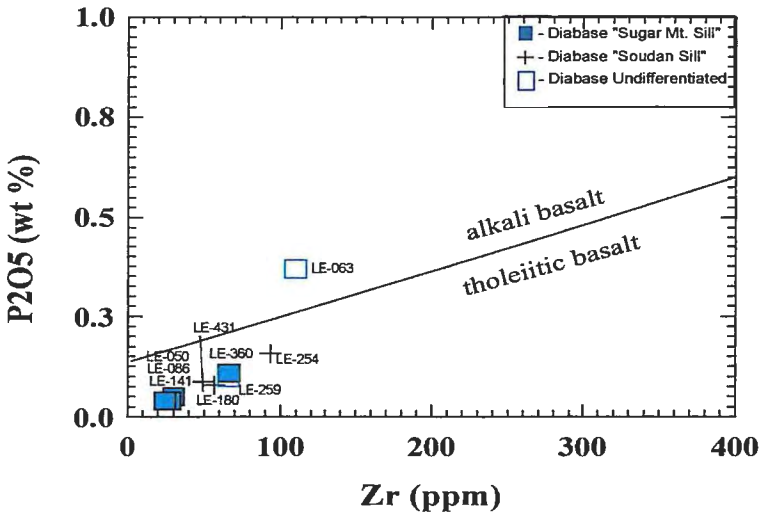

Figure 2.63. The P_2O_5-Zr discrimination diagram for basalts (after Winchester and Floyd, 1976). Mafic intrusive rocks in the Soudan Mine area plot mainly as tholeiitic basalts. Concentrations in parts per million.

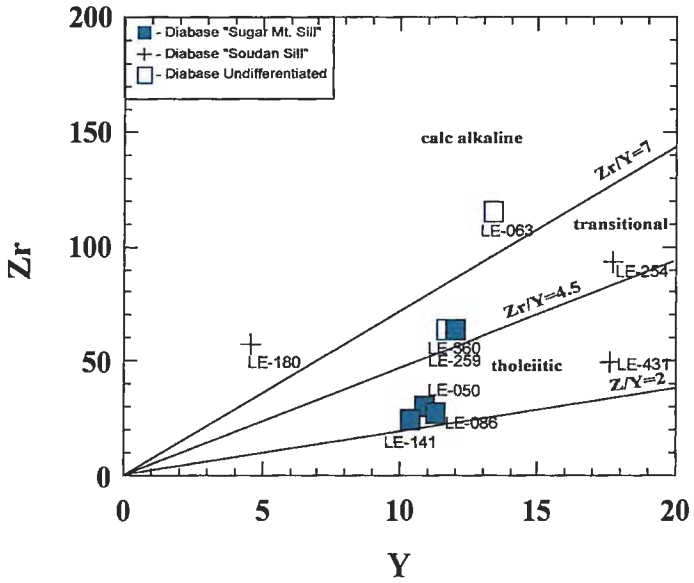

Figure 2.64. Immobile trace element plot of Zr vs. Y (after Barrett and Mclean, 1999) for mafic intrusive rocks in the Soudan Mine area. Mafic intrusive rocks plot in all fields. Concentrations in parts per million.

The relative enrichment and depletion of light rare earth elements (LREE) is depicted on chondrite normalized and primitive mantle normalized rare earth element spider diagrams (Figures 2.65 and 2.66) LREE enrichment in samples (LE-063, LE-259, LE-360, LE-254) may suggest fractionation in a magma chamber. Depletion in rare earth element in the remaining samples suggests that these magmas were derived from the depleted upper mantle. Nb, when compared to the other LREE is not depleted, which suggests a non-arc affinity.

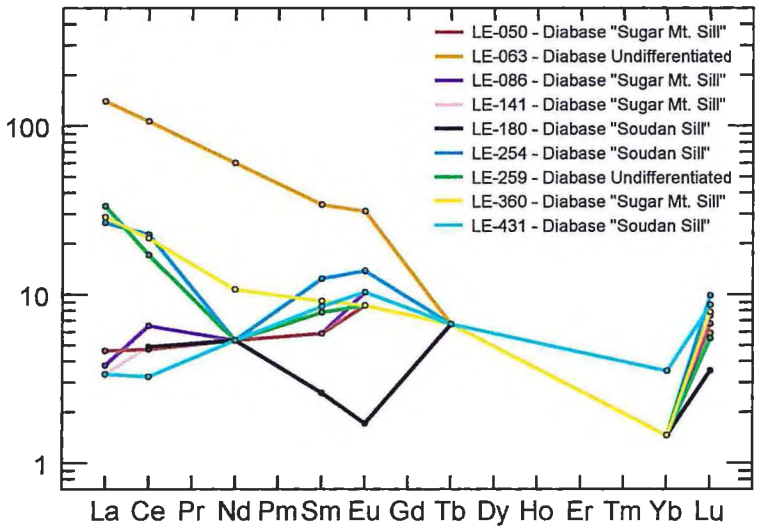

Figure 2.65. Rock vs. chondrite rare earth element spider diagram (after Sun and McDonough, 1989) for mafic intrusive rocks in the Soudan Mine study area. Notice the enrichment of the LREE in undifferentiated diabase, and the variability of LREE concentrations in the Sugar Mt. Sill and Soudan Sill. In general, the Sugar Mt. Sill and Soudan Sill have relatively flat REE patterns which suggests they were derived from the REE depleted upper mantle.

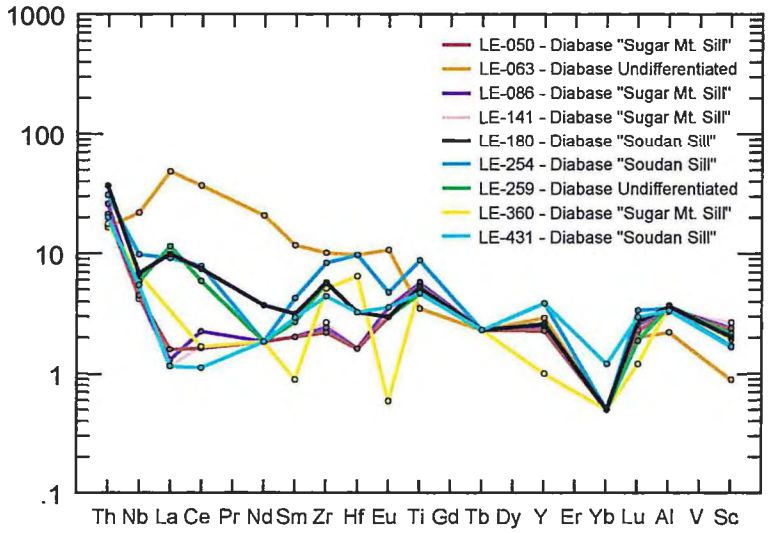

Figure 2.66. Rock vs. primitive mantle rare earth element spider diagram (after Sun and McDounough, 1989) for mafic intrusive rocks in the Soudan Mine Study area. Notice the absence of the negative Nb anomaly which suggests a non-arc affinity.

Tectonic diagrams (Winchester and Floyd, 1976; Pearce and Gale, 1977) suggest that undifferentiated diabase formed in a volcanic-arc, plate-margin setting, the Sugar Mt. Sill diabase formed in a volcanic-arc plate-margin to within-plate setting, and the Soudan Sill diabase formed in a volcanic-arc plate-margin to within-plate setting (Figure 2.67 and 2.68). Conversely, plots using relatively immobile trace elements (Figures 2.69) developed by Pearce and Cann (1973) indicate that undifferentiated diabase formed in a within-plate setting, the Sugar Mt. Sill diabase formed in an island-arc tholeiitic and calc-alkaline within-plate setting, and the Soudan Sill diabase formed in a within-plate to MORB setting.

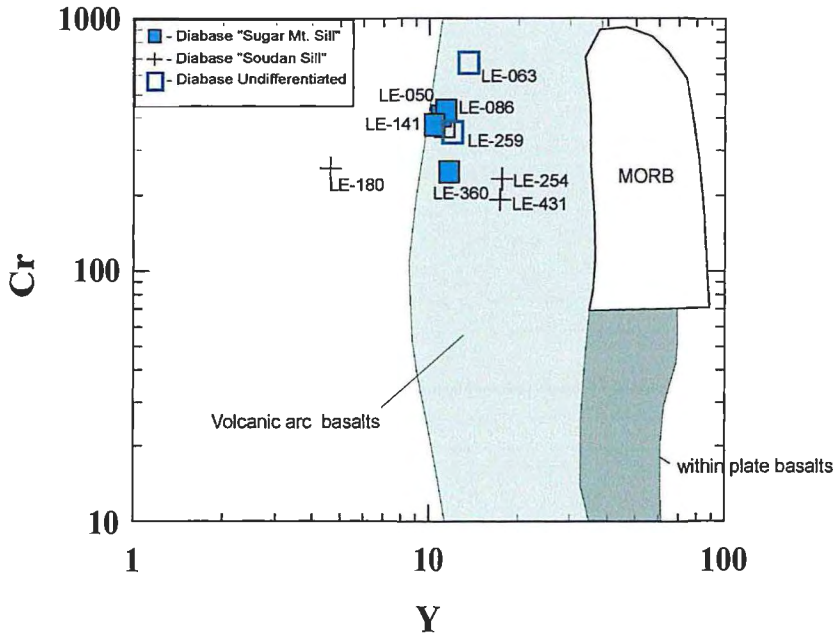

Figure 2.67. The Cr-Y discrimination diagram (after Winchester and Floyd, 1976). Intrusive rocks in the Soudan Mine area plot mainly as volcanic-arc basalts. Concentrations in parts per million.

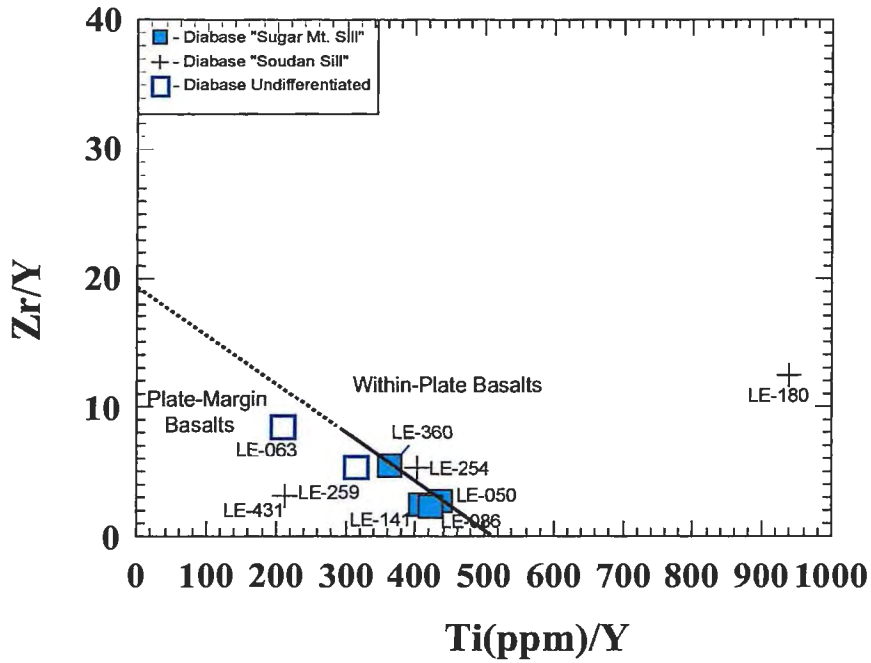

Figure 2.68. The Zr/Y vs. Ti/Y plot (after Pearce and Gale, 1977) for intrusive rocks in the Soudan Mine area. Intrusive rocks plot as both within-plate and plate-margin basalts.

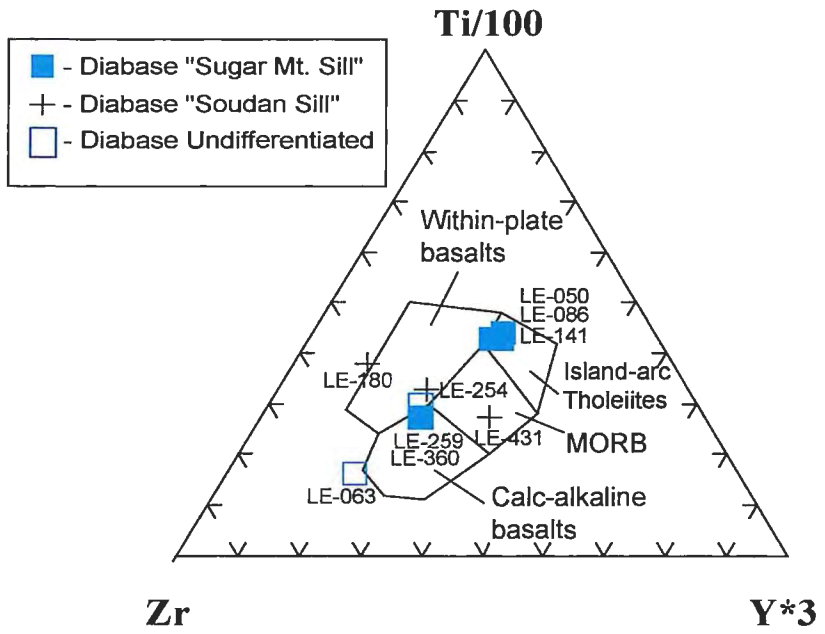

Figure 2.69. The Ti-Zr-Y discrimination diagram for basalts (after Pearce and Cann, 1973). Two suites of mafic intrusive rocks are present, island-arc tholeiites to calc-alkaline basalts (Sugar Mt. Sill), and within-plate to MORB (Soudan Sill). Concentrations in parts per million.

Basaltic Diabase Undifferentiated (*unit DbU*)

Basaltic diabase (undifferentiated) occurs as sill-like intrusions in the northwest and northeast quarter-sections of Section 26, and as a cross-stratal dike in the central portion of Section 25 (Plate 1). Diabase intrusions are 12-20 meters thick. As sills, they can be mapped along strike (80-120°), which parallels bedding, for approximately 150-180m. In the central portion of Section 25, basaltic diabase was present as a dike in only a single outcrop, so its vertical extents were inferred. Basaltic diabase (undifferentiated) intrusions have sharp contacts with all adjacent units (DbSS, US2c, CB1a, CB1b, DbSM). Contacts between adjacent units beyond outcrop exposure were inferred (Plate 1). Outcrops are generally small, variable in shape, and form moderate to steep terrain.

Peterson and Patelke's (2003) "Lamprophyre" unit was recognized in the northwest and northeast quarter-sections of Section 26. Mitchell (1994) defines lamprophyres by the presence of euhedral to subhedral phenocrysts of mica and/or amphibole together with lesser clinopyroxene and/or melilite set in a groundmass which may consist of plagioclase, alkali feldspar, feldspathoids, carbonate, monticellite, melilite, mica, amphibole, pyroxene perovskite, Fe-Ti oxides and glass. After further review of the field, lithogeochemical and petrographic data, the author has reclassified these rocks as diabase intrusions.

In outcrop, basaltic diabase is dominantly fine- to medium-grained, and appears to contain no primary minerals. Basaltic diabase is characterized by 80% red-gray-black, fine- to medium-grained massive matrix that hosts 10 cm – 1.5 m rounded-subrounded to elongated xenoliths of medium- to coarse-grained granitic rock (Figure 2.70). The contact relationship between the granite and host rock is sharp. In outcrop, the host rock (diabase) comprises 40% aphyric minerals, of which modal percentages were not estimated, and 60% secondary minerals. Secondary minerals comprise approximately 35% <1-2 mm subhedral to euhedral actinolite, 20% <1-2 mm subhedral albite plagioclase crystals and 5% 2-3 mm subhedral to euhedral Mg-chlorite crystals. In outcrop, granite xenoliths comprise approximately 20-30% aphyric groundmass, of which modal percentages were not estimated, and 70-80% phenocrysts. Phenocrysts comprise 35% 1-5 mm subhedral plagioclase, 25% 1-1.5 mm subhedral well-dispersed quartz crystals and 15-20% 1-3 mm anhedral to subhedral hornblende crystals.

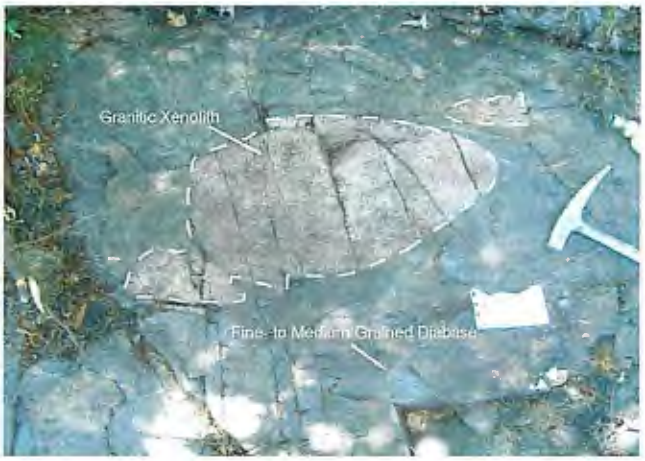

Figure 2.70. Typical appearance of granitic xenoliths in fine- to medium-grained diabase. Hammer head is approximately 15 cm long for scale. Outcrop 313.

Petrographic analysis on the host rock diabase (LE-63, LE-65, LE-354) indicates that these rocks comprise dominantly secondary minerals. Secondary minerals comprise 25-40% <1-1.5mm subhedral to euhedral well-dispersed actinolite lathes; 5-30% <1-2 mm euhedral albite plagioclase crystals; 25-30% <1-2 mm anhedral quartz crystals; 2-10% <1-4 mm subhedral to euhedral well-dispersed Mg-chlorite crystals; 4-10% <1-2 mm anhedral epidote that occurs as semi-opaque crystal aggregates; 6% 1mm anhedral to subhedral Fe-carbonate crystals; 1% <<1 mm well-dispersed anhedral sericite which occurs in the interstitial recrystallized groundmass; and 1% < 1mm subhedral clinozoisite crystals that occur dominantly in < 1mm veinlets. Petrographic analysis on the xenoliths (LE-064, LE-177, LE-354) indicates that these rocks comprise 10-85% groundmass and 15-90% phenocrysts. Secondary groundmass comprises up to 60% <<1mm well-dispersed recrystallized quartz groundmass, 16% <<1-1mm well-dispersed subhedral actinolite lathes, 9% <1mm subhedral well-dispersed platy sericite crystals, <1-4% anhedral well-dispersed circular epidote aggregates, <1-5% <1mm anhedral to subhedral

Fe-chlorite crystals and ~2% 1mm subhedral to euhedral well-dispersed Fe-carbonate crystals. Phenocrysts comprise 15-45% 1-6mm subhedral well-dispersed albite plagioclase, 15-25% 1-3mm subhedral to euhedral hornblende lathes, 18-25% 1-2 mm anhedral quartz crystals. The rock has a porphyritic texture. Petrographic analysis on the diabase dike (LE-259) indicates that this rock comprises 70% groundmass and 30% phenocrysts. Secondary groundmass comprises 35% <1mm anhedral well-dispersed sericite, 18% <1mm anhedral well-dispersed circular crystal aggregates of epidote, 10% 1-2mm cross-cutting Fe-chlorite stringers, 7% <1mm anhedral well-dispersed quartz crystals.

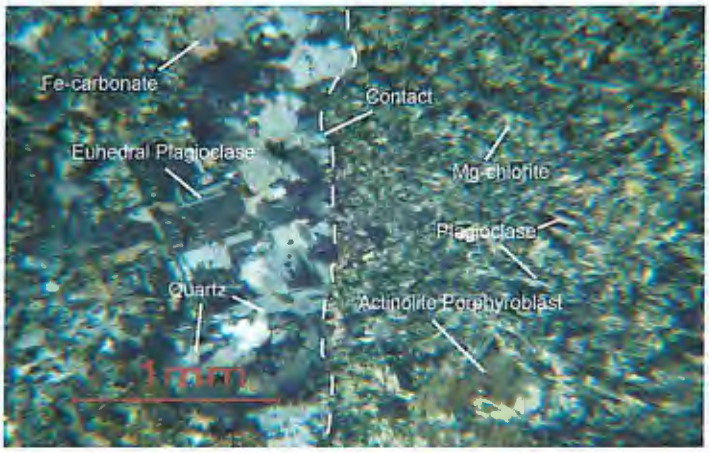

Figure 2.71. Photomicrograph of granitic contact with fine- to medium-grained diabase matrix. Contact relationship in this slide is sharp. Field of view 3 mm. Cross-polarized light. LE-354.

Porphyroblasts and phenocrysts comprise 15% 1-4 mm subhedral well-dispersed actinolite and 15% 1-4mm subhedral well-dispersed hornblende crystals. The rock has a porphyritic texture.

Based on lithogeochemical data, petrographic analysis, and field mapping, basaltic diabase (undifferentiated) appears to form sill-like intrusions and a cross-stratal

dike that cross cuts the Sugar Mt. Sill. Subrounded to rounded granitic xenoliths that are found within the diabase sills may represent injections of immiscible felsic magmas. According to Winter (2001), the mixing of different magma phases can be common in bimodal environments. This may explain the enigmatic appearance that these outcrops display in the field. The presence of minor foliation suggests these rocks are synvolcanic with respect to the Ely Greenstone Formation. The cross-stratal dike that cross-cuts the Sugar Mt. Sill has similar chemical affinities to basalts in the Central Basalt Sequence (see discrimination diagrams and REE plots). Therefore, this dike may represent a feeder for basalt lava flows up-section.

Basaltic Diabase (*unit DbSM*, "Sugar Mountain Sill")

A thin and laterally extensive diabase sill occurs between the Central Basalt Sequence and the Fivemile Lake Sequence. The sill strikes more or less east-west (80°-85°), varies in thickness from 70-200 m, and extends laterally 3.2 km from the center of Section 26, through Section 25, and into the northwest quarter-section of Section 30 (Plate 1). Contacts with adjacent units are sharp and include pillowed lava flows (CB1b, FM1b) foliated lava flows (FM1i) intrusive rocks (FPDD, DbU) and sheared rocks (5b, 5e). Outcrops are relatively large, abundant and create steep jagged terrain.

In outcrop, basaltic diabase is gray to light blue-gray, plagioclase-phyric with a fine-medium grained groundmass. The unit can be easily identified by its relative lack of veins and joints when compared to the adjacent volcanic strata (Figure 2.66). Locally, xenoliths of pillow basalt are 10's to 100's of meters in diameter. These xenoliths make up ~1% of the intrusion. Foliation within the intrusion is relatively absent; however,

locally the foliation is defined by the alignment of 1-4 mm subrounded chlorite aggregates. The Sugar Mountain Diabase comprises 2% phenocrysts and 98% fine-grained groundmass. Groundmass is comprised of approximately 50-60% <1-1mm well-dispersed epidote and 15-20% <1mm anhedral Fe-chlorite. Phenocrysts comprise 2% 1-2mm subhedral well-dispersed plagioclase lathes. Locally <2% 1-2 mm subrounded well-dispersed quartz amygdules and < 1% 1-3 mm wide cross-stratal epidote veins are present.

During their 2003 investigation, Peterson and Patelke compositionally classified this intrusion as diorite, based primarily on field observations. During the author's second stage of field work, several of these outcrops were revisited. Detailed studies of outcrops of this intrusion, along with petrographic and lithogeochemical data, indicate that these intrusive rocks are actually mafic in composition. Based on these studies, the previously named "Sugar Mountain Diorite Sill" (Peterson and Patlke, 2003) has been renamed "Sugar Mountain Diabase Sill".

Figure 2.72. Typical appearance of the Sugar Mountain Diabase Sill (unit DbSM). Rocks in this unit typically form steep and jagged terrain. Outcrop 130.

Petrographic analysis on three samples (LE-032, LE-080, LE-086) indicates that basaltic diabase is composed dominantly of secondary minerals, which include 20-60% <1mm anhedral well-dispersed epidote, which also occurs as <1mm semi-opaque spherical aggregates, 1mm anhedral crystals and in 1-3 mm wide cross-stratal veins, 5-30% <1-2 mm anhedral to subhedral quartz which occurs mostly as well-dispersed interstitial groundmass, 3-35% <1mm anhedral well-dispersed Fe-chlorite which also occurs as subhedral crystal aggregates, 20% <1-1mm subhedral actinolite lathe aggregates, 10% <1-1mm subhedral to euhedral localized clinozoisite, 2-10% <1-2mm sublinear anhedral Fe-carbonate crystals, 10% <1mm anhedral well-dispersed sericite, 5% skeletal 1-2mm anhedral to subhedral plagioclase, <1% <1mm anhedral to subhedral zoisite crystals. Locally, 5% of the rock comprises subrounded 1-3mm subhedral quartz + chlorite amygdules and 2-3% of the rock comprises 1-1.5 mm wide epidote + Fe-carbonate veins. The rock has a massive and locally felty texture.

Based on the emplacement geometry, the occurrence of hydrothermal alteration assemblages, and local occurrences of the regional D_2 foliation, the Sugar Mountain Sill is interpreted to be synvolcanic with respect to the Ely Greenstone Formation. It is very likely that during volcanism and sill emplacement, the Sugar Mountain Sill provided heat that contributed to forming semi-conformable and crosscutting hydrothermal alteration that is present up-section (see Chapter 3). Based on lithogeochemical similarities with massive and pillowed lavas in the Central Basalt Sequence, the Sugar Mt. Sill is believed to represent a hypabyssal staging magma chamber for volcanic rocks in the Central Basalt Sequence (Lower Member of the Ely Greenstone) and/or mafic rocks in the Upper Member of the Ely Greenstone.

Gabbro Porphyry (*unit Gb*)

A gabbro sill occurs at the contact between felsic fragmental rocks of the Upper Sequence (US2b), and the upper portion of the Central Basalt Sequence in the northern half of Section 26 (Plate 1). The sill is 130 m thick and has a strike length of approximately 1250 m. A small gabbro sill also occurs in the central portion of Section 27, where it is bounded by banded iron formation (US4a). In the northern half of Section 26, contacts with felsic fragmental rocks (US2b) are sharp. Contacts with all other adjacent units in this location (DbSS, Cb1a, Cb1b, DbU, US4a) were not observed in the field and are therefore approximated. Outcrops are large and form steep hilly terrain.

In outcrop, gabbro is dark-green to black, fine-medium grained, porphyritic and in some locations strongly magnetic (Figure 2.73). Gabbro commonly has a moderately developed east-west fabric (Peterson and Patelke, 2003). In outcrop, gabbro comprises 70% aphyric groundmass and 30% phenocrysts and porphyroblasts. Modal percentages were not estimated for the aphyric groundmass. Phenocrysts and porphyroblasts comprise approximately 15% 1-3mm well-dispersed anhedral to subhedral platy actinolite (which appears to pseudomorph pyroxene), and 15% 1-3 mm well-dispersed subhedral to anhedral skeletal plagioclase. Randomly oriented 1-3 cm wide quartz veins occur locally. Lithogeochemical analysis was not conducted for this unit.

Figure 2.73. Typical appearance of massive gabbro porphyry sill. Hammer 68 cm for scale. Outcrop 118.

Petrographic analysis on four samples (LE-173, LE-176, LE-252, 326) indicates that gabbro porphyry is comprised of 65-88% groundmass and 12-35% phenocrysts and porphyroblasts (Figure 2.68). Groundmass is composed of 10-35% <1-2mm anhedral to subhedral well-dispersed epidote crystals (which also occurs as <1mm well-dispersed semi-opaque spherical aggregates that pseudomorph plagioclase); 4-35% 1-2mm subhedral tabular actinolite that commonly occurs pseudomorphing pyroxene; 9-30% <1-1mm anhedral recrystallized quartz groundmass; 6-17% <1mm anhedral to subhedral well-dispersed Mg-chlorite crystals (which also occur as 1-1.5 mm well-dispersed tabular crystals); 2-15% <1-1.5 mm subhedral to euhedral well-dispersed clinozoisite; 2-5% <1-1mm subhedral well-dispersed albite plagioclase crystals; <1-5% <1mm anhedral to subhedral well-dispersed platy sericite crystals; 5% <1-1mm anhedral to subhedral zoisite crystals; 2-5% <1-1mm anhedral to subhedral crystals and blebs that pseudomorph

plagioclase; 2% <1mm anhedral opaque minerals; and 2% <1 mm anhedral to subhedral Fe-chlorite crystals. Phenocrysts and porphyroblasts comprise 8-17% 1-3mm anhedral

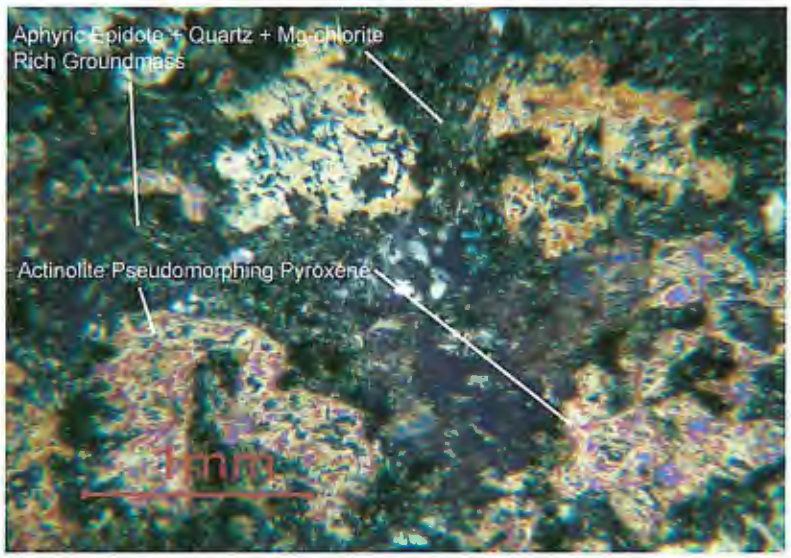

Figure 2.74. Photomicrograph of fine-grained gabbro intrusion. Notice actinolite pseudomorphing pyroxene and aphyric epidote + quartz + Mg-chlorite rich groundmass. Field of view 3 mm. Cross-polarized light. LE-252.

to subhedral tabular actinolite crystals that commonly pseudomorphs pyroxene and 4-15% 1-3 mm well-dispersed subhedral skeletal plagioclase lathes.

Gabbro porphyry is interpreted to be synvolcanic based on the presence of the regional D_2 fabric and the contained and peripheral hydrothermal alteration. The porphyritic texture and fine-grained groundmass of the gabbro porphyry sill suggests that it was emplaced in a partially crystalline state and cooled rapidly. The gabbro may represent a reservoir for basaltic lavas up-section (perhaps in the Upper Member of the Ely Greenstone), but a lack of lithogeochemical data from this sill precludes an unambiguous interpretation. Further lithogeochemical work is needed in order to determine the role this intrusion may have played in the generation of mafic volcanic rocks up section.

Basaltic Diabase (*unit DbSS*, "Soudan Sill")

A laterally continuous basaltic diabase sill crops out in the central and northeast quarter-section of Section 27, and can be mapped along strike for approximately 2000 m through the northwest quarter-section of Section 26 and the southeast quarter-section of Section 23 (Plate 1). The unit is dominantly bounded by banded iron formation (US4a). This unit was mapped by Sims and Southwick (1985) as basalt and banded iron formation (US1, 4). The sill ranges in thickness from 20-350 m. However, the original thickness is difficult to estimate in the western part of the field area due to the regional deformation of this unit. Sharp contacts occur with adjacent units, including felsic lapillistone and breccia deposits (US2b), felsic tuff deposits (US2c), banded iron formation (US4a), chlorite schist (5e) and Peterson and Patelke's (2003) schist n' BIF unit (Plate 1). The contact with diabase (undifferentiated) was not observed in the field and is therefore inferred. Outcrops are relatively large, abundant and create steep jagged terrain.

In outcrop, diabase is massive, fine-grained, red-orange in color and has <1- 10 m diameter xenoliths of laminated to thinly bedded banded iron formation. Basaltic diabase is dominantly fine-grained, so modal mineral percentages were not estimated in the field. Locally, mineralized zones contain 1-3 mm green euhedral chlorite, and 1-15mm concentrations of disseminated pyrite and chalcopyrite. Petrographic analysis was not conducted for this unit.

The Soudan Sill lacks physical and contact features consistent with extrusive volcanism. Therefore, these rocks are not basalt flows as previously interpreted by Sims and Southwick (1985) and Peterson and Patelke (2003). Due to the fine-grained nature of this intrusion, it likely crystallized at a shallow, hypabyssal depth, and cooled rapidly.

When comparing lithogeochemical data for the Soudan Sill with lithogeochemical data from Upper Ely basalts (data from Southwick et al., 1998), both sets of samples are relatively depleted in the light rare earth elements (LREE). The tectonic discrimination diagram (after Pearce and Cann, 1973) suggests that the Soudan Sill plots in the within-plate to MORB field, and the Upper Ely Basalts plot in the MORB field. Therefore, the Soudan Sill is interpreted as a feeder for lava flows in the Upper Ely Member of the Ely Greenstone Formation.

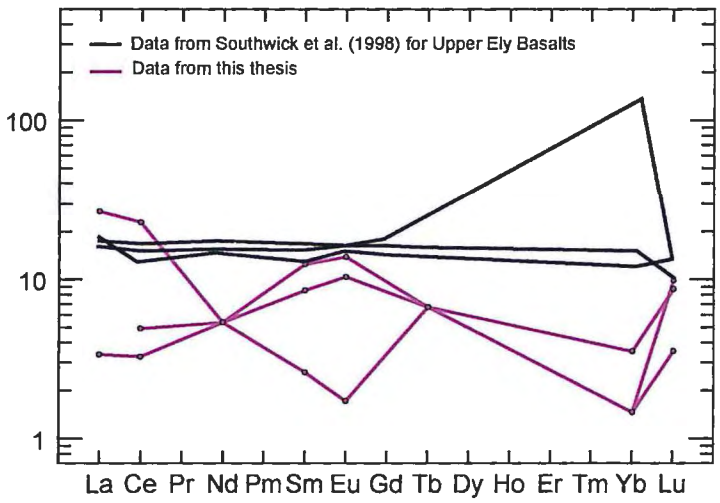

Figure 2.75. Notice the depletion in the light rare earth elements (LREE) in both the Soudan Sill and Upper Ely Basalts. Upper Ely data from Southwick et al. (1998). Concentrations in parts per million.

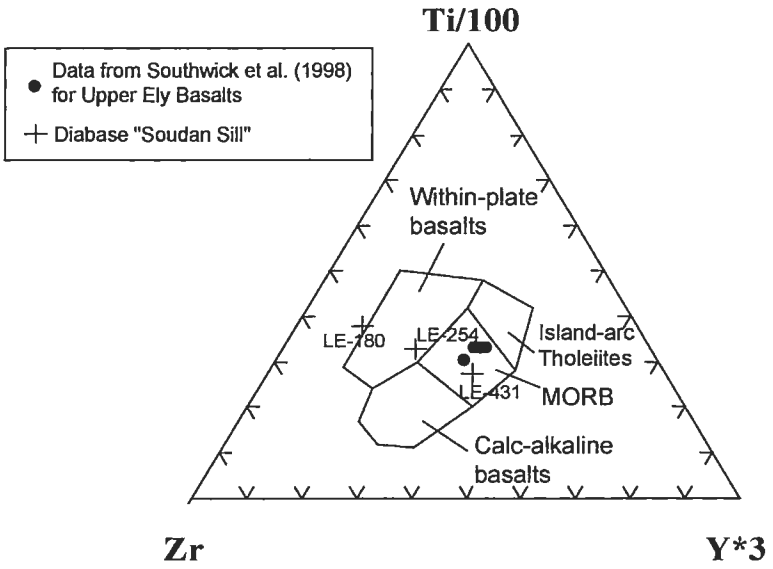

Figure 2.76. The Ti-Zr-Y discrimination diagram for basalts (after Pearce and Cann, 1973). Comparison between the Soudan Sill and Upper Ely basalts. Data for Upper Ely basalts from Southwick et al. (1998). The Soudan Sill plots in the Within-plate to MORB field, and the Upper Ely Basalts plot in the MORB field. Concentrations in parts per million.

Intermediate Intrusive Rocks

Six samples of intermediate intrusive rocks from the field area were analyzed. Five samples (LE-028, LE-160, LE-230, LE-321, LE-349) of intermediate dikes and one sample (LE-064) of dioritic xenolith (in unit DbU) were analyzed. Compositional classifications for intermediate intrusive rocks in the Soudan area were determined using relatively immobile trace elements (Zr, TiO2, Nb, Rb) (Winchester and Floyd, 1977; Pearce et al., 1984) and indicate that intrusive rocks plot as diorites and syeno-diorites that formed in a volcanic-arc setting (Figures 2.77 and 2.78).

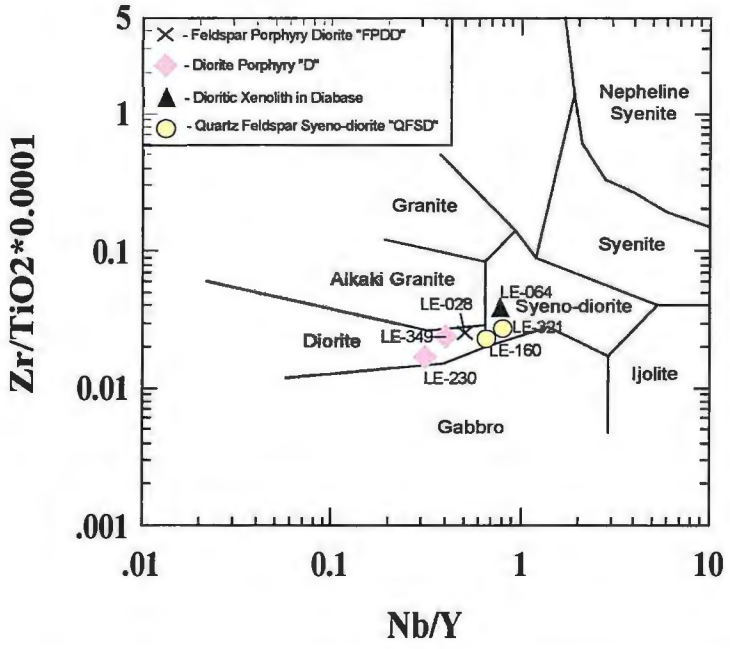

Figure 2.77. Immobile element classification for intermediate intrusive rocks near the Soudan Mine (after Winchester and Floyd, 1977).

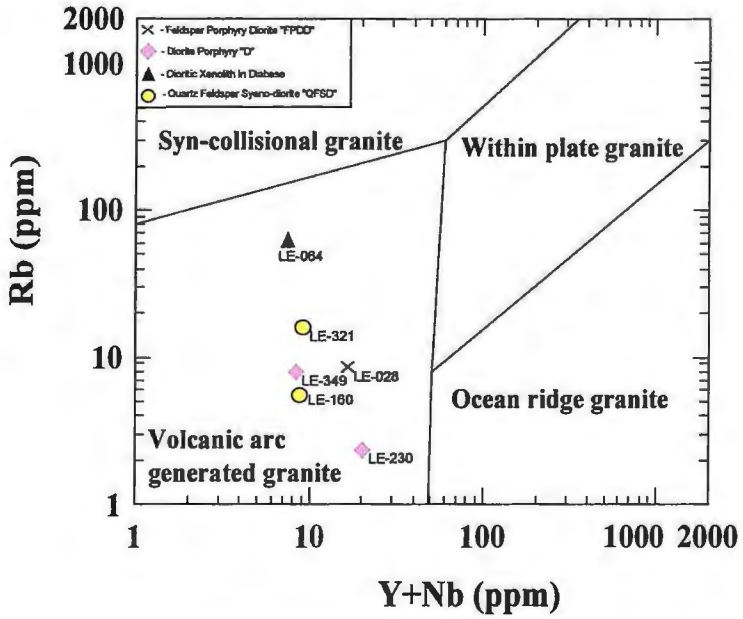

Figure 2.78. The Rb-(Y + Nb) discrimination diagram for granites (after Pearce et al., 1984). Intrusive rocks plot as volcanic-arc generated granites. Concentrations in parts per million.

A relative enrichment of light rare earth elements (LREE) and middle rare earth elements (MREE) is depicted on chondrite normalized and primitive mantle normalized rare earth element spider diagrams (Figure 2.79 and 2.80). These data suggest that diorite and syeno-diorite have a fractionated calc-alkaline trend and have geochemical signatures that are consistent with rocks that formed in an arc setting (e.g. negative Nb anomaly). This signature is consistent with rocks that formed by crystal fractionation in a magma chamber. Crystal fractionation enriches the existing liquid phases in the more incompatible elements (LREE).

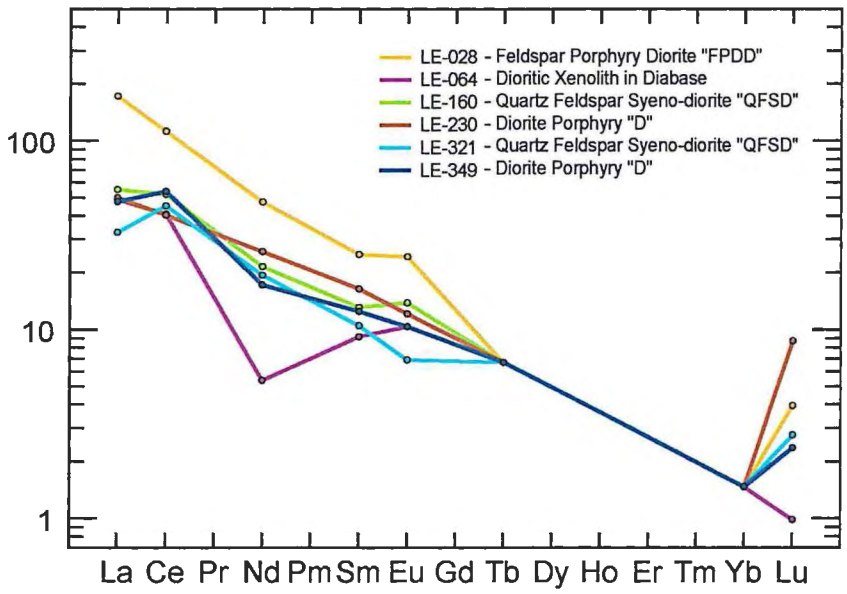

Figure 2.79. Rock vs. chondrite rare earth element spider diagram (after Sun and McDonough, 1989) for intermediate intrusive rocks in the Soudan Mine study area.

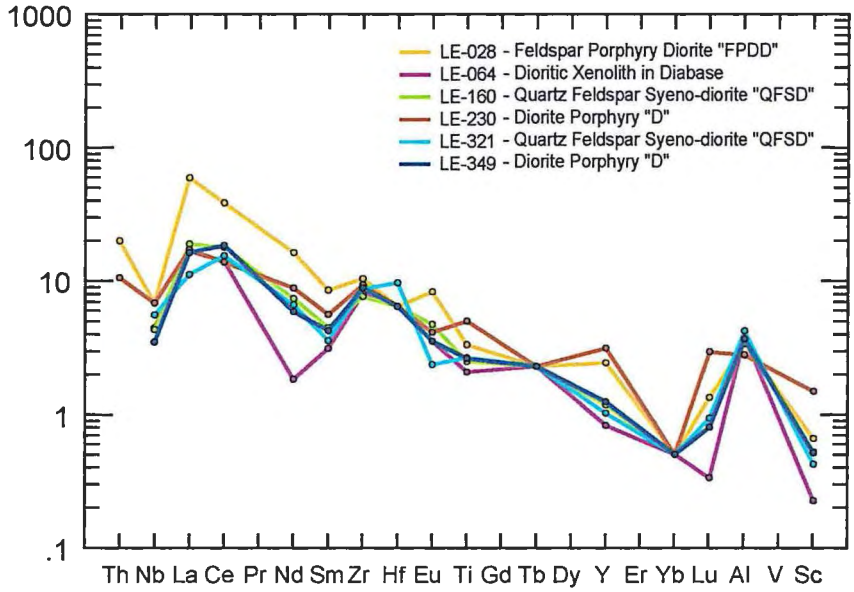

Figure 2.80. Rock vs. primitive mantle rare earth element spider diagram (after Sun and McDonough, 1989) for intermediate intrusive rocks in the Soudan Mine study area. Notice the enrichment of the LREE and the negative Nb anomaly typically associated with a volcanic-arc environment.

Diorite Porphyry (*unit D*)

Diorite Porphyry intrusions occur in the Fivemile Lake and Central Basalt Sequences. They occur as both isolated sill-like bodies and as cross-stratal dikes in the southwest, southeast, and northeast quarter-sections of Section 25, and in the northeast, northwest and southeast quarter-sections of Section 26. Sills can be mapped along strike for 200-500m and are 40-200 m thick. Dikes are generally <1-2m thick and occur in one outcrop so vertical continuity is difficult to establish. Sharp contacts with adjacent units include intrusive rocks (Gb) and pillowed and foliated lavas (CB1b, CB1i, FM1b, FM1i). Contacts with other adjacent units (5e, FM2c) were not observed in the field and are therefore inferred. Outcrops are generally small, narrow and form hilly terrain.

In outcrop, diorite porphyry sills and dikes are gray to light blue-gray and have fine-medium grained phenocrysts set in an aphyric groundmass. Diorite porphyry sills and dikes are composed of approximately 65% phenocrysts and 35% groundmass. Phenocrysts comprise approximately 40% 1-2mm subhedral well-dispersed plagioclase, 15% 1-2mm anhedral well-dispersed quartz and 10% <1-1.5mm euhedral well-dispersed orthoclase. Groundmass is dominantly aphyric so modal percentages were not estimated in the field. Quartz veins (<1%, 1-8 mm wide) are common. A poorly-developed D_2 oriented fabric is present; well-developed foliation is absent in these rocks.

Petrographic analysis on one sample (LE-230) indicates that diorite porphyry dikes are composed of 60% phenocrysts and 40% groundmass. Phenocrysts are composed of 30% 1-1.5 subhedral to euhedral well-dispersed albite plagioclase, 25% 1-1.5mm anhedral well-dispersed quartz (which also occurs in 1-2mm quartz + carbonate veins) and 5% <1-1mm subhedral to euhedral well-dispersed orthoclase. Groundmass comprises 16% 1-1.5 mm subhedral actinolite crystals that may be pseudomorphing relict hornblende crystals, 8% <1-1.5mm crystal aggregates of epidote that dominantly pseudomorph plagioclase, 8% <1-1mm anhedral to subhedral Mg-chlorite clots, 4% <1mm anhedral to subhedral Fe-chlorite clots and 4% <1mm anhedral Fe-carbonate blebs. Locally 1-2 mm quartz + carbonate veins are present.

Small diorite intrusions are interpreted to be synvolcanic in nature do to the presence of a slight east-west trending fabric and the presence of secondary minerals associated with seafloor hydrothermal alteration. These rocks may represent feeder dikes and sills for andesite lavas in the upper part of the Fivemile Lake and the Central Basalt Sequences.

Feldspar Porphyry Diorite Dikes (*unit FPDD*)

Feldspar porphyry diorite dikes occur in the south-central, southwest and southeast quarter-section of Section 26, and the northeast quarter-section of Section 25. Feldspar porphyry diorite dikes are 1-8 m wide and generally can be correlated across one or two outcrops. This makes vertical continuity (with respect to bedding) difficult to establish. Sharp contacts between adjacent units include intrusive rocks (DbSM) and pillowed lavas (CB1b). Contacts with volcanic units (CB1b, FM1b, FM1i) and contacts with fault bounded units (5b, 5e) were not observed and are therefore inferred. Outcrops are typically narrow and form gently sloping terrain.

In outcrop the dikes are white-gray, fine-medium grained, plagioclase- and hornblende-phyric, and locally contain 1-9 cm sigmoidal quartz and crystalline chlorite veins (Figure 2.81). Feldspar porphyry diorite dikes contain approximately 65% phenocrysts and 35% aphyric groundmass. Phenocrysts comprise 50% 1-4 mm subhedral to euhedral well-dispersed plagioclase feldspar and 10% 1-2 mm subhedral well-dispersed hornblende crystals, secondary minerals include 5% 1-2 mm anhedral well-dispersed chlorite aggregates and <1% 1-2 mm well-dispersed anhedral epidote which appears to pseudomorph primary plagioclase. Due to the fine-grained nature of the groundmass, modal mineral percentages were not estimated in the field. A poorly developed structural fabric exists that is consistent with the regional D_2 deformation. Petrographic analysis was not conducted for this unit.

Based on the presence of D_2 fabric and orientation with respect to volcanic bedding, feldspar porphyry diorite dikes are interpreted to be syn-volcanic with respect to the Ely Greenstone Formation. Lithogeochemical similarities between these

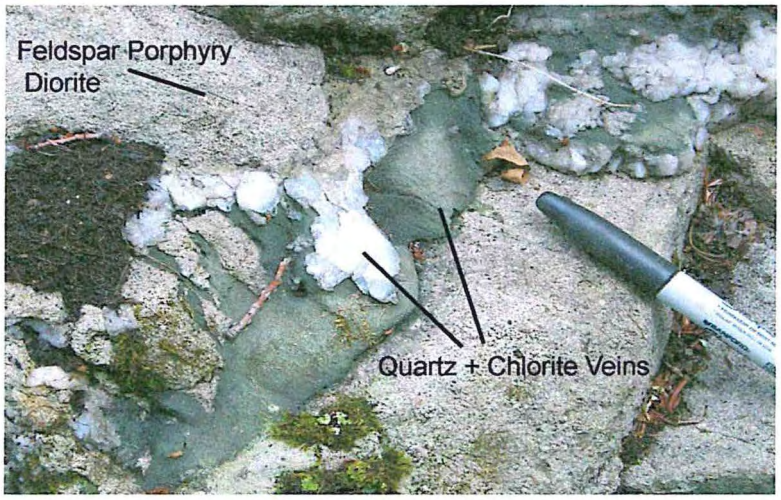

Figure 2.81. Feldspar porphyry diorite dike with 3-5 cm wide cross-cutting quartz + chlorite vein. Quartz and chlorite probably formed from upwelling hydrothermal fluids associated with the D_2 deformation (Peterson and Patelke, 2003). Black pen cap is 4 cm for scale. Outcrop 329.

dikes (LE-028) and basalt and andesite lavas in the Central Basalt Sequence (see REE plots), suggests that these dikes may be the feeders for volcanic rocks up-section.

Quartz Feldspar Syeno-Diorite Porphyry Dikes and Sills (unit QFSD)

Quartz feldspar syeno-diorite porphyry occurs within a sill and dike complex in the northeast quarter-section of Section 26, southeast-quarter-section of Section 23, and northwest quarter-section of Section 25 (Plate 1). Dikes dominantly trend to the north-northwest (320°-340°), and vary in width from 1-4 meters. Sill-like bodies can be mapped along strike for 180m, and vary in thickness from 12-50m. These rocks show a poorly developed regional D_2. Sharp contacts between adjacent units include mafic lava flows (CB1a, CB1b, Figure 2.82 and 2.83) and banded iron formation (CB4a). Contacts between other adjacent units (CB2b) were not observed and are therefore inferred. Outcrops are generally subrounded to narrow and are associated with hilly terrain.

In outcrop, syeno-diorite dikes are white to gray, and are plagioclase-, quartz-, orthoclase- and hornblende-phyric. Phenocrysts are fine- to medium-grained and set in an aphyric groundmass. Phenocrysts comprise approximately 40% and groundmass comprises approximately 60% of the rock. Phenocrysts comprise approximately 20% 1-4mm well-dispersed subhedral plagioclase crystals, 5% 1-4mm well-dispersed anhedral quartz crystals, 5% 1-2 mm anhedral to subhedral well-dispersed orthoclase crystals and 5% 1-3 mm subhedral well-dispersed hornblende crystals. Modal percentages for the aphyric groundmass was not estimated in the field. Randomly oriented quartz veins are common (<1%, 1-2mm).

Figure 2.82. Irregular contact relationship between basalt and quartz feldspar porphyry syeno-diorite dike. Notice the very sharp contact between these two units. Hammer 20 cm for scale. Outcrop 005.

Petrographic analysis on four samples (LE-008, LE-313, LE-321, 335) indicates that syeno-diorite dikes are porphyritic and composed of 65-80% groundmass and 20-35% phenocrysts. Phenocrysts comprise 2-25% 1-4mm anhedral to subhedral

plagioclase; 3-10% 1mm anhedral to subhedral well-dispersed orthoclase; 10% 1-4 mm subhedral well-dispersed quartz crystals; and 8% <1-3 mm tabular subhedral to euhedral hornblende crystals. The groundmass comprises 6-70% <1mm anhedral recrystallized quartz groundmass; <1-25% <1mm anhedral aggregates of Mg-chlorite; 16% <<1-1mm anhedral to subhedral well-dispersed hornblende; 2-15% <1-1.5 mm anhedral to subhedral platy sericite crystals (which commonly pseudomorph plagioclase and orthoclase); 8-10% <1-2mm anhedral to subhedral Fe-carbonate crystals and patches (which occur within the groundmass and also occur pseudomorphing plagioclase); 4-10% <1-1mm anhedral epidote (which occurs as fine grained crystals pseudomorphing plagioclase and as <1mm anhedral semi-opaque spherical aggregates). Also present are anhedral needle-like aggregates of actinolite (8%, <1mm) that pseudomorphs hornblende; 8% <<1-1mm subhedral to euhedral plagioclasE; 6% <1mm anhedral crystal patches of Fe-chlorite; 2% <1mm anhedral local sphene crystals; <1% <1-1mm subhedral local clinozoisite crystals; and <1% <1mm anhedral opaque minerals. Randomly oriented quartz and carbonate veins (<1-2% 1-3mm) cross-cut the primary and secondary mineralogy.

Syeno-diorite porphyry intrusions in the Central Basalt Sequence are interpreted to be syn-volcanic dikes that occupied syn-volcanic structures. These dikes appear to have intruded between the late stages of mafic and intermediate volcanism of the Central Basalts Sequence, and the beginning of low temperature chemical deposition of the Soudan Iron Formation, based on the following observations: 1) the most intense

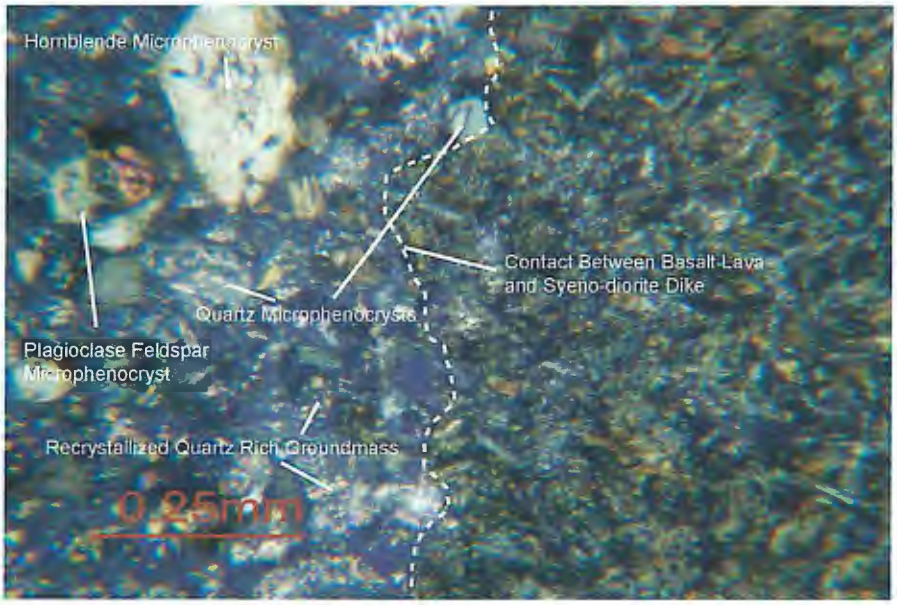

Figure 2.83. Photomicrograph of syeno-diorite intruding an epidote altered basalt in the Central Basalt Sequence. Notice the hornblende, plagioclase and quartz microphenocrysts. Contact relationship is sharp and irregular. Field of view 1mm. Cross-polarized light. LE-008.

hydrothermal alteration in the Central Basalt Sequence occurs proximal to, and concentrated within, zones where these dikes most frequently occur; 2) the morphology and variable thickness of dikes (their pinch- and swell-nature) suggests that the earlier formed structures may have been jagged fissures (Figure 2.82); and 3) there are no dikes in the Soudan Member, directly above this dike swarm. The presence of heavy impermeable iron formation may have helped the upwelling magma sill out along pre-existing mafic volcanic bedding planes.

Sheared Rocks (5x)

Sheared rocks occur as dominantly east-west trending, curvilinear bands of schist and phyllite that contain a diverse series of alteration minerals (Plate 1, Figure 2.78).

Peterson and Patelke (2003) have described three structural shear types in the field area. These include: 1) S-tectonites, with anastomozing bands composed of flattened sigmoidal domains with wrapping foliation and shear bands, or S-C structures; 2) L-tectonites, with pervasive lineation and local foliation; and 3) LS-tectonites, with both strong and pervasive foliation and lineation, the most common of the three. Geographic Information Systems (GIS) analysis performed on the study area map indicates that sheared rocks make up approximately 7% of the field area.

Sheared rocks have been interpreted by Peterson and Patelke (2003) as being formed during the late stages of the regional D_2 deformation event. Sheared rocks are part of two major sub-parallel structures (the Murray Shear Zone and Mine Trend Shear Zone) that displace rocks from west to east. Structural analysis by Peterson and Patelke (2003) indicate that large rock wedges were displaced approximately 7-14 kilometers respectively. For a thorough description of sheared rocks in the Soudan Mine area, see Peterson and Patelke (2003).

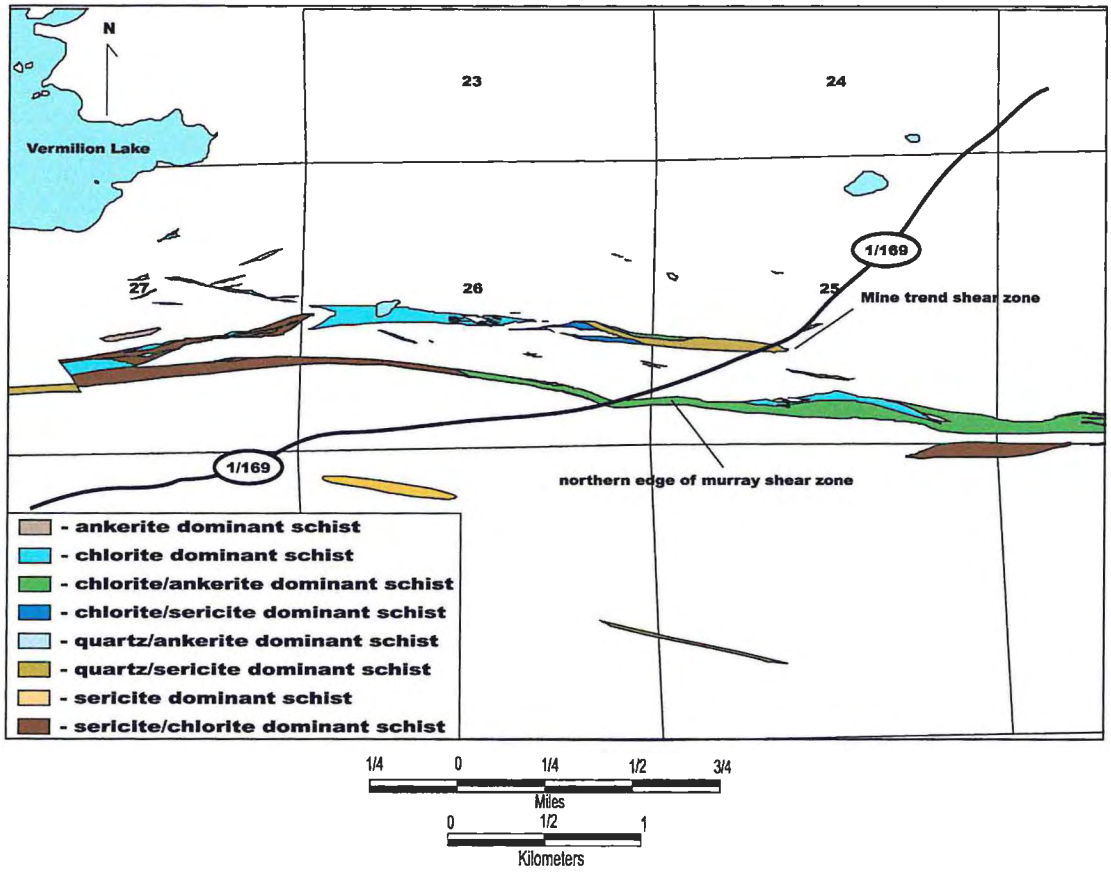

Figure 2.84. Location and mineralogy of sheared rocks in the Soudan Mine area after Peterson and Patelke (2003).

Chapter 3

HYDROTHERMAL ALTERATION DISTRIBUTION AND MINERAL ASSEMBLAGES

Introduction

Hydrothermal alteration is a complex, evolving, physical and chemical process involving mineralogical, chemical and textural changes that result from the interaction of aqueous fluids and adjacent rocks (Pirajno, 1992). According to Rose and Burt (1979), the main factors that control alteration processes are: 1) the nature of the wall rocks; 2) the composition of the fluids; and 3) the concentration, activity and chemical potential of the fluid components (e.g. H^+, CO_2, O_2, K^+, and S_2 etc.). Experimental work summarized by Seyfried et al. (1999) also suggests that fluid-rock ratios are extremely important in determining the final products of hydrothermal alteration.

The distribution and composition of alteration mineral assemblages in the study area reflects initial differences in rock bulk composition, primary and structurally induced permeability, water/rock ratios, and the compositions and temperatures of the altering fluids (Hudak, 1996). Economic geologists recognize the spatial relationships between alteration mineral assemblages and associated mineralization, and therefore, these alteration zones may provide useful guidance in the exploration for hydrothermal ore deposits (Franklin et al., 1981).

A detailed study of alteration assemblages using petrographic methods and field mapping at a 1:2000 scale was conducted for this thesis. The study area was selected for three reasons: 1) the Ely Greenstone has been regionally metamorphosed to greenschist grade through *in-situ* convective fluid/rock interaction; 2) the presence of banded iron

formation, provides evidence that hydrothermal systems existed in the area; and 3) hydrothermal-derived semiconformable and cross-cutting zones containing anomalous amounts of epidote, quartz, chlorite, actinolite, albite, sericite, carbonate, magnetite and garnet occur in the field area. Understanding the spatial distribution of alteration mineral assemblages in the study area allows a more accurate definition of various fluid transport zones, and may ultimately provide targets for future mineral exploration. Hydrothermal alteration processes and products must be evaluated and understood in order to develop efficient exploration methodologies for hydrothermal-associated ore deposits (Woodall, 1993).

Alteration Types

Rocks in the Soudan Mine area have experienced regional greenschist facies metamorphism and local to regional scale hydrothermal alteration. In general, the alteration minerals that were formed from these two processes are similar. Therefore, it is important to distinguish between regional greenschist facies mineral assemblages and true hydrothermal alteration (Hovis, 2001). This can be done by examining the textures and temporal relationships between greenschist facies minerals and the host rocks.

Regional Metamorphism:

Mineral assemblages formed from regional greenschist facies metamorphism are characterized by rocks containing non-anomalous concentrations of chlorite, albite, actinolite and epidote (Winter, 2001). Rocks that contain mineral abundances consistent with greenschist-facies metamorphism are classified as "least-altered" in this thesis.

Hydrothermal Alteration:

Hydrothermal mineral assemblages are believed to form at temperatures between 200-500°C (Pirajno, 1992). Morton and Franklin (1987), Gibson et al. (1999) and Franklin et al. (2005) subdivide hydrothermal alteration mineral assemblages into two types: 1) regional semi-conformable alteration zones which consist of upper and lower regimes; and 2) discordant "pipe-like" alteration zones.

Semi-conformable alteration zones occur hundreds of meters to many kilometers lateral to, and/or below, primary VMS targets (Franklin et al., 2005). The upper convective zone comprises large volumes of seawater circulating through the upper part of the hydrothermal system. The lower convective zone is comprised of evolved or modified seawater circulating through the capped lower part of the hydrothermal system. The evolved or modified seawater obtains heat and metals from the surrounding volcanic rocks (Franklin et al., 2005). These zones represent the products of large scale fluid/rock interaction within regional hydrothermal systems that commonly develop in the footwall rocks of VMS deposits (Gibson et al., 1999).

Discordant alteration occurs in disconformable zones that are laterally restricted, and generally occur below areas of anomalous sulfide mineralization (Gibson et al., 1999). These alteration zones form within regions of cross-stratal permeability where hot, hydrothermal fluids travel buoyantly toward the seafloor. Metal-rich moderately acidic high temperature (>300C°) hydrothermal fluids eventually dump metal sulfides as they rapidly cool and/or are neutralized at the water/seafloor interface (Franklin, 1996; Franklin et al., 2005). Discordant alteration zones are generally restricted to synvolcanic structures that control focused hydrothermal flow and discharge (Morton and Franklin, 1987; Gibson et al., 1999).

Alteration mineral assemblages that are similar to those present at Neoarchean VMS deposits are present in the Soudan Mine area. These assemblages can occur in veins or amygdules, and/or as patchy to pervasive replacement of volcanic and plutonic rocks. Pervasive and patchy replacement is both mineralogically and texturally destructive. Disconformable chlorite-epidote-garnet-magnetite-bearing mineral assemblages are recognized as the products of ancient pipe-like hydrothermal alteration processes in the Soudan Mine area.

Classification Method

Following petrographic analysis, percentages for each mineral present in a given sample were entered into the "Sample.shp" theme table in the inherited DUSEL (Peterson and Patelke, 2003) GIS database. This made data evaluation easy by sorting and querying modal mineral percentages within the table. Various hydrothermal alteration zones were classified by the modal mineral assemblage present. The distinct mineral assemblage was then assigned an alteration code.

Numerous alteration classification schemes (Hudak et al., 2002b; Santaguida, 1999) were evaluated in the Soudan Mine area, and a classification scheme similar to that of Hovis (2001) was applied in this study. The alteration mineral assemblage classification scheme used for this thesis is a derivative of that developed at the Eagles Nest VMS prospect. Alteration codes are listed in Table 3.01 and are described below. Figure 3.01 represents the distribution of the various alteration mineral assemblages in the Soudan Mine area.

Alteration Type	Mineral Abundance	Approximate Temperature of Mineral Formation in Hydrothermal Systems
0: Least-altered	<35% of common hydrothermal minerals consistent with regional greenschist facies metamorphism	260-430°C
1a: Epidote ± Quartz 1b: Mottled Epidote ± Quartz	Epidote 30-70%, Actinolite <30%	300->400°C
2: Quartz ± Epidote	Quartz 30-75%, Epidote <20%	150->400°C
3: Actinolite ± Epidote ± Quartz	Actinolite 30-50%, Epidote >10%	300-400°C
4: Mg-Chlorite ± Quartz ± Sericite	Mg-Chlorite 25-40%, Quartz >15%, Sericite <40%	80-350°C
5: Actinolite ± Epidote ± Garnet ± Magnetite	Actinolite >20%, Garnet 0-55%, Magnetite 0-15%	~400°C
6: Fe-Chlorite ± Quartz ± Sericite	Fe-Chlorite 25-55%, Quartz 30-40%, Sericite <15%	350-400°C
7: Sericite ± Quartz	Sericite > 35%, Quartz <50%	80-300°C

Table 3.01. Alteration types, mineral abundances and approximate temperatures of mineral formation recognized in the Soudan Mine area. Approximate temperature of mineral formation in hydrothermal systems is based on geochemical studies after Mottl and Seyfried (1980), Seyfried and Janecky (1985), Seyfried and Ding (1995), Seyfried et al. (1999) and Balangue-Tarriela (2004)

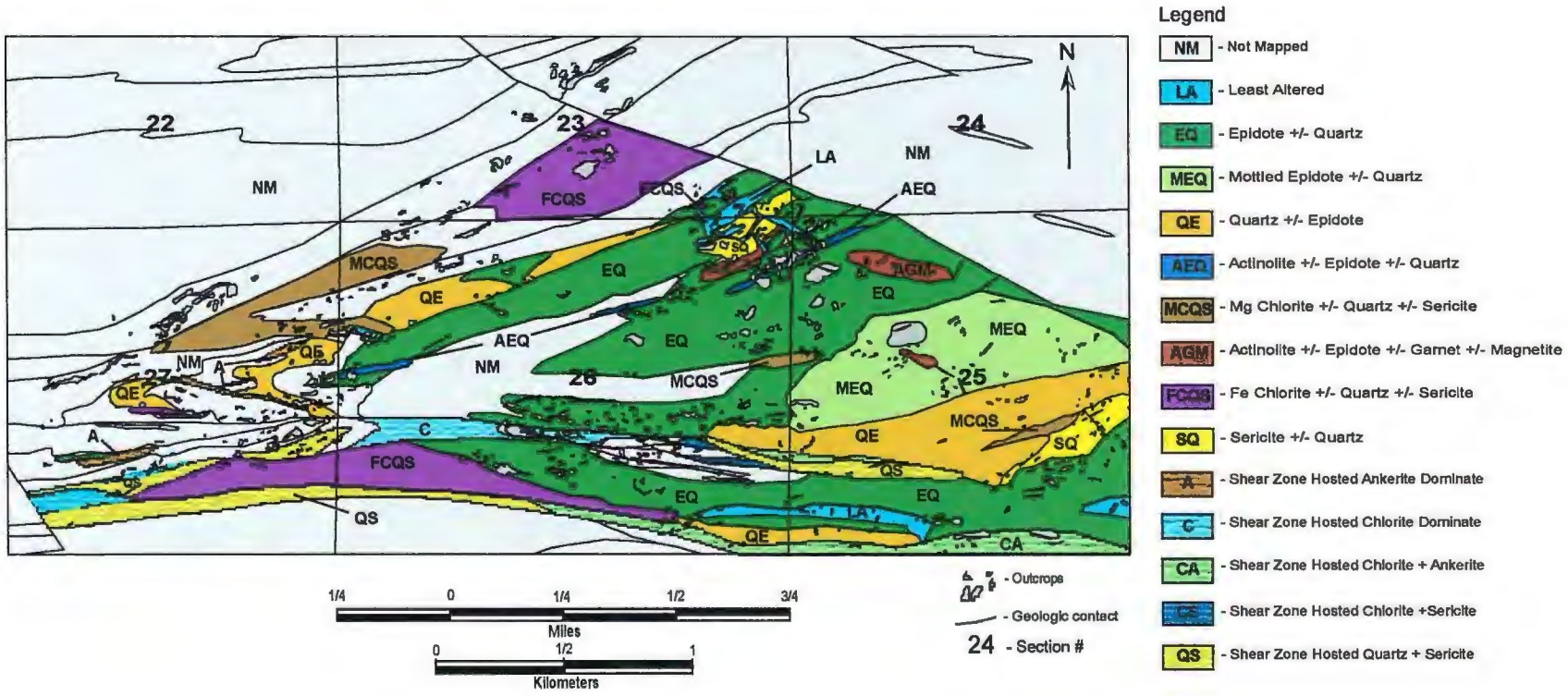

Figure 3.01. Alteration map of hydrothermal mineral assemblages found in the Soudan Mine area.

Descriptions of Alteration Mineral Assemblages

Least-Altered Assemblage (Alteration Code "0")

Least-altered rocks were recognized in the field by the presence of textures and mineral assemblages consistent with greenschist-facies metamorphism of their primary compositions. The least-altered assemblage occurs in coherent basalts, andesites, and in some cross-stratal dikes and sills throughout the field area. In basalts, the least-altered assemblage is green to black in color, whereas it is gray to black in least-altered andesites. Classification of the rocks was verified by petrographic analysis wherever possible.

In thin section, least-altered rocks (LE-227) contain approximately 35% <1-2mm well-dispersed subhedral to euhedral felty albite, <<1 mm anhedral to subhedral well-dispersed actinolite lathes, up to 30% <1mm anhedral patchy aggregates of epidote that commonly pseudomorphs plagioclase and occurs in the groundmass, 15% <1-1mm well-dispersed anhedral sericite crystals, 10% < 1mm anhedral to subhedral well-dispersed to localized concentrations of Fe-chlorite and 10% <1mm anhedral well-dispersed polygonal quartz groundmass (Figure 3.02).

The textures present in least-altered rocks appear to be similar to the textures present in their primary igneous equivalent. These include the presence of felty albite and fine-grained groundmass that are common in basalt and andesite lava flows. Least-altered rocks have been described in more detail in the previous chapter.

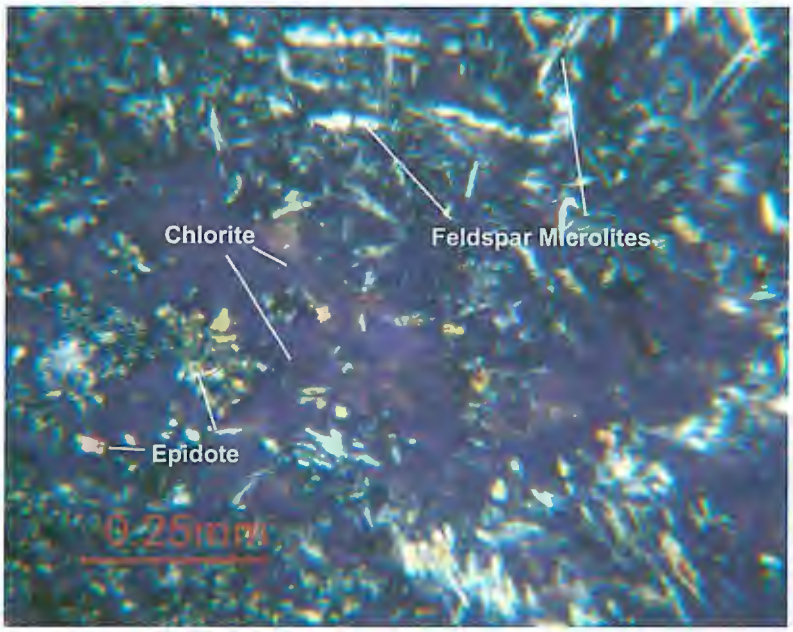

Figure 3.02. Photomicrograph of least-altered basalt from the Fivemile Lake Sequence. Plagioclase microlites gives the host rock a felty texture. Chlorite and disseminated quartz and epidote comprise the groundmass. Cross-polarized light. Field of view 1 mm. LE-372.

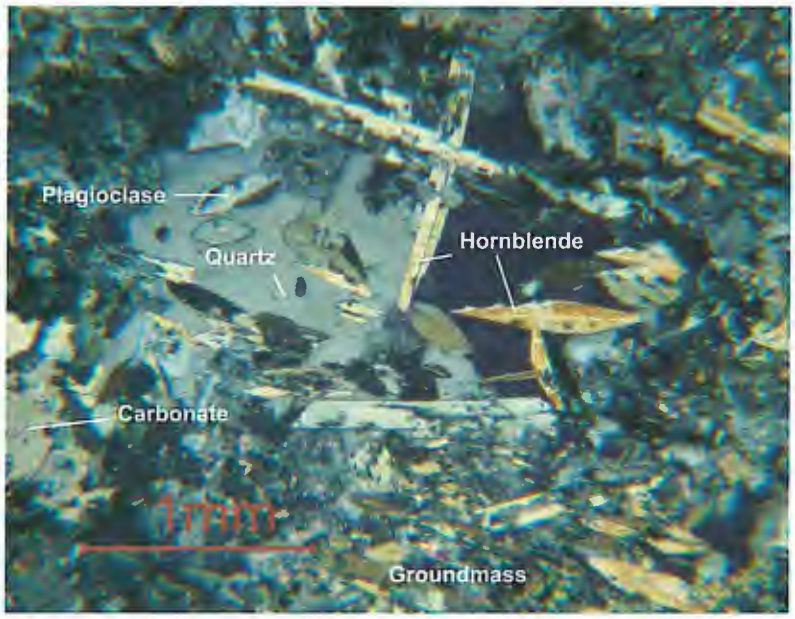

Figure 3.03. Photomicrograph of least-altered quartz feldspar syeno-diorite porphyry intrusion. Cross-polarized light. Field of view 3 mm. LE-313.

Epidote ± Quartz Assemblage (Alteration Code "1a")

The epidote ± quartz alteration assemblage encompasses rocks that contain 30-70% epidote, 5-45% quartz and less than 30% actinolite. The assemblage occurs in mafic and intermediate volcanic and plutonic rocks located primarily in the Fivemile Lake and Central Basalt Sequences in Sections 25 and 26 of the field area (Figure 3.01). The epidote ± quartz assemblage occurs adjacent to the mottled epidote ± quartz (1b), quartz ± epidote (2), sericite ± quartz (7) and actinolite ± epidote ± quartz (3) assemblages, and is adjacent to shear zone hosted alteration (C and CA) by means of faulting (Figure 3.01).

In outcrop, the epidote + quartz assemblage is characterized by 35-70% variable dark green and light blue-gray randomly oriented epidote, which occurs as a) <1-2 mm well-dispersed anhedral to subhedral crystal masses that pervasively alter the interiors of pillow lavas; b) alteration along joint surfaces; c) open space fillings such as amygdules; and d) in 1-1.5mm parallel cross-stratal epidote + quartz veins. Milky white quartz (30-40%) occurs as disseminated groundmass. Dark-green to black, randomly-oriented, 1-2mm subhedral actinolite lathes (5-25%) are disseminated and appear to be interstitial. Anhedral 1-3mm chlorite crystals occur as crystal aggregates (5-20%). Modal percentages for secondary aphyric minerals were not estimated in the field. Epidote ± quartz alteration is commonly cut by 1-2 mm wide white-tan-green epidote + quartz veins.

In thin section, the epidote ± quartz assemblage appears to have a fine-grained diffuse groundmass that is overprinted by patchy epidote. The most common alterations in this assemblage are saussuritization, uralitization, chloritization and seritization. Modal mineral percentages comprise 35-70% <1-2mm anhedral to subhedral epidote

crystals and crystal aggregates occur as localized 1-3 mm patches that overprint the groundmass; 5-54% <1-1mm well-dispersed anhedral recrystallized quartz groundmass; 5-25% <1-2mm well-dispersed subhedral actinolite lathe aggregates that may pseudomorph olivine or pyroxene; 15-20% <1-1mm well-dispersed anhedral Fe-chlorite crystals and crystal aggregates; 15-20% <1-1mm anhedral to subhedral Mg-chlorite crystals; 2-10% <1-1mm subhedral to euhedral localized clinozoisite crystals; 2-5% <1-2mm anhedral well-dispersed Fe-carbonate blebs; 2-5% <1mm well-dispersed platy sericite crystals that may pseudomorph fine-grained plagioclase; and 2% <1mm well-dispersed disseminated opaque minerals. 1-3mm epidote + quartz veins are comprised of 80% 1-3mm euhedral epidote crystals and <1-1mm subhedral interstitial quartz crystals (Figure 3.04). Where modal epidote concentration are <50%, crystalline epidote is more common and quartz is amorphous or present in a fine-grained crystalline groundmass (Figure 3.05). Where modal epidote is >50%, fine-grained, brown-colored grungy epidote masses are most common. Other minerals can be difficult to identify due to the intensity of this alteration. In gabbroic rocks, anhedral actinolite pseudomorphs relict pyroxene phenocrysts. Actinolite also commonly occurs in the interior of hyaloclastite. Chlorite composition ranges from magnesium- to iron-rich. Fe-rich chlorites were identified by the presence of purple to blue birefringence and Mg-rich chlorites were identified by the presence of brown to grey birefringence (Hey, 1954). Carbonate mineralization appears to overprint most other minerals and is interpreted to be secondary. Sulfide and oxide minerals occur only in trace amounts in this assemblage.

The epidote ± quartz alteration assemblage at Soudan is interpreted to represent a large-scale, semi-conformable alteration zone formed by hydrothermal fluids migrating

through deep seafloor aquifers. Similar semi-conformable zones have been documented to the east by Peterson (2001), Hudak et al. (2002a), Hudak et al. (2002b), and Hovis (2001) near the Fivemile Lake, Needleboy-Sixmile Lake and Eagles Nest areas, respectively. The semiconformable alteration near Soudan may form the western extension of the semi-conformable alteration found in the Fivemile Lake-Eagles Nest-Needleboy Lake-Six mile Lake areas, or may represent a separate semiconformable zone that occurs only in the vicinity of the Soudan Mine. Further mapping will be necessary to better constrain this interpretation.

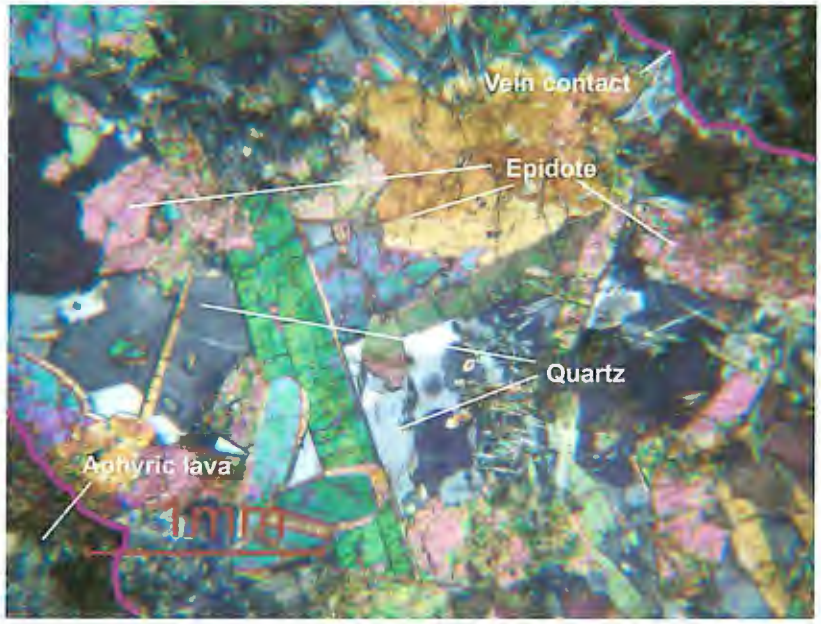

Figure 3.04. Photomicrograph of epidote ± quartz altered massive lava from the Central Basalt Sequence. Three millimeter epidote + quartz vein outlined in magenta. Cross-polarized light, field of view 3 mm. LE-154.

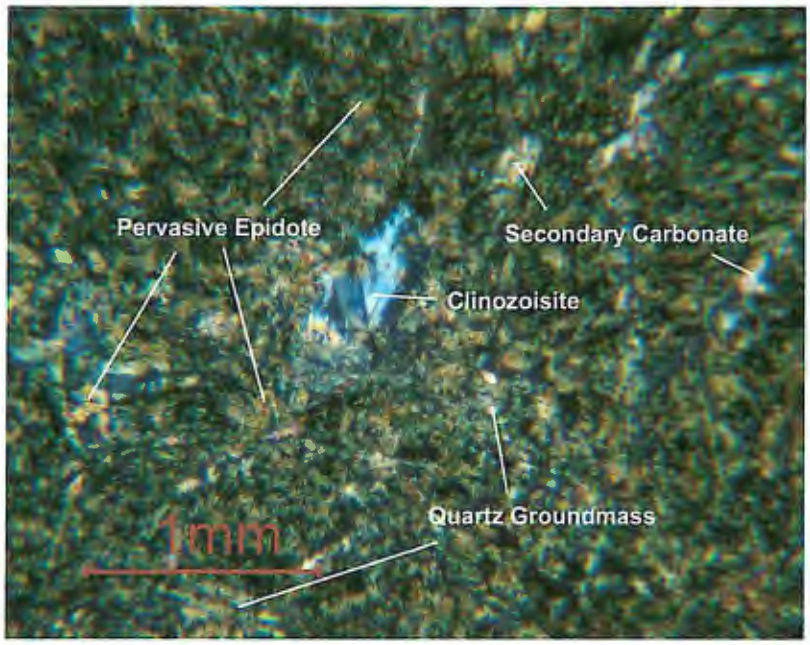

Figure 3.05. Photomicrograph of epidote ± quartz altered diabase (Sugar Mt. Diabase). Notice 1mm blue clinozoisite crystals and all encompassing epidote crystals. Cross-polarized light. Field of view 3 mm. LE-032.

Mottled Epidote ± Quartz Assemblage (Alteration Code "1b")

The mottled epidote ± quartz alteration assemblage comprises rocks containing 30-70% coarse epidote with <30% coarse actinolite and 2-10% quartz. This assemblage occurs in the central portion of Section 25 within mafic and intermediate pillowed and massive lavas of the Central Basalt Sequence. This alteration is approximately 500m thick and can be mapped along strike for approximately 1.5km (Figure 3.01). Adjacent alteration units include the epidote ± quartz (1a), quartz ± epidote (2), and the actinolite ± epidote ± garnet ± magnetite (5) assemblages.

In outcrop, the mottled epidote + quartz assemblage is characterized by 6-40 cm subrounded to amoeboid shaped patchy alteration zones that replace the interiors of pillows and interpillow hyaloclastite. This patchy alteration comprises 50-70% light

apple-green to dark yellow-green <1-2mm epidote crystals; 10-20% dark green to dark blue <1-2mm subhedral to euhedral actinolite porphyroblasts set in a <1mm dark blue soft chlorite-rich groundmass; and 10-20% pink-tan subhedral well-dispersed but locally patchy silicified zones that comprise <1-1mm secondary quartz. Interpillow hyaloclastite is altered to variable amounts of epidote, chlorite and actinolite. Due the fine-grained nature of secondary minerals in interpillow hyaloclastite, modal percentages were not estimated in the field. North-northwest trending cross-stratal veins up to 1 cm wide are composed of variable amounts of chlorite + epidote, quartz + chlorite, and quartz + carbonate.

Figure 3.06. Typical field appearance of mottled epidote + quartz alteration. Notice the 10-40cm zones of patchy epidote, quartz and actinolite + chlorite. Outcrop 331.

In thin section the mottled epidote ± quartz assemblage comprises 50-70% <<1-2mm well-dispersed subhedral epidote crystals (which also occurs in cross-stratal veinlets); 15-30% 1-2 mm subhedral to euhedral crystal lathes and <1mm lathe aggregates of actinolite; 10% <<1mm anhedral euhedral Mg-chlorite crystals; 10% 1mm anhedral to subhedral albite plagioclase lathes; 2-10% <1mm anhedral polygonal quartz crystals that occurs as fine-grained well-dispersed and locally concentrated groundmass; 2% <1mm anhedral platy sericite crystals that occur in the groundmass and pseudomorph fine-grained plagioclase; 1-2% <1-1mm anhedral Fe-carbonate blebs; and 2% 1-3mm wide veins of <1% zoisite + quartz + sericite + actinolite + Fe-carbonate. In general, epidote overprints the other secondary minerals present. In thin section, interpillow hyaloclastite comprises 35% <<1mm mostly subhedral to euhedral actinolite lathes, 30% <1-<<1mm subhedral to euhedral epidote crystals, 8% <<1mm-1mm euhedral Fe-carbonate crystals, 5% <<1mm anhedral local Fe-chlorite crystals, 2% <1mm subhedral clinozoisite crystals and 1% 1-1.5mm subhedral sub-cubic pyrite crystals. Chlorite and actinolite typically alter the interior of angular devitrified glass shards and epidote typically alters the rims of angular devitrified glass shards (Figure 3.07).

Based on the mottled appearance in the field, the large amount of epidote in the rocks, and the close spatial relationship between the assemblage and the synvolcanic Sugar Mt. Sill, the mottled epidote ± quartz assemblage may represent a more intense (higher temperature, higher water/rock ratio) epidote + quartz alteration than the (1a) assemblage. Patchy alteration probably resulted from the variable permeability in pillowed and massive lava flows. Hudak et al. (2006) have noted similar patchy epidote + quartz alteration zones immediately southeast of Six-Mile Lake. These zones clearly

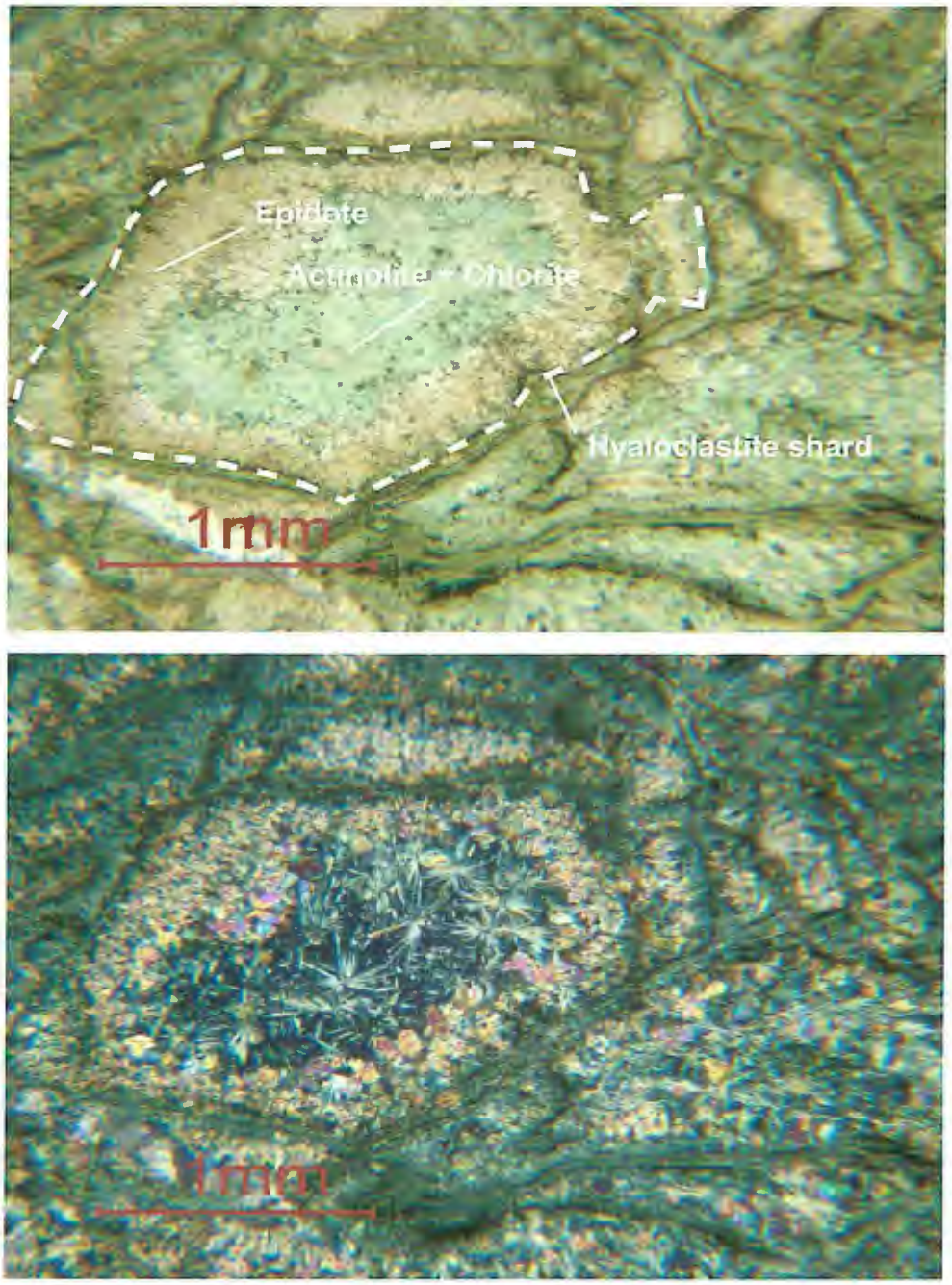

Figure 3.07. Photomicrograph of epidote + actinolite + chlorite alteration of interpillow hyaloclastite from pillow basalt (Central Basalt Sequence) in plane- and cross-polarized light (mottled epidote ± quartz assemblage). Mafic glass shards have a zoned actinolite + chlorite rich center, and epidote rich selvage. Field of view is 3 mm. LE-437.

formed from localized high temperature hydrothermal alteration associated with a small, sill-driven hydrothermal system.

Quartz ± Epidote Assemblage (Alteration Code "2")

The quartz ± epidote alteration assemblage comprises rocks containing 30-75% quartz and <20% epidote. This assemblage occurs in felsic volcaniclastic rocks in the northwest and northeast-central quarter-sections of Sections 26 and 27, directly below the Sugar Mountain Sill in the Fivemile Lake Sequence andesites and above the northern edge of the Murray Shear Zone in the southwest and southeast quarter-sections of Sections 25 and 26 respectively (Figure 3.01). Adjacent alteration units include the epidote ± quartz assemblage (1a), and the Fe-chlorite ± quartz ± sericite assemblage (6). The Mg-chlorite ± quartz ± sericite assemblage (4), chlorite + ankerite assemblage (CA), ankerite assemblage (A) and sericite + quartz assemblage (SA) locally occur within shear zones adjacent to or within the quartz ± epidote assemblage. The quartz ± epidote assemblage comprises felsic and mafic rocks that are silicified.

In outcrop, quartz ± epidote altered rocks are typically light gray to light green, although locally they may have a pink and orange tint. The quartz ± epidote assemblage comprises rock that contain approximately 50-75% <<1mm anhedral well-dispersed milky white quartz, 15-20% <1-2mm anhedral well-dispersed epidote crystal aggregates and 10-15% subhedral well-dispersed plagioclase crystals. The aphyric nature of the groundmass restricted accurate modal estimations in the field. In mafic rocks the alteration is patchy. Pillow cores locally appear to be intensely altered and interpillow

hyaloclastite is generally silicified. Locally, quartz ± epidote altered rocks are cut by up to 1cm wide quartz + epidote veins.

Figure 3.08. Typical field appearance of patchy quartz + epidote alteration of pillowed lavas in the Fivemile Lake Sequence. Locally the pillow interiors appear to be more intensely altered. Pen is 14 cm for scale. Outcrop 562.

The quartz ± epidote alteration assemblage comprises rocks that contain 35-70% <<1-3 mm anhedral quartz that occurs as fine-grained polygonal quartz groundmass or occurs as 3 mm interstitial well-dispersed anhedral crystals. Anhedral well-dispersed 1-2mm epidote (15%) occurs as semi-opaque crystal aggregates and well-dispersed anhedral crystals. Other minerals present include 8-15% <1mm well-dispersed anhedral platy sericite crystals that pseudomorph plagioclase; up to 25% 1-2mm subhedral plagioclase crystals; 14% <1mm anhedral Mg-chlorite crystals; 8% <<1mm anhedral to subhedral well-dispersed actinolite lathes; 10% <1mm anhedral Fe-chlorite crystals; and

2% well-dispersed sub-cubic opaque minerals. The identification of primary and secondary minerals was difficult because of the intense quartz overprinting.

The quartz ± epidote assemblage is interpreted to represent a large scale semi-conformable alteration zone related to the epidote ± quartz assemblage. This assemblage may be part of a larger regional alteration zone identified ~5km to the east that has been documented by Peterson (2001) and Hudak et al. (2002b).

Actinolite ± Epidote ± Quartz Assemblage (Alteration Code "3")

The actinolite ± epidote ± quartz assemblage is composed of rocks that contain 30-50% actinolite, and up to 40% epidote. This assemblage occurs primarily in pillowed basalt lavas in the Central Basalt Sequence (Figure 3.01). This alteration assemblage defines a 50 meter thick semiconformable zone that occurs immediately south of the syeno-diorite dike swarm in the northeast quarter-section of Section 26 and northwest quarter-section of Section 25 (Figure 3.01). A single outcrop containing this assemblage also occurs in the gabbroic intrusion in the west-central portion of Section 26. This alteration assemblage occurs adjacent to the epidote ± quartz assemblage (1a).

In outcrop, the actinolite ± epidote ± quartz assemblage is dark black with an orange hue. It occurs within pillow interiors as a pervasive alteration. The assemblage comprises approximately 40% <1-3mm well-dispersed randomly oriented subhedral to euhedral acicular actinolite lathes, and 40% <1-2mm anhedral local patchy epidote aggregates that are set in 10% <<1mm well-dispersed pervasive milky white anhedral quartz groundmass. Pillow selvages and interpillow hyaloclastite are altered to a dark

green to blue very fine-grained actinolite (60%) + chlorite (35%) with larger (<1-2mm) patches of secondary carbonate (~5%).

In thin section, the actinolite ± epidote ± quartz assemblage comprises 35-40% <1-1.5mm subhedral to euhedral well-dispersed acicular actinolite lathes and occurs as 1-2 mm euhedral lathe aggregates that pseudomorph pyroxene, 10-40% <1-2mm anhedral semi-opaque spherical epidote aggregates and 1-3mm patchy crystal aggregates, and 2-30% <1mm anhedral polygonal quartz groundmass (Figure 3.09). Accessory minerals include 5-10% <1-1mm anhedral to euhedral albite plagioclase crystals, 4-10% <1mm subhedral to euhedral tabular well-dispersed Fe-chlorite crystals, 5-8% <1-1mm anhedral to subhedral well-dispersed Mg-chlorite crystals, 2-3% <1-1mm anhedral to euhedral Fe-carbonate crystals, 3% 1-3mm euhedral local crystal masses of zoisite, 2% <1mm subhedral limonite staining, 2% <1mm anhedral well-dispersed platy sericite crystals and 1% <1-1mm local clinozoisite crystals.

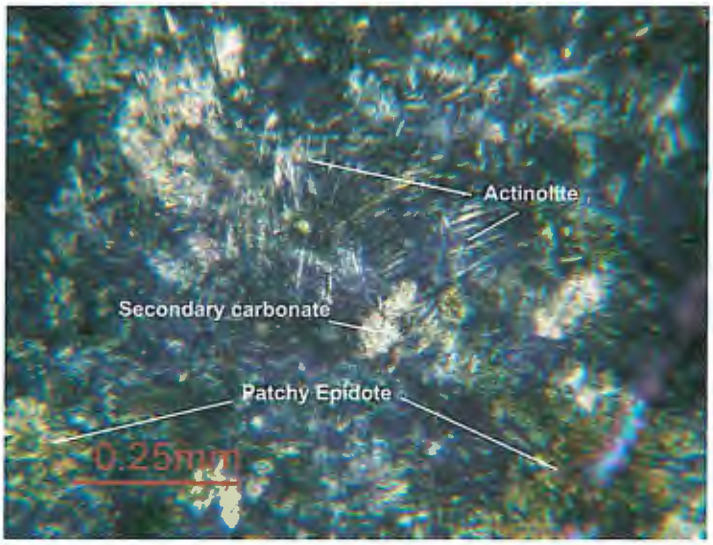

Figure 3.09. Photomicrograph of actinolite ± epidote ± quartz altered pillow basalt (Central Basalt Sequence). Notice intense patchy actinolite and epidote overprinted by iron-carbonate. Cross-polarized light. Field of view 1mm. LE-217.

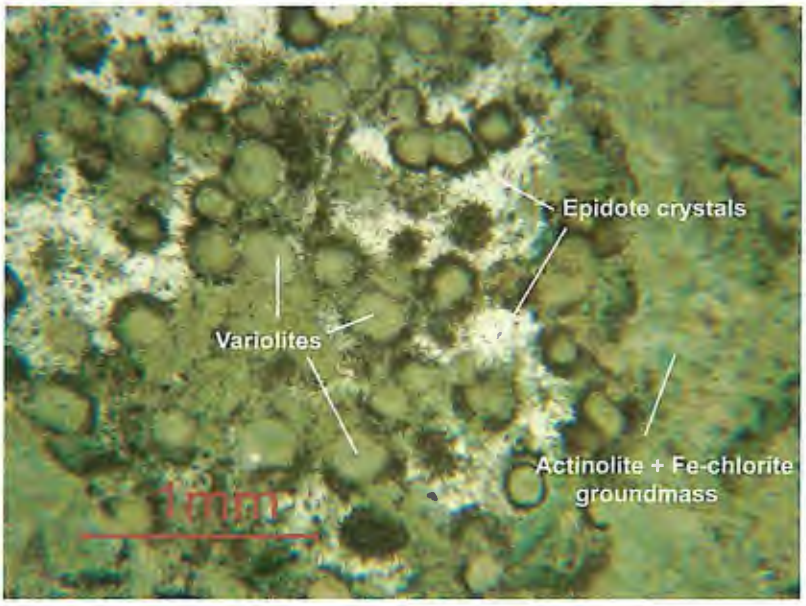

Figure 3.10. Photomicrograph of intense actinolite ± epidote ± quartz alteration in pillow basalt margin (Central Basalt Sequence). Round objects are interpreted to be varioles derived from quench induced crystallization (Cas and Wright, 1987; Fowler et al., 2001). Plane-polarized light. Field of view 3mm. Sample 007.

1-3mm cross-stratal actinolite + epidote rich veins contain equal proportions of 1-3mm euhedral epidote and <1-1mm felty actinolite lathes. Economic sulfide and/or oxide mineralization has not been recognized within this assemblage.

Disconformable actinolite-rich alteration zones occur in the footwall to sub-economic base-metal enriched exhalite deposits immediately northeast of Fivemile Lake (Peterson, 2001; Hudak et al., 2002b). At the present time, the spatial distribution of the semiconformable zones in the Soudan Mine area are poorly constrained due to lack of exposure. The relationship to potential economic or sub-economic VMS mineralization remains poorly understood.

Mg-chlorite ± Quartz ± Sericite Assemblage (Alteration Code "4")

The Mg-chlorite ± quartz ± sericite assemblage comprises mafic volcanic, mafic intrusive and felsic volcanic rocks with anomalous concentrations of magnesium-rich chlorite (25-40%), and lesser amounts of quartz (up to 35%) and sericite (up to 40%). This assemblage occurs primarily in the western portion of the Soudan Sill in the northwest and northeast quarter-sections of Section 26 and 27 respectively. The assemblage also occurs in the Central Basalt Sequence in the east-central portion of Section 26 and in the central portion of Section 25 in felsic volcanic rocks. Adjacent units include the least-altered assemblage (0), epidote ± quartz assemblage (1a), quartz ± epidote assemblage (2) and the sericite ± quartz assemblage (7).

In the field, the Mg-chlorite ± quartz ± sericite assemblage is dominantly aphyric. The rocks are generally gray, massive and have <1-2% disseminated pyrite and <1-2% disseminated anhedral well-dispersed hematite. Fractured surfaces display fine-grained recrystallized quartz that gives the rock a sugary texture. Due to the aphyric nature of the rocks, modal mineral percentages were not estimated in the field. The identification and distribution of alteration assemblage (4) was only possible via petrographic analysis because of the difficulties of distinguishing Mg-rich chlorite and Fe-rich chlorite in the field.

In thin section, the Mg-chlorite ± quartz ± sericite assemblage comprises 25-40% <1mm well-dispersed anhedral Mg-chlorite stringers that are <1-2mm wide; 25-35% <<1-1mm anhedral, well-dispersed recrystallized polygonal quartz groundmass; and 25-40% <<1mm anhedral patchy sericite which is typically closely associated with the quartz-rich groundmass and commonly pseudomorphs plagioclase crystals. Accessory

minerals include 2-20% <1mm anhedral, well-dispersed interstitial albite plagioclase lathes; 1-10% <1mm anhedral to subhedral well-dispersed Fe-chlorite crystals; 1-8% 1-2mm anhedral to subhedral well-dispersed Fe-carbonate crystals; 5% <1mm well-dispersed anhedral semi-opaque spherical aggregates of epidote, which also occurs as <1-1mm subhedral crystal aggregates and locally up to 3% <1mm anhedral opaque minerals (Figure 3.11). Locally, 15% 1-5mm amygdules are present consisting of variable amounts of Mg-chlorite + Fe-carbonate.

Accumulations of magnesium-rich chlorite are believed to form as a result of cool seawater drawn down that occurs in the upper part of low temperature, semiconformable zones on the seafloor. However, disconformable zones containing Mg-chlorite ± sericite also locally occur in the footwalls to VMS deposits (Franklin et al., 2005).

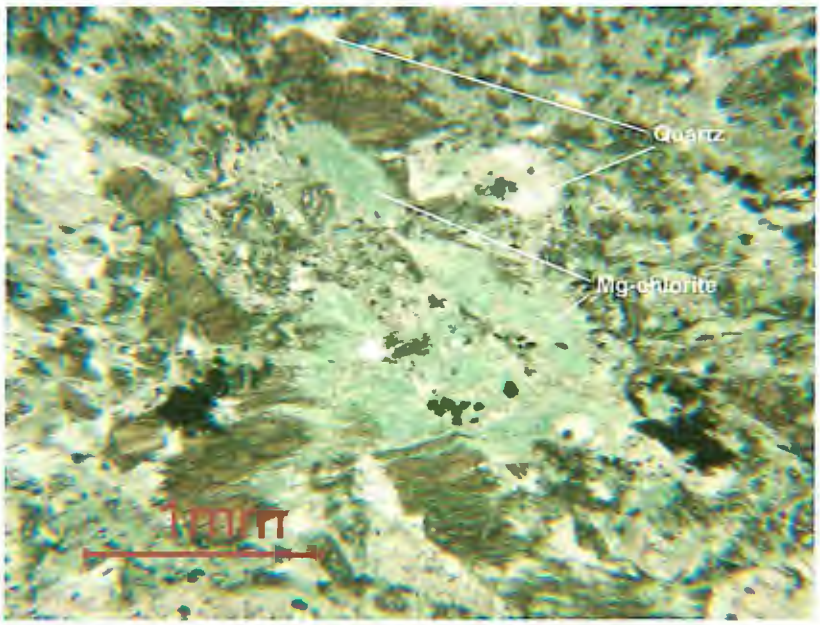

Figure 3.11. Photomicrograph of light green, stinger-like to pervasive Mg-chlorite alteration in pillow basalt (Central Basalt Sequence). Brown-orange mineral with high relief is locally concentrated subhedral epidote. Plane-polarized light. Field of view is 3mm. LE-003.

Actinolite + Epidote ± Garnet ± Magnetite Assemblage (Alteration Code "5")

The actinolite + epidote ± garnet ± magnetite assemblage occurs exclusively in basalt lava flows in the Central Basalt Sequence, and comprises rocks that contain an actinolite (up to 30%), epidote (up to 30%), garnet (up to 55%), and magnetite (up to 15%) assemblage. This discordant assemblage is located in the southeast quarter of Section 23, the central and northwest quarter of Section 25, and the northeast quarter of Section 26 (Figure 3.01). Adjacent alteration assemblages include the least-altered assemblage (0) by means of faulting, and the epidote ± quartz assemblage (1a), mottled epidote ± quartz assemblage (1b), and sericite ± quartz assemblage (7).

In the field, rocks with this alteration assemblage have a light- to dark-apple green tint. This assemblage comprises rocks that have approximately 30-50% 1-6mm local subhedral garnet porphyroblasts that occupy open spaced fillings such as interpillow hyaloclastite, 1-3mm subrounded amygdules, 1-6 cm long and 2-6 mm wide pipe vesicles and 20cm long and 2cm wide veins. Epidote (30%, 1-3mm) occurs as subhedral well-dispersed porphyroblasts. Fe-chlorite occurs as stringers (5-10%, 1-5mm wide), and anhedral magnetite crystals (15-20%, 15mm) occupy open space fillings within interpillow hyaloclastite, veins, vesicles, and locally occurs in the interiors of pillows (Figures 3.13. and 3.14.). Subhedral to euhedral pyrite (4%, 1-2mm) is closely associated with garnet. Fine-grained minerals were not estimated in the field. Field evidence suggests that garnet and magnetite mineralization is hydrothermally controlled and cross-cuts stratigraphy causing 1-4 cm breccia zones that contain 1-3 cm angular jigsaw puzzle fit clasts.

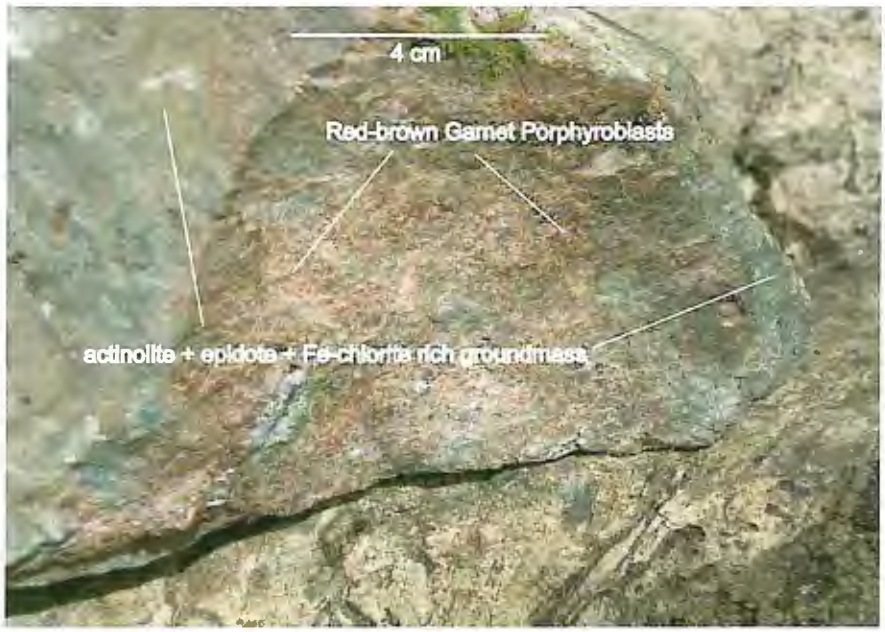

Figure 3.12. Red-brown cross-cutting garnet mineralization in actinolite + epidote altered basalt in the Central Basalt Sequence. 4 cm bar for scale. Outcrop 087.

Figure 3.13. Magnetite mineralization in fissure, hammer 68 cm for scale. Hammer represents the general strike of pillow lavas at this location. Outcrop 301.

Figure 3.14. Field appearance of magnetite replacing interpillow hyaloclastite. Outcrop 404.

In thin section, this assemblage comprises 25-55% <1-6mm subhedral to euhedral locally concentrated garnet porphyroblasts, 6-30% <<1-1mm subhedral to euhedral tabular actinolite crystals and local 1-2mm crystal lathe aggregates, 8-35% <<1-1mm subhedral well-dispersed crystal epidote aggregates and 1mm subhedral crystals, 5-20% <1-2mm anhedral well-dispersed quartz crystals, 8-20% <<1mm anhedral to subhedral well-dispersed Fe-chlorite crystals (which may also occur as locally concentrated crystal aggregates), and 15% 2-15mm zones of anhedral magnetite that appears to fill 1-3mm cross-stratal veinlets. Accessory minerals include 5-15% 1-4mm subhedral to euhedral Fe-carbonate, which occurs as well-dispersed blebs and in 1-2mm cross-cutting veinlets, as well as 4% non-magnetic anhedral well-dispersed opaque minerals and 1-2% <<1mm anhedral sericite crystal lathes. Approximately 15% of the rock contains 1-2mm wide cross-stratal veinlets that comprise dominantly quartz + carbonate veins that are cut by epidote + actinolite + magnetite veins. Locally breccias have a jigsaw puzzle fit

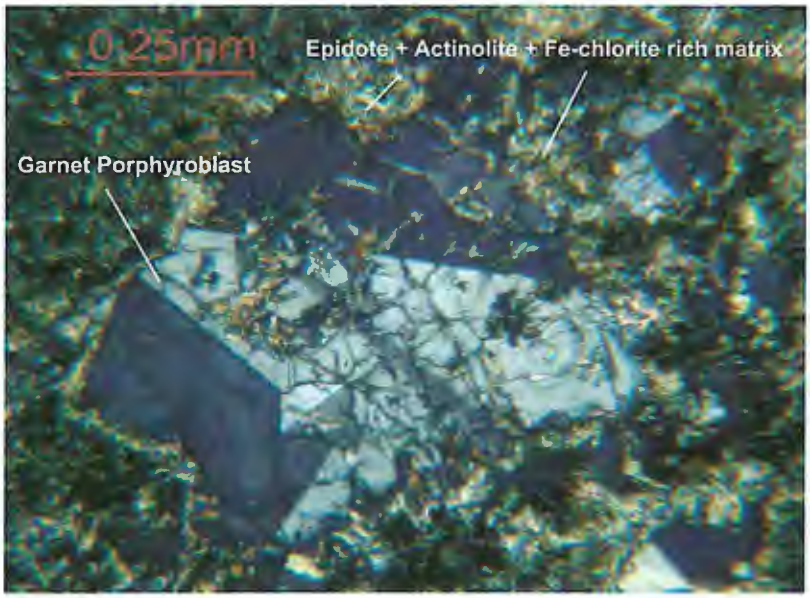

Figure 3.15. Garnet porphyroblast in actinolite + epidote altered basalt (Central Basalt Sequence). Note the weak birefringence of the garnet porphyroblast. Cross-polarized light. Field of view 1mm. Sample 222.

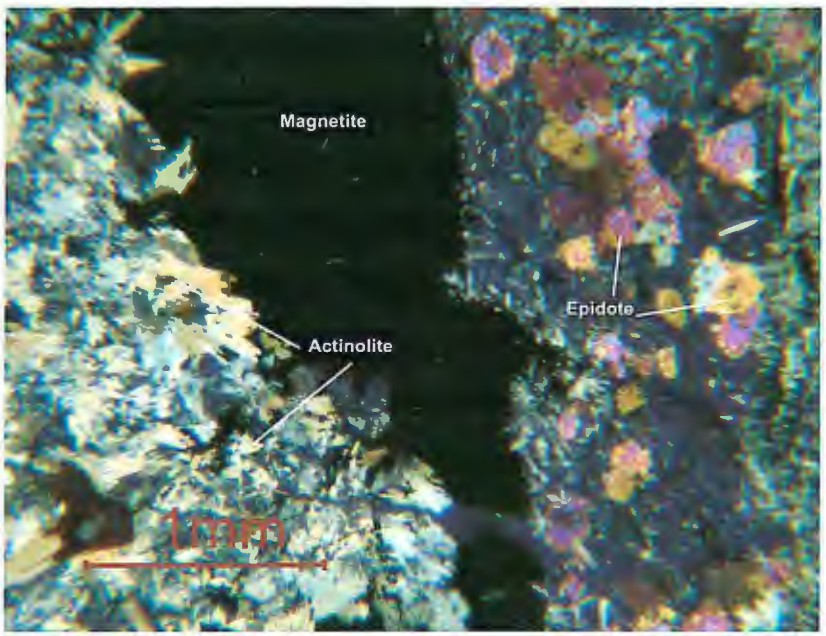

Figure 3.16. Magnetite vein cross-cutting tabular actinolite + epidote altered basalt (Central Basalt Sequence). Cross-polarized light. Field of view 3mm. Sample 401.

texture and are healed by epidote + actinolite. These breccias may have developed via hydrofracturing of the rock during alteration. All primary textures appear to have been destroyed during the development of this alteration assemblage. Phillips and Griffin (1981) suggest that garnets that show weak birefringence are typically of the ugrandite variety. Hudak (pers. comm.) has completed x-ray diffraction analysis of the garnets and indicates a composition of andradite.

Based on field evidence and petrographic data, the actinolite + epidote ± garnet ± magnetite assemblage is interpreted to represent the product of metasomatism involving iron-rich hydrothermal fluids. The development of garnet and magnetite may or may not have resulted from the subsequent regional metamorphism of the lower Ely Greenstone Formation. Similar garnet alteration has been noted by Hudak et al. (2002a, 2002b) near Six Mile Lake. X-ray analysis and SEM analysis indicates the garnets in this zone are andradite ($Ca_3Fe_2Si_3O_{12}$). Further work is needed on garnet and magnetite in the Soudan area to constrain their temporal relationship to the iron ores. If garnet and magnetite are primary, their presence may provide some clues to the relative temperature of the hydrothermal fluids that moved through the wall rocks. Schlatter (2005) indicates that intense chlorite + garnet alteration occurs immediately below the A and D ore lenses in the Petiknas south volcanic-hosted massive sulfide deposit in the Skellefte District, Sweden.

Fe-chlorite ± Quartz ± Sericite Assemblage (Alteration Code "6")

The Fe-chlorite ± quartz ± sericite assemblage comprises rocks that contain 25-55% Fe-chlorite, 30-40% quartz and <15% sericite. This assemblage occurs in foliated

lavas in the Fivemile Lake Sequence, the Soudan Sill, and in basalt lava flows in the southeast quarter-section of Section 23 in the Central Basalt Sequence (Figure 3.01). Adjacent alteration assemblages include the epidote ± quartz (1a) and quartz ± epidote (2), as well as local shear zone hosted alteration assemblages containing sericite + quartz (SC), chlorite + ankerite (CA) and chlorite (C).

In outcrop, Fe-chlorite ± quartz ± sericite assemblage occurs in broad semiconformable zones, as well as in pipe-like discordant zones (Figure 3.17 and 3.18). Semiconformable chlorite alteration initially was not identified in the field, but abundant chlorite-rich alteration was observed during petrographic studies. Discordant, pipe-like, chlorite-rich alteration was mapped in the field and occurs near the dike swarm within the upper Central Basalt Sequence (Figure 3.01, Plate 1) in two distinct morphologies: 1) disconformable braided chlorite stringers, with individual braids approximately 2-10cm wide (Figure 3.17.); and 2) 25-40cm wide linear "pipe-like" zones where 1-2 cm epidote-rich margins encompass a chlorite-rich core (Figure 3.18.). Both trend at approximately 130°, approximately perpendicular to the volcanic stratigraphy in this location. Discordant alteration comprises 50-60% <1mm patchy Fe-chlorite, 15% <1-1mm epidote (which occurs as 1-4 cm patchy alteration and in 1-2 cm wide healed fractures), 15% <1-1mm anhedral zoisite crystals which occur as subrounded patches in the core of the alteration pipe, and 1-5 cm patchy quartz + sericite alteration. Modal mineral percentages in the quartz and sericite rich patches were not estimated in the field due to the fine-grained nature of the minerals. Within discordant alteration zones <1% <1-1mm subhedral disseminated pyrite and chalcopyrite occurs in 1-3mm cross-stratal sulfide veins.

Figure 3.17. Outcrop appearance of Fe-chlorite ± quartz ± sericite alteration in the Central Basalt Sequence. Dark green areas represent crosscutting chlorite alteration, whereas gray-white colored areas represent patchy quartz + sericite alteration of mafic lava. Boot 5 cm thick for scale. Outcrop 192.

Figure 3.18. Alteration pipe crosscutting spherulitic rhyolite in Central Basalt Sequence. Green areas are chlorite- and epidote-rich. Contact strikes at approximately 130°. Outcrop 226.

Poor outcrop distribution limits further field documentation of the discordant alteration in the southeast quarter of Section 23.

Petrographic observations indicate that the Fe-chlorite ± quartz ± sericite assemblage comprises 50% <1mm-1cm wide Fe-chlorite stringers, 40% <1mm fine-grained recrystallized quartz groundmass, 20% <1mm well-dispersed anhedral disseminated epidote, 20% local anhedral Fe-carbonate blebs, 12% subhedral finely-disseminated sericite that pseudomorphs plagioclase, 2% subhedral local felty plagioclase microlites and 2% <1mm local subhedral clinozoisite.

The Fe-chlorite ± quartz ± sericite alteration assemblage is interpreted to represent a synvolcanic, generally discordant alteration formed by buoyant hydrothermal fluids that moved upward toward the seafloor in synvolcanic structures (e.g. fault zones) or zones of increased permeability. The mineralogy of this assemblage is typical of "pipe-like" alteration zones found beneath VMS deposits at the Noranda VMS camp in Quebec (Gibson, 1989; Santaguida et al., 1999), as well as many other lava flow dominated Precambrian VMS deposits (Morton and Franklin, 1987; Gibson et al., 1999). However, the relatively small size and discontinuous nature of this alteration differs from the extensive chlorite-rich alteration pipes typically found in footwalls of Archean VMS deposits.

Sericite ± Quartz Assemblage (Alteration Code "7")

The sericite ± quartz assemblage comprises rocks that contain greater than 35% sericite and up to 50% quartz. The sericite ± quartz assemblage occurs in the northeast quarter-section of Section 26 and southeast quarter-section of Section 23, and is

associated with mafic-intermediate and felsic lava flows of the Central Basalt Sequence. It also occurs in the southeast quarter-section of Section 25, where it is associated with felsic volcanic and volcaniclastic rocks in the Fivemile Lake Sequence (Figure 3.01). Adjacent alteration zones include the least-altered (0) assemblage, epidote ± quartz assemblage (1a) quartz ± epidote assemblage (2) and the actinolite + epidote ± garnet ± magnetite assemblage (5).

The sericite ± quartz assemblage is characterized in felsic rocks by its noticeably tan-milky-yellow color. The rocks generally can be easily scratched with a knife. Modal mineral percentages were difficult to estimate in the field because of the aphyric nature of the rocks. This alteration assemblage can be identified by local dark yellow 1-3cm wide patchy mottled zones that appear to be rich in sericite + quartz. The sericite ± quartz assemblage was difficult to identify in mafic rocks while mapping; therefore, this assemblage could only be identified by petrographic analysis. For mafic-intermediate volcanic rocks, thin section heels appear grayish-green in color and have a soft surface that can be scratched with a knife.

Petrographic analysis in felsic rocks indicates that the sericite ± quartz assemblage comprises 40% <1mm-1mm wide anhedral cross-cutting sericite stringers and <1-1mm crystal aggregates in interpillow hyaloclastite material, 35% <<1mm anhedral well-dispersed polygonal quartz groundmass, 15% <1mm anhedral epidote crystals, 6% 1mm anhedral limonite crystals, 2% <1mm anhedral Fe-carbonate crystals and 2% <1mm subhedral well-dispersed Fe-chlorite crystals. In mafic rocks the assemblage comprises 55% <1mm anhedral well-dispersed sericite crystals, 20% 1-1.5mm anhedral cross cutting Mg-chlorite stringers, 10% <1mm subhedral well-dispersed

Fe-carbonate crystals, 5% <1-1mm anhedral disseminated opaque minerals, 5% <1mm anhedral well-dispersed epidote crystals and 5% <1mm subhedral polygonal quartz groundmass.

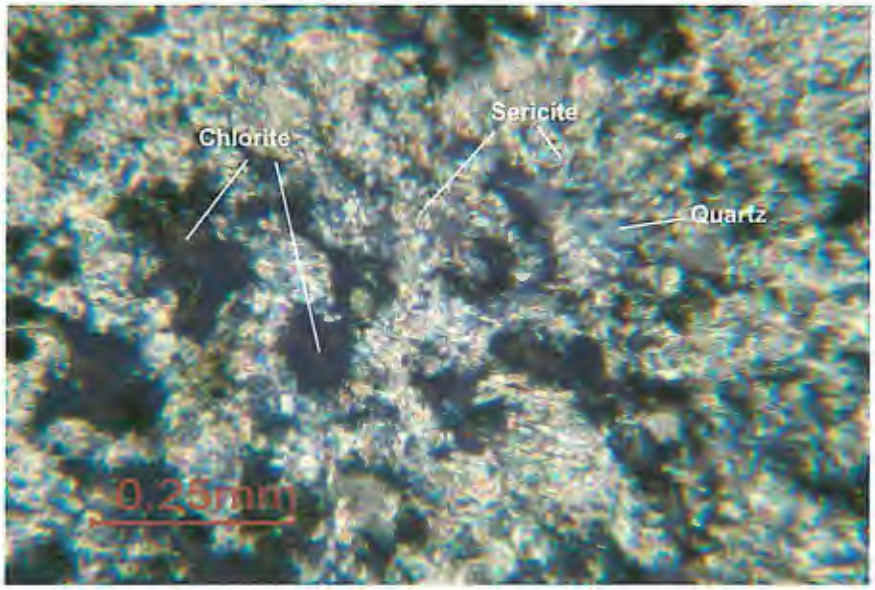

Figure 3.19. Photomicrograph of sericite ± quartz alteration in mafic-intermediate lava flow (Central Basalt Sequence). Cross-polarized light. Field of view approximately 2.5 mm. LE-333.

The addition of potassium ions from seawater drawdown into the subseafloor commonly alters primary feldspars (Winter, 2001). Sericite more readily forms in rocks where primary potassium feldspar is present, and is therefore typically more common in rocks with felsic bulk compositions. In mafic-intermediate volcanic rocks, the sericite ± quartz assemblage is interpreted to represent areas that underwent long-lived hydrothermal alteration at relatively high water: rock ratios (Hajash and Chandler, 1981). These rocks occur where cool downwelling seawater mixed with upwelling fluids from within the hydrothermal system.

Chapter 4

ALTERATION GEOCHEMISTRY

Introduction

Thirty-seven rock samples from the Soudan Mine area were analyzed for whole rock major oxide and trace element geochemistry (Appendix I). Thirty-three rock samples were analyzed by X-ray fluorescence spectrometry (XRF) at Macalester College for major and trace elements. Pulps from these thirty-three samples were subsequently sent to Activation Laboratories and analyzed by Inductive Coupled Plasma Mass Spectrometry (ICPMS) methods to provide analyses not available via XRF techniques. Four additional rock samples were sent to Activation Laboratories and analyzed by means of ICPMS methods for all major and trace elements.

In total, data for eleven major element oxides and forty-six trace elements were generated for the thirty-three rock samples analyzed at Macalester College and Activation Laboratories. Data for eleven major element oxides and fifty-one trace elements were obtained for the four samples processed by Activation Laboratories only (Table 4.01).

The results of these lithogeochemical analyses have been used to conduct mass balance calculations using the isocon method (Grant, 1986). The isocon method calculates the changes in elemental concentrations (as well as mass and volume changes if appropriate weight and volume data are incorporated) and was employed for four of the alteration mineral assemblages in the study area.

Major Oxides and Trace Elements	ICPMS (Activation Laboratories)	XRF Fused Bead (Macalester College)	XRF Pressed Pellet (Macalester College)	Major Oxides and Trace Elements	ICPMS (Activation Laboratories)	XRF Fused Bead (Macalester College)	XRF Pressed Pellet (Macalester College)
Al_2O_3	0.01%	0.1%		Nb	0.2		1
CaO	0.01%	0.1%		Ni	1		12
Cr_2O_3				P			
CuO				Pb	5		4
Fe_2O_3	0.01%	0.1%		Rb	1		1
K_2O	0.01%	0.02%		S	100		
MgO	0.01%	0.1%		Sb	0.2		
MnO	0.00%	0.002%		Sc	0.1		1
Na_2O	0.01%	0.04%		Se	3		
NiO				Sn	1		5
P_2O_5	0.01%	0.005%		Sr	2		4
SiO_2	0.01%	0.4%		Ta	0.01		
TiO_2	0.00%	0.02%		Th	0.05		2
LOI	0.01%	0.01%		Ti			
Ag	0.5			Tl	0.05		
As	0.5			U	0.01		3
Au	(2 ppb)			V	5		8
Ba	3		6	W	0.5		
Be	1			Y	0.5		2
Bi	0.1			Zn	1		1
Br	0.5			Zr	1		1
Ca				La	0.05		3
Cd	0.5			Ce	0.05		3
Co	1		4	Pr	0.01		
Cr	5		15	Nd	0.05		
Cs	0.1			Sm	0.01		
Cu	1		2	Eu	0.005		
Fe				Gd	0.01		
Ga	1		1	Tb	0.01		
Ge	0.5			Dy	0.01		
Hf	0.1			Ho	0.01		
In	0.1			Er	0.01		
Ir	(5 ppb)			Tm	0.005		
K				Yb	0.01		
Mo	2			Lu	0.002		

Table 4.01. Summary of lithogeochemical methods, elements analyzed, and detection limits in parts per million unless otherwise noted. XRF expressed as LDM values. *LDM = Limit of Determination of a Method = the minimum concentration that can be determined at the 95.4% level of confidence; calculated as recommended by Rousseau (2001); LMD = 2 x Standard Deviation (equation 12 in Rousseau, 2001); n = 10.

The Isocon Method

Grant's isocon method (1986) is used to determine the change in rock mass and the relative % change in individual components (oxides and trace elements) that accompany metasomatism associated with hydrothermal alteration. The isocon method provides a graphical solution to Gresens' (1967) equation (Grant, 1986), and allows mass and concentration changes to be calculated by comparing geochemical data from representative least-altered samples and from representative altered samples. This is accomplished by plotting the chemical data on an X-Y graph, and employs Gresens' (1967) equations for calculating volume and compositional changes of altered versus unaltered rocks.

	Gresens (1967)	Grant (1986)
Superscript for unaltered (original sample)	A	O
Superscript for altered (final) sample	B	A
Subscript for component	n	i
Specific gravity	g	ρ
Volume of sample	v	V
"Volume factor"	f_v	
Mass of sample		M
Mass of component i		M_i
Reference mass of original sample	a	M^O
Gain or loss of mass of component Relative to the reference mass	x	ΔM_i
Concentration	C	C

Table 4.02. Abbreviations for Gresens' (1967) and Grant's (1986) equations.

Gresens' (1967) presented an equation for calculating gains and losses from chemical analyses and specific gravities of altered and unaltered rocks (Grant, 1986). Gresens' basic equation is:

$$X_n = \left[f_v \left(g^B / g^A \right) C_n{}^B - C_n{}^A \right] a . \quad (1)$$

If chemical analyses are normalized to 100 wt %, the reference mass (a) in the equation will be equal to 100g.

According to Grant (1986), Gresens' (1967) equation really assesses mass rather than volume. Grant has rearranged Gresens' equation to show ratios of constant mass. Grants (1986) equation gives the ratio of equivalent masses after (M^A) and before (M^O) alteration, via the following equation:

$$\frac{M^A}{M^O} = \frac{V^A}{V^O} \bullet \frac{\rho^A}{\rho^O} = f_v \left(g^B / g^A \right) . \quad (2)$$

The mass of a component after alteration (M^A) equals its original mass plus any change in mass that has occurred:

$$M_i{}^A = M_i{}^O + \Delta M_i . \quad (3)$$

In order to express changes in terms of concentration units, it is necessary to divide the above equation by the mass of the original rock (M^O):

$$\frac{M_i{}^A}{{}^i M^O} = \frac{M_i{}^O}{M^O} + \frac{\Delta M_i}{M^O} . \quad (4)$$

The final concentration (M_i^A / M^A) is related to the original (M_i^O / M^O) by the following expression, which is obtained by multiplying equation (4) by (M^O/M^A):

$$\frac{M_i^A}{M^A} = \frac{M^O}{M^A} \bullet \frac{M_i^A}{M^O} = \frac{M^O}{M^A}\left(\frac{M_i^O}{M^O} + \frac{\Delta M_i}{M^O}\right). \quad (5)$$

Using concentration units, we obtain the following equation:

$$C_i^A = \frac{M^O}{M^A}\left(C_i^O + \Delta C_i\right). \quad (6)$$

This is Gresens' revised equation as can be seen by rearranging it into the form:

$$\Delta M_i = \left[\left(\frac{M^A}{M^O}\right) C_i^A - C_i^O\right] M^O. \quad (7)$$

For each component within the rock, there is an equation of this form in which (M^O/M^A) is constant. If immobile components (where $\Delta C_i = 0$) can be identified, then simultaneous equations can be solved of the form:

$$C_i^A = \left(\frac{M^O}{M^A}\right) C_i^O. \quad (8)$$

This can be accomplished by graphically plotting chemical data on an X-Y plot where C_i^O is plotted on the x-axis and C_i^A is plotted on the y-axis. Immobile components plot along a straight line through the origin with a slope of (M^O/M^A) which represents the constant mass before and after alteration. This line, where $\Delta C_i = 0$, is called an isocon. The equation for the isocon is:

$$C^A = \left(\frac{M^O}{M^A}\right) C^O. \quad (9)$$

If it is assumed that a component (alumina for example) has been constant (immobile) during metasomatism, equation (8) becomes:

$$\left(\frac{M^O}{M^A}\right) = \left(\frac{C^A{}_{Al2O3}}{C^O{}_{Al2O3}}\right), \quad (10)$$

and the isocon is:

$$C^A = \left(\frac{C^A{}_{Al2O3}}{C^O{}_{Al2O3}}\right) C^O. \quad (11)$$

If constant mass is assumed:

$$C^A = C^O. \quad (12)$$

The isocon representing constant volume is:

$$C^A = \left(\frac{\rho^O}{\rho^A}\right) C^O. \quad (13)$$

Once an isocon has been established, the relative gains and losses of components are graphically represented by the difference in slope of that component and that of the isocon. Grant (1986) suggests that concentration is generally the most useful means by which to measure metasomatic gains and losses.

In order to use concentration as a measure, it is imperative to compare the concentration of a component before and after alteration. This is done by dividing both sides of equation (6) by C_i^O and rearranging it to get:

$$\left(\frac{\Delta C_i}{C_i^O}\right) = \left(\frac{M^A}{M^O}\right)\left(\frac{C_i^A}{C_i^O}\right) - 1. \quad (14)$$

(M^A/M^O) is determined from the best fit isocon. For a constant component (alumina for example:

$$\left(\frac{\Delta C_i}{C_i}\right) = \left(\frac{C^O{}_{Al2O3}}{C^A{}_{Al2O3}}\right)\left(\frac{C_i{}^A}{C_i{}^O}\right) - 1. \quad (15)$$

For constant mass:

$$\left(\frac{\Delta C_i}{C_i}\right) = \left(\frac{C_i{}^A}{C_i{}^O}\right) - 1. \quad (16)$$

For constant volume:

$$\left(\frac{\Delta C_i}{C_i}\right) = \left(\frac{\rho^A}{\rho^O}\right)\left(\frac{C_i{}^A}{C_i{}^O}\right) - 1. \quad (17)$$

Mass Balance Analysis Methodology for the Soudan Mine Area

Perhaps the most important and difficult part of performing any type of mass balance analysis is selecting a representative least altered sample. The least altered sample must be taken from the same lithology as the altered rock if the comparison is to have merit. For this study, a least altered sample was selected by using petrographic studies (to evaluate sample mineralogy) and the Alteration Box Plot (Large et al., 2001) to evaluate sample geochemistry. The alteration box plot is a graphical representation that uses two alteration indices: 1) the Ishikawa Alteration Index (AI) (Ishikawa et al., 1976) and the Chlorite-Carbonate-Pyrite Index (CCPI); (Large et al., 2001). The alteration box plot is used to delineate zoned alteration assemblages in VMS systems. By plotting the AI versus CCPI, alteration trends within data sets associated with VMS deposits can be graphically evaluated (Figure 4.01). Least altered volcanic rocks typically plot toward the center of the diagram, and hydrothermally altered volcanics plot at different positions that correspond with various trends that reflect the hydrothermal minerals present (Large et al., 2001). Large et al. (2001) note that this technique is better

adapted for use with alteration geochemistry associated with felsic rock and works less well for alteration in mafic rock. However, this method was not employed to *distinguish* alteration types, but rather, to assist in the selection of a least altered sample for use in isocon mass balance analysis.

Several samples occur in the "least altered" field for mafic VMS systems. In order to pick a sample most representative of a pre-metasomatism protolith, the author used three criteria: 1) the sample must lie in the basalt field in a $Na_2O + K_2O$ vs. SiO_2 (TAS) diagram because Na, K, and Si are typically mobile in hydrothermal systems; 2) the sample must lie in the revised Winchester and Floyd field for basalt; and 3) the sample must be located in the least altered field in the alteration box plot. Petrographic methods were then used to verify the least altered characteristics of the samples.

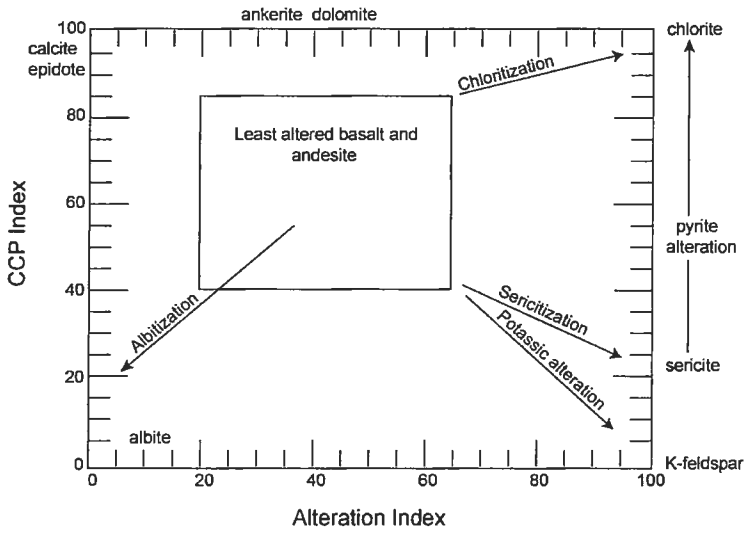

Figure 4.01. Standard alteration box plot for mafic and intermediate rocks from the Hellyer VHMS deposit (after Gemmel and Large, 1992). This box plot was used as part of a three step process to determine a least altered rock sample in the Soudan Mine area. Arrows indicate general trends associated with different types of metasomatism associated with VMS deposits.

Although two samples fit these criteria, one sample was eliminated by evaluating the CCPI and AI of the samples. The CCPI was similar in both samples, so the sample with the lower AI value was selected as the least altered sample (LE-227) for this thesis. Petrographical analysis reveals that this sample contains approximately 35% epidote, 25% fine-grained quartz + albite groundmass, 15% actinolite, 15% sericite, 10% iron chlorite and <1% carbonate. This sample appears to be a reasonable representation of regionally metamorphosed basalt that has not been exposed to more intense hydrothermal alteration.

In order to use the isocon method effectively, an element or group of elements that have been unaffected by hydrothermal activity must be identified. These species are used to define a best-fit isocon from which mass balance calculations for all other elements are calculated (Grant, 1986).

During hydrothermal processes associated with VMS hydrothermal alteration, high field strength elements (Ti, Zr, Hf, Nb, Ta, Y, and P), certain rare earth elements (Gd, Tb, Dy, Er, Yb, and Lu) and transitional elements (Cr, Ni, Sc, and V) are generally immobile (Jenner, 1996; Table 4.03). These immobile elements can be used to define a best-fit isocon to which all other elements are compared.

In the Soudan Mine area, discrimination diagrams have been used to evaluate the relative immobility of the "immobile" trace elements (Cann, 1970; Pearce, 1996; Hudak et al., 2002) identified above. In altered and unaltered rocks, strong linear relationships between two elements represent constant ratios. This implies relative immobility of the elements compared. Therefore, the relative mobility or immobility of elements can be evaluated when they are plotted against immobile elements on discrimination diagrams

(Figure 4.02). Statistical correlation coefficients were determined for immobile elements from the Soudan Mine area rocks (Table 4.04) using the statistical functions included in IGPET 2000 (Terra Softa Inc., 2000).

Elements	Mobility during seawater dominated conditions (fluid/rock>50)	Mobility during rock-dominated conditions (fluid/rock<50)	Comments
Low Field Strength Elements			
K, Rb, Cs, U, Pb	Mobile	Mobile	Assume immobile
Ba, Sr	Mobile	May be immobile	Generally mobile; in rock-dominated condition may be immobile and a useful petrogenetic indicator
Th	Mobile	May be immobile	In general appears to be immobile
High Field Strength Elements			
Ti, Zr, Hf, Nb, Ta	Immobile	Immobile	Immobile until proven mobile
P	Mobile	Immobile	Immobile to slightly mobile
Y	Immobile	Immobile	Immobile until proven mobile
Rare Earth Elements			
La, Ce, Nd, Sm	Generally Immobile	Immobile	Can be mobile, but for most altered volcanics seems to be immobile
Eu	Mobile	Mobile	The most unreliable of the REE for petrogenetic interpretation in altered rocks
Gd, Tb, Dy, Er, Yb, Lu	Slightly Mobile	Immobile	Generally immobile in water, but may be mobile in fluids with high carbonate concentrations
Transition Elements			
Cr, Ni, Sc, V	Immobile	Immobile	Ti-V is a useful immobile element ratio

Table 4.03. Trace element classification and behavior during hydrothermal alteration (seawater) and metamorphism (Jenner, 1996). Seawater and rock dominated conditions from Mottle and Seyfried (1980).

The Pearson's Product Moment Correlation Coefficient (r) is defined by the linear association between two components and has values ranging from +1 (a perfect positive correlation) to –1 (a perfect negative correlation). Positive or negative values near zero indicate that the components are not linearly related. The Coefficient of Determination (r^2) is a measure of the "goodness of fit" of the estimated regression line for the data, with higher r^2 values indicating a better fit. The Spearman's Rank Correlation Coefficient (r') is a measure of the association of the two variables when rank-order data are utilized (Anderson et al., 1986; *in* Hudak et al., 2002b).

For this thesis, the high field strength elements Ti, Zr, Hf, Nb, Y and P, and the transitional element Cr were determined to be immobile. Although Ti, P, and Cr did not show good correlation with the other immobile elements (Hf, Zr, Nb, Y), these elements consistently fell along the best-fit isocon. In all cases, the best-fit isocon was used for mass balance analysis for rocks in the Soudan Mine area.

Figure 4.03 shows an isocon diagram plotting the least altered sample LE-227 against a sample from the epidote ± quartz assemblage, LE-413. The major oxides plus Co, Cr, Cu, Ni, Nb, Pb, Zn, Zr, Ti and Y are plotted as components. All components have been scaled so they are more evenly distributed on the X-Y graph (see Grant, 1986 for an explanation of this procedure). This makes visualization easier and minimizes the crowding of data. Scaling for this thesis was accomplished by multiplying the least altered and altered analyses for each individual component by a unique factor so that the product of the analysis and the factor falls between zero and fifty, the maximum value for each axis on the X-Y graph.

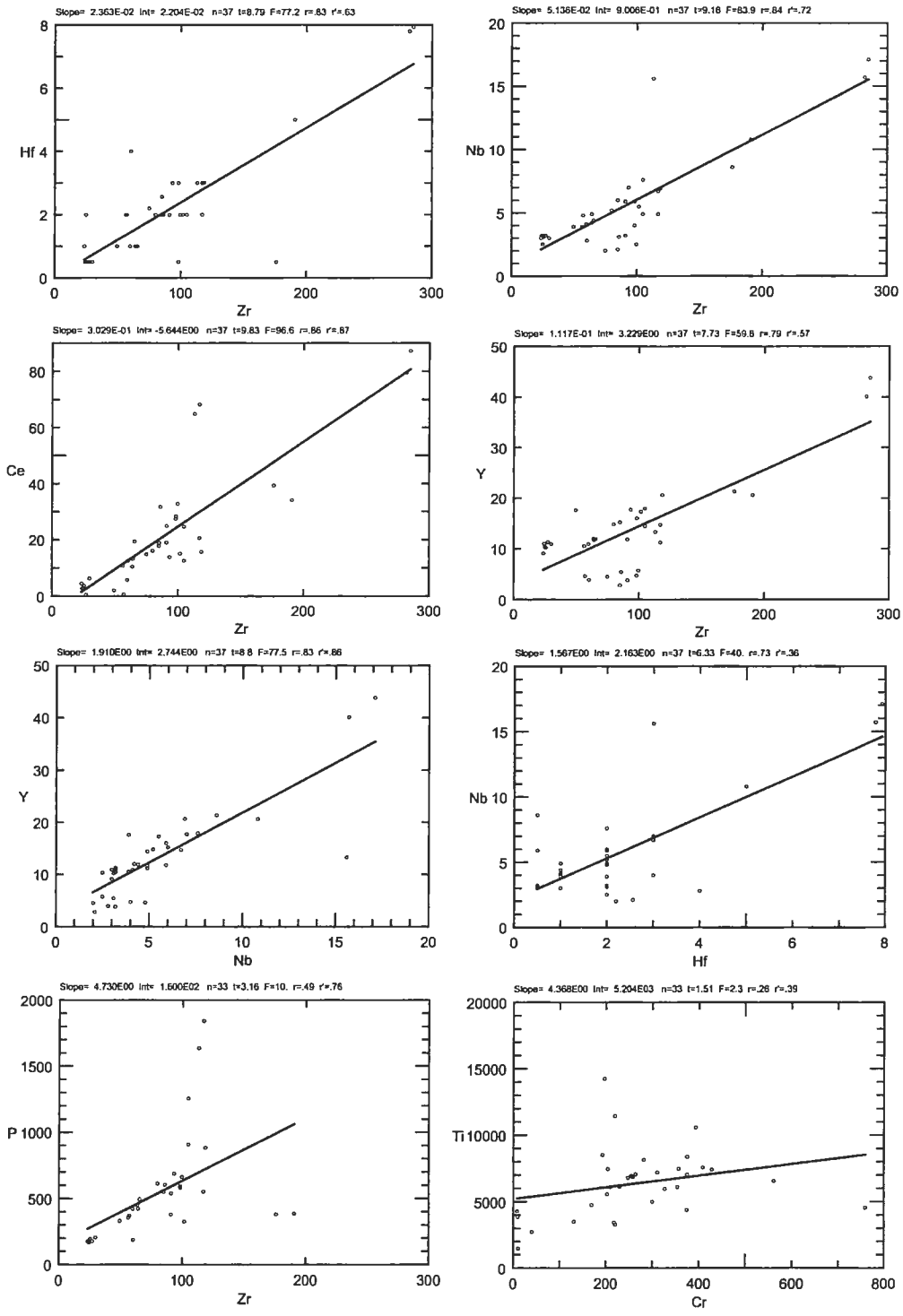

Figure 4.02. Variation diagrams showing the relative correlation of Hf, Zr, Nb and Y. "r" values between two components ranging from +1 (a perfect positive correlation) to –1 (a perfect negative correlation). Elements with higher r values are interpreted to be immobile during hydrothermal alteration. Concentration in parts per million.

Plot	Mafic Volcanic and Volcaniclastic Rocks in the Soudan Mine area		
	R	r^2	r'
Hf-Zr	0.83	0.69	0.63
Nb-Zr	0.84	0.71	0.72
Ce-Zr	0.86	0.73	0.87
Y-Zr	0.79	0.63	0.57
Cr-Zr	-0.45	0.20	-0.49
Ni-Zr	-0.35	0.12	-0.34
Sc-Zr	-0.69	0.47	-0.71
La-Zr	0.83	0.70	0.87
Th-Zr	.76	.59	.42
Ga-Zr	-0.34	0.12	-0.11
V-Zr	-0.69	0.47	-0.70
Nb-Hf	0.73	0.53	0.36
Ce-Hf	0.71	0.50	0.53
Cr-Hf	-0.44	0.19	-.49
Ni-Hf	-0.29	0.08	-0.27
Sc-Hf	-0.61	0.37	-0.61
V-Hf	-0.63	0.40	-0.60
Ce-Nb	0.78	0.61	0.50
Y-Nb	0.83	0.69	0.86
Cr-Nb	-0.63	0.00	-0.18
Ni-Nb	0.22	0.05	0.00
Sc-Nb	-0.44	0.16	-0.26
V-Nb	-0.39	0.15	-0.23
Ni-Cr	0.79	0.62	0.72
Sc-V	0.97	0.94	0.95
Al_2O_3-Nb	-0.74	0.54	-0.35
Al_2O_3-Zr	-0.55	0.3	-0.14
Al_2O_3-Hf	-0.48	0.23	0.03
Al_2O_3-Ce	-0.55	0.30	-0.05
Fe_2O_3-Zr	-0.59	0.34	-0.58
Na_2O-Zr	0.35	0.12	0.52
CaO-Zr	-0.60	0.36	-0.52
MgO-Zr	-0.49	0.24	-0.44
MnO-Zr	-0.58	0.34	-0.58

Table 4.04. Correlation coefficients for selected variation diagrams in the Soudan Mine area. The Immobile elements have the highest correlation coefficients (near 1 or -1), whereas the lower correlation coefficients (near zero) represent elements that may be more mobile.

An isocon with a slope of one is equivalent to a constant mass isocon, and indicates that no mass has been lost or gained during the alteration process. In the case illustrated in Figure 4.03, the constant aluminum isocon has a slope of $m = M^O/M^A = 1.0$, the best fit isocon has a slope of $m = (M^O/M^A) = 0.66$ which is equivalent to $(M^A/M^O) = 1.51$ and thus a mass increase of 51% which occurred to due the alteration process. All components that do not plot on the best fit isocon have been affected by hydrothermal alteration processes. Components that lie above the best-fit isocon (e.g. have a greater slope than) have been gained during hydrothermal alteration, whereas components that lie below the best-fit isocon have been leached during hydrothermal alteration (Grant, 1986). The larger the difference between the slope of the component and the slope of the isocon, the larger the magnitude of losses or gains of the species in the rock.

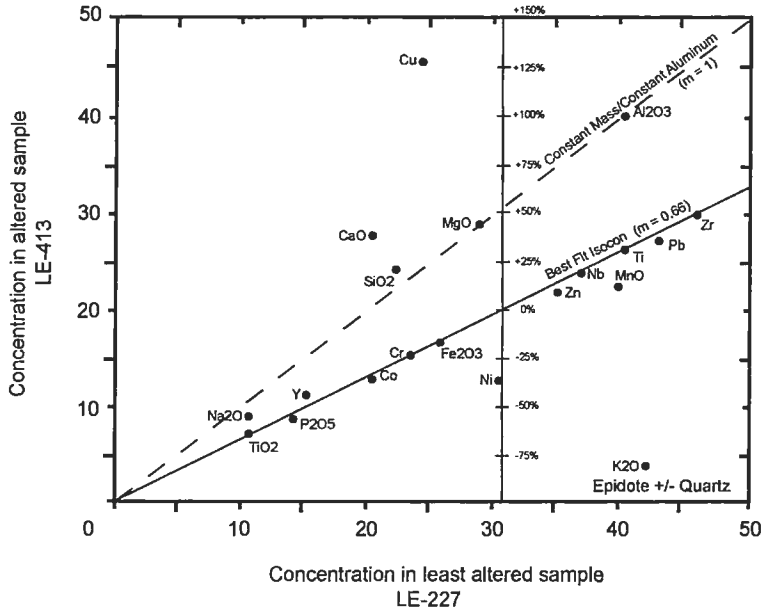

Figure 4.03. Isocon diagram comparing epidote ± quartz altered basalt LE-413, with least altered basalt sample LE-227. The best-fit isocon represents a straight line starting from the origin and passing through TiO_2, Cr, Nb, and Zr, which are interpreted to be immobile. The dashed lines represent the constant aluminum and constant mass Isocons.

A visual estimate of losses and gains can be used by superimposing a vertical scale onto the isocon diagram (Figure 4.03). A vertical line can be drawn anywhere along the X-axis. Where the vertical scale intersects the isocon of choice, the relative change (M^O/M^A) = 0. The vertical distance between this intersection to the X-axis equals 100%. This line can then be segregated so that the losses and gains of a component of interest can be measured by drawing a line from the origin through the component. Where the line intersects the scale, the losses and gains can be read.

Hovis (2001) used the constant aluminum isocon at the Eagles Nest VMS prospect. Although aluminum is not considered immobile at Soudan, constant aluminum isocons have been plotted so that direct comparisons to the results of Hovis (2001) can be done.

Mass Balance Analysis for the Soudan Mine Area

Mass balance analysis was conducted in order to measure the relative gains and losses of components in four of the seven alteration assemblages within the study area. Mass balance was conducted on basalts from the Central Basalt Sequence. Mass balance was not conducted in other rocks because of limited lithogeochemistry, the lack of least altered samples, and a variety of alteration assemblages that involve rocks with variable bulk compositions. Alteration assemblages analyzed include the epidote ± quartz assemblage (1a), mottled epidote ± quartz assemblage (1b), actinolite + epidote ± garnet ± magnetite assemblage (5), and the sericite ± quartz assemblage (7). Three other assemblages, the quartz ± epidote (2), Mg-chlorite ± quartz ± sericite (4) and Fe-chlorite

(6) occur in the Soudan Sill, Upper Sequence and Fivemile Lake Sequence, and therefore were not analyzed.

Epidote ± Quartz Assemblage

One sample from the epidote ± quartz alteration assemblage "1a" at the Soudan Mine are was analyzed using the isocon method (Figure 4.03). The sample is from mafic volcanic lavas of the Central Basalt Sequence (LE-413).

Table 4.05 indicates gains and losses associated with the epidote ± quartz assemblage. The addition of CaO (101%) is represented in outcrop and thin section by the abundance of epidote (Ca_2 (Al, Fe)$Al_2O(SiO_4)(Si_{12}O_7)(OH)$) and actinolite ($Ca_2$ (Mg, Fe)$_5$ (Si_4O_{11})$_2$ $(OH)_2$. An increases in Al_2O_3 (51%) and MgO (51%) and a slight loss of Fe_2O_3 (-1%) may be due to the varieties of chlorite present. Sodium shows a relative increase (29%) which probably resulted from the albitization of plagioclase to form epidote. Silicification in this assemblage is reflected by a gain in SiO_2 (65%). A total mass gain (51%) may be caused by epidote + quartz occupation in healed fractures. Large gains in Cu (187%) are not typically associated with epidote-rich zones, where instead metal depletion is usually more common (Hudak et al., 2002b). Gains in copper may also contribute to a total mass gain in the rock.

Element	Change % Best Fit	Change % Alum.	Change % Const. Mass
SiO2	65	9	9
TiO2	0	-35	-35
Al2O3	51	0	0
Fe2O3	-1	-34	-34
MnO	-15	-44	-44
MgO	51	0	0
CaO	101	33	33
Na2O	29	-15	-15
K2O	-85	-90	-90
P2O5	-7	-38	-38
LOI	40	-8	-8
Sc	73	14	14
V	45	-4	-4
Cr	0	-34	-34
Co	-4	-36	-36
Ni	-37	-58	-58
Cu	187	90	89
Zn	-7	-38	-38
Rb	-80	-87	-87
Sr	286	155	155
Y	5	-31	-31
Zr	0	-34	-34
Nb	0	-35	-35
Pb	-9	-40	-40
Ti	-2	-35	-35
K	-86	-90	-90
Au	51	0	0
Ag	51	0	0
As	-68	-79	-79
Ca	165	75	75
Fe	5	-30	-31
Hf	51	0	0
Sb	808	500	500
Total Mass Gain = 51%			

Table 4.05. Gains and losses of major element oxides and calculated trace elements from epidote + quartz altered basalt lava flow (Central Basalt Sequence, LE-413) by use of isocon analysis. The best fit (TiO_2, Cr, Zr, and Nb), constant aluminum and constant mass isocon are listed for comparison.

Mottled Epidote ± Quartz Assemblage

One sample from the mottled epidote ± quartz assemblage (1b) was analyzed using the isocon method. This sample (LE-437) is from pillowed mafic lavas (Central Basalt Sequence). The relative gains in CaO (436%) reflects the relatively large concentration of epidote (>50%) in these rocks. This is probably due to leaching of Ca^{2+} from plagioclase and its subsequent redeposition to form epidote (saussuritization) (Bernt et al., 1989). The lack of plagioclase and sericite is accounted for by the depletion of Na_2O (-85%) and K_2O (-60%). Increases in Fe_2O_3 (95%) and MgO (128%) reflect metasomatic changes resulting in Fe- and Mg-chlorite, and an increase in Cu (587%) may be due to deposition of copper by hydrothermal fluids originally generated deeper in the hydrothermal cell.

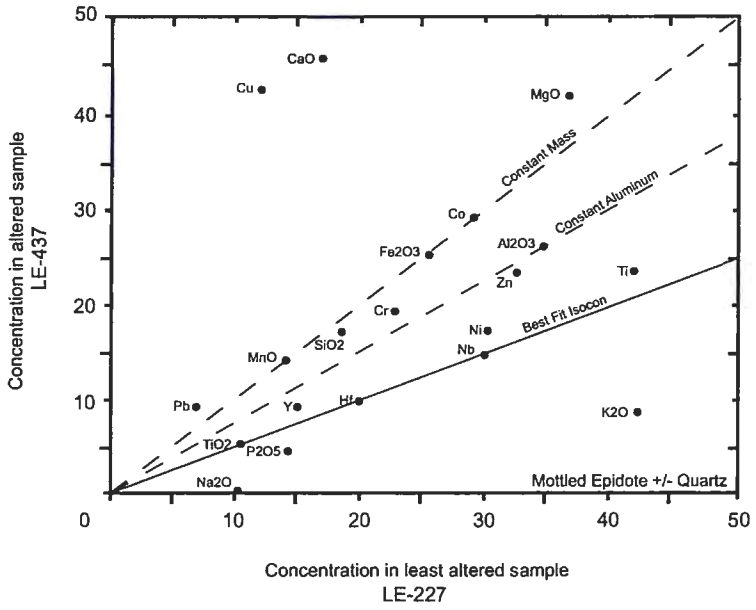

Figure 4.04. Isocon diagram comparing mottled epidote ± quartz altered mafic pillow lava (Central Basalt Sequence) LE-437, with least altered sample LE-227. The best fit isocon represents a straight line starting from the origin and passing through TiO_2, Hf, and Nb which have been interpreted to be immobile. The dashed lines represent the constant aluminum and constant mass Isocons.

Element	Change % Best Fit	Change % Alum.	Change % Const. Mass
SiO2	89	26	-6
TiO2	0	-24	-44
Al2O3	49	0	-25
Fe2O3	95	31	-3
MnO	100	34	0
MgO	128	53	14
CaO	436	260	168
Na2O	-85	-90	-93
K2O	-60	-73	-80
P2O5	-38	-59	-69
LOI	69	13	-15
Sc	151	68	25
V	95	31	-3
Cr	66	11	-17
Co	101	35	1
Ni	12	-25	-44
Cu	587	361	243
Zn	42	-5	-29
Rb	-71	-81	-86
Sr	279	154	90
Y	20	-20	-40
Zr	-44	-63	-72
Nb	0	-33	-50
Pb	180	88	40
Ti	0	-24	-44
K	-60	-73	-80
Au	100	34	0
Ag	100	34	0
As	-75	-83	-88
Ca	0	-33	-50
Fe	-69	-79	-85
Hf	0	-33	-50
Sb	700	437	300
Total Mass Gain = 100%			

Table 4.06. Gains and losses of major element oxides and calculated trace elements from mottled epidote ± quartz altered basalt lava flow (Central Basalt Sequence, LE-437). The best fit (TiO_2, Hf and Nb), constant aluminum and constant mass isocon are listed for comparison.

Silicification in this assemblage is reflected by a gain in SiO_2 (89%). A total mass gain (100%) occurs, and may be caused by epidote + quartz occupation in healed fractures. Large gains in Cu (587%) are not typically associated with mottled assemblages where the depletion of metal is usually more common (Hudak et al., 2002b). However, seemingly large amounts of copper, may be related to very miniscule amounts of chalcopyrite in the rock samples since copper is measured in parts per million, not weight percent.

Actinolite + Epidote ± Garnet ± Magnetite Assemblage

One sample from the Central Basalt Sequence containing the actinolite + epidote ± garnet ± magnetite assemblage (LE-222) was analyzed using the isocon method.

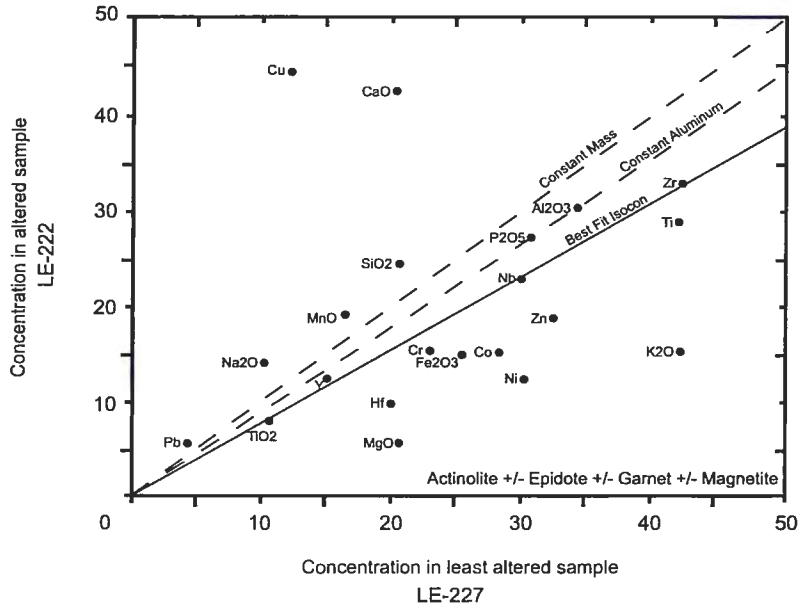

Figure 4.05. Isocon diagram comparing actinolite ± epidote ± garnet ± magnetite sub alkaline pillow basalt from the Central Basalt Sequence LE-222, with least altered sample LE-227. The best fit isocon represents a straight line starting from the origin and passing through TiO_2, Nb, and Zr which have been interpreted to be immobile. The dashed lines represent the constant aluminum and constant mass Isocons.

Element	Change % Best Fit	Change % Alum.	Change % Const. Mass
SiO2	47	22	11
TiO2	0	-27	-34
Al2O3	21	0	-9
Fe2O3	-19	-33	-39
MnO	76	46	32
MgO	-57	-65	-68
CaO	171	125	103
Na2O	84	52	38
K2O	-50	-59	-63
P2O5	13	-7	-15
LOI	-27	-39	-45
Sc	57	30	18
V	15	-5	-14
Cr	-11	-26	-33
Co	-27	-39	-45
Ni	-46	-55	-60
Cu	382	299	261
Zn	-26	-39	-45
Rb	-59	-66	-69
Sr	182	133	111
Y	4	-14	-22
Zr	0	-15	-23
Nb	0	-19	-27
Pb	75	45	31
Ti	-11	-26	-33
K	-50	-59	-62
Au	33	10	0
Ag	33	10	0
As	-29	-41	-47
Ca	233	176	150
Fe	-7	-23	-30
Hf	-33	-45	-50
Sb	2567	2109	1900
Total Mass Gain = 33%			

Table 4.07. Gains and losses of major element oxides and calculated trace elements from the actinolite + epidote ± garnet ± magnetite altered basalt lava flow (Central Basalt Sequence, LE-222) by use of isocon analysis. The best-fit (TiO_2, Nb and Zr), constant aluminum and constant mass isocon are listed for comparison.

The mineralogy and textures in the sample indicate it has experienced intense hydrothermal alteration.

Table 4.07 illustrates the results of the isocon analysis for this assemblage. An increase in CaO (171%) is consistent with the large modal abundances of actinolite within this assemblage. Increases in Na_2O (84%) likely reflect albitization of original feldspar in the rock. The large gain in Cu (382%) reflects the abundance of opaque copper sulfide minerals that occur in this assemblage. Losses of Fe_2O_3 (-19%) and MgO (-57%) reflects the breakdown of primary ferromagnesian phases (e.g. pyroxene) and the loss of K_2O (-50%) reflect the absence of sericite in the sample. Depletion of Zn (-36%) likely reflect base metal leaching. It is clear, however, that some areas with this alteration assemblage contain zones where crosscutting magnetite and garnet is present; therefore a large gain in iron would be expected. However, garnet and magnetite occupy open space fillings such as veins and interpillow hyaloclastite; the sample that was taken represents the pillow cores and therefore did not incorporate large amounts of magnetite and garnet.

Sericite ± Quartz Assemblage

One sample from the sericite ± quartz assemblage (LE-337) was analyzed by the Isocon method. This sample is of basalt lava from the Central Basalt Sequence.

Table 4.08 illustrates the results of the mass balance analysis of the sericite ± quartz assemblage. Gains in K_2O (421%), SiO_2 (56%), and MgO (78%) reflect the high modal abundances of sericite, Mg-chlorite and quartz-rich groundmass that occur in this

assemblage, respectively. Losses in CaO (-18%) are indicative of the relative lack of epidote and plagioclase in this assemblage.

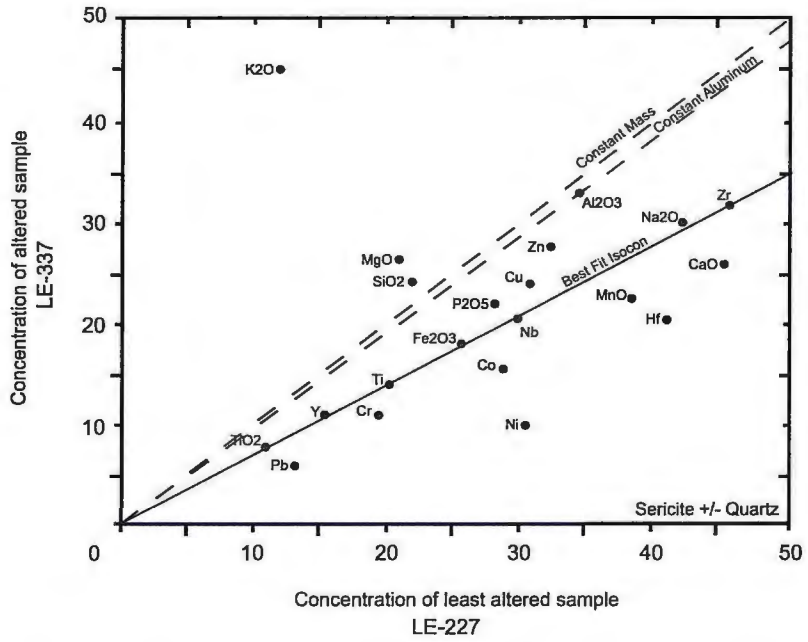

Figure 4.06. Isocon diagram comparing sericite ± quartz sub alkaline massive basalt (Central Basalt Sequence) LE-337, with least altered sample LE-227. The best fit isocon represents a straight line starting from the origin and passing through TiO_2, Y and Zr which have been interpreted to be immobile. The dashed lines represent the constant aluminum and constant mass isocons.

Element	Change % Best Fit	Change % Alum.	Change % Const. Mass
SiO2	56	15	9
TiO2	0	-26	-30
Al2O3	36	0	-5
Fe2O3	-2	-28	-32
MnO	-14	-37	-40
MgO	78	31	24
CaO	-18	-40	-43
Na2O	0	-26	-30
K2O	421	284	264
P2O5	10	-19	-23
LOI	32	-3	-8
Sc	33	-2	-8
V	38	2	-3
Cr	-25	-45	-48
Co	-20	-41	-44
Ni	-52	-65	-67
Cu	7	-21	-26
Zn	20	-11	-16
Rb	214	131	119
Sr	243	153	140
Y	0	-24	-28
Zr	0	-26	-30
Nb	-2	-28	-32
Pb	-30	-48	-51
Ti	1	-26	-30
K	422	284	264
Au	43	6	0
Ag	43	6	0
As	-92	-94	-94
Ca	8	-21	-25
Fe	-2	-28	-32
Hf	-28	-47	-50
Sb	43	6	0
Total Mass Gain = 43%			

Table 4.08. Gains and losses of major element oxides and trace elements from the sericite ± quartz altered sub-alkaline basalt (Central Basalt Sequence, LE-337) calculated via isocon analysis. The best fit (Zr, Nb, TiO_2 and Y), constant aluminum and constant mass isocon are represented for comparison.

	Alteration Assemblages			
	Quartz ± Epidote "1a" LE-413	Mottled Quartz ± Epidote "1b" LE-437	Actinolite + Epidote ± Garnet ± Magnetite "5" LE-222	Sericite ± Quartz "7" LE-337
SiO2	65	89	47	56
TiO2	0	0	0	0
Al2O3	51	49	21	36
Fe2O3	-1	95	-19	-2
MnO	-15	100	76	-14
MgO	51	128	-57	78
CaO	101	436	171	-18
Na2O	29	-85	84	0
K2O	-85	-60	-50	421
P2O5	-7	-38	13	10
LOI	40	69	-27	32
Sc	73	151	57	33
V	45	95	15	38
Cr	0	66	-11	-25
Co	-4	101	-27	-20
Ni	-37	12	-46	-52
Cu	187	587	382	7
Zn	-7	42	-26	20
Rb	-80	-71	-59	214
Sr	286	279	182	243
Y	5	20	4	0
Zr	0	-44	0	0
Nb	0	0	0	-2
Pb	-9	180	75	-30
Ti	-2	0	-11	1
K	-86	-60	-50	422
Au	51	100	33	43
Ag	51	100	33	43
As	-68	-75	-29	-92
Ca	165	0	233	8
Fe	5	-69	-7	-2
Hf	51	0	-33	-28
Sb	808	700	2567	43
Δ Mass (%)	51	100	33	43

Table 4.09. Summary table of major element oxides and trace elements calculated via the isocon method. These data were generated using the elements Ti, Zr, Hf, Nb, Y, P and Cr which were interpreted to be immobile and in general comprise the best-fit isocon. Notice that some immobile elements (Nb, Zr, Hf) show large net losses when their immobility should suggest a value approximately = 0. These irregular data represent "below detection" analyses.

This assemblage may have resulted from cool downwelling seawater (addition of Mg^{2+} and K^{+}) mixing with higher temperature upwelling hydrothermal fluids (K^{+} and Silica dumping). The large increases in K_2O and MgO are consistent with relatively low temperature, high water: rock alteration conditions.

Summary of Data

Best-fit isocons were used to evaluate gains and losses of chemical components that occurred from hydrothermal alteration processes in the Soudan Mine area. The high field strength elements Ti, Zr, Hf, Nb, Y and P, and the transitional element Cr, were used to define the isocons.

Table 4.09 summarizes the best-fit isocon data. The epidote ± quartz assemblage is characterized by gains in Ca (101%), Al_2O_3 (51%), MgO (51%), Na_2O (29%), Cu (187%), SiO_2 (65%) and a mass gain of 51%. The mottled epidote ± quartz assemblage is characterized by gains in CaO (436%), Al_2O_3 (49%), MgO (120%), Cu (587%), and SiO_2 (89%) and a loss in Na_2O (-85%) with a mass gain of 100%. The actinolite + epidote ± garnet ± magnetite assemblage is characterized by gains in CaO (171%), Al_2O_3 (21%), Na_2O (84%), SiO_2 (47%), Cu (382%) and losses of MgO (-57%) and Fe_2O_3 (-19%) with a mass gain of 133%. The sericite ± quartz assemblage is characterized by gains in SiO_2(56%), Al_2O_3 (36%), MgO (78%), K_2O(421%), and a total mass gain of 43%.

Chapter 5

VOLCANIC RECONSTRUCTION AND HYDROTHERMAL ALTERATION MODEL

Introduction

Volcanic reconstruction is an essential tool used in the exploration of all volcanic-associated ore bodies, including volcanogenic massive sulfide deposits (Cas, 1992; Gibson et al., 1999). Volcanic reconstruction through stratigraphic correlations, facies mapping and lithogeochemical and structural analysis is a powerful tool for determining the geotectonic and paleogeographic environment of older volcanic successions (Gibson et al., 1999).

Estimating water depth, although sometimes difficult and always contentious, also has significance in targeting VMS deposits. Water depth has a direct correlation with hydrostatic pressure, and when paired with temperature, salinity and gas content, control the depth of boiling of an ascending hydrothermal fluid (Franklin et al., 2005). Boiling, and the resulting phase separation of a hydrothermal fluid, can result in the formation of a base metal poor vapor and a base metal-rich residual fluid (Franklin et al., 2005). Therefore, a reliable criterion for determining water depth has significance in targeting VMS deposits. Franklin et al. (2005) suggests that lithofacies alone can not be a reliable tool to estimate water depth. Recent studies suggest that pyroclastic eruptions (historically considered shallow-water phenomena) have occurred on the modern day seafloor at depths of 2000-4000m (Butterfield et al., 1990; Hannington et al., 1991 Sherlock et al., 1999). The eruption and emplacement of lava flows, domes and cryptodomes are not constrained by water depths. Therefore, the ability to confidently

estimate water depths between storm wave base and 3,000+ m based on lithofacies alone has been impossible (Franklin et al., 2005).

The well-preserved nature of the Vermilion Greenstone belt provides an excellent opportunity to evaluate Neoarchean volcanism and volcanic-associated submarine hydrothermal systems. In order to piece together the geologic history of the Soudan Mine area, it is important to look at each major rock sequence individually. This chapter will briefly review the physical characteristics of all the rock types in the Soudan Mine area, as well as evaluate geochemical characteristics indicative or their genetic environment.

Interpretation of the Stratigraphic and Tectonic Evolution of Major Sequences

Four major volcanic sequences occur in the Soudan Mine area. From oldest to youngest, these are: 1) the Fivemile Lake Sequence; 2) the Central Basalt Sequence; 3) the Upper Sequence; and 4) the Gafvert Lake Sequence. Recent physical and geochemical data collected by the author and others working in the Vermilion District (Southwick et al., 1998; Hudak et al., 2004; Peterson and Patelke, 2003) suggest that rocks in this region were created by a variety of volcanic processes in various depositional environments, were affected by a variety of hydrothermal processes, and were formed during a continuous tectonic evolution. Accordingly, the following discussion describes the processes that occurred and the environments that were present during the development of this ancient geologic terrain. The depositional environments, genetic processes, and tectonic setting will be discussed as a whole in four separate stages, which represent the four major rock successions in the field area.

Stage I – The Fivemile Lake Volcanic Sequence

Based on geochemical and physical similarities throughout the Ely Greenstone belt, the Fivemile Lake Sequence represents part of a laterally extensive Neoarchean mafic-intermediate shield volcano complex that extends south and southeast (down-section) well beyond the mapping boundaries for this thesis. Hudak et al. (2002a), Hudak et al. (2002b), Hovis (2001) and Peterson (2001) have completed the majority of work in other parts of the Fivemile Lake volcanic sequence. The Fivemile Lake Sequence studied in the Soudan Mine area represents the upper and therefore latter stages of this particular volcanic shield environment.

The Fivemile Lake Volcanic Sequence is composed dominantly of basalt and andesite lava flows with minor felsic lava flows and volcaniclastic rocks. Rocks of this composition are common in most greenstone terrains of Archean age (Thurston and Chivers, 1990). In stratigraphic terms, Archean arc and back-arc sequences are composed of broad basal lava plains which transition stratigraphically upwards into mafic shield volcanoes that commonly develop central bimodal volcanic complexes (Ayers, 1982). The Fivemile Lake Sequence appears to have developed in this manner.

Hudak et al. (2002b) suggest that the Fivemile Lake Sequence rocks are associated with an island-arc volcanic system. Lithogeochemical diagrams (see Chapter 2) also suggest that these rocks formed in an arc setting. Therefore, the Fivemile Lake Sequence developed from magmas generated in an oceanic-oceanic plate compressional environment, involving the subduction of oceanic lithosphere beneath overriding oceanic crust. This subduction generated a juvenile, low-density mafic melt that propagated upwards through the overriding slab, initiating volcanic activity. This melt may have

been brought to the seafloor through a stock work of synvolcanic faults, but the distribution of synvolcanic intrusions feeding this system is poorly constrained due to a paucity of outcrop and structural deformation associated with the Murray Shear Zone.

Volcanic Stratigraphy

Persistent mafic and intermediate lava flows comprise the bulk of the volcanic strata in the Fivemile Lake Sequence. Submarine mafic and intermediate pillowed lava flows are likely believed to represent the subaqueous equivalent of subaerial tube-fed pahoehoe flows in modern submarine environments (Ballard et al., 1979). These flows are products of sustained eruptions with low-moderate effusion rates (Gibson et al., 1999). Mafic volcaniclastic deposits (e.g. tuffs and lapillistone) probably form from the explosive interaction of magma and external water (Gibson et al., 1999). As is similar in many ancient volcanic terrains (Franklin et al., 2005), it is difficult to tell the water depth under which these volcanic processes take place. However, the presence of abundant large vesicles, an increased amount of interpillow hyaloclastite (when compared to the Central Basalt Sequence), stratigraphic correlations to pillow sequences containing a large number of multi-rind pillows (Hudak et al., 2002a), and the presence of short-lived explosive lapillistone and tuff deposits, it is reasonable to conclude that these processes occurred at water depths less than 1500m (McBirney, 1963; Kokelaar, 1986; Gibson et al., 1999; Wright and Gamble, 1999).

The presence of rhyodacite lava flows and small dikes and stock-like intrusions in the Fivemile Lake Sequence, suggests the emplacement of numerous small hypabyssal magma chambers during volcanism. Intrusive rocks indicate that a portion of these melts did not erupt, but instead, stalled in the upper crust during upward migration. Andesite

and rhyodacite volcanic rocks resulted from magma migration from these hypabyssal intrusions upward through the seafloor, through synvolcanic faults or other synvolcanic structures.

Persistent andesite volcanism was periodically interrupted by rhyodacite to dacite volcanism that produced localized explosive eruptions followed by effusive lava flows. In the southeast quarter-section of section 25, a 135m thick, central volcanic pile consists of basal, felsic, small-volume co-ignimbrite-like deposit that transitions quickly into rhyodacite to dacite lava flows. The base of the volcanic pile consists of a moderately thick (up to 68m), poorly-bedded, poorly-sorted and locally clast-supported breccia that comprise 50-70% rounded-subangular, silicified, aphyric (20-40%) fine-lapilli to block pumice fragments and angular fine- to medium-lapilli rhyodacite lava fragments that are well-dispersed and set in 30-50% quartz-phyric recrystallized coarse-ash matrix. Contacts between felsic volcaniclastic rocks and adjacent units are not visible in the field area due to scattered outcrop exposures. Felsic volcaniclastic rocks transition upwards into felsic lava flows which are 10-50m thick and extend laterally for 400 and 550 meters respectively. Lava flows are massive, aphyric to quartz-phyric, and exhibit subtle flow banding. Medium lapilli to block sized angular to sub-rounded felsic lava accessory fragments are well-dispersed within the flows.

The felsic components in the Fivemile Lake Sequence appear to make up the transition from explosive volcanism to effusive volcanism. The presence of highly-vesiculated, poorly-sorted volcaniclastic material and angular lava clasts that resemble the massive flow facies, paired with the absence of bedding and grading and a lack of broken crystals, suggests that initially, the felsic edifice erupted in a moderately violent

fashion (Gibson et al., 1999). The presence of the massive lava facies suggests that magma chamber pressure and hence effusion rate rapidly decreased after the explosive initiation of felsic volcanism.

Rhyodacite to dacite lava flows are overlain and adjacent to mafic lapillistone deposits. These deposits are thickly to very thickly bedded, poorly-sorted, non-graded, and composed of vesicular scoria-lapilli to block-sized fragments (65%) set in 35% recrystallized fine-medium ash. This deposit is correlated stratigraphically with a poorly-bedded, well-sorted mafic tuff deposit 1000m to the southwest of the lapillistone deposit, which may suggest a cogenetic relationship. Mafic lapillistone deposits in this area are laterally restricted and do not fit the criteria of scoria cones or scoria flow deposits suggested by Cas and Wright (1989). However, the location and morphology of lapillistone deposits above and adjacent to rhyodacite to dacite lava flows suggests they may represent the weathered or resedimented equivalents of primary scoria cone or scoria flow deposits. The presence of scoria deposits marks the transition from dominantly explosive volcanism with intermittent effusive eruptions, to long-lived effusive andesite eruptions.

Conclusions

Geochemically, the majority of samples analyzed in the Fivemile Lake Sequence suggest that these rocks formed in a plate-marginal volcanic-arc setting (See Chapter 2). The introduction of rhyolite volcanism in mafic-dominated volcanic successions is commonly associated with mature arc construction, arc-rifting and the beginning of back arc development (Chown et al., 1992; Corcoran and Dostal, 2001). The occurrence of

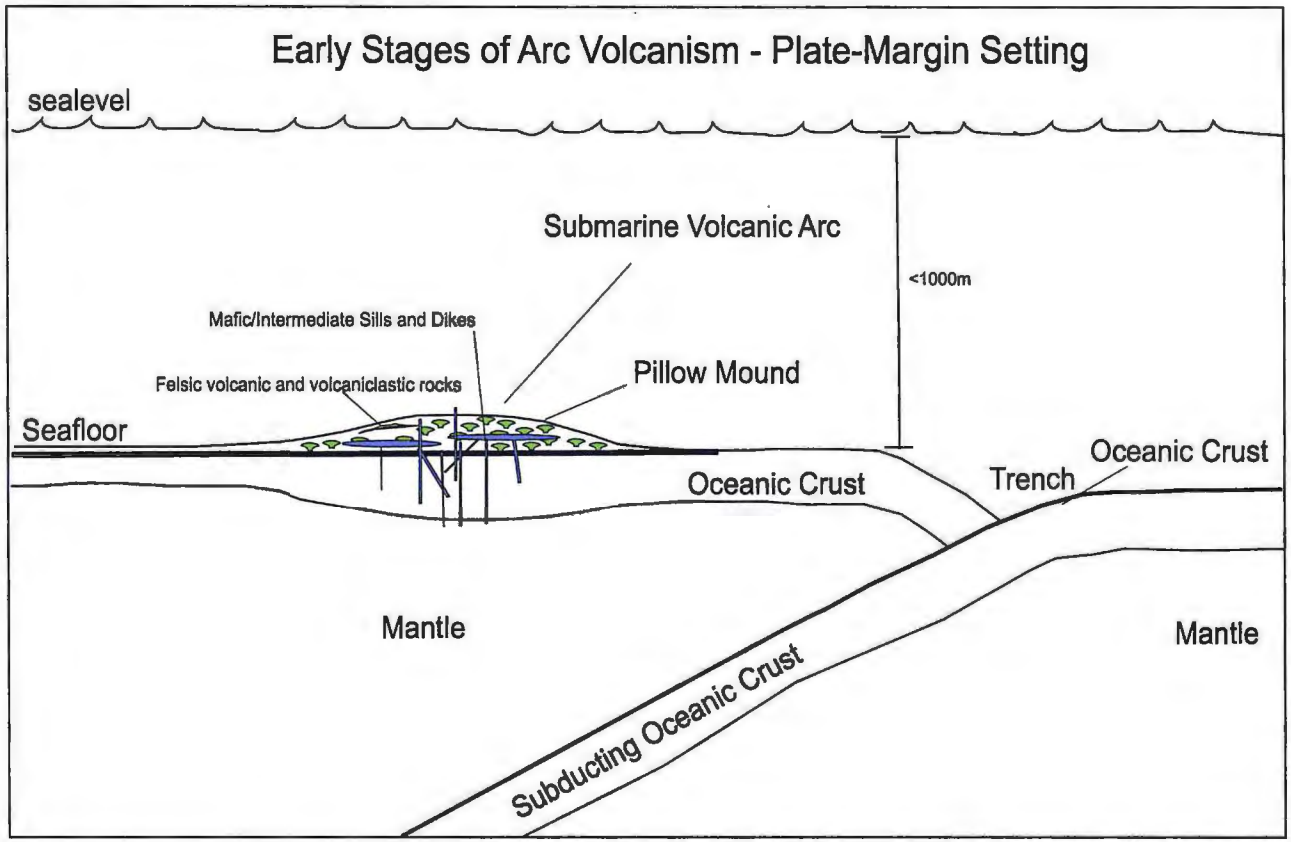

Figure 5.01. Schematic cross section illustrating the early stages of arc-volcanism as an analogy to the formation of the Fivemile Lake Sequence (modified after Corcoran, 2000). Not to scale.

felsic rocks represents the latter stages of plate marginal arc rifting and the beginning of post-collisional within-plate volcanism.

Stage II – The Central Basalt Volcanic Sequence

Lithological, stratigraphic, and geochemical similarities throughout the Lower Member of the Ely Greenstone Formation suggest that the Central Basalt Sequence is also part of a large mafic shield complex that extends at least 5 kilometers east of the study area. Geochemical studies performed for this thesis indicate that the Central Basalt Sequence lavas in the Soudan Mine area represent the products of both volcanic-arc and post-collisonal within-plate associated volcanism (see Chapter 2). The Central Basalt Sequence is composed of basalt lava flows with minor andesite flows and associated felsic volcanic and volcaniclastic rocks. Lithogeochemical data (see Chapter 2) suggests that syn-collisional arc and post-collisional within-plate basalts are coeval. The coeval relationship between arc and within-plate magmas is unclear. Within-plate volcanism commonly occurs in the interior of oceanic plates and produces ocean island volcanism that form seamounts or large accumulations that may never breach the water surface (Winter, 2001). Within-plate volcanism is usually associated with hot spots or plumes generated by thermal anomalies originating in the deep mantle (Winter, 2001). Their deep mantle source typically results in an enriched LREE pattern. LREE's at Soudan show depletion which suggests partial melting of the REE depleted upper mantle.

Isley and Abbott (1999) have correlated mantle plume activity (to the 99% confidence interval) with the age of banded iron formation. They suggest that mantle plume activity may promote BIF deposition by increasing the iron flux to the global

oceans through continental weathering and/or through submarine hydrothermal processes.

The presence of within-plate volcanism (also promoted by plume activity) in the footwall of the Soudan iron formation may present further evidence that reinforces Isley and Abbott's (1999) hypothesis. This however, does not shed light on the coeval relationship between island-arc and ocean island volcanism and is best explained by the author as either the mixing of source regions, or a two source cyclicity between partial melts from the contaminated mantle and partial melts from deep mantle plumes. The overlapping of shield magmas from different sources is very common in Archean shield terrains (Dimroth and Rocheleau, 1979; Thurston and Chivers, 1990). According to Thurston and Ayres (2004), this two source cyclicity can develop from (1) competition between upwards growth of volcanoes by intermittent or continuous eruptions, simultaneous with downwards movement resulting from erosional degradation and isostatic rebound; (2) interaction between intermittent volcanic processes and sedimentation (Anhaeusser, 1971); and (3) temporal changes in source regions.

Volcanic Stratigraphy

Mafic and intermediate lavas that comprise the Central Basalt Sequence are the product of sustained subaqueous eruptions with variable effusion rates. The lack of vesicles and multiple-selvage pillows, a paucity of epithermal-like zinc mineralization (as seen at the Fivemile Lake Prospect) and a close association with banded iron formation (which are generated during sea transgressions; Clout and Simonson, 2005), suggest that these lavas formed at greater water depths than those of the Fivemile Lake Sequence.

Sedimentary structures indicate these rocks formed at depths greater than storm wave base (Hudak pers. comm. 2006).

Persistent mafic and intermediate volcanism was periodically interrupted by felsic volcanism that produced rhyolite lava flows and lapillistone deposits. These deposits occur in the southeast corner of Section 23 (Plate 1) and comprise a 60m thick volcanic pile that extends laterally to the southwest and northeast at a trend of 035°-205°. At the base, felsic volcaniclastic rocks are composed of non-bedded, poorly-sorted, matrix supported fragments. Clasts are composed of 40% <1-3 cm angular to subrounded rhyolite lava lapilli, <1-3 cm angular to subrounded dark grey chert lapilli and 2-4cm subrounded well-dispersed silicified pumice set in recrystallized fine- to coarse-ash matrix. Felsic volcanic rocks transition up-section into aphyric to plagioclase-phyric, felsic lavas that are locally spherulitic. These flows contain 1-15cm, subangular, spherical to elongated, medium- to coarse-lapilli to block sized massive rhyolite lava accessory fragments. A 10m wide mafic dike is located in the center of the edifice. This dike is cut by a felsic dike, suggesting that subsequent volcanism utilized the same, possibly reactivated synvolcanic structures.

The felsic components in the Central Basalt Sequence may represent a blocky rhyolite dome. Blocky domes are aerially restricted and have small volumes of lava which travel <2 km from their source. Typically blocky domes are characterized by steep-sides that are located immediately adjacent to, and above, their feeding fissure or conduit (Gibson et al., 1999). According to Gibson et al. (1999), blocky domes are characterized by three flow facies: (1) an interior of microcrystalline to spherulitic non-vesicular to poorly vesicular massive and flow-banded lava that occurs as dikes, lobes

and autobreccia blocks that grade outwards into (2) a monolithic, block and hyaloclastite-rich carapace breccia that mantles and underlies the massive lava, and (3) flank breccias. Therefore, it appears that the massive and spherulitic lavas that overly lapillistone deposits (with local block and hyaloclastite) comprise a blocky rhyolite dome (Figure 5.02).

Felsic volcanic and volcaniclastic rocks in the Central Basalt Sequence lie approximately 1300m stratigraphically above felsic volcanic and volcaniclastic rocks of the Fivemile Lake Sequence (see Plate 1). A lithogeochemical comparison of chondrite and primitive mantle normalized spider diagrams indicates that felsic volcanic rocks in the Central Basalt Sequence are more enriched in LREE, MREE and HREE which suggests the eruption of a more evolved magma. Their relative location (Plate 1) may suggest the presence of a central long-lived, series of deep penetrating reactive faults and fractures which acted as conduits for periodic felsic volcanism (Franklin et al., 2005).

Conclusions

The Central Basalt Sequence was produced during the latter stages of arc construction simultaneous with the onset of post-collisonal, within-plate volcanism. By comparing the chemical affinities for Fivemile Lake (dominantly plate-marginal arc) and Central Basalt (plate-marginal arc to within-plate) environments, it appears that the Central Basalt Sequence represents part of the latter stages of plate-marginal arc rifting and the beginning of post-collisional within-plate volcanism. The co-genetic relationship between volcanic-arc and within-plate volcanism is unclear. However, within-plate volcanism may be directly related to BIF deposition as suggested by Isley and Abbott (1999). A lack of geochemical data in the Soudan BIF prevents lithogeochemical

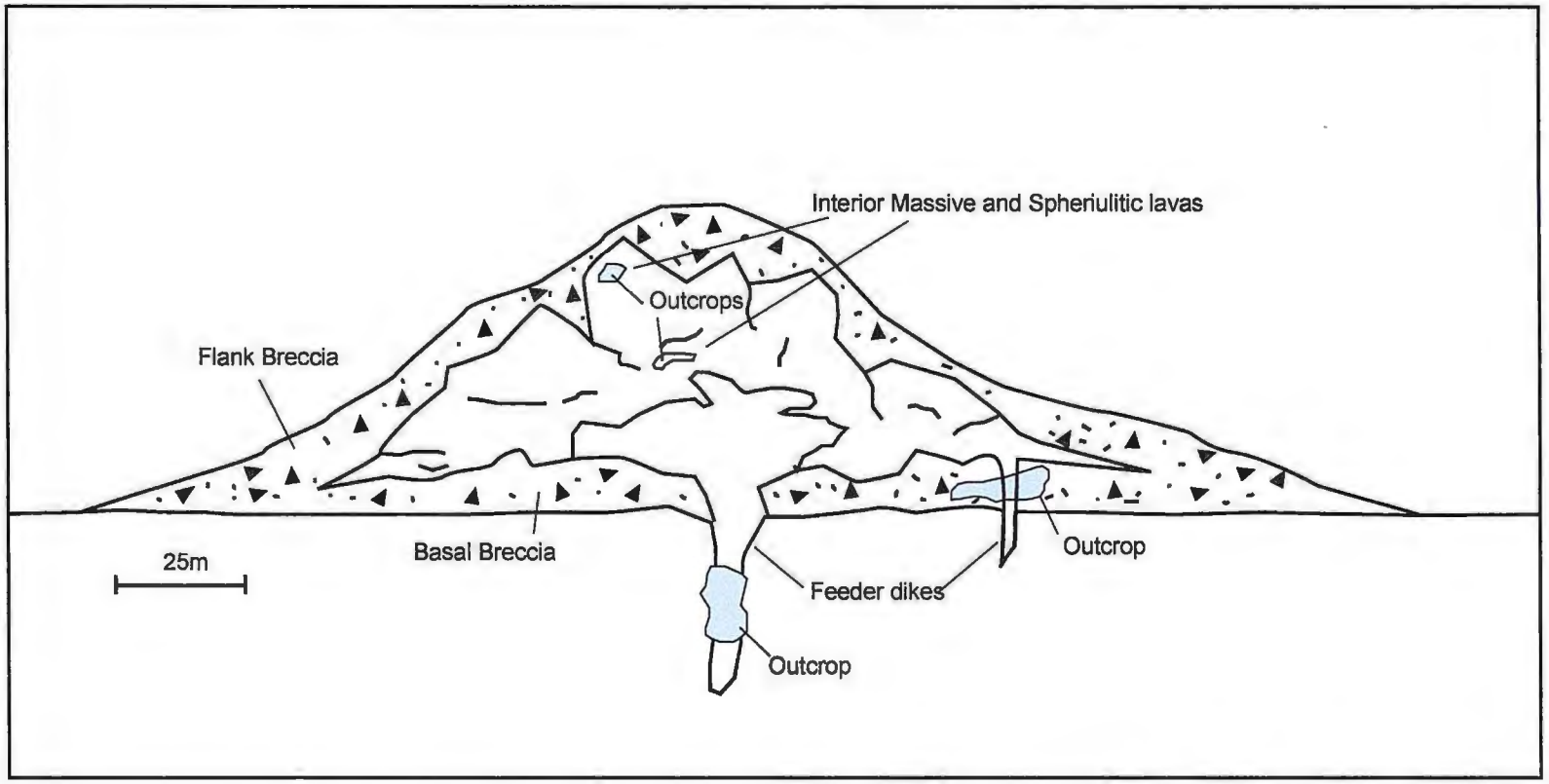

Figure 5.02. Schematic cross section through a blocky rhyolite flow illustrating flow morphology and typical flow and volcaniclastic facies. Gray polygons represent shape and location of outcrops (see Plate 1) in the Central Basalt Sequence (after Gibson et al., 1999)

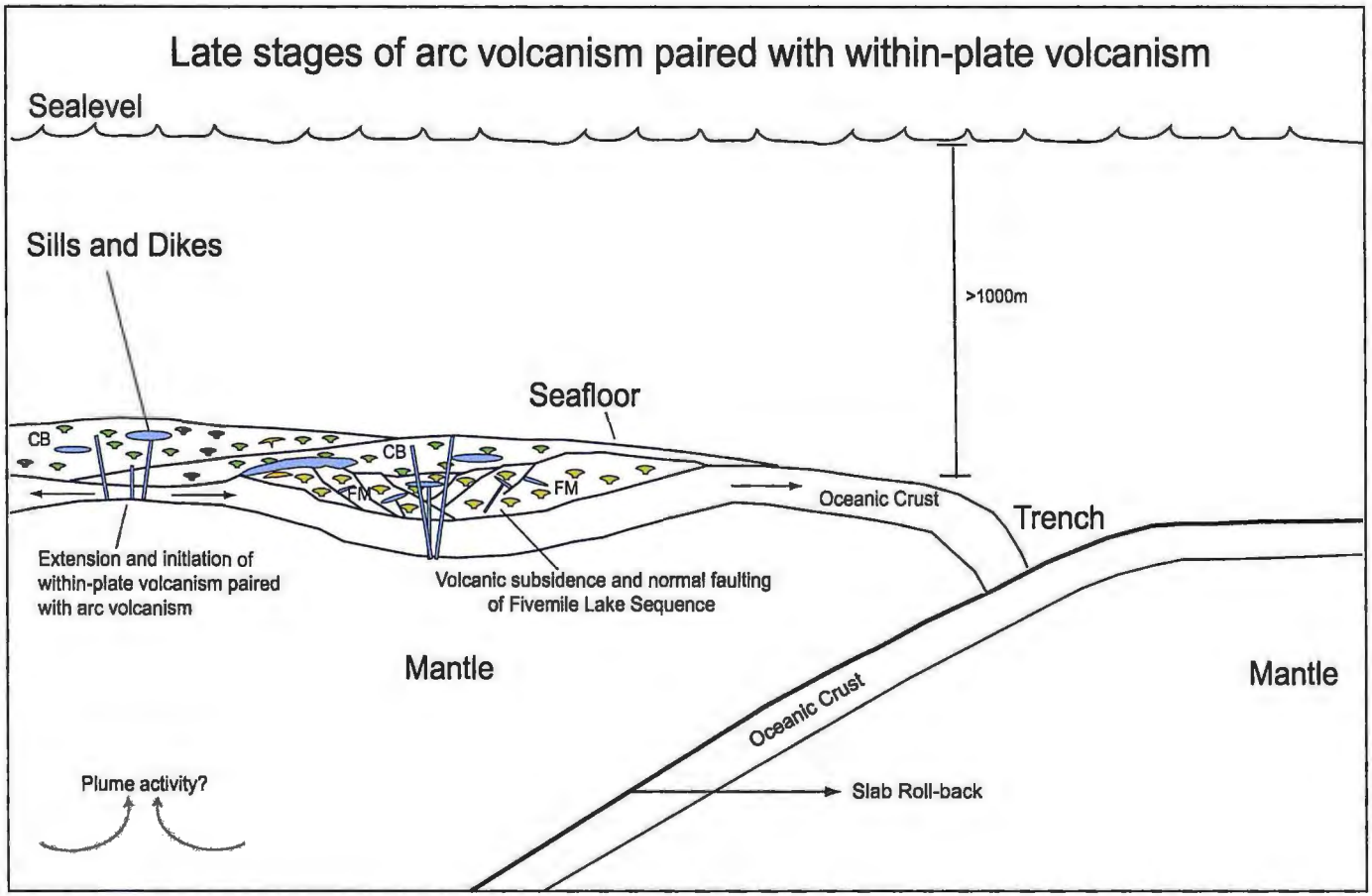

Figure 5.03. Schematic cross section illustrating the late stages of arc volcanism and initiation of slab roll back/early within-plate development and associated volcanism responsible for the formation of the Central Basalt Sequence. Not to scale.

comparisons between within-plate volcanics and BIF. The relationship between these rocks should be explored more thoroughly in the future.

A strong vertical correlation exists between 1) felsic volcanic and volcaniclastic rocks in both the Central Basalt Sequence and Fivemile Lake Sequence; 2) chemical sediments in the Central Basalt Sequence; 3) structurally induced cross-stratal hydrothermal alteration in the Central Basalt Sequence; and 4) cross-stratal synvolcanic syeno-diorite dikes. This correlation provides strong evidence that a central, deep penetrating structural zone exists between the blocky rhyolite dome and felsic volcanic and volcaniclastic rocks in the Fivemile Lake Sequence. Following bimodal volcanism in the Central Basalt Sequence, long lived volcanic quiescence and hydrothermal activity deposited ~650m of BIF, formally known as the Soudan Member of the Ely Greenstone Formation.

Stage III – The Upper Volcanic Sequence

The Upper Sequence comprises volcaniclastic rocks and chemical sediments that blanket several dissected shield volcanoes. The Upper Sequence includes the deposition of felsic lapillistone and breccia deposits, felsic tuff deposits and chemical sediments. The Upper Sequence is intruded by stock and sill-like intrusions of diabase and gabbro that have a within-plate to mid ocean ridge basalt (MORB) signature.

Volcanic Stratigraphy

The lower most 140m-240m of the Upper Sequence comprises felsic volcaniclastic rocks that are monolithic, thinly- to medium-bedded but locally massive, poorly-sorted and dominantly clast-supported. Lapillistone and breccia deposits

comprise 66% subrounded to subangular fine- to block sized rhyolite lava lapilli fragments set in 34% recrystallized medium- to very coarse-ash matrix with randomly oriented quartz and feldspar grains. This rock unit is deformed in the west and pinches out to the northeast but can be followed along strike for approximately 1500 meters (Plate 1). Based on the criteria of Cas and Wright (1987), lapillistone and breccia deposits in the Upper Sequence are interpreted as epiclastic deposits. Stratigraphically above felsic lapillistone and breccia deposits lie laminated to very thinly bedded, non-graded, quartz- and plagioclase-phyric tuff deposits. These deposits are interpreted to represent primary or resedimented subaqueously deposited tuffs.

Volcaniclastic material provides additional evidence that supports the development of a basin through extensional rifting in which these sediments may have been deposited. A lack of geochemical data does not permit the relationship between this unit and the Gafvert Lake Sequence to be determined. However, the volcanic center (edifice) in the Gafvert Lake Sequence documented by Peterson (2001), northeast of the field area, is the most likely source for deposition of primary or resedimented tuff deposits.

Over 600m of oxide facies banded iron formation occurs stratigraphically above felsic volcaniclastic rocks at the base of the Upper Sequence, and basalts and andesites of the Central Basalt Sequence (Plate 1). This unit can be followed along strike for several kilometers to the northeast.

The origins of iron formations remain controversial (Kimberley, 1979, 1989; Dimroth, 1986). It is believed that Algoma-type (Gross, 1965) iron formations are the products of proximal volcanic-driven hydrothermal processes. They may represent the

distal and more diluted equivalent of massive sulfide deposits (Chown et al., 2000), although, research by Chown et al. (2002) on iron formations in the Hunter Mine Group in the Abitibi Subprovince of Canada suggests that iron formation there may have formed from low temperature alteration of subaqueous sediments.

The Neoarchean age, thinly laminated chert-iron oxide bands close association with volcanic rock, and sub-wave base sedimentary strata indicate that the Soudan Iron Formation is an Algoma-type iron formation. Laterally restricted iron formation horizons that occur within the Central Basalt Sequence indicate waxing and waning volcanic and hydrothermal systems.

The sequence of events that led to the deposition of the Soudan Iron Formation consist of three phases; 1) continued extensional rifting of the Central Basalt Sequence and Fivemile Lake Sequence shield volcanoes creating deep submarine basins; 2) development of hydrothermal systems that led to leaching of wall rocks to form silica and iron rich solutions, and their subsequent upward migration, cooling, and precipitation of silica-iron oxide bands on the seafloor; and 3) uplifting of the basin, possibly due to magma-driven tumescence, causing the iron and silica rich sediments to slump prior to lithification. This final process led to the development of sediment convolution, interpreted by Lundy (1985) as soft sediment deformation.

Conclusions

A lack of geochemical data for felsic volcaniclastic rocks and banded iron formation precludes an unambiguous interpretation of the tectonic relationship between the Upper Sequence and its adjacent stratigraphy. However, the stratigraphic make up of the area indicates the development of a basin which must be associated with a divergent

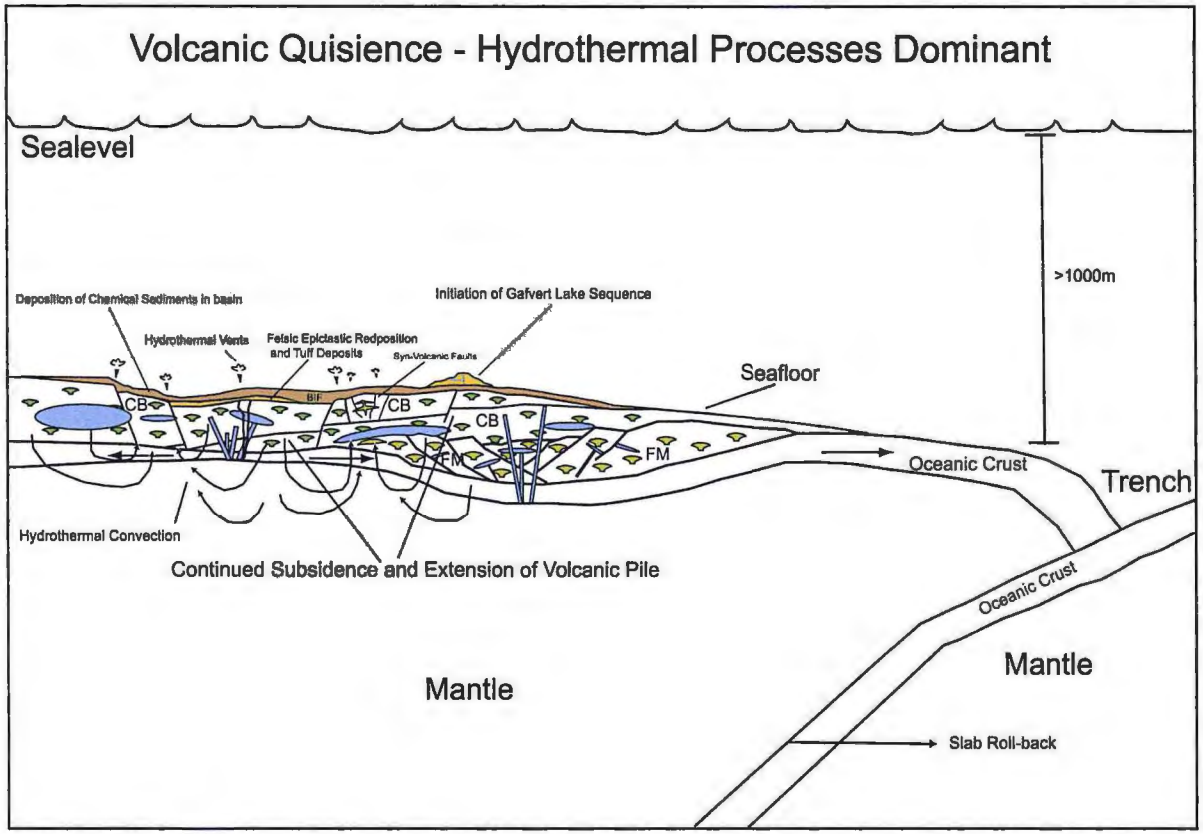

Figure 5.04. Schematic cross section illustrating the deposition of the Soudan Iron Formation by means of hydrothermal convection and the initiation of felsic volcanism related to the Gafvert Lake Volcanic Complex. Analogy for the formation of the Upper Volcanic Sequence. Not to scale.

tectonic setting.

The presence of chemical sediments and large concentrations of epiclastic rocks and primary or resedimented tuff deposits provides strong evidence for quiescence of effusive volcanism. These sediments probably accumulated in basins that may have developed from extension of the overriding plate caused by slab role back (Figure 5.04).

The presence of Algoma-type banded iron formation suggests that hydrothermal processes were dominant during volcanic quiescence.

Stage IV - The Gafvert Lake Volcanic Sequence

Felsic volcanic rocks that lie immediately above the Soudan Iron Formation comprise the base of the Gafvert Lake Volcanic Sequence. According to Peterson (2001), the Gafvert Sequence is composed of felsic lava flows, associated volcaniclastic deposits, and related intrusions that are believed to represent deposits formed in association with one or more Neoarchean stratovolcanoes that formed upon the Lower and Soudan Members of the Ely Greenstone. This edifice is located northeast of the field area (Figure 1.04.).

Volcanic Stratigraphy

In the thesis study area, the base of the Gafvert Lake Sequence is composed of poorly-sorted, clast-supported, non-graded volcaniclastic rocks that comprise <1-400mm angular to subrounded medium-lapilli to block-sized fragments set in 45% dominantly angular recrystallized fine- to coarse-ash to fine-lapilli matrix. Clasts are comprised of plagioclase phyric lava fragments, pumice, chert, and rip-up fragments of banded iron formation. Photomicrographs reveal poorly sorted clasts of felsic volcanic rock set in a

recrystallized coarse grained felsic recrystallized ash matrix that contains broken angular quartz and feldspar grains. Petrographic analysis and field data are consistent, and reveal that these rocks are dominantly massive in nature. The massive texture of this rock may suggest that the base of the Gafvert Lake Sequence near the Soudan Mine study area represents abundant pyroclastic rocks either deposited from primary flows or remobilized and deposited down slope via mass flow processes (Figure 5.05). These rocks may represent the massive basal division (Gibson et al., 1999) of a subaqueous mass flow deposit. Further work in the field needs to be done to better constrain the origin of these deposits.

Lithogeochemical analyses indicate that the Gafvert Lake Sequence was formed by magma generated in an arc setting. The advent of dominantly felsic volcanism is often associated with a mature volcanic arc undergoing simultaneous arc-rifting and back arc basin development (Chown et al., 1992; Corcoran and Dostal, 2001). As indicated above, both arc-type and within-plate-type mafic volcanic rocks are present within the Central Basalt Sequence, which underlies the Gafvert Lake Sequence. Therefore, the Gafvert Lake Sequence appears to represent the products of volcanism associated with a rifting mature volcanic arc.

Conclusions

Felsic volcaniclastic rocks that comprise the Gafvert Lake Sequence lie directly above the Soudan Iron Formation. The presence of banded iron formation rip-up clasts suggests that the base of the Gafvert Lake Sequence scoured the Soudan Iron Formation after lithification. Therefore, the contact between the base of the Gafvert Lake Sequence

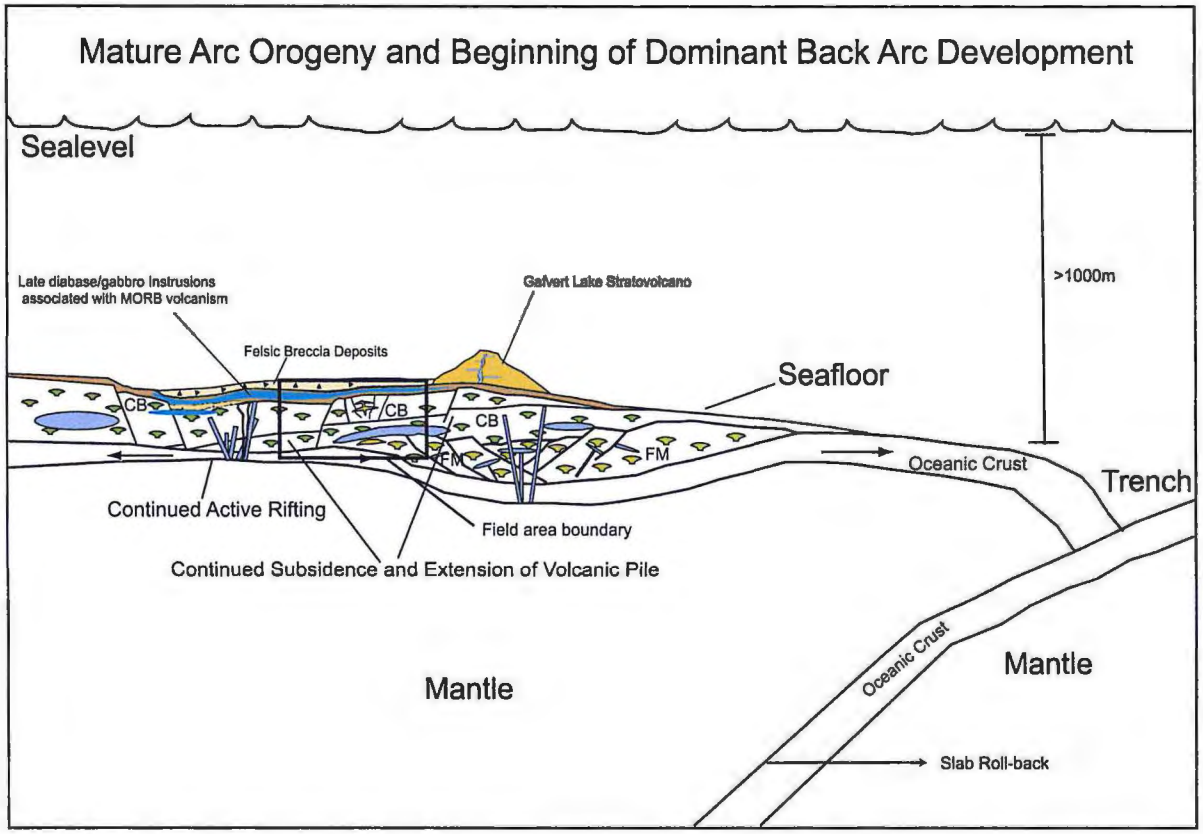

Figure 5.05. Schematic cross-section illustrating mature arc Orogeny and Gafvert Lake Volcanic Complex construction marking the end of arc volcanism and the beginning of dominant back arc development. Analogy for the formation of the Gafvert Lake Sequence. Not to scale.

and the Soudan Iron Formation appears to represent a disconformity. The source of volcaniclastic rocks remains unknown; however these rocks are probably associated with the Neoarchean Stratovolcano (Peterson, 2001) located to the northeast of the field area. Lithogeochemistry of lapillistone and breccia deposits at the base of the Gafvert Lake Sequence suggests that these rocks formed in a volcanic-arc setting. Therefore, the source area for these rocks probably represents volcanism associated with a mature volcanic-arc undergoing rifting and back arc development.

Lithogeochemistry suggests that the Soudan Sill has a within-plate to MORB signature and is therefore interpreted to have intruded after or near the end of arc maturity. The massive intrusion is probably a large reservoir for MORB-type mafic volcanic rocks that have been documented in the Upper Ely Formation by Schultz (1980) and Southwick et al. (1998). The advent of MORB-type rocks within, and stratigraphically above the study area suggests a transition from volcanic-arc to back arc volcanism.

Interpretation of Hydrothermal Processes in the Soudan Mine Area

Alteration mineral assemblages in the Soudan Mine area were produced by a combination of syn-volcanic ancient seafloor hydrothermal activity and overprinted by regional greenschist facies metamorphism. Numerous studies of the physical and chemical characteristics of greenschist facies metamorphism alteration assemblages found in VMS mining camps exist (Gibson et al., 1983; Gibson et al., 1999; Morton and Franklin, 1987; Alt, 1995; Franklin; 1996, Franklin et al., 1981; Seyfried et al., 1999; Santaguida et al., 1999; Franklin et al., 2005). The distribution and mineralogy of these

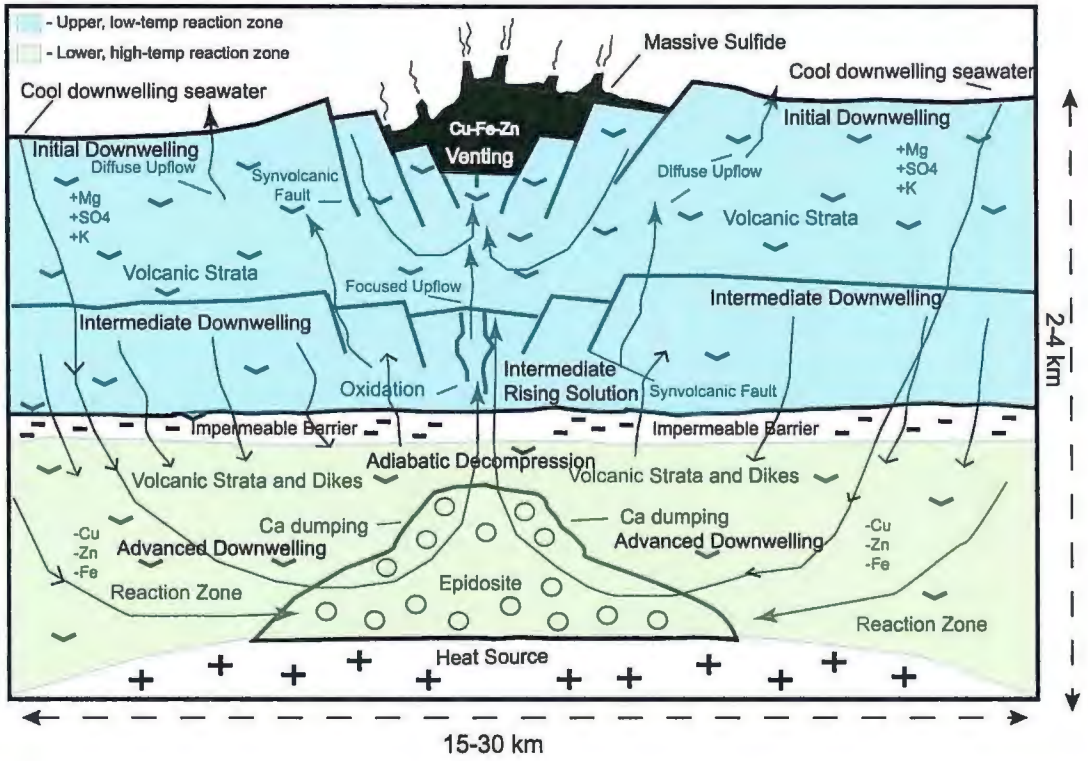

Figure 5.06. Generalized illustration of a hydrothermal cell in a subaqueous volcanic setting, after Mottl (1988), Alt (1995), Franklin (1996), Seyfried et al. (1988), Seyfried et al. (1999) and Franklin et al. (2005). Cool seawater is drawn down and heated by a synvolcanic intrusion. Metasomatic reactions involving magnesium, calcium sulfate and base metals take place creating an evolved metalliferous fluid. The hot fluid buoyantly rises adiabatically back towards the seafloor through synvolcanic structures such as faults. As the fluid approaches the seafloor, the pH increases and the fluid cools, causing base metals to precipitate as sulfide minerals. Water that continues through the system makes up black smoker (>250°) and white smoker (<250°C) hydrothermal vents (Hudak et al., 2002b). Various hydrothermal zones indicated on figure are elaborated on in the text.

assemblages has been documented (see Chapter 3). They appear to be, on a large scale, consistent with the model for syn-volcanic hydrothermal alteration developed for VMS associated hydrothermal systems (Franklin, 1993; Franklin; 1996; Franklin et al., 2005). The Soudan area alteration mineral assemblages will be evaluated and interpreted with respect to this model.

The Chemical/Physical Hydrothermal Process: Comparisons to the Soudan Mine Area

Initial Downwelling Environment

In modern submarine hydrothermal systems, the first major reaction between subseafloor strata and downwelling hydrothermal fluids takes place at temperatures close to ~150°C, and water/rock ratios of >50:1 (Seyfried et al., 1999; Franklin et al., 2005). This reaction involves the removal of Mg as an $Mg(OH)_2$ component from seawater and subsequent incorporation into the rock to form Mg-chlorite. Simultaneously, feldspars and ferromagnesian minerals are broken down in the rocks, and alkali elements, iron, and manganese are given up to the hydrothermal fluid:

$$Mg^{2+} + H_2O + \text{Pyroxene} = \text{Mg (OH) silicates} + H^+ \qquad (1)$$

In modern seafloor systems, the resulting mineralogy in the wall rocks comprises Mg-chlorites, quartz, talc, serpentine and anhydrite. As the water-rock interaction increases chlorite chemistry increases in Mg, Al, and H_20 and decreases of Si and Mn (Seyfried et al., 1988).

The initial downwelling zone is represented in the Soudan Mine area by mineral assemblage (4). The abundance of Mg-chlorite, quartz, and the pseudomorphing of feldspar into sericite is common. The mineral talc was never found in the field or in thin section most likely due to Mg/(Mg + Fe) ratios in the fluid (see Saccocia et al., 1994 and Seyfried et al., 1999). Rocks within mineral assemblage (4) were not geochemically analyzed for major oxide and trace elements. Therefore, the isocon method was not employed and the exact metasomatic gains and losses were not measured for this assemblage.

Intermediate Downwelling

In the intermediate downwelling zone, water rock ratios are typically 10-40:1 and temperatures are 150-350°C. Magnesium becomes scarce in the fluid because of the formation of talc and/or Mg-chlorite in the rocks. There is a continuous increase in Ca, Na, Fe, Mn, SiO_2, K, Rb, Li, B and Bi, as feldspars and ferromagnesian minerals continue to breakdown. Silicate hydrolysis consumes H^+ from the solution and results in the production of micas (sericite ± chlorite/clays/smectites) and a simultaneous increase in fluid pH. Rock minerals are altered to Mg-chlorite and talc and retrograde solubility occurs in and along veins, contacts and selvages resulting in the formation of anhydrite in these areas (Seyfried et al., 1988).

In the Soudan Mine area, the intermediate downwelling zone may represent advanced stages of mineral assemblage (4). The mineral anhydrite was not found during field or petrographic analysis, although sericite was common, especially in more felsic epiclastic rocks found below the iron formation. The lack of anhydrite in ancient VMS

systems is common and is believed to be due to the retrograde solubility of anhydrite once the hydrothermal system wanes.

Advanced Downwelling Environment

As the fluid moves deeper below the seafloor (>2 km), water/rock ratios decrease, to approximately <10:1, and temperatures increase to ~350->400°C. Within this part of the hydrothermal cell, all magnesium has been removed from the seawater by the formation of Mg-rich phyllosilicates; the seawater solution is now referred to as an evolved fluid. As the fluid approaches temperatures of ~350°C, calcium is released from the evolved fluid (as $Ca(OH)_2$ compounds) into the rocks, and results in the formation of secondary Ca-bearing silicates such as epidote and/or Ca-rich plagioclase feldspar (Berndt et al., 1989; 1993). As this occurs, the pH of the hydrothermal fluid falls to approximately 3-4 (Seyfried et al., 1988).

$$CaAl_2Si_2O_8\,(\text{Anorthite}) + Ca^{2+} + 2H_2O \leftrightarrow 2\text{Clinozoisite} + 2H^+ \quad (2)$$

$$NaAlSi_3O_8\,(\text{Albite}) + Ca^{2+} \leftrightarrow CaAl_2Si_2O_8\,(\text{Anorthite}) + 4SiO_2 + 2Na^+ \quad (3)$$

As the temperature increases deeper within the hydrothermal system, the evolved fluid becomes increasingly rich in Na-Cl-K-Fe-Mn as the weathering of feldspars and primary ferromagnesian minerals continues. The resulting mineralogy of the rocks consists of a quartz, epidote and Ca-rich plagioclase feldspar. If all calcium is consumed from the evolved fluid prior to the complete alteration of plagioclase feldspar, albite may remain (Hudak pers. comm., 2006).

The advanced downwelling environment appears to be represented by the alteration mineral assemblages' epidote ± quartz (1a) and quartz ± epidote (2) found in mafic and intermediate rocks in the Soudan Mine Area. The relative gains and losses of components in epidote ± quartz assemblage rocks (Chapter 4) are characterized by gains in Ca (101%), Al (51%), Mg (51%) and Na (29%), and losses in Mn(-15%) and K(-85%).

In general, the metasomatic changes in this alteration assemblage are consistent with those in the advanced downwelling environments in models proposed by Mottl (1988), Alt (1995), Franklin (1996), Seyfried et al. (1988), Seyfried et al. (1999) and Franklin et al. (2005) (See Figure 5.06).

The variable presence of magnesium chlorite in mineral assemblage (1) and (2) may have resulted from: a) high water/rock ratios throughout the initial and intermediate down welling stages, or; b) late stage cold seawater flushing through the system as the hydrothermal system waned.

Epidosite (Mottled Environment)

As the evolved fluid moves deeper (> 3km) into the seafloor, water/rock ratios generally approach 1:1, but can locally exceed 1000:1. At this level in the crust, the fluid temperature increases to ≥ 400°C, and the pressure approaches ~400 bars (Seyfried et al., 1988). Metasomatism includes the leaching of Cu, Zn, Fe, Mn, Mg, and possibly Al from the wall rocks. Transitional elements and base metals (Cu, Zn, Fe, Mn) are mobilized primarily as chloride complexes in the fluid (Saccocia et al., 1994). Quartz + epidote ± actinolite assemblages result in the wall rocks from the addition of Ca, Sr, H_20, and Fe^{3+}. At this point the fluid approaches a supercritical state, and a chlorine-poor

"vapor" phase and a chlorine-rich "brine" phase may separate from one another (Berndt et al., 1989; Berndt and Seyfried, 1993). The rocks are left rich in epidote and quartz, and Fe^{3+} is consumed by the rock from the hydrothermal fluid to form iron-bearing epidote (e.g. pistacite). Minor amounts of Al^{3+} may be added to the hydrothermal fluid as shown by equation 4 below:

$Ca_2Al_3O\ (SiO_4)\ Si2O7\ (OH)$ (clinozoisite) + $Fe^{3+} \leftrightarrow$

$Ca_2\ (Al,Fe)\ Al_2O\ (SiO_4)\ (Si_2O_7)\ (OH)$ (epidote) + Al^{3+} (4)

Experimental studies and field studies in ophiolite complexes (Harper, 1999) indicate that this environment comprises ~75% epidote and ~25% quartz, with minor ferromagnesian minerals such as chlorite and actinolite (Saccocia et al., 1994). In the footwall rocks of most VMS deposits this area may be called the cracking front, as it commonly occurs at or near the top of synvolcanic intrusions.

According to Harper (1999), epidosites are recognized by the presence of granoblastic epidote + quartz + chlorite + titanite ± magnetite, and represent the interactions of wall rocks with large volumes of highly reacted seawater derived fluids. The location and distribution of the mottled epidote ± quartz (1b) assemblage suggests that the Sugar Mt. Sill represents the heat source that drove hydrothermal alteration in the field area. However, an intrusion capable of driving a large regional scale hydrothermal system has yet to be recognized in the Soudan Mine area. Therefore, the mottled epidote ± quartz (1b) assemblage may represent a lower temperature deep-seated epidosite-like environment typically formed in the footwall of VMS deposits. Hudak et al. 2002b has

documented a mottled epidosite-like zone (assemblage 3CM) near Fivemile Lake. The Mottled Epidote + Quartz ± Actinolite assemblage at Fivemile Lake appears to be confined to synvolcanic fault zones and areas where focused hydrothermal fluid flow would be anticipated. At Fivemile Lake, this assemblage has been interpreted to represent a synvolcanic, semiconformable to disconformable alteration zone formed by high temperature fluid: rock interactions deep within a sub-seafloor hydrothermal cell (Hudak et al., 2002b).

Isocon analysis of the mottled epidote ± quartz altered rocks (see Chapter 4) in the Soudan Mine area indicates gains in Si (89%), Ca (436%), Sr (279%) and Fe (95%). This is consistent with the gains and losses in the hydrothermal alteration models proposed by Mottl (1988), Alt (1995), Franklin (1996), Seyfried et al. (1988), Seyfried et al. (1999) and Franklin et al. (2005) (see Figure 5.06). However, gains in Cu (587%), Zn (42%), Mn (100%), Mg (128%) and Al (49%) are not consistent with these models, as these elements are typically depleted in the epidosite environment (Harper, 1999). The relative increases in base metals within the mottled epidosite ± quartz assemblage (1b) suggest that: 1) the evolved fluid was not buoyant enough to rise to the seafloor and may have instead pooled in the footwall rocks; or 2) base metal deposition by later, lower-temperature hydrothermal fluids occurred as the hydrothermal system waned.

Adiabatic Decompression Environment

As the evolved fluid attains its maximum temperature, it starts to rise buoyantly upward through the seafloor. This fluid rises adiabatically at rates of 1-5 m/s. During its upward journey, the fluid decompresses as the sum of hydrostatic and lithostatic pressure

decreases (Seyfried, 1999). Adiabatic decompression leads to increases in Fe^{3+}/Fe^{2+} and increased rates of oxidation in the fluid. Epidote formation continues, and the production of iron silicates (Fe-chlorite + Fe-actinolite) is stimulated (Seyfried et al., 1988).

The presence of magnetite in healed fissures in the Soudan Mine area may represent mineralization as a result of an adiabatically cooled evolved fluid rising through the volcanic stratigraphy. The formation of the actinolite + epidote ± garnet ± magnetite assemblage (5) near and adjacent to the intersection of Sections 23, 24, 25 and 26, likely resulted from metasomatism between rising evolved fluid and the adjacent rocks.

Isocon analysis of the actinolite + epidote ± garnet ± magnetite assemblage (5) rocks are enriched in Ca (171%) and Na (84%), and depleted in Fe (-19%), and K (-50%). The gains in Ca are consistent with rocks formed within an up-flow environment. However, the losses of Fe in the rock are not consistent with an up-flow environment (Seyfried et al., 1988). Isocon analysis was performed on a sample that did not contain magnetite and garnet occupied open spaced fillings such as interpillow hyaloclastite and/or cross-stratal veins. Instead, the sample was from pillow interiors where garnet and magnetite are typically absent except in amygdules or cross-stratal veinlets. Healed fissures containing magnetite and garnet suggests that large amount of iron were liberated from the rock into the fluid as they moved towards the seafloor.

Intermediate Rising Solution Environment

The rising evolved hydrothermal fluid generally >350°C, is enriched in base- and alkali- metals, silica, and H_2, depleted in Mg and Ca, and has a moderately acidic (3-5)

pH (Seyfried et al., 1988). This fluid continues to rise adiabatically at 1-5 m/s. The rapid decrease in pressure may cause silica dumping (Figure 5.07).

Alteration mineral assemblage (6) Fe-chlorite ± quartz ± sericite may have formed in this environment. This assemblage occurs in coherent felsic rocks which contain chlorite-rich "pipe-like" alteration, and in mafic volcanic rocks containing "braided" disconformable chlorite-rich alteration zones. The abundance of quartz may have resulted from silica dumping during adiabatic decompression, or, more likely, a decrease in fluid temperature as the upwelling fluid mixes with cooler hydrothermal solutions shallower in the seafloor. Further geochemical studies will need to be

med to further constrain the processes responsible for silica dumping in these rocks.

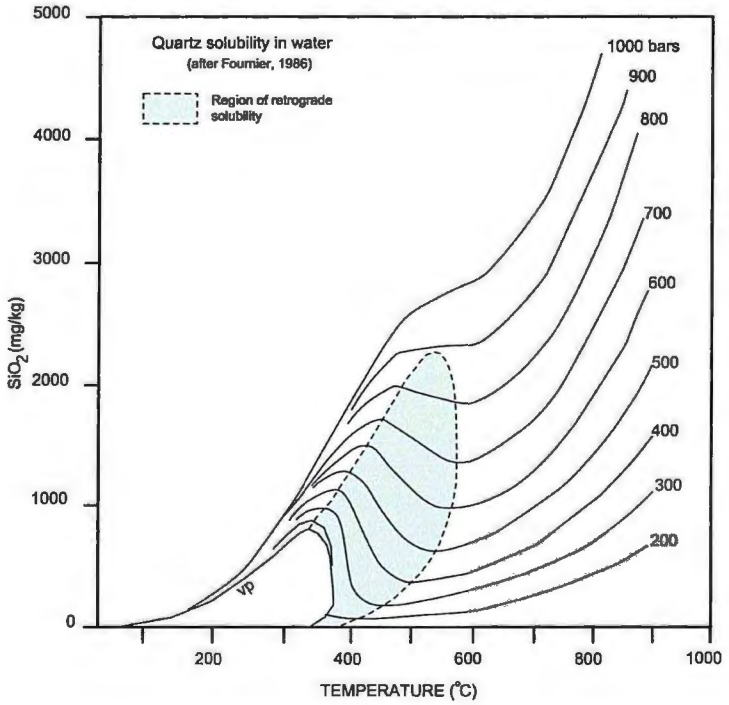

Figure 5.07. The relative solubility of silica in water with respect to temperature and pressure (after Fournier, 1986).

Hydrothermal Vent or Seafloor Deposition Environment

As the evolved fluid approaches the seafloor, base metals precipitate out as the fluid is cooled by, and mixes with, ambient and/or shallow seafloor ground waters. The pH rises to near neutral ambient seawater levels as the moderately acidic evolved fluid mixes with, and is diluted by, fresh sea water. This decreases the evolved fluid's ability to transport base-metals as chloride complexes, and as a result, base metal-bearing sulfide minerals are precipitated. Additional silicate phases that form in this environment include quartz, albite, Mg- and or Fe-chlorite, clays, and sericite and/or paragonite.

The sericite ± quartz alteration mineral assemblage is believed to have formed as rising evolved fluid mixed with cool seawater in a near seafloor environment. Sericite altered rhyolite and basalt lavas are interpreted to represent altered rocks formed near a vent zone.

Isocon analysis indicates that the sericite ± quartz assemblage (7) is characterized by gains in Cu (7%), Zn (20%), Mg (78%), Si (56%), LOI (32%) and K (421%), and losses in Mn (-14%) and Fe (-2%). These gains and losses are, in a general sense, consistent with the gains and losses suggested by submarine hydrothermal alteration models proposed by Mottl (1988), Alt (1995), Franklin (1996), Seyfried et al. (1988), Seyfried et al. (1999) and Franklin et al. (2005) (See Figure 5.06).

Conclusions

Alteration mineral assemblages in the Soudan Mine area resulted from a combination of syn-volcanic ancient seafloor hydrothermal activity and subsequent regional greenschist facies metamorphism. The distribution and mineralogy of these assemblages have been documented, and appear to be, on a broad scale, similar in

distribution and composition of hydrothermal alteration assemblages that occur in the footwall rocks of many lava-flow dominated Archean VMS deposits (Franklin, 1993; Franklin, 1996; Morton and Franklin, 1987; Franklin et al., 2005).

The mottled epidote ± quartz assemblage is associated with anomalous concentrations of copper and zinc immediately up-section from the Sugar Mountain Sill. This suggests that fluid temperature and pH were at the proper conditions for transporting base metals (Figure 5.08). Based on the alteration distribution, the Sugar Mountain Sill is believed to have been the local heat source for hydrothermally altered rock in the Soudan Mine area. This intrusion may have generated numerous small localized hydrothermal cells that mobilized, and subsequently deposited, copper and zinc over short distances. However, its small sized suggests it did not posses a sufficient amount of heat required to establish a broad, long-lived, hot hydrothermal system necessary to form VMS. The absence of a discrete synvolcanic structural zone may have led to unfocused fluid migration and discharge, also preventing anomalous concentrations of base metal sulfide minerals from being precipitated.

The relative high solubility of iron versus copper and zinc (Figure 5.09) suggests that iron would be leached from deep in the footwall rocks. Isocon analysis suggests that low concentrations of iron are present in the footwall rocks when compared to copper and zinc. The upward migration of iron may be partly responsible for the local concentrations of banded iron formation in the hanging wall of the Central Basalt Sequence. The presence of magnetite in more permeable zones (interpillow material, vesicles, and fissures) may be a strong indication that the alteration at the Soudan Mine area is related to the formation of the Soudan Member of the Ely Greenstone rather than

base metal massive sulfide deposits. Few published studies of hydrothermal alteration zones associated with Algoma-type BIF exist in the literature; therefore further detailed work is needed in the vicinity of the Soudan Mine and surrounding areas (between the Soudan Mine study area and Fivemile Lake) in order to better understand the significance of the alteration zones and the genesis of the Soudan BIF in the Vermilion District.

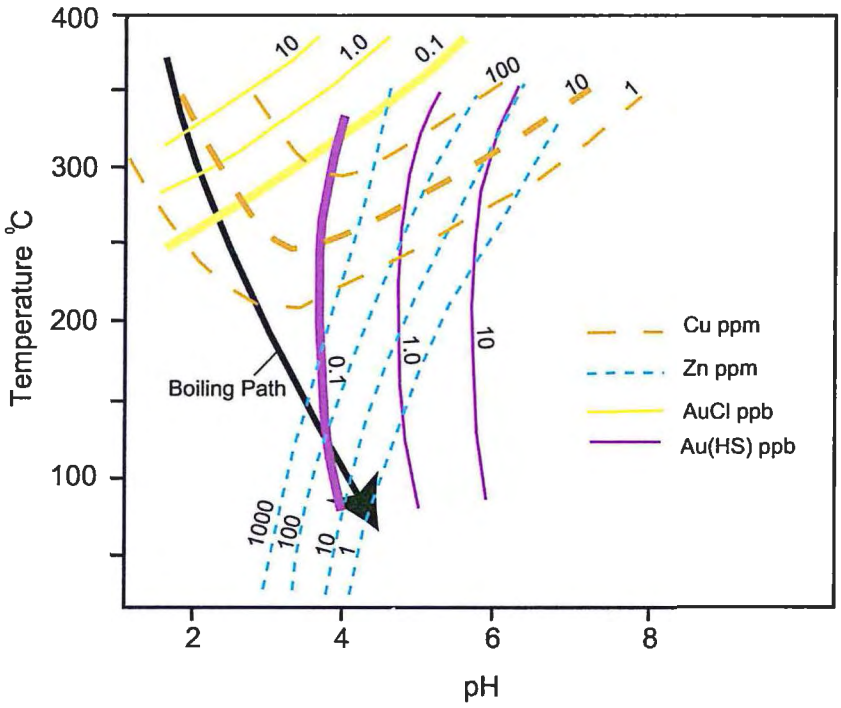

Figure 5.08. Solubility curves for Cu, Zn, and Au complexes under typical fluid conditions in sea-floor VMS systems (Hannington et al., 2005). Thick lines represent compositions for typical ridge-crest hydrothermal fluids. Copper content in fluid is most influenced by temperature, whereas zinc content is most influenced by pH (Franklin et al., 2005).

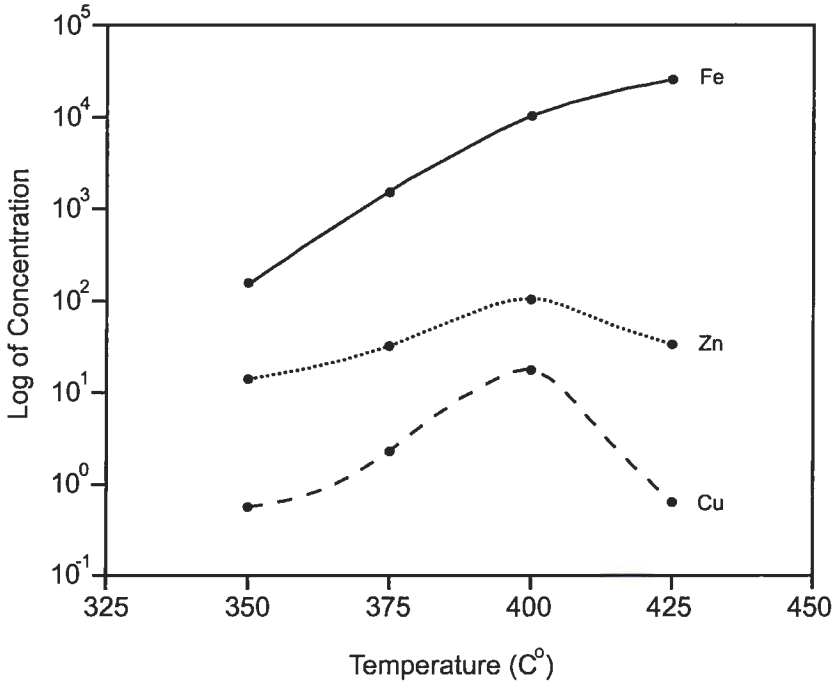

Figure 5.09. Relative concentration of Fe, Zn and Cu (in μmolal) in an experimental hydrothermal fluid at 400 bars. As temperature increases from 350-425°C the solubility of iron increases exponentially with respect to zinc and copper (after Seyfried and Janecky, 1985).

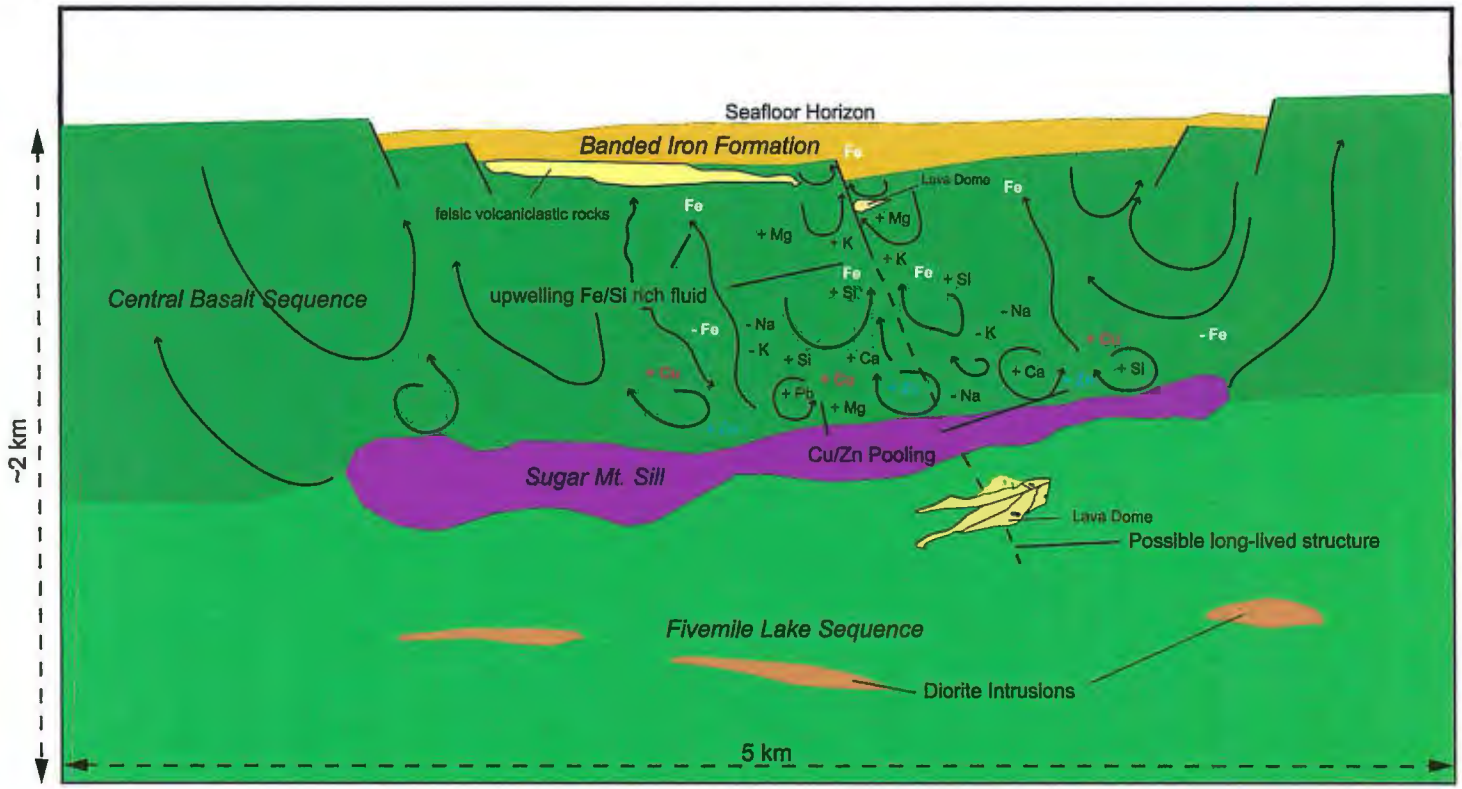

Figure 5.10. Alteration model showing the relative losses and gains of components in the Soudan Mine area. Notice the deposition of copper and zinc and the relative loss of Fe (Table 4.06). This suggests that Fe is being mobilized from the footwall volcanic rocks in the hydrothermal fluids. Such iron metasomatism may ultimately be related to the formation of the Soudan BIF.

Chapter 6

SUMMARY AND CONCLUSIONS

Summary

The stratigraphy in the Soudan Mine area was determined via detailed field mapping, petrographic analysis, and lithogeochemical methods. Together these data have played a major role in establishing lithological boundaries and evaluating the volcanic, volcaniclastic, and intrusive rocks. They have also provided essential information that led to the development of a volcanological and hydrothermal alteration model. These data have provided a better understanding of the origins of hydrothermal alteration that may have been associated with the development of oxide facies banded iron formation, and have led to a better understanding concerning the apparent lack of VMS in this part of the Lower Member of the Ely Greenstone.

The generalized stratigraphy, from oldest to youngest, consists of a) the Fivemile Lake Sequence; b) the Central Basalt Sequence; c) the Upper Sequence; and d) the Gafvert Lake Sequence. Intrusive rocks are syn-volcanic with respect to the Ely Greenstone Formation. Post-volcanic regional deformation (D_2) and metamorphism produced sheared rocks and regional greenschist facies mineral assemblages which characterize the study area.

The oldest volcanic strata in the Soudan Mine study area comprise the Fivemile Lake Sequence. The Fivemile Lake Sequence is a north-facing, steeply dipping bimodal succession of subaqueous aphyric to plagioclase-phyric andesite and rhyodacite pillowed and massive lavas, pillow flow top breccias, and basalt and rhyodacite lapillistone and

breccia deposits that subsequently underwent structural deformation and hydrothermal alteration.

Pillows in the Fivemile Lake Sequence are mainly amoeboid or mattress-shaped, and range in size from 50-150 cm along strike and are 30-75 cm thick. The pillows contain vesicles up to 15 mm in diameter. Rocks in the Fivemile Lake Sequence are similar in affinity to plate-margin, island arc tholeiitic basalts. Lithogeochemical similarities suggest that volcanic rocks at Soudan are correlative with volcanic rocks 5 km east, near Fivemile Lake (Hudak et al., 2002b).

Felsic rhyodacite to dacite volcanic and volcaniclastic rocks in the Fivemile Lake Sequence occur as three distinct lithologies: 1) rhyodacite to dacite lava flows; 2) lapillistone and breccia deposits that have characteristic consistent with co-ignimbrite deposits; and 3) lapilli-bearing tuff deposits. Rhyodacite to dacite rocks in the Fivemile Lake Sequence have chemical affinities consistent with granites that formed in a syn-collisional, volcanic-arc setting. High field strength elements and rare earth element concentrations suggest that felsic rocks resemble FII-type rhyolites (Lesher et al., 1986; Hart et al., 2004).

The Central Basalt Sequence is a north-facing, steeply-dipping, mafic-dominated, bimodal succession of subaqueous volcanic, volcaniclastic, intrusive, and chemical sedimentary rocks that are locally deformed, texturally well-preserved, and moderately to extensively hydrothermally altered. Rock types in the Central Basalt Sequence include pillowed basalt and massive andesite lavas, pillow- and flow-top breccias, rhyolitic volcanic and volcaniclastic deposits, and chemical sedimentary rocks.

Pillowed and massive lavas in the Central Basalt Sequence are poorly-vesiculated, aphyric to plagioclase-phyric, and have associated pillow breccias, mafic tuff deposits, and interpillow and flow-margin hyaloclastite. Pillows are mainly ovoid or bun-shaped with some amoeboid shaped pillows occurring locally. Pillows generally range in size from 8-75 cm along strike, and are 7-40 cm thick. Pillows in the Central Basalt Sequence are generally smaller than pillows in the Fivemile Lake Sequence.

Rhyolitic volcanic and volcaniclastic rocks in the Central Basalt Sequence have chemical affinities similar to within-plate generated granites. High field strength elements and rare earth element concentrations suggest that felsic rocks in the Central Basalt Sequence resemble FIIIa-type rhyolites (Lesher et al., 1986; Hart et al., 2004)

The Upper Sequence is a north-northwest facing, steeply-dipping, well-preserved (but locally deformed) suite of rocks that is well exposed throughout the field area. The sequence includes the Soudan BIF and felsic volcanic and volcaniclastic rocks immediately in the footwall of the Soudan BIF. The Upper Sequence is interpreted to represent epiclastic redeposition deposits that were preceded by primary or resedimented tuff deposits interpreted to be associated with a Neoarchean stratovolcano located to the northeast of the field area. Felsic volcaniclastic rocks are preceded by long-lived volcanic quiescence and low temperature hydrothermal alteration that produced ~650m of oxide facies banded iron formation.

The Gafvert Lake Sequence is a north-northwest facing, steeply-dipping, well-preserved suit of rhyodacite-dacite-trachyandesite volcaniclastic rocks that have chemical affinities consistent with volcanic-arc syn-collisonal generated granites. The textures found in the field and in thin section suggest that rocks at the base of the Gafvert Lake

Sequence represent the massive facies of a mass flow deposit. High field strength elements and rare earth element concentrations in these rocks suggest that rocks in the Gafvert Lake Sequence have FI-type rhyolite affinities (Lesher et al., 1986; Hart et al., 2004). The presence of angular rip-up clasts of BIF and black chert, suggest that the mass flow was deposited following lithification of the BIF. Therefore, this contact may represent a disconformity.

Intrusive rocks in the Soudan Mine area are syn-volcanic with respect to the Ely Greenstone based on: 1) the occurrence of structural fabric; 2) the occurrence of hydrothermal alteration associated with seafloor metamorphism; and 3) cross-cutting relationships to bedding. Intrusive rocks mainly occur along major sequence contacts, within sequences, or as thin 1-4 m wide pseudo-linear northwest-northeast trending porphyry dikes and east-west trending sills.

Synvolcanic intrusions comprise diorite porphyry dikes and sills, mafic diabase sills (Sugar Mt. Sill, Soudan Sill, and undifferentiated diabase), gabbro porphyry sills, feldspar porphyry diorite dikes, quartz feldspar syeno-diorite porphyry dikes and sills. In general, intrusive rocks in the Fivemile Lake Sequence have chemical affinities suggestive of genesis in a plate-marginal volcanic arc setting. Intrusive rocks in the Central Basalt Sequence have chemical affinities suggestive of rocks that formed in a plate-marginal volcanic-arc to within-plate post-collisonal setting. The Sugar Mountain Sill has chemical affinities similar to rocks that formed in a plate marginal volcanic-arc to post-collisional within-plate setting. The Soudan Sill has chemical affinities similar to rocks that formed in a within-plate, mid ocean ridge (MORB) setting.

Sheared rocks occur as dominantly east-west trending, curvilinear bands of schist and phyllite that contain diverse assemblage of alteration minerals believed to have been derived from metasomatism associated with deep-seated hydrothermal fluids during the 2680-2685 Ma (D_2) structural events (Corfu and Stott, 1998). Sheared rocks are part of two major sub-parallel structures that displace rocks from west to east. These structures comprise the Murray Shear Zone and Mine Trend Shear Zone.

A detailed study of alteration assemblages using petrographic methods and field mapping at a 1:2000 scale was conducted for this thesis. *Semiconformable* epidote ± quartz, mottled epidote ± quartz, quartz ± epidote, actinolite ± epidote ± quartz, Mg-chlorite ± quartz ± sericite, and sericite ± quartz assemblages, and *discordant* actinolite + epidote ± garnet ± magnetite and Fe-chlorite ± quartz ± sericite were mapped in the field area. Mass balance analysis was completed via the isocon method. The high field strength elements Ti, Zr Hf, Nb, Y and P and the rare earth element Cr were found to be immobile during seawater-dominated metasomatism in the Soudan Mine area. The isocon method was used to calculate the elemental gains and losses in four of the seven hydrothermal alteration assemblages (see Chapter 4 for results). Mass gains (33-100%) consistently occurred for the four alteration assemblages analyzed via the isocon method.

Conclusions

The Fivemile Lake Sequence represents part of a laterally extensive Neoarchean mafic shield volcano. This volcano comprises dominantly andesite lava flows, with minor basalt and rhyodacite lava flows and volcaniclastic rocks. It formed in a submarine, subduction generated, juvenile mantle-derived ocean-ocean plate island-arc

system during Neoarchean time. The presence of numerous small diorite dikes and stock-like intrusions in the Fivemile Lake Sequence suggests the presence of numerous hypabyssal magma chambers during volcanism. The felsic components in the Fivemile Lake Sequence comprise a series of explosive co-ignimbrite eruptions followed by effusive rhyodacite lava flows. The introduction of rhyolite volcanism in mafic-dominated volcanic successions is commonly associated with mature arc construction, arc rifting and the beginning of back arc development (Chown et al., 1992; Corcoran and Dostal, 2001).

The Central Basalt Sequence is part of a large mafic shield complex that extends at least 5 kilometers to the east of the present study area. Geochemical studies indicate that the Central Basalt Sequence lavas in the Soudan Mine area represent the products of coeval island-arc and within-plate associated volcanism. The coeval relationship between island-arc and within-plate volcanism is unclear. Isley and Abbott (1999) suggest that the presence of plume related (within-plate, ocean island) volcanism may be directly related to the deposition of banded iron formation. Further geochemical studies need to be completed to constrain this relationship.

The lack of vesicles and multiple-selvage pillows in mafic lava flows, and the close association with banded iron formation, suggest that these lavas likely formed at greater water depths than those of the Fivemile Lake Sequence.

The felsic lithofacie in the Central Basalt Sequence are consistent with the presence of a blocky rhyolite dome. Felsic volcanic and volcaniclastic rocks in the Central Basalt Sequence lie approximately 1300m stratigraphically above felsic volcanic and volcaniclastic rocks of the Fivemile Lake Sequence (see Plate 1). This may suggest

the presence of a long-lived series of deep penetrating reactive faults and fractures which acted as conduits for periodic felsic volcanism (Franklin et al., 2005).

The Upper Sequence represents chemical and volcaniclastic rock suites that blanket several dissected shield volcanoes. The Upper Sequence is intruded by stock and sill-like intrusions of diabase and gabbro that have a within-plate, mid ocean ridge (MORB) signature. The deposition of banded iron formation is interpreted to have occurred in basins created by extensional rifting of the Central Basalt Sequence and Fivemile Lake Sequence shield volcanoes. Rifting created deep sea basins, enhanced cross-stratal permeability, and promoted the development of hydrothermal systems that led to leaching of wall rocks to form silica and iron rich solutions. The subsequent upward migration, cooling, and precipitation of silica-iron-rich hydrothermal fluids resulted in approximately 650 m of BIF.

The Gafvert Lake Sequence rocks in the Soudan Mine area represent the basal facies of a mass flow deposit associated with a Neoarchean Stratovolcano located to the northeast of the field area. The presence of BIF rip-up clasts and black chert within the mass flow suggests emplacement after lithification of the Soudan BIF. The contact relationship between the Soudan BIF and the base of the Gafvert Lake Sequence in this location may represent a disconformity. Lithogeochemical analyses indicate that the source rocks for the Gafvert Lake Sequence mass flow were formed in an arc setting. Therefore, the Gafvert Lake Sequence appears to represent the products of volcanism associated with a rifting mature volcanic-arc.

Alteration mineral assemblages in the Soudan Mine area resulted from a combination of ancient syn-volcanic seafloor hydrothermal activity and subsequent

regional greenschist facies metamorphism. The distribution and mineralogy of these assemblages appear to be, on a large scale, similar with those associated with syn-volcanic hydrothermal alteration that occurs in the footwall of VMS deposits (Franklin, 1993; Franklin, 1996; Franklin et al., 2005). Isocon analysis reveals that there are anomalous concentrations of copper and zinc in the mottled epidote ± quartz alteration assemblage in the rocks directly above the Sugar Mountain Sill. Therefore, the Sugar Mountain Sill is recognized as the local heat source for hydrothermally altered rock in the Soudan Mine area. Heat derived from this intrusion may have resulted in numerous local hydrothermal cells that continuously mobilized and deposited copper and zinc on a small scale. However, its small size yielded insufficient heat to produce the long lived high temperature hydrothermal system necessary to make VMS. The lack of an impermeable barrier in the field area (see Figure 5.07), and the relative lack of copper-zinc sulfide mineralization in what has been interpreted to be the "venting environment", may have resulted from low sulfur fugacity in the Sugar Mountain Sill. The relatively high solubility of iron versus copper and zinc (Figure 5.10) suggests that iron would have been extensively leached in the footwall rocks, an observation that has been documented. Isocon analysis suggests that relative low concentrations of iron are present in the footwall rocks when compared to copper and zinc. Therefore, iron was probably mobilized in the upwelling hydrothermal fluids. The migration of iron may be partly responsible for the local concentrations of banded iron formation in the hanging wall of the Central Basalt Sequence. The presence of magnetite in more permeable zones (interpillow material, vesicles, veins), if primary, may be a strong indication that the alteration at the Soudan Mine area is related to the formation of the Soudan Member of

the Ely Greenstone, and that the proper thermal and structural conditions were not met to promote the formation of massive sulfide deposits.

References Cited

Alt, J. C., 1995, Subsea-floor processes in mid-ocean ridge hydrothermal systems, *in* Humpris, S. E., Zierenberg, R. A., Mullineaux, L. S., and Thomson, R. E. (eds.), Seafloor hydrothermal systems: physical, chemical, biological, and geological interactions: Geophysical Monograph, v. 91, pp. 85-114.

Anhaeusser, C.R., 1971, Cyclic volcanicity and sedimentation in the evolutionary development of Archaean greenstone belts of shield areas. In: J.E. Golver (Ed.), Symposium on Archaean rocks. Geol. Soc. Australia, Sydney, Spec. Publ., 3, pp. 57-70.

Ayers, L.D., 1982, A subaqueous to subaerial transition zone in the Early Proterozoic metavolcanic sequence, Amisk Lake, Saskatchewan. In: Centre for Precambrian Studies, Annual Report, 1981, University of Manitoba, pp. 49-61.

Balangue-Tarriela, M.I.R., 2004, Chemical reaction path modeling of hydrothermal mineralization in the Tongonan geothermal field, Leyte (Philippines): Geothermics v. 33, p. 143-179.

Ballard, R. D., Holcomb, R. T., and van Andel, T., 1979, The Galapagos Rift at 86°W: Sheet flows, collapse pits, and lava lakes of the Rift Valley: Journal of Geophysical Research, v. 84, p. 5407-5422.

Barrett, T. J., and MacLean, W. H., 1999, Volcanic sequences, lithogeochemistry, and hydrothermal alteration in some bimodal volcanic-associated massive sulfide systems: Reviews in Economic Geology, v. 8, p. 101-131.

Barrie, C. T., and Hannington, M. D., 1997, Introduction: Classification of VMS Deposits Based on Host Rock Composition: *in* Barrie, C. T., and Hannington, M. D. (eds.), Volcanic Associated Massive Sulphide Deposits: Processes and Examples in Modern and Ancient Settings: GAC-MDD-SEG Short Course Volume, May 17-18, Ottawa, Ontario, Canada, p. 1-12.

Barrie, C.T., and Hannington, M.D., 1999, Classification of Volcanic-Assoicated Massive Sulfide Deposits Based on Host-Rock Composition: Reviews in Economic Geology, v. 8, pp. 1-11.

Barrie, C.T., Ludden, J.N., and Green, T.H., 1993, Geochemistry of volcanic rocks associated with Cu-Zn and Ni-Cu deposits in the Abitibi Subprovince: Economic Geology, v. 88, p. 1341-1358.

Bauer, R.L., 1985, Correlation of early recumbent and younger upright folding across the boundary between an Archean gneiss belt and greenstone terrane, northeastern Minnesota: Geology, v. 13, p.657-660.

Berndt, M. E., and Seyfried, W. E., Jr., 1993, Calcium and sodium exchange during hydrothermal alteration of calcic plagioclase at 400°C and 400 bars, Geochimica et Cosmochimica Acta, v. 57, pp. 4445-4451.

Berndt, M. E., Seyfried, W. E., Jr., and Janecky, D.R., 1989, Plagioclase and epidote buffering of cation ratios in mid ocean ridge hydrothermal fluids: experimental results in and near the supercritical region, Geochimica et Cosmochimica Acta, v. 53, pp. 2283-2300.

Blatt, H. and Tracy, R.J., 1996, Petrology: Igneous, Sedimentary, and Metamorphic, 2nd Edition, W.H. Freeman and Company, New York.

Blundell, D.J., 2002, The timing and location of major ore deposits in an evolving orogen: The geodynamic context: Geological society Special Publication 204, p. 1-12.

Boerboom, T.J., and Zartman, R.E., 1993, Geology, geochemistry, and geochronology of the central Giants Range batholith, northeastern Minnesota: Canadian Journal of Earth Science, v. 30, pp. 2510-2522.

Butterfield, D.A., Massoth, G.J., McDuff, R.E., Lupton, J.E., and Lilley, M.D., 1990, Geochemistry of hydrothermal fluids from Axial Seamount hydrothermal emissions study vent field, Juan de Fuca Ridge: Subseafloor boiling and subsequent fluid-rock interaction: Journal of Geophysical Research, v. 95, sec. B, p. 12,895-12,912.

Card, K. D., and Ciesielski, A., 1986, DNAG No. 1. Subdivisions of the Superior province of the Canadian Shield: Geosci. Canada, v. 13, pp. 5-13.

Cas, R.A.F., 1992, Submarine volcanism: Eruption styles, products, and relevance to understanding the host-rock successions to volcanic-hosted massive sulfide deposits: Economic Geology, v. 87, p. 511-541.

Cas, R. A., F., and Wright, J. V., 1987, Volcanic Successions: Modern and Ancient: London, Allen and Unwin, 528 p.

Chown, E.H., Daigneault, R., Mueller, W. and Mortensen, J., 1992. Tectonic evolution of the northern volcanic zone, Abitibi belt, Quebec. Can. J. Earth Sci., 29: 2211-2225.

Chown, E.H., N'Dah, E. and Mueller, W.U., 2000. The relation between iron-formation and low temperature hydrothermal alteration in an Archean volcanic environment. Precambrian Res., 101: 263-275.

Clements, J.M., 1903, The Vermilion iron-bearing district of Minnesota: U.S. Geological Survey, Monograph 45, 463 p.

Clout, J.M.F., and Simonson, B.M., 2005, Precambrian Iron Formations and Iron Formation-hosted Iron Ore Deposits: Economic Geology 100th Anniversary Volume, p. 643-649.

Corcoran, P.L., 2000. Recognizing distinct portions of seamounts using volcanic facies analysis: examples from the Archean Slave Province, NWT, Canada. Precambrian Research., 101: 277-261.

Corcoran, P.L., and Dostal, J., 2001. Development of an ancient back-arc basin overlying continental crust: the Archean Peltier Formation, Northwest Territories, Canada. J. Geol., 109: 329-348.

Corfu, F., and Stott, G.M., 1998, Shebandowan greenstone belt, western Superior Province: U-Pb ages, tectonic implications, and correlations: Geological Society of America Bulletin, v. 110, pp. 1467-1484.

Cox, K. G., Bell, J. D., and Pankhurst, R. J., 1979, The Interpretation of Igneous Rocks: London,George Allen and Unwin, 450 p.

de Rosen-Spence, A.P., Provst, G., Dimroth, E., Gochnauer, K. and Owen, V., 1980. Archean subaqueous felsic flows, Rouyn-Noranda, Quebec, Canada and their Quaternary equivalents. Precambrian Res., 12: 43-78.

Dimroth, E., 1986, Depositional environments and tectonic settings of the cherty iron-formations of the Canadian Sheild. Geol. Soc. India 28, 239-250.

Dimroth, E. and Rocheleau, M., 1979. Volcanology and sedimentology of the Rouyn-Noranda area, Quebec. Geol. Assoc. Canada, Field Trip A-1, Guide Book, Universite´ Laval, Quebec, 193 pp.

Fisher, R.V., 1961, Proposed classification of volcaniclastic sediments and rocks: Geological Society of American Bulletin, v. 72, pp. 1409-1414.

Fisher, R.V., 1966, Rocks composed of volcanic fragments, Earth Science Reviews, v. 1, pp. 287-298.

Fisher, R.V., and Schmincke, H.-U., 1984. Pyroclastic Rocks. Springer-Verlag, New York, 472 pp.

Floran, R. J. and Papike, J.J., 1978, Mineralogy and petrology of the Gunflint iron formation, Minnesota-Ontario: correlation of compositional and assemblage variations at low to moderate grade. Journal of Petroleum 19, p. 215-288.

Fournier, R. O., 1986, Chapter 3 - The Behavior of Silica in Hydrothermal Solutions: in Berger, B. R., and Bethke, P. M., eds., Geology and Geochemistry of Epithermal Systems: Reviews in Economic Geology, v. 2., p. 45-59.

Fowler, A.D., Berger, B., Shore, M., Jones, M.I., and Ropchan, J., 2001, Supercooled rocks: development and significance of varioles, spheriulites, dendrites and spinifex in Archean volcanic rocks, Abitibi Greenstone belt, Canada. Journal of Precambrian Research V. 115, p. 311-328.

Franklin, J.M., 1993, Volcanic-associated massive sulphide deposits, *in* Kirkham, R.V., Sinclair, W.D., Thorpe, R.L., and Duke, J.M., eds., Mineral deposit modeling: Geological Association of Canada Paper 40, p. 315-334.

Franklin, J. M., 1996, Volcanic-associated massive sulfide base metals, *in* Eckstrand, O. R., Sinclair, W. D., and Thorpe, R. I. (eds.), Geology of Canadian Mineral Deposit Types. Geological Survey of Canada, no. 8, p. 158-183.

Franklin, J.M., Sangster, D.M., and Lydon, J.W., 1981, Volcanic associated massive sulfide deposits, in Economic Geology 75th Anniversary Volume B.J. Skinner (ed.), pp. 485-627.

Franklin, J.M., Gibson, H.L., Jonasson, I.R., and Galley A.G., 2005, Volcanogenic Massive Sulfide Deposits, in Society of Economic Geology 100th Anniversary Volume, pp. 523-560.

Fyon, J. A., Breaks, F. W., Heather, K. B., Jackson, S. L., Muir, T. L., Stott, G. M, and Thurston, P. C., 1992, Metallogeny of metallic mineral deposits in the Superior Province of Ontario: *in* Thurston, P. C., Williams, H. R., Sutcliffe, R. H., and Stott, G. M. (eds.), Geology of Ontario: Ontario Geological Survey, Special Volume 4, Part 2, p. 1091-1176.

Giagrande, P., 1981, Geology and sulphide mineralization of the Skeleton Lake prospect: Unpublished M. S. thesis, University of Minnesota, Duluth, 118 p.

Gibson, H. L., 1989, The mine sequence of the Central Noranda Volcanic Complex: Geology, alteration, massive sulfide deposits and volcanological reconstruction: unpublished Ph. D. dissertation, Carleton University, Ottawa, Ontario, Canada, 800 p.

Gibson, H.L., 1990, The mine sequence of the Central Noranda Volcanic Complex: Geology, alteration, massive sulphide deposits and volcanogical reconstruction: Unpublished Ph.D. thesis, Ottawa, Carleton University, 715 p.

Gibson, H. L., Watkinson, D. H., and Comba, C. D. A., 1983, Silicification: hydrothermal alteration in an Archean geothermal system within the Amulet Rhyolite Formation, Noranda, Quebec: Economic Geology, v. 78, p. 954-971.

Gibson, Harold L., Morton., Ronald L., and Hudak, George J., 1999 Submarine volcanic processes, deposits, and environments favorable for the location of volcanic-associated massive sulfide deposits, in Volcanic Associated Massive Sulphide Deposits: Processes and Examples in Ancient and Modern Settings; Eds., Barrie, T. and Hannington, M. in Reviews in Economic Geology, pp. 13-51.

Gifkins C.C. and Allen R.L. 2001, Textural and Chemical Characteristics of Diagenetic and Hydrothermal alteration in Glassy Volcanic Rocks: Examples from the Mt. Reed Volcanics Tasmania. Economic Geology Volume 96 #5 pp 973-1002.

Gordan, M. P., and Schandl, E. S., 2000, From continents to island arcs: a geochemical index of tectonic setting for arc-related and within-plate felsic to intermediate volcanic rocks: The Canadian Mineralogist, v. 38, p. 1065-1073.

Grant, James A., 1986, The isocon diagram- A simple solution to Gresens' equation for Metasomatic alteration, Economic Geology, v. 81, pp. 1976-1982.

Gresens, R.L., 1967, Composition-volume relationship of metasomatism: Chem. Geology, v. 2, p. 47-55.

Gross, G.A., 1965, Geology of Iron Deposits in Canada; Vol. I, General Geology and Evaluation of Iron Deposits. Geol. Surv. Can., Econom. Geol. Rep. 22, 181 pp.

Hannington, M., Herzig, P., and Scott, S.D., 1991, Auriferous hydrothermal precipitates on the modern sea floor, in Foster, R.P., ed., Gold metallogeny and exploration: Glasgow, Blackie and Son, p. 242-282.

Hargraves, R., and Ayres, L. D., 1979, Morphology of Archean metabasalts flows, Utic Lake, Manitoba: Canadian Journal of Earth Sciences, v. 16, p. 1452-1466.

Harper, G.D., 1999, Structural Styles of Hydrothermal Discharge in Ophiolite/Sea-floor Systems, Volcanic Associated Massive Sulphide Deposits: Processes and Examples in Ancient and Modern Settings, Reviews in Economic Geology v. 88 p. 53-73.

Harris, N. B. W., Pearce, J. A., and Tindle, A. G., 1986, Geochemical characteristics of collision zone magmatism, *in* Coward, M. P. and Reis, A. C. (eds.), Collision Tectonics: Special Publication of the Geological Society 19, p. 67-81.

Hart, T., Gibson, H.L., and Lesher, C.M., 2004, Trace element geochemistry and petrogenesis of felsic volcanic rocks associated with volcanogenic Cu-Zn-Pb massive sulfide deposits: Economic Geology, v. 99, p. 1003-1013.

Hajash, A., and Chandler, G.W., 1981, An Experimental Investigation of High Temperature Interaction Between Seawater and Rhyolite, Andesite, Basalt, and Peridotite: Contributions to Mineralogy and Petrology, V. 78 p. 240-254.

Heiling, C., 2003, Peperites of the Gafvert Lake Volcanic Complex, St.Louis County, Minnesota: in Woodruff, L. G., and Bornhorst, T., eds., Institute on Lake Superior Geology, Volume 49, Part 1 - Proceedings and Abstracts, p. 27-28.

Hey, M.H., 1954, A New Review of the Chlorites: Mineralogical Magazine, V. 31, p. 277-292.

Hocker, S.M, Hudak, G.J., and Heine, J., 2003, Electron microprobe analysis of alteration mineralogy at the Archean Fivemile Lake volcanic-associated massive sulfide mineral prospect in the Vermilion District of NE Minnesota: Natural Resources Research Institute, University of Minnesota Duluth, Report of Investigation NRRI/RI-2003/17, 49 p.

Hoffman, P. F., 1990, On Accretion of Granite-Greenstone Terranes: Nuna Conference on Greenstone Gold and Crustal Evolution, Val D'OR, 15 p.

Hooper, P., and Ojakangas, R., 1971, Multiple deformation in the Vermilion district, Minnesota: Canadian Journal of Earth Sciences, v. 8, p.423-434.

Hovis, S. T., 2001, Physical Volcanology and Hydrothermal Alteration of the Archean Volcanic Rocks at the Eagles Nest Volcanogenic Massive Sulphide Prospect, Northern Minnesota. M.S. Thesis, University of Minnesota Duluth, Duluth, Minnesota, 10 p.

Http://www.physics.umn.edu/research/underground.html

Hudak, G.J., 1996, The Physical Volcanology and Hydrothermal Alteration Associated with Late Caldera Volcanic and Volcaniclastic Rocks and Volcanogenic Massive Sulfide Deposits in the Sturgeon Lake Region of Northwestern Ontario, Canada. University of Minnesota PhD thesis. P. 198-220.

Hudak, G.J., 2005, Personal communication, University of Wisconsin Oshkosh.

Hudak, G.J., and Morton, R.L., 1999, Mineral Potential Study, Minnesota Department of Natural Resources Project 326, Bedrock and Glacial Drift Mapping for VMS and Lode Gold Alteration in the Vermilion-Big Fork Greenstone Belt, Part A:

Discussion of Lithology, Alteration, and Geochemistry at the Five Mile Lake, Eagles Nest, and Quartz Hill Prospects: Minnesota Department of Natural Resources Division of Minerals Project 326 Report, 136 p.

Hudak G.J., and Peterson D.M., 2003 Personal communication, University of Minnesota Duluth.

Hudak G.J., Heine J., Hocker., Hauck., 2002a, Geologic Mapping of the Needleboy Lake-Six Mile Lake Area, Northeastern Minnesota: A Summary of Volcanogenic Massive Sulfide Potential. Report of Investigations NRRI/RI-2002/14.

Hudak, G.J., Heine, J., Newkirk, T., Odette, J., and Hauck, 2002b. Comparative Geology, Stratigraphy, and Litho-Geochemistry of the Five Mile Lake, Quartz Hill, and Skeleton Lake VMS Occurrences, Vermilion District, NE Minnesota: A report to the Minerals Coordinating Committee, Minnesota Dept. of Natural Resources, 390 p.

Hudak, G. J., Heine, J., Jirsa, M., and Peterson, D., 2004, Volcanic stratigraphy, hydrothermal alteration, and VMS potential of the Lower Ely Greenstone, Fivemile Lake to Sixmile Lake Area: in Severson, M. and Heinz, J., 2004, 50th Annual Meeting Institute on Lake Superior Geology, Proceedings Volume 50, Part 2 - Field Trip Guidebook, p. 1-44.

Hudak, G.J., Hocker-Finamore, S.M., and Heine, J., 2006, Field Distribution, Petrography, and Lithogeochemistry of Epidosites in the Vicinity of Fivemile, Needleboy and Sixemile Lakes, Vermilion District, NE Minnesota: Procedings of the 52nd ILSG Annual Meeting, Volume 52, Part 1, p. 30-31.

Hudak G.J., 2006 Personal communication, University of Minnesota Duluth.

Hudleston, P.J. 1976, Early deformation history of Archean rocks in the Vermilion district, northeastern Minnesota: Canadian Journal of Earth Sciences, v. 13, p. 579-592.

Hudleston, P.J., Schultz-Ela, D., and Southwick, D.L., 1988, Transpression in an Archean greenstone belt, northern Minnesota: Canadian Journal of Earth Sciences, v. 25, p. 1,060-1,068.

Isley, A.E., and Abbott, D.H., 1999, Plume-related mafic volcanism and the deposition of banded iron formation, Journal of Geophysical Research, Vol. 104, No. B7, pp. 15,461-15,477.

Jenner, G. A., 1996, Trace element geochemistry of igneous rocks: geochemical nomenclature and analytical geochemistry: *in* Wyman, D. A. (ed.)., Trace

Element Geochemistry of Volcanic Rocks: Applications for Massive Sulphide Exploration: Geological Association of Canada, Short Course Notes 12, p. 1-77.

Jirsa, M.A., 2000, The Midway sequence: a Timiskaming-type pull-apart basin deposit in the western Wawa subprovince, Minnesota: Canadian Journal of Earth Science, v. 37. p. 1-15.

Jirsa, M. A., Southwick, D. L., and Boerboom T. J., 1992 Structural evolution of Archean rocks in the western Wawa Subprovince, Minnesota; refolding and of precleavage nappes during D2 transpression, Canadian Journal of Earth Science, v. 29, p. 2146-2155.

Kimberley, M.M., 1979. Geochemical distinctions among environmental types of iron formations. Chem. Geol. 25, 185-212.

Kimberley, M.M., 1989. Exhalative origins of iron formations. Ore Geol. Rev. 5, 13-145.

Kokelar, P., 1986, Magma-water interactions in subaqueous and emergent basaltic volcanism: Bulletin of Volcanology, v. 48, p. 275-289.

Large, R.R., Gemmell J.B., Paulick, H., The Alteration Box Plot: A Simple Approach to Understanding the Relationship between Alteration Mineralogy and Lithogeochemistry Associated with Volcanic-Hosted Massive Sulfide Deposits. Economic Geology, v. 96, 2001, pp. 957-971.

LeMaitre, R.W., 1984, A proposal by the IUSG Subcommission on the Systematics of Igneous Rocks for chemical classification of volcanic rocks based on the total alkali silica (TAS) diagram. Australian Journal of Earth Sciences 31, v.2, pp 243-255.

Lentz, D. R., 1998, Petrogenetic evolution of felsic volcanic sequences associated with Phanerozoic volcanic-hosted massive sulfide systems: the role of extensional geodynamics: Ore Geology Reviews, v. 12, p. 289-327.

Lundy, J.R., 1985, Clues to Structural History in the Minor Folds of the Soudan Iron Formation, NE Minnesota, Minneapolis, University of Minnesota, 144 p., unpublished M.S. Thesis.

Lesher, C. M., Goodwin, A. M., Campbell, I. H., and Gorton, M. P., 1986, Trace-element geochemistry of ore-associated and barren felsic metavolcanic rocks in the Superior Province, Canada; Canadian Journal of Earth Science, v. 23, p. 222-237.

McBirney, A.R., 1963, Factors governing the nature of submarine volcanism: Bulletin of Volcanology, v. 30, p. 337-363.

McPhie, J., Doyle, M., Allen, R., 1993, Volcanic Textures: Centre for Ore Deposit and Exploration Studies, Key Center, University of Tasmania, 198 p.

Mitchell, R.H., 1994, The lamprophyre facies, Mineralogy and Petrology, 51 p.137-146.

Morey, G.G., Green, J.C., Ojakangas, R.W. and Sims, P.K., 1970, Stratigraphy of the Lower Precambrian rock in the Vermilion District, northeastern Minnesota., Minnesota Geological Survey, Report of Investigation 14, 33 p.

Morton, R.L., 2003, personal communication, University of Minnesota-Duluth.

Morton, R.L., and Franklin, J.M., 1987, Twofold classification of Archean volcanic-associated massive sulfphide deposits: Economic Geology, v. 82, pp. 1057-1063.

Mottl, M.J., and Seyfried, W.E., 1980, Sub-sea floor hydrothermal systems: Rock-vs. seawater-dominated, *in* Rona P.A., and Lowell R.P., eds., Seafloor spreading centers and hydrothermal systems, Benchmark papers in geology, v. 56: Dowden, Hutchinson & Ross, p. 66-82.

Mueller, W.U., and White, J.D.L., 2004. Terminology of Volcaniclastic and Volcanic Rocks: The Precambrian Earth: Tempos and Events: Developments in Precambrian Geology V. 12, p. 273-277.

Newkirk, T., Hudak, G. J., and Hauck, S. A., 2001b, Preliminary lava flow morphology studies at the Five Mile Lake VMS prospect, Vermilion District, NE Minnesota: Implications for volcanic processes, volcanic paleoenvironments, and VMS exploration (abstract): Geological Society of America Abstracts and Programs v. 33, no. 6, p. A-398.

Odette, J. D., Hudak, G. J., Suszek, T., and Hauck, S. A., 2001b, Preliminary evaluation of hydrothermal alteration mineral assemblages and their relationship to VMS-style mineralization in the Five Mile Lake area of the Archean Vermilion Greenstone Belt, NE Minnesota (abstract): Geological Society of America Abstracts and Programs v. 33, no. 6, p. A-420.

Orton, G. J., 1996, Volcanic Environments: *in* Reading, H. G. (Ed.), Sedimentary Environments: Processes, Facies, and Stratigraphy: Oxford, Blackwell, 3rd Edition, p. 485-567.

Pearce, J. A. and Cann, J. R., 1973, Tectonic setting of basic volcanic rocks determined using trace element analysis: Earth and Planetary Science Letters, v. 19, p. 290-300.

Pearce, J. A., and Gale, G. H., 1977, Identification of ore-deposition environment from trace element geochemistry of associated igneous host rocks: Geological Society Special Publication, v. 7, p. 14-24.

Pearce, J. A., Harris, N. B. W., and Tindle, A. G., 1984, Trace element discrimination diagrams for the tectonic interpretation of granitic rocks: Journal of Petrology, v. 25, p. 956-983.

Peterson, D.M., 1998, IRRRB Exploration Report: Geological and Mineral Potential Report on the Purvis Road Cu-Zn Prospect, Northeastern Minnesota, Economic Volcanological Research Laboratory, Department of Geology, University of Minnesota Duluth. 19 p.

Peterson, D.M., 2003, personal communication, University of Minnesota-Duluth.

Peterson, D.M., and Patelke, R.L., 2003 National Underground Science and Engineering Laboratory (NUSEL): Geologic Site Investigation for the Soudan Mine, Northeastern Minnesota.

Peterson, D.M., 2001 Development of Archean lode gold and massive sulfide exploration models using Geographic Information System applications: Targeting mineral exploration in northeastern Minnesota from analysis of analog Canadian mining camps: University of Minnesota Ph.D. thesis.

Peterson, D.M., and Jirsa, M.A., 1999a, Bedrock geologic map and mineral exploration data, western Vermillion district, St. Louis and Lake Counties, northeastern Minnesota: MGS Miscellaneous Map M-98, scale 1:48,000.

Peterson, D.M., and Jirsa, M.A., 1999b, Lode gold and massive sulfide prospects in the Archean western Vermilion district: Minnesota Exploration Association, Minnesota Exploration Conference, Field Trip Guidebook, 10 maps, 30 p.

Peterson, D.M., Gallup, C., Jirsa, M.A., and Davis, D.W., 2001, Correlation of Archean assemblages across the U.S.-Canadian border; Phase I geochronology, abstract and oral presentation, Institute on Lake Superior Geology, 47th Annual Meeting, Thunder Bay, Ontario, v. 47.

Peterson, D.M., Jirsa, M. A., and Hudak, G. J., 2005, Field Trip 9 - Architecture of an Archean Greenstone Belt: Stratigraphy, Structure, and Mineralization: *in* Robinson, L., ed., Field Trip Guidebook for selected geology in Minnesota and Wisconsin: Minnesota Geological Survey Guidebook 21, p. 154-180.

Phillips, W.R., and Griffin, D.T., 1981, Optical Mineralogy-The Non-opaque Minerals: W.H. Freeman and Co., San Francisco, 677 p.

Piercey, S.J., Paradis, S., Murphy, D. C., and Mortensen, J. K., 2001, Geochemistry and paleotectonic setting of felsic volcanic rocks in the Finlayson Lake volcanic-hosted massive sulfide district, Yukon, Canada: Economic Geology, v. 96, p. 1877-1905.

Piercey S.J., 2005, Lithogeochemistry of mafic rocks associated with VMS systems: In Franklin J.M., Gibson H.L., Hannington M, Piercey S., Hart T, Riverin G., Hudak G., Target Selection Criteria for VMS deposits: Annual workshop in mineral exploration. Laurentian University April 2005.

Pirajno, F., 1992, Hydrothermal mineral deposits: principles and fundamental concepts for the exploration geologist, Berlin; New York: Springer-Verlag, 100-155 p.

Rollinson, H.R., 1993, Using geochemical data: evaluation, presentation, interpretation, Longman Scientific and Technical, Essex, England, pp.133-157.

Rose, A.W., Burt, D.M., 1979, Hydrothermal alteration. In: Barnes, H.L., (ed) Geochemistry of hydrothermal ore deposits. John Wiley & Sons, New York, pp 173-227.

Rousseau, R.M., 2001, Detection Limit and Estimate of Uncertainty of Analytical XRF Results: The Rigaku Journal, v. 18, no.2 p. 33-47.

Saccocia, P. J., Ding, K., Berndt, M. E., Seewald, J. S., and Seyfried, W. E., Jr., 1994, Experimental and theoretical perspectives on crustal alteration at mid-ocean ridges, *in* Lentz, D. R. (ed.), Alteration and alteration processes associated with ore-forming systems: Geological Association of Canada, Short Course Notes, v. 11, p. 403-431.

Santaguida, F., Gibson, H. L., and Watkinson, D. H., 1999, Hydrothermal alteration mineral assemblages associated with volcanic-hosted massive sulphide mineralization in the Noranda area, Quebec: Geological Association of Canada / Mineralogical Association of Canada Field Trip Guidebook B8, 57 p.

Schlatter, D.M., 2005, Volcanic Stratigraphy, Chemical Stratigraphy and Hydrothermal Alteration of the Petiknas South Volcanic-Hosted Massive Sulfide Deposit Sweden. Published Thesis, 128 pp.

Schultz, K.J., 1980, The magmatic evolution of the Vermilion greenstone belt, NE Minnesota, Precambrian Research, V. 11, pp. 215-245.

Seyfried, W.E. Jr., and Janecky, D.R., 1985, Heavy metal and sulfur transport during subcritical and supercritical hydrothermal alteration of basalt: Influence of fluid pressure and basalt composition and crystallinity: Geochimica et Cosmochimica Acta, v. 49, p. 2545-2560.

Seyfried, W.E. Jr., and Ding, K., 1995, Phase equilibria in subseafloor hydrothermal systems: A review of the role of redox, temperature, pH and dissolved Cl on the chemistry of hot spring fluids at mid-ocean ridges: Geophysical Monograph 91, p. 248-272.

Seyfried, W. E. Jr., Berndt, M.E., and Seewald, J.S., 1988, Hydrothermal alteration processes at mid-ocean ridges: Constraints from diabase alteration experiments, hot-spring fluids and composition of the oceanic crust: Canadian Mineralogist, v. 26, p. 787-804.

Seyfried, W. E. Jr., Ding, K., Berndt, M. E., and Chen, X., 1999, Experimental and theoretical controls on the composition of mid-ocean ridge hydrothermal fluids: Reviews in Economic Geology, v. 8, p. 181-200.

Sherlock, R.L., Roth, T., Spooner, E.T.C., and Bray, C.J., 1999, Origin of the Eskay Creek precious metal-rich volcanogenic massive sulfide deposit: Fluid inclusion and stable isotope evidence: Economic Geology, v. 94, p. 803-824.

Sims, P. K., 1976, Early Precambrian tectonic - igneous evolution in the Vermilion District, northeastern Minnesota: Geological Society of America Bulletin, v. 87, p. 379-389.

Sims, P.K., and Southwick, D.L., 1980, Geologic map of the Soudan quadrangle, St. Louis County, Minnesota: U.S. Geological Survey, Geologic Quadrangle Map GQ-1540, scale 1:24,000.

Sims, P.K., and Southwick, D.L., 1985, Geologic map of Archean rocks, western Vermilion district, northern Minnesota: U.S. Geological Survey, Miscellaneous Investigations Map I-1527, scale 1:48,000.

Southwick, D.L., compiler., 1993, Geologic map of Archean bedrock, Soudan-Bigfork area, northern Minnesota: Minnesota Geological Survey Miscellaneous Map Series M-77, scale 1:100,000.

Southwick, D.L., Boerboom, T.J., Jirsa, M.A., 1998, Geologic Setting and Descriptive Geochemistry of Archean Supracrustal and Hypabyssal Rocks, Soudan-Bigfork Area, Northern Minnesota: Implications for Metallic Mineral Exploration. Minnesota Geological Survey Report of Investigations 51. 69 p.

Stix, J., 1991, Subaqueous, intermediate to silicic-composition explosive volcanism; a review. Earth Sci. Rev., 31: 21-53.

Streckenstein, A.L. 1976, to each plutonic rock its proper name. Earth Sci. Rev., 12, 1-33.

Sun S.S., and McDonough W.F., 1989, Chemical and isotopic systematics of oceanic basalts: implications for mantle composition and processes. In: Saunders A.D. and Norry M.J., (eds.), Magmatism in ocean basins. Geol. Soc. London. Spec. Pub. 42, pp. 313-345.

Thurston, P.C. and Chivers, K.M., 1990, Secular variation in greenstone sequence development emphasizing Superior Province, Canada. Precambrian Res., 46: 21-58.

Thurston, P.C. and Ayers L.D., 2004 Archean and Proterozoic Greenstone Belts: Setting and Evolution; *In* The Precambrian Earth: Tempos and Events, Developments in Precambrian Geology v. 12 p. 311-334.

White, J.D.L., 1994. Review of: McPhie J., Doyle M., Allen R.L. (1993) Volcanic textures: a guide to the interpretation of textures in volcanic rocks. Bull. Volcanol., 56: 412-413.

Williams, H.R., Stott, G.M., Heather, K.B., Muir, T.L., and Sage, R.P., 1991, Wawa Subprovince, in Thurston, P.C., Williams, H.R., Sutcliffe, R.H., and Stott, G.M., eds., Geology of Ontario: Ontario Geological Survey Special Volume 4, Part 1, p. 485-539.

Wilson, M., 1989, Igneous Petrogenesis: London, Unwin Hyman, 466 p.

Winchester, J. A., and Floyd, P. A., 1976, Geochemical magma type discrimination; application to altered and metamorphosed basic igneous rocks: Earth and Planetary Science Letters, v. 28, p. 459-469.

Winchester, J.A., and Floyd, P.A., 1977, Geochemical discrimination of different magma series and the differentiation products using immobile elements, Chemical Geology, v. 20, pp. 325-343.

Winter, J.D., 2001 An introduction to Igneous and Metamorphic Petrology, Prentice-Hall Inc. Upper Saddle River, New Jersey.

Woodall, R., 1993, The multidisciplinary team approach to successful mineral exploration: Society of Economic Geologists Newsletter, no. 14, p.1-11.

Wright, I.C., and Gamble, J.A., 1999, Southern Kermadec Submarine Caldera Arc Volcanoes (SW Pacific): Caldera Formation by Effusive and Pyroclastic Eruption, Marine Geology, vol. 161, no. 2, pp. 207-227.

Appendix 1: Major Oxide and Trace Element Lithogeochemistry

Sample	UTM (east)	UTM (north)	Map_Unit	Lithology	SiO2 %	TiO2 %	Al2O3 %	Fe2O3 %	MnO %	MgO %
LE-028	559544.89	5296877.31	FPDD	Feldspar Porphyry Diorite	52.93	0.46	15.83	5.95	0.1	7.53
LE-050	559765.33	5296869.24	DbSM	Sub-Alkaline Basaltic Diabase	45.3	0.79	15.61	12.57	0.19	8.13
LE-055	559458.97	5297373.83	CB1b	Sub-Alkaline Basalt	44.43	0.78	13.84	12.42	0.24	9.87
LE-063	559211.31	5297305.34	DbU	Sub-Alkaline Basaltic Diabase	50.05	0.47	10.3	6.88	0.14	11.83
LE-064	559214.64	5297309.38	QFSD	Syeno-Diorite	64.82	0.28	18.04	1.6	0.03	1.93
LE-086	558960.74	5296615.05	DbSM	Sub-Alkaline Basaltic Diabase	45.83	0.77	16.14	12.82	0.25	4.03
LE-141	559098.64	5296853.17	DbSM	Sub-Alkaline Basaltic Diabase	46.98	0.73	15.32	11.91	0.19	8.18
LE-160	559608.22	5297718.7	QFSD	Quartz Feldspar Syeno-diorite	60.03	0.34	17.54	3.23	0.06	4.3
LE-180	558150.01	5297191.45	DbSS	Alkaline Diabase	51.39	0.72	17.22	13.7	0.13	8.17
LE-222	560301.92	5297443.57	CB1b	Sub-Alkaline Basalt	51.66	0.73	15.79	7.96	0.33	2.29
LE-225	560162.34	5297476.77	CB1a	Sub-Alkaline Andesite	50.86	0.63	16.94	13.16	0.19	4.44
LE-227	559876.14	5297238.24	CB1b	Sub-Alkaline Basalt	46.73	1.1	17.44	13.11	0.25	7.17
LE-230	559666.56	5297115.91	D	Diorite Porphyry	55.22	0.68	13.06	7.81	0.13	7.71
LE-254	558540.38	5297501.8	DbSS	Sub Alkaline Diabase	49.63	1.19	16.38	10.01	0.1	6.8
LE-259	560338.94	5297005.44	DbU	Sub-Alkaline Basaltic Diabase	49.58	0.63	17.01	9.34	0.15	8.71
LE-288	560513.74	5296561.85	FM2a	Rhyodacite/Dacite Lava	74.78	0.45	13.34	2.06	0.03	1.21
LE-289	560537.92	5296625.43	FM1h	Sub-Alkaline Basaltic Lapillistone	60.22	0.88	15.74	5.65	0.1	5.13
LE-295	559538.89	5296486.9	FM1b	Andesite	58.43	0.58	16.36	6.04	0.08	6.63
LE-321	559783.48	5297620.89	QFSD	Syeno-Diorite	56.51	0.36	19.73	1.98	0.06	3.27
LE-337	559594.05	5297508.73	CB1b	Sub-Alkaline Basalt	50.94	0.77	16.52	8.95	0.15	8.91
LE-349	558362.51	5297181.96	D	Diorite Porphyry	61.39	0.36	17.2	3.79	0.05	3.97
LE-360	559117.82	5296814.11	DbSM	Sub-Alkaline Basaltic Diabase	46.84	0.71	16.82	10.53	0.2	4.31
LE-402	559883.8	5297211.88	CB1b	Sub-Alkaline Basalt	55.66	1.48	14.68	11.69	0.19	5.66
LE-413	558152.81	5297007.64	CB1b	Sub-Alkaline Basalt	51.07	0.71	17.43	8.6	0.14	7.15
LE-420	560172.59	5297067.18	CB1b	Sub-Alkaline Basalt	45.12	0.75	13.18	12.09	0.3	7.5
LE-425	560144.76	5297091.06	CB1b	Sub-Alkaline Basalt	50.43	0.84	15.99	10.07	0.14	9.16
LE-431	557552.46	5296878.48	DbSS	Basaltic Andesitic Diabase	54.39	0.64	15.61	15.02	0.06	7.6
LE-437	560166.53	5297208.18	CB1b	Sub-Alkaline Basalt	44.05	0.62	13	12.77	0.25	8.17
LE-451	559711.54	5297646.57	CB1b	Sub-Alkaline Basalt	0	0	0	0	0	0
LE-461	557349.09	5296696.56	US2b	Trachy Andesitic Lapillistone	71.09	0.15	15.67	1.9	0.03	0.94
LE-500	560868.21	5296890.57	FM2a	Rhyodacite/Dacite lava	76.13	0.4	12.13	1.66	0.03	0.89
LE-1507	560647.47	5296534.39	FM1b	Sub-Alkaline Basalt	55.7	0.49	17.04	7.19	0.15	4.18
LE-1512	560675.55	5296372.8	FM1i	Foliated Sub-Alkaline Basalt	54.26	0.52	18.77	4.96	0.08	4.5
CBD3	559720.00	5297708.00	CB2a	Rhyolite Lava	80.03	0.137	9.34	3.02	0.019	1.84
CBD2	559720.00	5297708.00	CB2a	Rhyolite Lava	83.8	0.131	8.33	1.3	0.016	0.69
LE-1018	558959.00	5298283.00	GL2b	Rhyodacite Lapillistone/Breccia	67.48	0.191	17.25	2.9	0.041	1.12
LE-1014	559042.00	5298262.00	GL2b	Trachyandesite Lapillistone	65	0.218	20.32	1.53	0.021	0.52

Appendix 1: Major Oxide and Trace Element Lithogeochemistry

Sample	CaO	Na2O	K2O	P2O5	LOI	Sc	V	Cr	Co	Ni	Cu	Zn	Ge
	%	%	%	%	%	ppm	ppm	ppm	ppm	ppm	ppm	ppm	ppm
LE-028	8.68	4.48	0.4	0.42	3.81	11.4	102	374.2	30.7	229.4	11.3	71.3	0
LE-050	13.99	0.72	0.05	0.05	2.73	45.9	262.4	408.8	61.9	171.7	77.7	77.9	0
LE-055	12.16	0.99	1.26	0.04	4.47	42.5	271.3	356.8	66.6	228.8	70.4	119.1	0
LE-063	10.02	3.65	0.69	0.37	5.66	15.4	116.1	760.5	47.4	351	48	93.5	0
LE-064	2.9	6.89	2.81	0.12	0.98	3.9	39.6	40.2	1	24	6.5	28.1	0
LE-086	13.29	0.64	0.02	0.04	6.34	41.5	270.1	428.2	62.2	217.3	23.8	75.3	0
LE-141	11.53	1.48	0.19	0.04	3.37	40.9	249.8	375.1	64.6	198.7	101.2	81.1	0
LE-160	7.01	5.1	0.48	0.14	1.54	9	65	220.3	15.1	92.8	6.2	47.5	0
LE-180	0.38	2.95	0.81	0.08	5	33.4	224.7	255.2	68.3	142.3	11.7	131.5	0
LE-222	14.06	4.69	0.45	0.11	1.99	34.5	194.5	264	31.3	122.5	88.9	60.3	0
LE-225	9.18	0.22	1.37	0.07	3.22	31.5	228.5	209.8	43.5	114.7	76	82.1	0
LE-227	6.91	3.4	1.21	0.13	3.62	29.3	226.2	393.5	56.8	304	24.6	109.1	0
LE-230	7.03	4.57	0.24	0.29	3.05	25.7	177.4	561.2	31.9	68.1	65.7	85.1	0
LE-254	6.38	3.6	0.58	0.16	6.16	29.5	216.2	219.8	40.7	131.9	91.3	96	0
LE-259	7.09	1.92	3.12	0.1	3.03	37.3	191.1	353.9	44.4	155.9	28.4	80	0
LE-288	0.98	4.51	1.5	0.09	1.48	4.7	31.1	8.1	4.1	8.5	8.1	40.2	0
LE-289	2.75	5.59	0.14	0.21	3.84	18.1	160	192.8	26.4	151	73.8	81.3	0
LE-295	4.77	3.23	1.15	0.13	3.49	16.7	125.4	202.9	31.5	163.7	39	74.5	0
LE-321	8.9	6.31	0.75	0.14	2.7	7.3	57	130.7	11.7	82.6	10.2	28	0
LE-337	3.96	2.37	4.4	0.1	3.34	27.1	218.4	204.5	31.7	101.2	18.3	91.7	0
LE-349	5.72	4.53	0.42	0.15	2.69	8.9	65.7	218.1	15.5	81.1	14.8	49.7	0
LE-360	9.97	3.73	0.34	0.1	6.72	34.7	264.8	247.6	41.4	119.5	66.2	70	0
LE-402	3.77	4.29	0.64	0.2	2.73	29.6	156.4	196.8	37.4	128.7	41.6	137.2	0
LE-413	9.18	2.9	0.12	0.08	3.34	33.5	217.1	258.4	36.1	126.3	46.6	67.1	0
LE-420	18.14	0.48	0.14	0.04	3.47	38.8	234.4	311.1	64.9	183.2	11.1	95.3	0
LE-425	6.03	3.8	1.38	0.14	2.66	34.8	222.3	281.8	35.5	123.2	47.4	77.3	0
LE-431	0.15	0.51	0.28	0.08	5.33	28.8	208.7	229.6	50.8	124.5	8.4	92.9	0
LE-437	18.52	0.25	0.24	0.04	3.06	36.7	220.4	326.9	57.2	169.6	84.5	77.6	0
LE-451	0	0	0	0	0	0	0	0	0	0	0	0	0
LE-461	1.83	4.48	1.44	0.04	2.21	2.5	18.4	10.7	5.5	16.9	14.6	46.7	0
LE-500	1.83	2.9	2.28	0.09	2.19	4.5	29.6	9.2	5.1	15.6	13.2	19.5	0
LE-1507	5.91	3.17	1.34	0.09	5.03	14.3	109.6	169.3	24.2	147	12.6	81.5	0
LE-1512	5.29	4.79	2.25	0.13	5.63	18.8	162.6	300.2	24.4	197.3	62.7	82.1	0
CBD3	0.54	2.4	1.11	0.02	1.59	2	2.5	37	5	0	0	0	1
CBD2	0.65	3.94	0.28	0.03	0.86	0.5	6	19	3	0	0	0	0.8
LE-1018	2.46	5.09	1.17	0.05	2.03	5	32	51	10	0	0	0	1
LE-1014	3.32	4.46	3.08	0.06	1.52	3	19	14	0.5	0	0	0	1

Appendix 1: Major Oxide and Trace Element Lithogeochemistry

Sample	Ga ppm	Rb ppm	Sr ppm	Y ppm	Zr ppm	Nb ppm	Ba ppm	La ppm	Ce ppm	Pb ppm	Th ppm	U ppm	Ti ppm
LE-028	17.1	8.3	538.9	11.2	117.1	4.9	187.9	40.6	68.2	6	1.7		4379
LE-050	16.4	1.8	232.7	10.9	29.9	3	41.4	0.8	3	2	1.7		7573
LE-055	17.2	32.2	90.6	11	24.2	3.2	307.4	2.3	2.8	5.5	2		7469
LE-063	14.9	14.9	494.2	13.3	113.2	15.6	358.7	33	64.8	5.4	1.4		4549
LE-064	18.8	57.5	483.8	3.8	91	3.2	1239.6	11.5	24.9	9.8		1.6	2733
LE-086	18.8	1.4	137.4	11.3	27.2	3.2	21.2	0.9	4	4.6	2.2	0.7	7403
LE-141	15.7	6.1	108.3	10.4	24.7	3.2	52.7	1.1	2.9	2.2	1.8		7031
LE-160	17.7	5.6	630.6	5.4	86	3.1	231.8	13	31.7	2		1.1	3275
LE-180	12.1	45.7	38.4	4.6	57.2	4.8	73.7	-0.7	3	4.3	1.5		6918
LE-222	12.9	8.5	211.3	11.9	65.6	4.4	134.6	9.2	19.4	5.9	2.3	1.3	7057
LE-225	17	56.6	47.9	17.3	101.7	5.5	98.1	10	15.1	5.2	3.3	2	6087
LE-227	20.2	27.6	100	15.2	84.9	6	318.5	10.1	17.8	4.5	2.3	3.1	10576
LE-230	17	2.4	580.7	14.4	104.8	4.9	139.3	11.8	24.6	6	0.9		6557
LE-254	19.8	14.5	137	17.7	93.5	7	79.1	6.3	13.9	4.9	2.6		11441
LE-259	17.8	93.8	154.3	12	63.9	4.2	582.9	7.9	10.5	4.5		0.9	6091
LE-288	13.4	37.1	36.1	20.6	190.7	10.8	304.6	22.5	34.1	2	5	1.5	4284
LE-289	14.6	5	98.7	17.9	104.8	7.6	58.1	7.4	12.6	4.8	1.4	1.7	8500
LE-295	16.6	22.4	169.7	14.7	117.1	6.7	311.8	13.3	20.6	6.1	2.3		5568
LE-321	17.2	16	629	4.7	98.2	4	200.2	7.7	27.5	2.3		3.8	3503
LE-337	16.8	60.5	239.6	10.9	59.8	4.1	815.2	1.6	5.8	2.2			7443
LE-349	18	8.4	872.8	5.7	99.7	2.5	290.4	11.2	32.8	2.6			3447
LE-360	19.4	4.4	197.4	11.7	64.2	4.9	85.3	6.8	13.2	2.1	3.1	1.6	6792
LE-402	17.2	10.9	245.1	20.6	118.6	6.9	206	11.4	15.7	5.6	2.2		14239
LE-413	17.8	3.6	255	10.5	56.4	3.9	46.8	1.7	7	2.7	0.8	1.2	6838
LE-420	14.7	2.7	217.7	10.2	25.7	3.1	48.3	2.2	3.7	4.2	1.5		7184
LE-425	17.1	28.2	170.9	14.8	80	5.2	252.1	9.1	16.1	3	0.9		8131
LE-431	16	10.3	37.8	17.6	49.5	3.9	37	0.8	2	4.2	1.7	0.4	6131
LE-437	15.2	4	189.5	9.1	23.6	3	109.4	3	4.5	6.3	1.8		5954
LE-451	0	0	0	0	0	0	0	1.3	4	0	0	0	0
LE-461	15.3	27.7	373	3.9	60.3	2.8	327.5	5.3	12.5	5		1.3	1460
LE-500	11.2	66.6	54.7	21.3	176.1	8.6	352.9	19.6	39.4	7	4.7	2.6	3849
LE-1507	16.5	38	169	11.8	90.9	5.9	252.2	11.8	19	3.35	2.2		4752.477
LE-1512	24.6	61.4	78.1	16	98.4	5.9	409.4	13.5	28.3	5.9	1.6	1.1	5001.872
CBD3	14	37	56	40.1	282	15.7	156	34.1	79.5		5.283	1.407	0
CBD2	10	11	83	43.8	285	17.1	66	39.9	87.2		5.191	1.548	0
LE-1018	21	27	415	4.5	75	2	323	7.6	14.9		0.631	0.326	0
LE-1014	25	63	610	2.8	85	2.1	552	8.65	18.9		0.76	0.364	0

Appendix 1: Major Oxide and Trace Element Lithogeochemistry

Sample	K	P	Au	Ag	As	Bi	Br	Ca	Cs	Dy	Fe	Gd	Ho
	ppm	ppm	ppm	ppm	ppm	ppm	ppm	ppm	ppm	ppm	ppm	ppm	ppm
LE-028	3302	1841	6	2.5	1.8		0.25	4	0.5	0	2.83	0	0
LE-050	427	206	6	2.5	7.3		0.25	10	0.5	0	7.45	0	0
LE-055	10494	178	1	2.5	1.4		0.25	8	0.5	0	6.99	0	0
LE-063	5751	1636	1	2.5	4.3		0.25	6	0.5	0	4.15	0	0
LE-064	23329	538	1	2.5	2.4		0.25	0.5	0.5	0	1.09	0	0
LE-086	154	177	1	2.5	2		0.25	10	0.5	0	7.25	0	0
LE-141	1618	181	1	2.5	3		0.25	8	0.5	0	7.16	0	0
LE-160	3974	603	1	2.5	2.9		0.25	5	0.5	0	2.2	0	0
LE-180	6758	370	1	2.5	2.7		0.25	0.5	3	0	8.27	0	0
LE-222	3767	495	1	2.5	7.7		0.25	10	0.5	0	5.07	0	0
LE-225	11400	326	6	2.5	3.7		0.25	6	0.5	0	7.72	0	0
LE-227	10034	549	1	2.5	14.4		0.25	4	0.5	0	7.24	0	0
LE-230	1996	1256	1	2.5	3.8		0.25	0.5	0.5	0	4.51	0	0
LE-254	4847	687	2	2.5	3.3		0.25	4	2	0	5.54	0	0
LE-259	25858	452	1	2.5	2.1		0.25	4	0.5	0	4.65	0	0
LE-288	12444	386	2	2.5	2.3		0.25	0.5	1	0	1.34	0	0
LE-289	1135	907	1	2.5	1.5		0.25	3	0.5	0	3.3	0	0
LE-295	9516	551	1	2.5	1.5		0.25	3	0.5	0	3.41	0	0
LE-321	6226	593	1	2.5	3		0.25	4	0.5	0	1.27	0	0
LE-337	36522	422	1	2.5	0.8		0.25	3	1	0	4.93	0	0
LE-349	3527	662	1	2.5	1.8		0.25	4	0.5	0	2.38	0	0
LE-360	2843	424	1	2.5	2.4		0.25	8	0.5	0	6.17	0	0
LE-402	5289	881	1	2.5	3.9		0.25	4	0.5	0	6.78	0	0
LE-413	956	356	1	2.5	3		0.25	7	0.5	0	5.03	0	0
LE-420	1193	194	5	2.5	3.5		0.25	12	0.5	0	6.78	0	0
LE-425	11468	614	1	2.5	2.5		0.25	3	2	0	5.35	0	0
LE-431	2313	331	4	2.5	2.5		0.25	0.5	0.5	0	8.75	0	0
LE-437	1997	176	1	2.5	1.8		0.25	2	0.5	0	1.12	0	0
LE-451	0	0	1	2.5	2		0.25	12	0.5	0	6.98	0	0
LE-461	11921	188	3	2.5	3.7		0.25	2	1	0	1.29	0	0
LE-500	18909	381	1	2.5	1.8		0.25	9	0.5	0	4.47	0	0
LE-1507	11083.48	379.858	1	2.5	2.7		0.25	4	2	0	2.97	0	0
LE-1512	18695.39	580.848	1	2.5	1.1		0.25	0.5	0.5	0	0.02	0	0
CBD3	0	0	0.5		1.9	0.111	0.25		0.5	7.413		7.006	1.574
CBD2	0	0	0.5		0.25	0.05	0.25		0.209	7.931		8.65	1.477
LE-1018	0	0	4		0.25	0.309	0.25		0.667	0.745		0.923	0.146
LE-1014	0	0	0.5		2.2	0.502	0.25		1.351	0.468		0.88	0.078

Appendix 1: Major Oxide and Trace Element Lithogeochemistry

Sample	Hf	Hg	Ir	In	Mo	Na	Pr	Sb	Se	Sn	Ta	Tb	Tm
	ppm	ppm	ppm	ppm	ppm	ppm	ppm	ppm	ppm	ppm	ppm	ppm	ppm
LE-028	2	0.5	2.5	0	0.5	2.33	0	0.05	1.5	0.005	0.25	0	0
LE-050	0.5	0.5	2.5	0	0.5	0.5	0	1	1.5	0.005	0.25	0	0
LE-055	0.5	0.5	2.5	0	0.5	0.62	0	0.7	1.5	0.005	0.25	0	0
LE-063	3	0.5	2.5	0	0.5	2.35	0	0.05	1.5	0.005	0.25	0	0
LE-064	2	0.5	2.5	0	0.5	4.37	0	0.05	1.5	0.005	0.25	0	0
LE-086	0.5	0.5	2.5	0	0.5	0.46	0	0.05	1.5	0.005	0.25	0	0
LE-141	0.5	0.5	2.5	0	0.5	0.97	0	0.05	1.5	0.005	0.25	0	0
LE-160	2	0.5	2.5	0	0.5	3.15	0	0.05	1.5	0.005	0.25	0	0
LE-180	2	0.5	2.5	0	0.5	2	0	0.05	1.5	0.005	0.25	0	0
LE-222	1	0.5	2.5	0	10	3.2	0	1	1.5	0.005	0.25	0	0
LE-225	2	0.5	2.5	0	0.5	0.18	0	0.3	1.5	0.005	0.25	0	0
LE-227	2	0.5	2.5	0	0.5	2.21	0	0.05	1.5	0.005	0.25	0	0
LE-230	2	0.5	2.5	0	0.5	2.91	0	0.7	1.5	0.005	0.25	0	0
LE-254	3	0.5	2.5	0	0.5	2.22	0	0.05	1.5	0.005	0.25	0	0
LE-259	1	0.5	2.5	0	0.5	1.07	0	0.3	1.5	0.005	0.25	0	0
LE-288	5	0.5	2.5	0	0.5	2.82	0	0.2	1.5	0.005	0.25	0	0
LE-289	2	0.5	2.5	0	0.5	3.57	0	0.8	1.5	0.005	0.25	0	0
LE-295	3	0.5	2.5	0	0.5	1.96	0	0.05	1.5	0.005	1.3	0	0
LE-321	3	0.5	2.5	0	101	3.91	0	0.3	1.5	0.005	0.25	0	0
LE-337	1	0.5	2.5	0	0.5	1.49	0	0.05	1.5	0.005	0.25	0	0
LE-349	2	0.5	2.5	0	0.5	2.85	0	0.3	1.5	0.005	0.25	0	0
LE-360	1	0.5	2.5	0	0.5	2.39	0	0.5	1.5	0.005	0.25	0	0
LE-402	3	0.5	2.5	0	0.5	2.75	0	0.6	1.5	0.005	0.25	0	0
LE-413	2	0.5	2.5	0	0.5	1.83	0	0.3	1.5	0.005	0.25	0	0
LE-420	0.5	0.5	2.5	0	0.5	0.33	0	0.8	1.5	0.005	0.25	0	0
LE-425	2	0.5	2.5	0	0.5	2.3	0	0.05	1.5	0.005	0.25	0	0
LE-431	1	0.5	2.5	0	0.5	0.37	0	0.3	1.5	0.005	0.25	0	0
LE-437	1	0.5	2.5	0	0.5	2.61	0	0.2	1.5	0.005	0.25	0	0
LE-451	0.5	0.5	2.5	0	0.5	0.18	0	0.7	1.5	0.005	0.25	0	0
LE-461	4	0.5	2.5	0	0.5	1.74	0	0.3	1.5	0.005	0.25	0	0
LE-500	0.5	0.5	2.5	0	0.5	0.93	0	0.4	1.5	0.005	0.25	0	0
LE-1507	2	0.5	2.5	0	0.5	2.98	0	0.3	1.5	0.005	0.25	0	0
LE-1512	0.5	0.5	2.5	0	0.5	0.005	0	0.05	1.5	0.005	0.25	0	0
CBD3	7.796	0	2.5	0.05	1	0	9.228	0.05	1.5	2.012	1.5	1.295	0.863
CBD2	7.931	0	2.5	0.05	1	0	9.985	0.05	1.5	2.144	2.8	1.38	0.601
LE-1018	2.2	0	2.5	0.05	1	0	1.603	0.05	1.5	0.5	0.25	0.122	0.068
LE-1014	2.564	0	2.5	0.05	1	0	2.088	0.05	1.5	1.171	0.25	0.165	0.033

Appendix 1: Major Oxide and Trace Element Lithogeochemistry

Sample	Tl	W	Nd	Sm	Eu	Er	Tb	Yb	Lu
	ppm	ppm	ppm	ppm	ppm	ppm	ppm	ppm	ppm
LE-028	0	0.5	22	3.8	1.4	0	0.25	0.25	0.1
LE-050	0	0.5	2.5	0.9	0.5	0	0.25	0.25	0.15
LE-055	0	0.5	2.5	0.8	0.4	0	0.25	0.25	0.18
LE-063	0	0.5	28	5.2	1.8	0	0.25	0.25	0.15
LE-064	0	0.5	2.5	1.4	0.6	0	0.25	0.25	0.025
LE-086	0	0.5	2.5	0.9	0.6	0	0.25	0.25	0.19
LE-141	0	0.5	2.5	0.9	0.5	0	0.25	0.25	0.17
LE-160	0	0.5	10	2	0.8	0	0.25	0.25	0.07
LE-180	0	0.5	2.5	0.4	0.1	0	0.25	0.25	0.09
LE-222	0	0.5	2.5	1.5	0.1	0	0.25	0.25	0.17
LE-225	0	0.5	8	2	0.7	0	0.25	0.25	0.28
LE-227	0	0.5	12	2.2	0.7	0	0.25	0.25	0.21
LE-230	0	0.5	12	2.5	0.7	0	0.25	0.25	0.22
LE-254	0	0.5	2.5	1.9	0.8	0	0.25	0.25	0.25
LE-259	0	0.5	2.5	1.2	0.5	0	0.25	0.25	0.14
LE-288	0	0.5	14	2.9	0.5	0	0.25	0.25	0.29
LE-289	0	0.5	10	2	0.7	0	0.25	0.25	0.23
LE-295	0	0.5	8	1.8	0.6	0	0.25	0.25	0.19
LE-321	0	0.5	9	1.6	0.4	0	0.25	0.25	0.07
LE-337	0	0.5	2.5	1	0.5	0	0.25	0.25	0.17
LE-349	0	0.5	8	1.9	0.6	0	0.25	0.25	0.06
LE-360	0	0.5	5	1.4	0.5	0	0.25	0.25	0.2
LE-402	0	2	7	2.3	0.9	0	0.25	0.25	0.29
LE-413	0	0.5	2.5	1	0.4	0	0.25	0.25	0.15
LE-420	0	0.5	2.5	0.8	0.4	0	0.25	0.25	0.14
LE-425	0	0.5	9	1.8	0.7	0	0.25	0.25	0.19
LE-431	0	0.5	2.5	1.3	0.6	0	0.25	0.6	0.22
LE-437	0	0.5	2.5	0.6	0.1	0	0.25	0.25	0.025
LE-451	0	0.5	2.5	0.7	0.4	0	0.25	0.25	0.14
LE-461	0	0.5	12	2.9	0.7	0	0.25	0.25	0.29
LE-500	0	0.5	12	2.9	0.4	0	0.25	0.25	0.14
LE-1507	0	0.5	10	1.9	1.2	0	0.25	0.25	0.21
LE-1512	0	0.5	10	1.9	1.2	0	0.25	0.25	0.025
CBD3	0.088	0.552	23	7.263	1.187	5.293	0.8	5.643	0.904
CBD2	0.0025	1.2	33.329	8.481	1.627	4.215	0.25	3.728	0.527
LE-1018	0.123	0.25	2	1.097	0.425	0.442	0.25	0.456	0.077
LE-1014	0.304	0.25	5.504	1.227	0.479	0.224	0.25	0.21	0.034

Appendix 2: Thin section descriptions. * Indicates lithogeochemical analysis.

LE-002 35% Skeletal Feldspar, <1mm subhedral. 30% Epidote, <1-1mm anhedral forms semi opaque aggregates. 20% Mg-chlorite, <1mm anhedral-subhedral. 8% Quartz, <1mm anhedral grains. 5% Actinolite, 1-2mm spiny subhedral aggregates. 2% Fe-carbonate, 1-2mm anhedral. Slide has a felty texture. Fine-grained massive basalt lava, Central Basalt Sequence (CB1a).

LE-003 40% Mg-Chlorite, <1mm anhedral. 35% Quartz, <<1mm, anhedral mostly recrystallized. 25% Fe-carbonate, <1-1.5mm subhedral, occurs in 1.5-2mm aggregates. <1% well-dispersed opaque minerals. Mg-chlorite shows fluid migration direction. Fine-grained massive basalt lava, Central Basalt Sequence (CB1a).

LE-004 30% Plagioclase, 1-4mm, subhedral crystals, albite twinning very apparent. 25% Quartz, 1-4mm, anhedral, recrystallized. 25% Hornblende, 1-2mm, subhedral. 10% Carbonate, 1-2mm, anhedral. 5% Epidote, 1-4mm, anhedral-subhedral. 4% Mg-chlorite, 1-2mm, subhedral, commonly replacing hornblende. <1% Opaque minerals, 1mm sub-euhedral. White-gray-pink medium grained diorite dike, Central Basalt Sequence (D).

LE-007 40% Actinolite, <1-1mm, sub-euhedral lathes. 25% Epidote, <1mm patches and ~1mm anhedral semi opaque aggregates. 15% Varioles, 1-2mm. 10% Fe-chlorite, <1mm, subhedral tabular crystals. 3% Fe-carbonate, 1mm, anhedral blebs. 3% Zoisite, 1-3mm, euhedral crystal masses. 2% Sericite, <1mm,

anhedral-subhedral. 2% Quartz, <<1mm, anhedral groundmass. 10% 1-4mm hyaloclastite shards. Fine-grained pillow basalt, Central Basalt Sequence (CB1b).

LE-008 Slide consists of two lithologies. Lithology 1, 50% of slide: 25% Epidote, ~1-2mm, anhedral-euhedral, very fine-grained in some areas. 8% Actinolite, <1mm, subhedral and tabular. 8% Plagioclase, ~1mm, skeletal, subhedral. 4% Fe-chlorite, <<1mm, anhedral. 2% Sericite, <1mm, anhedral, occurs mostly as alteration product of plagioclase. 2% Quartz, <<1mm, anhedral. 1% Clinozoisite, <1-1mm, an-subhedral. Lithology 1 has a felty texture. Fine-grained pillow basalt, Central Basalt Sequence (CB1b). Lithology 2, 50% of slide: 35% Quartz, <<1mm, anhedral. 8% Hornblende, ~1-<<1mm, anhedral-subhedral. 4% Plagioclase, <<1-2mm, subhedral-euhedral. 2% Epidote, <1-1mm, anhedral, occurs as semi-opaque spherical aggregates and crystal venires. 1% Sericite, ~1mm, anhedral. Lithology 2 has a porphyritic texture. White-gray medium grained syeno-diorite porphyry, Central Basalt Sequence (QFSD).

LE-032 40% Epidote, <1-1mm, mottled anhedral crystals. 20% Actinolite, <1-1mm, subhedral lathe aggregates. 10% Sericite, <1mm, anhedral, mostly well-dispersed. 10% Clinozoisite, <1-1mm, sub-euhedral crystals. 10% Quartz, <1mm, anhedral groundmass. 5% Skeletal Plagioclase, 1-2mm, an-subhedral. 3% Fe-chlorite, <1mm, anhedral, occurs in aggregates. 2% Fe-carbonate, <1-

2mm, subhedral crystals, occurs primarily in 1-3mm veins. Rock has a slight felty texture. Fine-grained massive diabase intrusion, Sugar Mountain Sill (DbSM).

LE-063* 30% Plagioclase, <1-2mm, euhedral crystals, twinning very apparent. 25% Quartz, 1-2mm, anhedral. 25% Actinolite, <1-1mm, euhedral lathes. 10% Mg-chlorite, up to 4mm, subhedral-euhedral platy crystals. 6% Fe-carbonate, 1mm, anhedral-subhedral. 4% Epidote, 1-2mm, anhedral semi-opaque aggregates, well-dispersed. Rock has a felty texture. Light pink-gray medium grained sub-alkaline diabase (DbU).

LE-064* Slide contains 85% groundmass and 15% phenocrysts. Groundmass consists of: 60% Quartz, <<1mm, anhedral groundmass, also occurs as deformed crystals with bladed texture. 12% Actinolite, ~1-<<1mm, subhedral lathes. 9% Sericite, <1mm, subhedral, occurs as platy crystals. 4% Epidote, <1mm, anhedral circular aggregates. Phenocrysts consist of: 15% Plagioclase, 1-3mm, subhedral. Plagioclase crystals are zoned and dominantly sericite epidote altered. Pink-gray medium grained syeno-diorite porphyry (QFSD).

LE-065 40% Actinolite, <1-1.5mm euhedral crystals. 30% Quartz, <1mm anhedral crystalline groundmass. 10% Epidote, <1-1mm anhedral, occurs as semi-opaque crystal aggregates. 8% Mg-Chlorite, <1mm, subhedral crystals. 5% Fe-carbonate, <1-1mm, an-euhedral crystals. 5% Plagioclase, <1mm,

anhedral-subhedral crystals. 2% Limonite, <1mm, subhedral. Rock has a felty texture. Light pink-gray medium grained sub-alkaline diabase (DbU).

LE-080 35% Quartz, <1-2mm, anhedral-subhedral, occurs mostly as groundmass with some larger crystal aggregates. 35% Fe-chlorite, <1mm, anhedral. 20% Epidote, <1mm, anhedral well-dispersed semi-opaque aggregates and some larger 1mm anhedral crystals. 10% Fe-carbonate, <1mm, anhedral-subhedral. <1% Zoisite, <1mm, anhedral-subhedral. 5% Quartz + Chlorite 1-3 mm subrounded amygdules. Fine-grained basaltic diabase, Sugar Mountain Sill (DbSM).

LE-086* 65% Epidote, <1mm, anhedral well-dispersed crystals and semi-opaque aggregates, crystals occur primarily in veins. 20% Fe-chlorite, <1mm, anhedral well-dispersed aggregates. 5-10% Quartz, <1mm, anhedral interstitial groundmass. 5% Fe-carbonate, 2mm linear anhedral blebs and <1mm anhedral crystals. 2-3% 1-1.5mm euhedral epidote rich veins. Fine-grained sub-alkaline basaltic diabase, Sugar Mountain Sill (DbSM).

LE-100 60% Sericite, << 0.25 mm, anhedral crystals, micas are imbricated along foliation plane and show relict fluid pathways. 25% Quartz, <1-1mm, anhedral-subhedral crystals occurring mostly in amygdules and veins. 10% Fe-carbonate, <1mm, anhedral-euhedral crystals, dominantly associated with

quartz, some carbonate crystals are lined by chlorite. 5% Fe-chlorite, <1mm anhedral-subhedral crystals. Alteration derived from D_2 shearing, unrelated to seafloor hydrothermal alteration. Slide contains <1mm wide quartz carbonate veins that run the entire slide length. Slide contains 5% quartz filled amygdules that exhibit pressure shadows and dextral shear indicators. Fine-grained sericite + quartz phyllite/schist (5b).

LE-126 Slide consists of two lithologies. Lithology 1: 80% of slide: 40% Epidote, <1-1mm and in veins as 1-3mm, sub-euhedral crystals, occurs as fine-grained semi-opaque aggregates. 35% Actinolite, 1-1.5mm, subhedral-euhedral. 10-15% Skeletal Feldspar, <1mm, subhedral. 5% Mg-Chlorite, <1-1mm, anhedral. 2-3% Fe-carbonate, 1-2mm, subhedral-anhedral. 2% Sericite, anhedral-subhedral, occurs in small aggregates in distinct fluid pathways and commonly occurs replacing plagioclase. This portion of the slide has a felty matrix. Small 1-4mm veins are well-dispersed and are composed dominantly of epidote + actinolite. This portion of the slide is fine-grained pillow basalt, Central Basalt Sequence (CB1b). Lithology 2: 20% of slide: 35% Quartz, 1mm, anhedral, appears to be mostly recrystalized. 20% Epidote, <1mm, occurs as fine-grained semi-opaque aggregates. 10-15% Hornblende, 1-2mm, subhedral lathes. 10-15% Sericite, <1mm, anhedral, commonly replacing 1-3 mm feldspars but occurs within clast matrix. 10% Actinolite, <1-1mm, subhedral. 5% Mg-chlorite, <1mm, occurs as imbricated wisps. This portion

Appendix 2: Thin section descriptions. * Indicates lithogeochemical analysis.

of slide is a white-gray medium grained syeno-diorite, Central Basalt Sequence (QFSD).

LE-135 Slide consists of 85% groundmass and 15% clasts. Groundmass consists of: 65% Quartz, <<1-1mm, anhedral to subhedral grains. 15% Sericite, <1mm, anhedral. ~2% Epidote, <1mm, anhedral circular aggregates. 2% Pyrite, <1-1mm, sub-euhedral, disseminated crystals. ~1% Mg-Chlorite, <1mm, anhedral crystals. Grains consist of: 10% Plagioclase, ~1-<1mm subhedral broken angular grains. 4% Quartz, ~1mm anhedral grains. 1% Orthoclase, <1mm anhedral angular grains. Felsic lapillistone and breccia deposit (US2b).

LE-154 60% Epidote, <1mm aggregates, 5mm subhedral crystals. 15% Quartz, <1mm, anhedral groundmass. 8% Mg-Chlorite, <1mm, well-dispersed anhedral wisps. 5% Actinolite, <1mm, subhedral lathes. 5% Zoisite, <1mm, subhedral-euhedral crystals, well-dispersed. 3% Stelpnomelane, <1mm, anhedral, occurs mostly in veins. 2% Sericite, <1mm, subhedral, occurs primarily in what appear to be fluid pathways. 2% Opaque minerals, <1-2mm, subhedral-euhedral pyrite and unknown sulfides. Mineral assemblages appear to be overprinted several times. An extremely fine grain assemblage of quartz + sericite + actinolite is found dispersed in the matrix and may represent one of the overprinting assemblages. Fine-grained mottled massive basalt, Central Basalt Sequence (CB1a).

Appendix 2: Thin section descriptions. * Indicates lithogeochemical analysis.

LE-173 35% Actinolite, 1-2mm subhedral patchy tabular crystals that pseudomorph pyroxene. 25% Quartz, <1mm anhedral recrystallized groundmass. 15% Clinozoisite, <1mm subhedral-euhedral crystals. 10% Epidote, <1mm, well-dispersed subhedral crystals. 6% Mg-Chlorite, <1mm, subhedral crystals, some occurs as 1-1.5mm tabular crystals. 5% Sericite, <1mm anhedral-subhedral crystals. 2% Plagioclase, <1mm, anhedral-subhedral. 2% Fe-carbonate, <1mm, anhedral blebs, prefers to grow on albite phenocrysts. Dark green-black medium grained gabbro porphyry (Gb).

LE-176 35% Quartz, <1mm, anhedral groundmass. 35% Epidote, <1mm, anhedral, occurs as fine-grained aggregates. 10% Mg-chlorite, <1mm, anhedral-subhedral crystals. 5% Clinozoisite, <1-1.5mm, subhedral-euhedral crystals. 5% Fe-carbonate, <1-1mm, subhedral crystals. 5% Plagioclase, subhedral crystals, mostly skeletal remnants. 4% Actinolite, 1mm subhedral tabular crystals,. <1% Sericite, <1mm anhedral crystals. Dark green-black medium grained gabbro (Gb).

LE-177 Slide contains 90% phenocrysts and 10% groundmass. Phenocrysts consists of: 45% Plagioclase, 1-1.5mm, subhedral crystals. 25% Hornblende, 1-2mm, subhedral-euhedral lathes. 18% Quartz, 1-1.5mm, anhedral crystals. Groundmass consists of: <1% Fe-chlorite, <1mm, an-subhedral crystals. <1% Epidote, 1mm, well-dispersed anhedral aggregates. Slide has a porphyritic felty texture. Fine-medium grained hornblende diorite clast in diabase (D).

Appendix 2: Thin section descriptions. * Indicates lithogeochemical analysis.

LE-180* 25% Quartz, <1-1mm, recrystallized anhedral crystals. 25% Sericite, <<1/4 mm, anhedral crystals mostly associated with quartz groundmass. 20% Plagioclase, <1mm, anhedral skeletal feldspar lathes. 15% Mg-Chlorite, <1mm, anhedral crystals. 10% Fe-chlorite, <1mm, an-subhedral crystals. 5% Epidote, <1mm, well-dispersed anhedral aggregates. 40% of slide contains deformed 1-4mm quartz sericite amygdules. This slide is very fine-grained (aphyric) and is completely metasomatically recrystallized. Fine-grained alkaline basaltic diabase (DbSS).

LE-188 40% Epidote, <1mm, euhedral crystals and anhedral semi-opaque aggregates. 35% Quartz, <1mm, anhedral groundmass. 10% Mg-Chlorite, <1mm anhedral-subhedral crystal aggregates. 10% Actinolite, 1-2mm platy crystals, anhedral-subhedral. 5% Clinozoisite, <1mm, euhedral crystal aggregates. <1% Limonite, <1mm, anhedral. Fine-grained pillow lava, Fivemile Lake Sequence (FM1b).

LE-204 35% Quartz, <<1mm, anhedral, occurs as crystals and fine-grained groundmass. 25% Fe-chlorite, <1mm, anhedral-subhedral wisps. 20% Fe-carbonate, ~1-<1mm subhedral crystals, appear to be primary. 15% Epidote, <1mm, anhedral circular aggregates. 4% Plagioclase, <1mm subhedral-anhedral crystals. <1% Sericite, <<1mm anhedral crystals. White-tan fine-grained well-foliated dacite lava (5b).

Appendix 2: Thin section descriptions. * Indicates lithogeochemical analysis.

LE-212 40% Quartz, <<1mm, anhedral groundmass, 20% of which is represented by 1-1.5mm deformed quartz amygdules. 25% Fe-chlorite, <<1mm anhedral crystals. 18% Fe-carbonate, 1-1.5mm subhedral blebs, carbonate occupies a small fraction of amygdules. 12% Sericite, <1mm, anhedral. 2% Biotite, <<1mm, anhedral. 2% Zoisite, <<1mm, subhedral. <1% Epidote, <1mm, anhedral circular aggregates. A large portion of the very fine-grained matrix has an alteration assemblage of Quartz + Chlorite + Sericite. Foliated fine-grained mafic pillow lava, Fivemile Lake Sequence (FM1i).

LE-217 40% Actinolite, <1mm, subhedral linear aggregates, occur in a cross stitch pattern. 35% Epidote, <1mm, anhedral, occurs as patchy aggregates. 12% Plagioclase, <1-1mm, subhedral skeletal lathes. 8% Quartz, <1mm, anhedral groundmass. 4% Fe-carbonate, <1mm anhedral blebs. ~1% Fe-chlorite, <1mm, anhedral crystals. <1% ~1mm Actinolite + Epidote veins with larger 1-2mm Epidote crystals within veins. Rock has a felty texture. Fine-grained pillow basalt, Central Basalt Sequence (CB1b).

LE-218 70% Epidote, <1-2mm, anhedral-subhedral crystals, epidote overprints a lot of slide as patchy aggregates. 15% Actinolite, <1mm, subhedral. 5% Clinozoisite, <1mm, subhedral crystals. 5% Sericite, <1mm, anhedral crystal aggregates. 5% Fe-chlorite, <1mm, anhedral crystals. ~5% 1-1.5mm

actinolite + epidote veins that run parallel to each other. Fine-grained pillow basalt, Central Basalt Sequence (CB1b).

LE-222* Slide contains 82% groundmass and 18% phenocrysts. Groundmass consists of: 32% Epidote, <1mm, anhedral semi-opaque aggregates, large amounts of epidote occur near garnet crystals. 28% Actinolite, <1mm, subhedral lathes, some ~1mm subhedral crystal aggregates. 16% Quartz, <1mm, anhedral groundmass. 4% Plagioclase, <<1-1mm, anhedral lathes. 1% Fe-carbonate, <1mm, anhedral blebs. 1% Opaque minerals, <1mm, anhedral crystals. Phenocrysts consist of: 18% Garnet, 1-4mm, anhedral-subhedral, occurs as what appears to be filled pipe vesicles or veins. Garnet is likely Grossular. Slide has a felty texture. Fine-grained porphyritic sub-alkaline pillow basalt, Central Basalt Sequence (CB1b).

LE-225* 35% Epidote, <1mm-1mm aggregates. 20% Quartz, <1mm, anhedral groundmass. 25% Fe-chlorite, <1mm anhedral crystals. 12% Actinolite, <1mm, anhedral crystals. 5% Sericite, <1mm anhedral crystals, mostly well-dispersed. 1% Opaque minerals, <1mm anhedral crystals. Slide contains roughly 2% 4-5mm well-rounded quartz + chlorite amygdules. 1-4mm oxides/sulfide burns. Fine-grained massive sub-alkaline basalt flow, Central Basalt Sequence (CB1a).

Appendix 2: Thin section descriptions. * Indicates lithogeochemical analysis.

LE-226 45% Epidote, 1-2mm, anhedral circular aggregates. 25% Actinolite, <1mm, subhedral lathes, occurs mostly in veins. 15% Fe-chlorite, <1-1mm, subhedral crystals. 5% Quartz, <1mm, anhedral crystals, occurs mostly in veins. 5% Fe-carbonate, <1mm anhedral blebs. 2% Clinozoisite, <1-1mm subhedral crystals. 2% Opaque minerals, <1mm disseminated anhedral crystals. <1% 1mm varioles present but somewhat overprinted. <1% 1-2mm hyaloclastite. Fine-grained pillow lava, Central Basalt Sequence (CB1b).

LE-227* 35% Epidote, <1mm, anhedral, occurs as patchy aggregates. 15% Actinolite, <<1mm, anhedral, some subhedral lathes visible. 15% Plagioclase, <1mm, anhedral, difficult to see in some areas because of epidote overprinting. 15% Sericite, <1-1mm, anhedral crystals, occurs in patches. 10% Quartz, <1mm, anhedral groundmass. 10% Fe-chlorite, <1mm, anhedral-subhedral, in some spots chlorite is very concentrated. Alteration is local and intense for most minerals except for epidote which is fairly well-dispersed. 1-2mm wide Actinolite + Quartz + Carbonate veins. Rock has a felty texture. Fine-grained sub-alkaline pillow basalt, Central Basalt Sequence (CB1b).

LE-230* Slide contains 60% phenocrysts and 40% groundmass. Phenocrysts consist of: 30% Plagioclase, ~ 1-1.5mm, subhedral-euhedral. 25% Quartz, 1-1.5mm, anhedral crystals. 5% Orthoclase, <1-1mm, subhedral-euhedral. Groundmass consists of: 16% Actinolite, 1-1.5mm, subhedral crystals. 8% Mg-Chlorite

Appendix 2: Thin section descriptions. * Indicates lithogeochemical analysis.

~1-<1mm clots of anhedral-subhedral crystals. 8% Epidote, <1-1.5mm crystal aggregates, subhedral, occurs most commonly as replacement of plagioclase crystals. 4% Fe-chlorite, <1mm clots, anhedral-subhedral. 4% Fe-carbonate, <1mm, anhedral crystals. ~1mm Quartz + Carbonate veins present. Fine-grained diorite dike, Central Basalt Sequence (D).

LE-239 35% Fe-chlorite, <1mm, anhedral crystals. 30% Quartz, <1mm, anhedral groundmass. 30% Pyrite, <1-4mm, anhedral-subhedral crystals. 4% Hematite, anhedral, product of pyrite weathering. 1% Fe-carbonate, <1mm, anhedral-subhedral. Sheared texture. Shear zone derived alteration. Quartz + Chlorite Schist (5e).

LE-240 40% Sericite, <1mm anhedral crystals. 35% Quartz, ½-2mm, quartz amygdules and <<1mm groundmass, 10% of total quartz is represented in amygdules. 10% Fe-chlorite, <<1mm, anhedral well-dispersed crystals. 8% Epidote, <1mm, anhedral circular aggregates. 5% Opaque minerals, <1mm, anhedral-subhedral. 2% Fe-carbonate, <1mm, anhedral-subhedral. <1% Limonite, anhedral, represented in curvilinear trends that occur in foliation planes. This slide has a sheared texture. Pressure shadows are not prominent but mica mats are located in some areas adjacent to amygdules. Shear zone derived alteration. Quartz + Sericite + Chlorite Schist (5b).

Appendix 2: Thin section descriptions. * Indicates lithogeochemical analysis.

LE-245 75% Sericite, <1mm well-dispersed play anhedral crystals. 25% Quartz, <1mm anhedral crystals. <1% Fe-carbonate, <1mm anhedral-subhedral crystals, contains sericite inclusions. <1% Stelpnomelane, <1mm anhedral crystals, occurs mostly as staining. <1% Mg-Chlorite, <1mm occurs interstitially and in amygdules, chlorite fills center and quartz lines rims. A few 1-2mm zoned chlorite + quartz amygdules. Felsic tuff deposit, Upper Sequence (US2c).

LE-246 Slide contains 98% groundmass and 2% phenocrysts. Groundmass consists of: 78% Quartz, <1mm anhedral crystals. 20% Sericite, <<1mm anhedral crystals. Phenocrysts consist of: 2% Quartz, 1-2mm round-subangular grains. Felsic tuff deposit, Upper Sequence (US2c).

LE-252 Rock contains 88% groundmass and 12% phenocrysts. Groundmass consists of: 35% Epidote, 1-2mm, anhedral-subhedral semi-opaque spherical crystal aggregates. 30% Quartz, <1-1mm anhedral groundmass. 15% Mg-Chlorite, <1mm anhedral-subhedral. 2% Fe-chlorite, <1mm anhedral-subhedral. 2% Fe-carbonate, <1mm anhedral crystals. 2% Clinozoisite, <1mm euhedral crystals. 2% Sericite, <1mm anhedral crystals. Phenocrysts and porphyroblasts consist of: 8% Actinolite, 1-3mm, anhedral crystals that pseudomorph pyroxene. 4% Plagioclase, <1mm, skeletal subhedral lathes. Rock has a porphyritic texture. Dark green-black medium grained gabbro porphyry (Gb).

Appendix 2: Thin section descriptions. * Indicates lithogeochemical analysis.

LE-253 25% Quartz, <<1mm spheriods. 25% Jasper spheroids, <<1mm. 25% Hematite spheroids, <<1mm. 25% gray chert spheroids, <1mm. <<1mm circular hematite/quartz spheroids that may represent single celled algae. Alternating quartz and hematite bands are 1-9mm thick and are generally not continuous along bedding. Soudan oxide facies banded iron formation (US4a).

LE-254* 30% Quartz, <1mm anhedral groundmass. 25% Mg-Chlorite, 1-3mm anhedral-subhedral circular aggregates. 20% Clinozoisite, <1-1mm anhedral-subhedral, occurs as acicular plates and crystal aggregates. 18% Fe-carbonate, <1-1mm, subhedral crystals. 5% Fe-chlorite, <1mm, anhedral-subhedral crystals. 2% Sericite, <<1mm, anhedral crystals. Fine-grained sub-alkaline basaltic diabase (DbSS).

LE-259* Slide consists of 70% groundmass and 30% phenocrysts. Groundmass: 35% Sericite, <1mm, anhedral 18% Epidote, <1mm, anhedral, occurs and circular aggregates with a small amount of <1mm subhedral crystals. 15% Actinolite, 1-4mm, subhedral-euhedral, large tabular crystals and fine crystal lathes. 10% Fe-chlorite, 1-2mm wide stringers, anhedral. 7% Quartz, <1mm, anhedral crystals. Phenocrysts: 15% Hornblende, 1-4mm, subhedral crystals. Very fine-grained matrix consists mostly of Quartz + Actinolite + Sericite. Slide

has a porphyritic felty texture. Dark green medium grained sub-alkaline basaltic diabase dike (DbU).

LE-288* 75% Quartz, <1mm-1mm, anhedral crystals and interstitial groundmass. 12% Sericite, <1mm, anhedral, mineral readily depicts relict fluid pathways. 5% Orthoclase, <1mm, anhedral-subhedral crystals. 5% Epidote, <<1mm, occurs as well-dispersed anhedral circular aggregates. 3% Fe-carbonate, <1mm, anhedral-subhedral elongated crystal masses. Rock has a silicified texture. Tan fine-grained rhyodacite/dacite lava flow, Fivemile Lake Sequence (FM2a).

LE-290 40% Mg-Chlorite, <1mm anhedral-subhedral crystals. 30% Quartz, <<1mm anhedral groundmass. 20% Plagioclase, 1-2mm anhedral-subhedral, mostly relict, some twinning still apparent. 4% Limonite, <<1mm biotite staining. 3% Epidote, ~1mm anhedral grunge aggregates. 2% Sericite, <1mm, subhedral lathes. 1% Fe-carbonate, <1mm anhedral crystals. Slide contains some very fine-grained quartz + chlorite patches. Very fine-grained matrix is composed of quartz + chlorite + sericite. Medium grained gabbro porphyry, Fivemile Lake Sequence (Gb).

LE-295* 20% Quartz, <<1mm anhedral crystals. 20% Actinolite, <1mm euhedral radiating aggregates. 15% Epidote, <1mm subhedral-euhedral. 15% Mg-Chlorite, 1-2mm subhedral-euhedral crystals, occurs interstitially and as large tabular crystals. 10% Sericite, <<1mm anhedral crystals. 8% Fe-carbonate,

Appendix 2: Thin section descriptions. * Indicates lithogeochemical analysis.

<1mm subhedral-euhedral crystals. 5% Orthoclase, <1mm anhedral crystals. 5% Plagioclase, <1mm subhedral lathes. 2% Zoisite, <1mm subhedral crystals. <1% Stelpnomelane, <1mm anhedral crystals. Fine-grained pillowed andesite lava flow, Fivemile Lake Sequence (FM1b).

LE-297 50% Epidote, <1-2mm, anhedral grunge aggregates. 45% Quartz, <<1mm, anhedral groundmass. 5% Fe-chlorite, ~1-2mm, anhedral, some chlorite filling 1-3mm amygdules. Rock has a sheared texture. Fine-grained pillowed lava, Fivemile Lake Sequence (FM1b).

LE-299 Slide contains 60% phenocrysts and 40% groundmass. Phenocrysts consist of: 30% Quartz, 1-3mm anhedral crystals. 25% Plagioclase, 1-2mm subhedral crystals. 5% Orthoclase, <1-2mm anhedral-subhedral. Groundmass consists of: 15% Epidote, <1mm anhedral crystals, occurs as splotches and semi-opaque grunge aggregates. 8% Sericite, <1mm, anhedral, well-dispersed crystals that commonly occur as a feldspar alteration product. 8% Fe-chlorite, <1mm aggregates, anhedral and interstitial crystals. 8% Actinolite, <<1mm, subhedral bladed aggregates. 1% Hematite, <1mm, anhedral crystal aggregates. Fine-grained pillowed andesite lava flow, Fivemile Lake Sequence (FM1b).

LE-312 35% Epidote, <1mm, anhedral circular aggregates, 1-2mm anhedral crystals, epidote completely replaces most of the original Plagioclase. 25% Quartz,

Appendix 2: Thin section descriptions. * Indicates lithogeochemical analysis.

<<1mm, anhedral groundmass. 18% Sericite, <1mm anhedral crystals well-dispersed throughout rock. 15% Actinolite, <1mm euhedral lathe aggregates. 4% Plagioclase, <1mm needle aggregates mostly replaced by epidote. 3% Fe-chlorite, <1mm anhedral crystals. Rock has a felty texture. Secondary alteration type is 8B: Sericite ± Carbonate. Fine-grained pillow lava, Central Basalt Sequence (CB1b).

LE-313 Slide contains 80% groundmass and 20% phenocrysts. Groundmass consists of: 25% Magnesium-Chlorite, <1mm anhedral crystals. 20% Quartz, <1mm recrystallized anhedral crystal aggregates. 8% Fe-carbonate, <1-2mm anhedral-subhedral crystals. 8% Actinolite, <1mm needle aggregates and patches, subhedral-euhedral. 6% Epidote, <1mm circular anhedral aggregates. 6% Fe-chlorite, <1mm anhedral crystals patches. 4% Sericite, <1mm anhedral crystals, occur primarily on feldspar crystals. 2% Sphene, <1mm anhedral crystals. 1% Opaque minerals, <1mm, disseminated anhedral crystals. Phenocrysts consists of: 10% Quartz, 1-4mm, subhedral crystals. 6% Hornblende, <1-1mm, subhedral lathes. 2% Plagioclase, 1-2mm, subhedral-euhedral crystals. 3% Orthoclase, <1-1mm anhedral-subhedral crystals commonly being altered to Sericite. Rock has a porphyritic texture. Pink-tan medium-coarse grained syeno-diorite (QFSD).

LE-321* Slide contains 70% groundmass and 30% phenocrysts. Groundmass consists of: 35% Quartz, <1mm, dominantly recrystallized crystals. ~15% Sericite,

<1mm, anhedral and commonly associated with Actinolite making it difficult to interpret modal percent. 10% Fe-carbonate, <1-2mm, subhedral-anhedral crystals. ~8% Actinolite, <1mm anhedral crystals, commonly mixed with sericite making it difficult to interpret modal percent. <1% Mg-chlorite, <1mm anhedral crystals. <1% Clinozoisite, <1-1mm, subhedral crystals, occurs most commonly in veins. Phenocrysts: 12% Epidote, occurs as <1mm anhedral grunge aggregates and replaces relict plagioclase crystals. 10% Plagioclase, highly altered subhedral <1-2mm crystals. Most feldspar is altered to Epidote but cleavage and some twinning are still recognizable in thin section. 8% Hornblende, tabular 1-3mm subhedral-euhedral crystals. Slide contains 1-3mm randomly oriented veins. Rock has a porphyritic texture. Pink-tan medium grained syeno-diorite.

LE-325 60% Quartz, <1mm, anhedral groundmass and 1-3mm spherical quartz amygdules. 15% Epidote, 1-2mm, anhedral patchy crystal aggregates. 10% Sericite, <1mm anhedral crystals, occurs as local aggregates sometimes replaces quartz and feldspar. 8% Actinolite, <1mm subhedral-euhedral crystal lathes, mostly well-dispersed, some local lathe aggregates. 5% Orthoclase, <1mm anhedral-subhedral crystals. 2% Fe-chlorite, <1mm anhedral crystals. Fine-grained felsic lava lapilli in lapillistone and breccia deposit, Upper Sequence (US2b).

Appendix 2: Thin section descriptions. * Indicates lithogeochemical analysis.

LE-326 Slide consists of 85% groundmass and 15% phenocrysts. Groundmass consists of: 35% Epidote, <1mm, subhedral crystals and <<1mm semi-opaque spherical aggregates. 17% Mg-Chlorite, <1-1mm subhedral well-dispersed crystals. 17% Actinolite, 1-1.5mm subhedral platy crystals. 9% Quartz, <1-1mm anhedral crystals. 5% Zoisite, <1-1mm, anhedral-subhedral crystals. 2% Opaque minerals, <1mm, anhedral crystals. Phenocrysts consist of: 15% Plagioclase, <1-3mm subhedral crystals commonly being replaced by epidote. Fine-grained gabbro (Gb).

LE-333 55% Sericite, <1mm anhedral well-dispersed crystals. 20% Mg-Chlorite, 1-1.5mm anhedral linear aggregates. 10% Fe-carbonate, <1mm subhedral crystals. 5% Opaque minerals, <1-1mm anhedral crystals. 5% Epidote, <1mm anhedral crystals. 5% Quartz, <1mm anhedral crystal groundmass. Fine-grained massive lava, Central Basalt Sequence (CB1a).

LE-335 Slide contains 65% groundmass and 35% phenocrysts. Groundmass consists of: 23% Quartz, <1-1mm anhedral crystal groundmass. 10% Orthoclase, <1-1mm anhedral-subhedral crystals. 10% Mg-Chlorite, <1mm anhedral circular crystal aggregates. 10% Epidote, <1mm anhedral grunge aggregates. 7% Sericite, <<1-1.5mm subhedral-euhedral crystals. 5% Fe-carbonate, <1-1mm, anhedral-subhedral crystal blebs, occurs on only one large feldspar phenocryst. Phenocrysts consist of: 25% Plagioclase, 1-4mm, anhedral-subhedral crystals. 6% Quartz, <1-2mm anhedral crystals. 4% Orthoclase,

Appendix 2: Thin section descriptions. * Indicates lithogeochemical analysis.

<1-1mm, anhedral-subhedral crystals. Pink-tan-white medium grained syeno-diorite porphyry (QFSD).

LE-337* 35% Quartz, <1mm, anhedral crystal groundmass. 30% Sericite, <1mm anhedral crystals. 20% Mg-Chlorite, <1mm, anhedral crystal aggregates. 15% Epidote, <1mm anhedral crystal aggregates. 2% Plagioclase, 1-1.5mm anhedral crystals. Rock has a felty texture. 2% Quartz + Chlorite filled Amygdules, 1-4mm in diameter. Fine-grained sub-alkaline amygdaloidal pillow basalt, Central Basalt Sequence (CB1b).

LE-338 Slide contains 55% porphyroblasts and 45% groundmass. Porphyroblasts consist of: 55% Garnet, 1-6mm, subhedral crystals. Groundmass consists of: 23% Actinolite, <<1mm, subhedral crystal lathes and tabular crystal aggregates. 8% Epidote, <<1-1mm, subhedral circular crystal aggregates. 6% Fe-carbonate, 1-4mm subhedral-euhedral crystals, commonly occurs between garnet crystals. 5% Quartz, <1mm anhedral crystal groundmass. 2% Fe-chlorite, <<1mm anhedral crystals. 1% Sericite, <1mm anhedral crystals. Slide has a porphyritic/felty texture with groundmass dominant. Fine-grained mafic pillow lava, Central Basalt Sequence (CB1b).

LE-354 Slide consists of two lithologies. Lithology 1: 10 % of slide: 4% Actinolite, <1-1mm subhedral crystal lathes. 2% Mg-chlorite, <1mm anhedral crystals. 1% Sericite, <<1mm, occurs mostly as interstitial anhedral crystals. 1%

Clinozoisite, <1mm subhedral crystals that occur mostly in 1mm veinlets. <1% Quartz, <<1mm anhedral crystals. <1% Plagioclase, <1mm subhedral crystals. Lithology 2: 90%: 35% Plagioclase, 1-6mm subhedral crystals. 25% Quartz, 1-2mm anhedral crystals, 1-3mm recrystallized pods, individual crystals <1mm. 15% Hornblende, 1-3mm anhedral-subhedral crystals. 5% Fe-chlorite, <1-1mm anhedral crystals. 4% Epidote, <1-1mm anhedral-subhedral crystal aggregates. 4% Sericite, <<1mm anhedral crystals. 2% Fe-carbonate, 1-2mm subhedral-euhedral crystals. Contact between lithologies is extremely sharp and curvilinear. Modal sericite and carbonate occur together as interstitial material. Lithology 1 has a felty texture. Primary alteration assemblage is 1: Least Altered. Lithology 2 has a porphyritic texture and is least altered. Brick red medium-coarse grained diorite (D), intruding fine-grained diabase (DbU).

LE-356 40% Sericite, <1mm anhedral, occurs as patchy aggregates. 30% Mg-chlorite, <1-2mm anhedral-subhedral wisps. 15% Quartz, <1mm anhedral angular crystal groundmass. 8% Carbonate, 1-2mm anhedral-subhedral aggregates, also occurs in groundmass. 5% Epidote, subhedral crystals up to 4mm and <1mm round spherical grunge aggregates. 2% Plagioclase, <1mm interstitial anhedral-subhedral crystals. <1% Fe-chlorite, <1mm anhedral crystals. 15% Chlorite/Carbonate Amygdules, 1-5mm, contains anhedral chlorite and subhedral carbonate crystals. Rock appears to show two stages of chlorite alteration. Sericite mostly present as plagioclase alteration product. Fine-

grained felsic lava lapilli clast in felsic lapillistone and breccia deposit, Upper Sequence (US2b).

LE-362 Slide contains 92% groundmass and 8% phenocrysts. Groundmass consists of: 30% Plagioclase microlites, <1mm subhedral crystals. 30% Mg-Chlorite, <1mm subhedral tabular crystals. 20% Quartz, <1mm anhedral crystal groundmass. 5% Epidote, <1mm anhedral circular crystal aggregates. 5% Sericite, <1mm anhedral crystals. 5% 1-3mm deformed chlorite + carbonate filled amygdules. 2% Opaque minerals, <1mm subhedral-euhedral crystals. <1% Biotite, <1mm localized anhedral crystals. <1% Fe-carbonate, <1mm, anhedral-subhedral crystals. Phenocrysts consist of: 7% Plagioclase, 1-3mm subhedral crystals. Slide has a felty texture. Fine-grained rhyodacite lava flow, Fivemile Lake Sequence (FM2a).

LE-371 Slide contains 90% groundmass and 10% phenocrysts. Groundmass consists of: 54% Plagioclase, <<1mm anhedral-subhedral microlites that appear to be recrystallized. 16% Mg-Chlorite, 1-1.5mm anhedral pod-like aggregates. 8% Epidote, <<1mm, anhedral aggregates, well-dispersed. 8% Quartz, <1mm anhedral groundmass. 3% Sericite, <<1mm anhedral crystals. <1% Actinolite, 1-1.5mm anhedral crystal aggregates, aggregates are rounded to curvilinear. Phenocrysts consists of: 10% Plagioclase, 1-2mm euhedral crystals. Rock has a felty texture. Fine-medium grained andesite lava flow, Fivemile Lake Sequence (FM1b).

Appendix 2: Thin section descriptions. * Indicates lithogeochemical analysis.

LE-372 40% Plagioclase, <1-2mm subhedral skeletal crystal lathes. 20% Mg-Chlorite, ~1mm subhedral crystal aggregates. 15% Actinolite, <1-1mm subhedral lathes and lathe aggregates, well-dispersed but can be locally concentrated. 15% Epidote, <1-1mm anhedral patchy aggregates, also occurs in small veins. 5% Fe-chlorite, <1-1mm subhedral crystal aggregates. 2% Sericite, <1mm anhedral crystals. 2% Quartz, <1mm very fine-grained crystalline groundmass. 1% Limonite, <1mm anhedral crystals that occur in veinlets. Rock has a felty texture. 5% of slide is composed of zoned 1-4mm chlorite + quartz amygdules. Mg-chlorite is commonly in the center with Fe-chlorite on the rims. <1mm fine-grained mafic lava. This slide represents a clast found in a felsic breccia. Fine-grained mafic pillow lava clast (FM1b).

LE-401 35% Epidote, 1mm subhedral crystals. 30% Actinolite, <1mm subhedral-euhedral crystals. 20% Fe chlorite, <1mm anhedral-subhedral crystals. 15% Magnetite, 2-15mm, occurs as large irregular accumulations. Roughly 15% of slide has veining, 1-2mm wide veinlets. Vein mineral assemblages include, quartz + epidote, quartz + actinolite + chlorite, quartz + actinolite, epidote + chlorite, oxide only, actinolite only. Alteration is intense and patchy. Rock has a felty texture. Fine-grained pillow lava, Central Basalt Sequence (CB1b).

LE-402* 35% Plagioclase, <1mm, subhedrdal-euhedral crystal lathes. 15% Fe-chlorite, <1mm anhedral crystals. 15% Pyrite, <1-1mm subhedral-euhedral cubic

crystals. 10% Actinolite, <1mm anhedral-subhedral crystal lathes. 10% Epidote, <1mm anhedral crystal aggregates, also occurs as 1-2mm euhedral crystals in 1mm veinlets. 10% Quartz, <1mm anhedral crystals. 3% Opaque minerals, <1-1mm anhedral-subhedral crystals. 2% Fe-carbonate, <1mm anhedral crystals. Slide contains undeformed quartz veins, <1% of slide. Deformed sigmoidal epidote + Fe-carbonate + sericite veins ~1%. Deformed epidote vein ~1%. Rock has a felty texture. Fine-grained sub-alkaline pillow basalt, Central Basalt Sequence (CB1b).

LE-409 Rock contains roughly 98% groundmass and 2% angular fragments. Groundmass consists of: 70% Quartz, <1-1mm anhedral crystals. 15% Sericite, <1mm anhedral crystals and 1-3mm curvilinear bands and patches. 10% Fe-chlorite, <1mm anhedral, occurs as fine-grained crystal aggregates. 2% Epidote, 1mm anhedral, occurs as fine-grained crystal aggregates. <1% Fe-staining, <<1mm, anhedral, occurs in foliation planes. Fragments consist of: 2% Subangular Quartz Clasts, 1-2mm. Veining and foliation have roughly the same trend. Rock has a silicified texture. Felsic tuff deposit, Upper Sequence (US2c).

LE-413* 35% Epidote, 1mm anhedral, occurs primarily as patchy crystal aggregates and also as <1mm circular crystal aggregates. 25% Quartz, <1mm anhedral crystal groundmass. 16% Actinolite, <1-1mm subhedral crystal lathes. 10% Mg-Chlorite, <1mm anhedral crytals. 10% Sericite, <1mm anhedral crystals.

Appendix 2: Thin section descriptions. * Indicates lithogeochemical analysis.

3% Fe-carbonate, 1mm subhedral crystals, <<1mm anhedral crystals. 1% Clinozoisite, <1mm subhedral crystal aggregates. Fine-grained sub-alkaline pillow basalt, Central Basalt Sequence (CB1b).

LE-419 60% Epidote, mostly <<1mm, anhedral crystals, but some 1-2mm subhedral crystals occur in veinlets. 15% Actinolite, 1-2mm subhedral-euhedral crystal lathes. 10% Mg-Chlorite, <<1mm anhedral crystal. 10% Plagioclase, 1mm subhedral-euhedral crystal lathes. 2% Quartz, <1mm anhedral crystals. 2% Sericite, <1mm anhedral crystals. 1-2% Fe- Carbonate, <1-1mm anhedral crystals. 1-3mm veins consists mostly of zoisite + quartz + sericite + actinolite + Fe-carbonate. Veins make up <2% of slide. Slide has a felty texture. Fine-grained pillow lava, Central Basalt Sequence (CB1b).

LE-420* 60% Sericite, <1mm-1mm anhedral-subhedral crystal aggregates, occurs mostly in veins and on hyaloclastite shards. 20% Fe-carbonate, 1-3mm subhedral-euhedral crystals. 12% Actinolite, <1mm euhedral crystal lathes. 5% Quartz, <1mm anhedral crystals, mostly overprinted. 2% Fe-chlorite, <1mm anhedral-subhedral crystals. 1% Epidote, <<1mm anhedral crystals, some 1-2mm anhedral crystal aggregates. Roughly 20% of slide is composed of mineralized hyaloclastite. Interstitial veins are mostly carbonate + actinolite + sericite. Inner pillow material of pillow lava, Central Basalt Sequence (CB1b).

Appendix 2: Thin section descriptions. * Indicates lithogeochemical analysis.

LE-431* 55% Fe-chlorite, <1mm anhedral-subhedral crystals. 32% Quartz, <<1mm anhedral crystalline groundmass. 5% Sericite, <<1mm anhedral crystals. 5% Epidote, <1mm circular anhedral crystal aggregates. 3% Limonite, <1mm anhedral crystals that occur primarily in curvilinear veinlets. Fine-grained basaltic andesitic diabase (DbSS).

LE-437* 50% Epidote, <1mm subhedral-euhedral crystals. 35% Actinolite, <1-<<1mm mostly anhedral-subhedral lathes with some euhedral lathes. 8% Fe-carbonate, <1-1mm euhedral crystals. 5% Fe-chlorite, <<1mm anhedral crystals. 2% Clinozoisite, <1mm subhedral crystals. 1% Pyrite, ~1-1.5mm subhedral sub-cubic crystals. Slide contains hyaloclastite that are rimmed with coarse epidote and centers rich in actinolite. Inner pillow hyaloclastite of fine-grained pillow basalt, Central Basalt Sequence (CB1b).

LE-461* Slide consists of 60% fragments and 40% groundmass. Fragments: composed dominantly of 1-4mm sub-angular quartz. Phenocrysts consist of: 32% Quartz, <1mm, anhedral crystals. 15% Sericite, <1mm anhedral crystals, defines fluid migration paths and also occurs as small crystal aggregates. 10-15% Plagioclase, <1-2mm subhedral-euhedral crystal lathes. 5% Orthoclase, 1-2mm anhedral-subhedral crystals. 5% Epidote, <1-1mm anhedral crystals that occur as small circular aggregates. 4% Mg-Chlorite, <1-1mm anhedral-subhedral crystals aggregates. 3% Fe-carbonate, <1mm anhedral-subhedral crystals. 1% Zoisite, <1mm anhedral crystals aggregates. 1% Opaque

minerals, <1mm crystals, some show cubic cleavage. Trachyandesitic lapillistone and breccia deposit (GL2b).

LE-469 Slide contains 75% groundmass and 25% porphyroblasts. Groundmass consists of: 20% Quartz, 1-2mm anhedral crystals. 20% Epidote, <1mm anhedral crystals. 15% Fe-carbonate, <1mm anhedral-subhedral crystals. 8% Fe-chlorite <<1-1/2mm anhedral-subhedral crystals. 6% Actinolite, <1mm subhedral-euhedral crystal lathes. 4% Opaque minerals, <<1-1mm subhedral-euhedral crystals. 2% Sericite, <<1mm anhedral-subhedral crystal aggregates. Phenocrysts consists of: 25% Garnet, <1-3mm subhedral porphyroblasts, Grossular. Slide is hydrofractured and broken into angular fragments with minimal distance between fragments, jigsaw puzzle fit. Slide contains quartz + Fe-carbonate veins <1-1mm that are cut by epidote + actinolite veins. Epidote veins are parallel fractured suggesting brittle extension. Fine-grained porphyroblastic pillow lava, Central Basalt Sequence (CB1b).

LE-496 40% Sericite, <1mm anhedral crystals. 35% Quartz, <<1mm anhedral crystalline groundmass. 15% Epidote, <1mm anhedral crystal circular aggregates. 6% Limonite, 1mm anhedral crystals, occurs in curvilinear alteration zones. 2% Fe-carbonate, <1mm anhedral crystals. 2% Fe-chlorite, <1mm subhedral crystals. Rock contains roughly 15% zoned quartz + chlorite amygdules, quartz lines the exterior and chlorite fills the center of amygdules.

Limonite appears to occur along a foliation. Basaltic lapillistone deposit, Fivemile Lake Sequence (FM1h).

LE-602 65% Quartz, <1mm anhedral crystalline groundmass. 15% Plagioclase, <1mm anhedral crystals. 8% Sericite, <1mm anhedral crystals, occurs mostly in foliation planes. 5% Fe-chlorite, <1-1mm anhedral tabular crystals. 4% Limonite, <<1mm anhedral crystals, occurs mostly in foliation planes. 3% Opaque minerals, <<1mm, subhedral cubic crystals. Shear indicators suggest sinistral deformation. Rock has a silicified texture. Shear zone derived alteration. Sericite + Quartz Schist (5b).

LE-604 50% Quartz, <1mm anhedral crystals. 40% Sericite, <1mm anhedral crystals. 8% Fe-carbonate, <1mm anhedral-subhedral crystals. <1% Pyrite, <1mm subhedral-euhedral crystals. <1% Plagioclase, ~1mm subhedral crystals. Pressure shadows suggest dextral shear sense. Sheared texture with shear zone derived alteration. Sericite + Quartz Schist (5b).

LE-605 60% Quartz, <<1mm, anhedral crystalline groundmass. 20% Plagioclase, <1-1.5mm, subhedral-euhedral crystals. 10% Fe-carbonate, <1mm anhedral-euhedral crystals. 4% Sericite, <1mm anhedral well-dispersed crystals. 4% Pyrite, 1-2mm subhedral-euhedral crystals, a majority of crystals are plucked out but cavities still exist and show relict cleavage. 1% Fe-chlorite, <1mm, anhedral-subhedral. <1% Hematite, <1mm anhedral crystals, occurs in veins

and adjacent to pyrite crystals. Silicified texture with shear zone derived alteration. Quartz + Carbonate + Pyrite Schist.

LE-611 55% Quartz, ~1-<<1mm anhedral crystal aggregates. 25% Mg-Chlorite, <1mm subhedral crystals, occurs primarily as linear relict fluid pathways. 15% Fe-carbonate, ~1-<1mm subhedral-euhedral crystals. 2% Sericite, <1-2mm anhedral crystals, occurs as strange bladed spherical pod-like aggregates. 1% Pyrophyllite, ~1mm, anhedral crystals. 1% Epidote, <1mm anhedral crystals, occurs primarily in veins. <1% Limonite, <<1mm anhedral crystals. 1-2% <1mm curvilinear veins. Some shear indicators show sinistral shear sense. Shear zone derived alteration. Quartz + Chlorite Schist (5b).

LE-621 45% Quartz, <<1mm, anhedral groundmass. 25% Mg-chlorite, <1mm anhedral crystals. 20% Fe-carbonate, <<1-1.5mm, subhedral crystals, probably ankerite. 5% Sericite, <1mm anhedral crystals. 5% Plagioclase, <1-1mm subhedral crystal lathes. <1% Epidote, <<1mm anhedral circular pod-like crystal aggregates. Rock has a slight sheared texture, shear indicators are not prominent. Secondary alteration is 8BSZ: Sericite ± Carbonate, Shear zone derived alteration. Chlorite + Ankerite Schist (5c).

LE-1004 50% Quartz, <1-2mm anhedral crystals. 30% Epidote, <<1mm anhedral semi-opaque crystal aggregates. 12% Actinolite, <<1mm anhedral-subhedral crystals, occurs as anhedral aggregates and small microlites, also occurs in 1-

2mm relict fluid pathways. 8% Sericite, <<1mm anhedral-subhedral crystals. <1% Fe-carbonate, <1mm anhedral pod-like crystal aggregates. Fine-grained pillow lava, Fivemile Lake Sequence (FM1b).

LE-1018 40% Quartz, <1mm anhedral angular to subrounded recrystallized grains and crystals. 30% <1-2mm angular to subrounded well-dispersed quartz grains. 10% <1-1mm subhedral well-dispersed plagioclase grains. 10% <1mm anhedral well-disseminated sericite. 8% 1-2mm aphyric lava fragments that consist of 70% <<1mm recrystallized quartz and 20% <<1mm anhedral sericite, 5% <1mm anhedral quartz phenocrysts and 5% <1mm plagioclase phenocrysts. <1% Fe-carbonate, <<1mm anhedral blebs. <1% Epidote, <1mm anhedral to subhedral crystals and semi-opaque crystal aggregates. <1% Fe-chlorite, < 1mm anhedral crystals. Felsic lapillistone and breccia deposit (GL2b).

LE-1020 30% Quartz, <<1mm anhedral recrystallized aggregates. 25% Fe-chlorite, 2-3mm anhedral patchy aggregates. 25% Fe-carbonate, <1mm anhedral-subhedral crystals. 10% Plagioclase, 1mm anhedral crystals. 10% Sericite, <1mm anhedral crystal aggregates that commonly occur as inclusions in quartz crystals. Rock has a sheared texture. Shear zone derived alteration. Quartz + Chlorite + Carbonate Schist (5e).

LE-1106 Slide contains 65% groundmass and 35% phenocrysts. Groundmass consists of: 20% Epidote, <1mm well-dispersed anhedral circular crystal aggregates.

20% Mg-Chlorite, 1-2mm subhedral imbricated crystals that occur as elongated wisps. 10% Quartz, <1mm anhedral crystals. 8% Fe-carbonate, <<1-1mm anhedral crystal blebs. 4% Skeletal Plagioclase, <1mm subhedral crystal lathes, mostly sericite altered. 3% Sericite, <1mm, anhedral-subhedral crystals, well-dispersed, commonly occurs as inclusions. Phenocrysts consist of: 30% Plagioclase, 1-3mm, subhedral-euhedral crystals. 5% Quartz, 1-2mm anhedral-subhedral crystals. Medium grained diorite (D).

LE-1500 35% Quartz amygdules, amygdules are ~1mm in diameter, quartz is anhedral and occurs as spherical crystal aggregates. 25% Fe-chlorite, <1mm anhedral crystals. 20% Plagioclase, <1-<<1mm subhedral-euhedral crystals. 10% Opaque minerals, <<1-1/2mm subhedral sub-cubic crystals. 10% Fe-carbonate, <<1-2mm subhedral-euhedral crystals, 5% is represented in 4-5mm thick Fe-carbonate veinlets. <1% Epidote, <1mm anhedral spherical crystal aggregates. Slide contains substantial iron staining. Slide has a sheared and felty texture. Some alteration may be shear zone derived. Foliated fine-grained pillowed andesite lava, Fivemile Lake Sequence (FM1i).

LE-1512* 65% Plagioclase, ~1-<<1mm subhedral-euhedral crystal microlites. 15% Quartz, ~1-<1mm anhedral crystals. 10% Fe-chlorite, <1mm anhedral well-dispersed interstitial crystals. 5% Sericite, <<1mm, anhedral crystals. 5% Fe-carbonate, 1-2mm, anhedral-subhedral crystals. Slide has a felty texture. Fine-grained pillowed andesite lava flow, Fivemile Lake Sequence (FM1b).

Appendix 2: Thin section descriptions. * Indicates lithogeochemical analysis.

CBD1 50% Quartz, < 1mm anhedral well-dispersed recrystallized groundmass and 1-2 mm angular crystal grains. 20% Sericite, < 1mm anhedral to subhedral well-dispersed interstitial grains, also pseudomorphs plagioclase. 15% orthoclase, < 1m-1mm angular well-dispersed grains. 10% plagioclase, occurs dominantly as <1-1 mm well-dispersed subhedral crystals and <1-2 mm well dispersed angular grains. 5% Fe-chlorite, < 1mm well-disseminated platy crystals. <1 % Fe-carbonate, < 1mm well-dispersed anhedral blebs. Matrix portion of felsic lapillistone deposit (CB2b).

CBD2* 60% Quartz, < 1mm anhedral well-dispersed groundmass. 20% Sericite, < 1mm anhedral-subhedral well-dispersed interstitial groundmass. 10% Orthoclase, < 1mm anhedral well-dispersed groundmass. 8% Fe-chlorite, < 1mm anhedral well-dispersed groundmass and 1- 2 mm cross-cutting stringers. 1% Fe-carbonate, < 1mm andhedral well-dispersed and interstitial blebs. 1% plagioclase, <1-1mm subhedral-euhedral well-dispersed crystals. Rhyolite lava flow, Central Basalt Sequence (CB2a).

CBD3* 60% Sericite, < 1-1mm anhedral-subhedral well-dispersed groundmass and 1-3mm stringers. 15%, Fe-chlorite, < 1-1mm anhedral to subhedral local cross-cutting stringers. 15% Quartz, < 1mm anhedral well dispersed groundmass and < 1mm anhedral crystals. 5% Fe-carbonate, < 1mm anhedral well-

dispersed blebs. 5% Pyrite, < 1-3 mm subhedral. Rhyolite lava flow, Central Basalt Sequence (CB2a).

CBD3-2 40% Quartz, < 1mm-1mm anhedral recrystallized groundmass. 30% Hematite, < 1-1mm anhedral crystals that form 1-2mm patchy alteration zones. 20% Spherulites, well-rounded local accumulations composed dominantly of quartz + orthoclase and locally altered to hematite which either pervasively replaces spherulite, or alters the rims of the spherulite. 10% Fe-chlorite < 1mm well-dispersed anhedral crystals. Spherulitic rhyolite lava flow, Central Basalt Sequence (CB2a).